Microbubble Driven Airlift Bioreactor for CO_2 Sequestration and Algal Biomass Production

KEZHEN YING

Degree of Doctor Philosophy

Department of Chemical and Biological Engineering

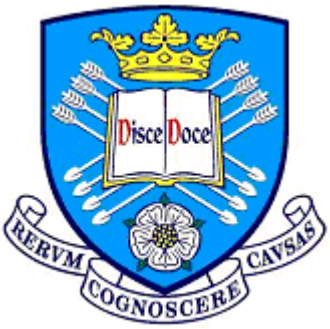

University of Sheffield

September 2013

Summary

This doctoral thesis is mainly focused on improving the microalgal growth and CO_2 capture efficiency by introducing microbubbles into an airlift bioreactor.

The effect of microbubbles on overall gas-liquid mass transfer (CO_2 dissolution and O_2 removal) was studied. The results showed that the K_La can be enhanced by either increasing the dosing flowrate or reducing the bubble size; however, increasing the flow rate to achieve a higher K_La would ultimately lower the CO_2 capture efficiency. In order to achieve both higher CO_2 mass transfer rate and capture efficiency, reducing bubble size (e.g. using microbubbles) has proved more promising than increasing flow rate. Microbubble (250 - 450 μm) dosing of 5% CO_2 gas showed improved K_La by 30 – 100% across different flow rates, compared to fine-bubble (400 - 800 μm) dosing.

The microalga *Dunaliella salina* was cultivated in both microbubble induced airlift bioreactor and conventional airlift bioreactor. About 20% - 40% increase in specific growth rate of *D. salina* was achieved in the proposed microbubble driven bioreactor compared with the conventional bioreactor cultures. A periodic CO_2 dosing model was later proposed for optimal algal (*D. salina*) biomass production and CO_2 sequestration. By applying this model, the culture dosed periodically achieved a much higher CO_2 capture efficiency (10-20%) compared to the one dosed continuously (0.25%). Finally, a 'pH^*-$NaHCO_3$-CO_2% system' was proposed to control the pH of the culture. An empirical equation correlating pH^* to $NaHCO_3$ and CO_2% was obtained. Additionally, the sole impact of either pH or CO_2 concentration on *D. salina* growth was studied by adapting 'pH^*-$NaHCO_3$-CO_2% system'. pH around 6 - 9 was found to support growth of *D. salina* cultures. The specific growth decreased when the CO_2 concentration increased. 0.02 mol L^{-1} CO_2 concentration (i.e. constant dosing of 50% CO_2) resulted in a strong inhibition of growth.

Acknowledgements

First of all, I would like to express my sincere gratitude to my supervisor Professor William Zimmerman, a respectable, responsible and resourceful person, who has provided me with valuable guidance, advice and encouragement all through my PhD studies. His insightful suggestions and vigorous academic observations enlighten me not only in this study but also in my future study/career. Thanks for his endless helps. I would also like to appreciate the helps I received from my co-supervisor Dr. Jim Gilmour. Thanks for his encouragements I could always find inspirations in my study. Furthermore, his kindness and patience are impressive.

Moreover, I want to show my great appreciation to Prof. Steve Wilkinson and Dr. Seetharaman Vaidyanathan who helped me with valuable comments over the years. I am also grateful to every technician in our department, who did a fantastic work on my experimental equipments, especially, Andy, Stuart, Adrian and Mark.

Content

List of Tables

List of Figures

Nomenclature

ε	the gas holdup, (V/V ratio)
μ	the overall specific growth rate, d^{-1}
$\triangle G$	the Gibbs free energy change for the reaction, J mol^{-1}
$\triangle G^0$	the standard Gibbs free energy change for the reaction, J mol^{-1}
$\triangle$[Chl]	changes in the concentration of chlorophyll content, mg L^{-1}
$\triangle[CO_2]_{dosed}$	the difference between the concentration of dissolved CO_2 before and after dosing, mol L^{-1}
$\triangle[CO_2]_{uptake}$	changes in the concentration of CO_2(aq) due to the CO_2 consumption by algal growth, mol L^{-1}
$\triangle[Na^+]$	the concentration of sodium ions in the liquid which comes from $NaHCO_3$, mol L^{-1}
C_0	initial concentration of algal biomass, mg L^{-1}
C_{NaHCO3}	concentration of $NaHCO_3$ in the culture, mol L^{-1}
C_t	instantaneous concentration of algal biomass, mg L^{-1}
CO_2%	the concentration of CO_2 in the gas stream, % (V/V)
d_B	the bubble size, m
η	the CO_2 capture efficiency, %
I%	the percentage increase in K_La, %
K_1	first equilibrium constant for bicarbonates buffer
K_2	second equilibrium constant for bicarbonates buffer
K_La	volumetric mass transfer coefficient (min^{-1}), where 'K_L' is the CO_2 gas-liquid mass transfer coefficient (m min^{-1}); 'a' means the gas-liquid interfacial area (m^{-1})
K_w	hydrolysis constant of the water
P	standard atmospheric pressure, 101.325 Kpa
pH	the pH value of the liquid

pH^* / pH_{eq}	equilibrium pH
R	universal gas constant, 8.314 J mol^{-1} K^{-1}
T	the temperature, K
t_C	culture time period, d
t_d	CO_2 dosing time, min
t_i	CO_2 dosing interval, min
ν_{Chl}	instantaneous productivity of chlorophyll content, mg L^{-1} d^{-1}
ν'_{Chl}	average productivity of chlorophyll content, mg L^{-1} d^{-1}
$\nu_{CO2\ uptake}$	instantaneous algal CO_2 uptake rate, mol L^{-1} min^{-1}
$\nu'_{CO2\ uptake}$	average algal CO_2 uptake rate, mol L^{-1} min^{-1}
Q	the gas dosing flowrate, L min^{-1}
ν_{MTR}	CO_2 instantaneous mass transfer rate, mol L^{-1} min^{-1}
ν'_{MTR}	CO_2 average mass transfer rate, mol L^{-1} min^{-1}
V_L	the volume of the liquid, L
$[An^-]$	total concentration of anions, mol L^{-1}
$[Cat^+]$	total concentration of cations, mol L^{-1}
$[C_T]$	total concentration of inorganic carbon in the liquid, mol L^{-1}
$[C_T]_{pH=A}$	total concentration of inorganic carbon in the liquid at pH=A, mol L^{-1}
$[C_T]_{pH=B}$	total concentration of inorganic carbon in the liquid at pH=B, mol L^{-1}
[Chl]	concentration of chlorophyll content in the culture, mg L^{-1}
$[Chl]_0$	initial concentration of chlorophyll content at the beginning of log growth phase, mg L^{-1}
$[CO_2]$	dissolved carbon dioxide concentration in the liquid, mol L^{-1}
$[CO_2]^*$	dissolved carbon dioxide equilibrium concentration in the liquid, mol L^{-1}
$[CO_2]_0$	initial dissolved carbon dioxide concentration in the liquid, mol L^{-1}

$[CO_2]_t$	dissolved carbon dioxide concentration in the liquid at time t, mol L^{-1}
$[CO_2]_{pH=A}$	dissolved carbon dioxide concentration in the liquid at pH=A, mol L^{-1}
$[CO_2]_{pH=B}$	dissolved carbon dioxide concentration in the liquid at pH=B, mol L^{-1}
$[CO_3^{2-}]$	the concentration of carbonate, mol L^{-1}
$[H^+]$	the concentration of hydrogen ions, mol L^{-1}
$[HCO_3^-]$	the concentration of bicarbonate, mol L^{-1}
$[NaHCO_3]$	the concentration of sodium bicarbonate, mol L^{-1}
$[OH^-]$	the concentration of hydroxyl ions, mol L^{-1}
$[P_A],\ldots[P_D]$	the partial pressure of the reactant(s) and product(s)

Chapter 1: Introduction

1.1 Research background

Nowadays, climate change and energy crisis are two major challenges for humanity. Consequently, governments around the world have paid a lot of attention to dealing with both problems and issued several measures, such as encouraging renewable energy production, increasing the price of fossil fuel, controlling CO_2 emissions, charging certain tax on different emission levels, investing in projects on CO_2 reduction and biofuel production, etc. (BBC news, 2007; EU Commission Brochure, 1987) These have become the major driving forces for developing new technologies to mitigate the CO_2 level, and many physical and chemical technologies have been in use for CO_2 capture from flue gas. In fact, the conventional chemical/physical approaches are relatively expensive and energy costly which causes the benefits of CO_2 mitigation to become marginal. (Gupta and Fan, 2002; Shi and Shen, 2003) According to the previous cost analysis of CO_2 removal from industry processed gases, the cost of CO_2 removal would essentially double the electricity and fossil fuel costs and this does not include the ultimate disposal fee for the sequestrated CO_2. (Herzog et al., 1991) Compared with chemical/physical CO_2 mitigation, biological CO_2 capture has attracted more attention as an alternative mainly because it can capture CO_2 via photosynthetic activities and meanwhile produce biomass energy. (Kondili and Kaldellis, 2007) However, conventional terrestrial plants were estimated to contribute only 3-6% of CO_2 capture from fossil fuel emissions, due to their slower growth rates. (Skjanes et al., 2007) For submerged aquatic higher plants, they present relatively low productivities even under optimal conditions of CO_2 and nutrient supply which does not appear to be practical for CO_2 capture. (Benemann, 1993) Compared with submerged plants, seaweeds exhibit higher productivities. For the seaweeds cultured on-shore, they have certain benefits for growth due to higher control of conditions, better nutrients supply, etc. However,

the requirement of considerable mixing and turbulence to allow effective mass transfer of nutrients, especially CO_2, results in the dramatic energy inputs and consequently makes such culture impractical. (Benemann, 1993) Among other options, microalgae, due to their unique properties, are a reasonable choice for CO_2 capture and biomass production, and could thus provide many benefits to industry.

Microalgae are a large and diverse group of typically autotrophic, photosynthetic microorganisms, producing complex organic compounds from simple inorganic molecules by using energy from light and inorganic chemical reactions. There are thousands of algal species, ranging from unicellular to multi-cellular form, and some of them are obligately photoautotrophic while some are mixotrophic, deriving energy both from photosynthetic activities and uptake of organic carbon. Microalgae are simple in structure so that solar energy is directed into growth and reproduction rather than maintaining complex tissues or organs. (Walker et al., 2005) Besides, microalgae are very efficient solar energy converters and grow faster than any terrestrial plants. They are capable of producing the highest possible annual yield of biomass, and most of them have a wide range of tolerance to environmental conditions. Some microalgae can survive extreme conditions such like extreme pH, salinity or temperature etc., which are undesirable for conventional plants. Since fast growing algae require a lot of CO_2 and industry is one of the major CO_2 producers and fossil fuel consumers, responsible for more than 7% of total world CO_2 emissions, (Sakai et al., 1995) algal mass culture might be one of the quickest and most efficient solutions for reducing CO_2. The algal biomass produced can be used as food, animal feed, fertilizers and sources of oils and valuable chemicals, etc. (Chaumont, 1993; Borowitzka & Borowitzka, 1988; Spolaore et al., 2006; Becker, 2007; Chisti, 2008) Therefore, microalgae culture for CO_2 sequestration and biomass production seems to be win-win on both sides.

Since microalgae have been proposed as a sustainable and cost-competitive resource for biomass/biofuel production and CO_2 reduction (Benemann, 1993), a lot of algal projects have got underway around the world. However, only a few of them have achieved an advanced stage of development due to many challenges such as insufficient CO_2 supply, O_2 inhibition, mixing/circulation, illumination problem and contamination, etc. (Richmond, 2008) Many investigations have also been carried out to solve these problems. Among these major challenges, technical issues associated with light have been studied by many researchers, with various solutions arising (e.g. using an optimal mixing rate and light/dark ratio, combining artificial light with natural light, and increasing harvest frequency etc.). (Richmond et al, 2003; Suh & Lee, 2003;) For mixing, various methods were developed (e.g. re-design the reactor geometry, stirring, pumping and bubbling etc.), bubbling seems to hold the promise for a proper mixing. However, the techniques to solve CO_2 supply and O_2 accumulation problems are still at the 'bottle neck' of the development. Therefore, design of a bioreactor with low energy cost and particularly high gas mass transfer for both CO_2 dissolution and O_2 removal tends to be a major consideration for cost-competitive microalgae culture.

1.2 Research hypothesis and objectives

Since an innovative microbubble generation mechanism by fluidic oscillation was developed by Zimmerman et al. (2008), the idea of adapting this novel microbubble generation technique into microalgae culture to solve the CO_2 supply and O_2 accumulation problems is considerable. The new microbubble dosing technology promises to bring many benefits to microalgae cultrue. First, it contributes to a high CO_2 mass transfer rate by reducing the bubble size and by increasing the residence times. Second, when combined with an airlift loop design in bioreactor, it provides a proper mixing feature for suspending microalgae cells and evenly distributing nutrients and illumination. Furthermore,

this fluidic oscillator approach saves energy, compared to conventional microbubble generation approach, by avoiding the friction loss near the stagnation point and by disrupting boundary layer formation to reduce the skin friction loss. Therefore, the hypothesis of this thesis is that introducing microbubbles generated by oscillating flow into a conventional airlift bioreactor can enhance the mass transfer for both CO_2 dissolution and O_2 stripping, which will ultimately enhance microalgal biomass productivity and CO_2 sequestration efficiency. The main objectives are listed below:

1. Study the mass transfer property of the novel culture system – microbubble driven airlift bioreactor (ALB) and build up a matrix or model relating mass transfer with operational parameters.
2. Study the performance of microbubble driven ALB on microalgae (*D. salina*) culture and compare it with conventional ALB culture.
3. Study the pH-CO_2 interaction on microalgal growth.
4. Build up models correlating mass transfer to microalgal growth and optimize the operational parameter (CO_2 bubbling) to improve algal biomass productivity and CO_2 sequestration efficiency.

1.3 Organization of the thesis

Chapter 2 reviews the literatures involving the use of microalgae, general knowledge on photosynthesis, the major problems for conventional algal culture systems, basic principle of CO_2 mass transfer and microbubble generation systems etc. Chapter 3 describes the major experimental equipment and methods (while the detailed experimental designs for different studies are addressed in Chapters 4-7). The major analysis methods to determine the mass transfer, CO_2 uptake rate and algal growth etc. are described as well. From Chapter 4 to Chapter 7, the studies carried out to achieve the research objectives are discussed. In Chapter 8, the work is concluded and the main findings and recommendations for future work are given.

Chapter 2: Literature review

2.1 Microalgae

2.1.1 Introduction to microalgae

Microalgae are a large and diverse group of typically autotrophic, photosynthetic microorganisms, producing complex organic compounds from their simple inorganic molecules by using energy from light and inorganic chemical reactions. (Richmond, 1986) They contain thousands of species, ranging from unicellular to multi-cellular form, and some of them are obligately photoautotrophic while some are mixotrophic, deriving energy both from photosynthetic activities and uptake of organic carbon either by osmotrophy, myzotrophy, or phagotrophy. (Van den Hoek, 1995)

Unlike terrestrial plants producing certain desired chemicals only in parts of their overall structure such as leaves, roots, or seeds, microalgae can produce such chemicals in their entire biomass. (Wijffels et al., 2010) Additionally, they are simple in structure so that solar energy is directed into growth and reproduction rather than maintaining complex tissues or organs. (Walker et al., 2005) Besides, microalgae are very efficient solar energy converters and grow faster than any terrestrial plants, having the ability to fix carbon dioxide with an efficiency one order of magnitude (10-50 times) higher than those of terrestrial plants. (Li et al., 2008b) Furthermore, most microalgae have a wide range of tolerance to environmental conditions and some of them even can survive in extreme conditions such like extreme pH, salinity or temperature etc. which are undesirable for conventional plants. (Borowitzka & Borowitzka, 1988) Due to these features, microalgae have been suggested as a commercial and renewable resource for a long time. Most species are used as food, animal feed, fertilizers and sources of oils and valuable chemicals, etc. (Chaumont, 1993; Spolaore et al., 2006; Becker, 2007; Chisti, 2008)

2.1.2 Products and uses of microalgae

2.1.2.1 Microalgae for fine chemicals production

Microalgae require vitamins for growth, but on the other hand they also contain and excrete vitamins of which some have particular commercial interest. For example, the vitamin B_{12} in some algae species produced through a symbiotic interaction with bacteria is particularly in demand as a health food. (Croft et al., 2005) Vitamin E, especially used as an anti-oxidant and having a great market potential, also can be produced by some algae. (Klaui, 1976; Azzi & Stocker, 2000) Besides, microalgae also form a wide range of carotenoids which have many commercial applications such as 'natural food' colourings (Emodi, 1978; Del Campo et al., 2007), improvement of feed nutrition (Spolaore et al., 2006; Becker, 2007) and colour enhancement of fish such as salmon (Schiedt et al., 1985; Zaťková et al., 2011). In addition, the derivatives of carotenoids, such as abscisic acid and retinol, can be used as growth promoters and aid in cancer prevention (Peto et al. 1981). Also some carotenoids, such as neoxanthin and fucoxanthin in some edible brown algae, were found to have the potential to reduce the risk of cancer (Kotake-Nara et al., 2001). The green alga *Dunaliella salina* was considered to be one of the richest algal sources of β-carotene and glycerol which have massive commercial benefits. (Chen&Chi, 1981; Chengala et al., 2010)

2.1.2.2 Microalgae for aquaculture and animal consumption

In aquaculture, microalgae are an essential component of the diet of marine bivalve mollusks, larvae of saltwater shrimp, some fish species and zooplankters. (Lazo, et al., 2000; Brown, 2002) Algal supplements increase significantly the survival of the larvae, and it is suggested that microalgae may add a growth factor to the culture or may act as a bactericidal agent. (Lazo, et al., 2000) Green algae such as *Dunaliella* spp. are the most frequently used species in such

commercial operations for aquaculture. (Borowitzka & Borowitzka, 1988) Microalgae are not only important as a food source for aquatic organisims, they also play an important role in oxygen and carbon dioxide balance due to their photosynthetic activities. (Pruder, 1983; Cheng et al., 2006) Microalgae are also considered to be used as an alternative high quality protein supplement to replace soybean meal or other conventional protein sources for animal feed. (Becker, 2007) Some sewage grown algae species were tested in Israel with the view to replacing soya protein used in poultry feed. The results showed that all the species tested can successfully replace 25% of the soybean protein with e.g. 7.5% algae, although the feed conversion efficiency was lowered with higher percentage of algae. (Borowitzka & Borowitzka, 1988; Lipstein & Hurwitz, 1980) In principle, microalgae can also be utilized as an ingredient in pig feed preparations. Yap et al. (1982) successfully replaced 33% protein by using *Spirulina* and *Chlorella* in pig feed, with no negative symptoms observed. He et al. (2002) found that the supplementation of algae to the diet of pigs could increase daily body weight by 10%.

2.1.2.3 Microalgae in wastewater treatment

With regard to wastewater treatment, microalgae when used as alternatives to active sludge are able to remove contaminants, especially nitrogen/phosphorus and heavy metals, while conventional physical/chemical and biological methods fail to achieve an effective elimination (Chaumont, 1993). In the process of wastewater purification, the oxygen produced by algal photosynthesis is used by aerobic bacteria to meet the BOD. (Rawat et al., 2011) On the other hand, the aerobic bacteria break down the organic matter, with carbon dioxide generated, contributing to the growth of algal biomass of which a part is harvested for further commercial uses. Combination of wastewater treatment and CO_2 microalgal fixation has become more attractive recently as it provides additional economic incentives due to the savings in nutrient supply and the environment

benefits. (Mallick, 2002) In a feasibility study, *C. vulgaris* was cultivated in wastewater discharged from a steel plant, presenting a CO_2 fixation rate of 0.624 g L^{-1} d^{-1} and an ammonia removal rate of 0.92 g m^{-3} h^{-1}. (Yun et al., 1997)

2.1.2.4 Microalgal culture for CO_2 sequestration

Microalgae are among the fastest growing species, having the ability to fix carbon dioxide with an efficiency of 10-50 times higher than those of land-based plants. (Li et al., 2008b) Industrially processed gas contains varying amounts of CO_2 which can also be considered as a carbon-rich source for microalgae and thus can be directly injected into the microalgal culture. By dosing in this way, it could simplify CO_2 separation from stack gas and reduce the capital cost. (Wang, 2008) Besides, some microalgae species showed satisfactory tolerance to moderate levels of NOx and SOx which can be effectively used by them as nutrients. (Matsumoto et al., 1997; Olaizola, 2003) This also simplifies the scrubbing system required for industrial exhaust gas. The high value commercial products yielded by microalgae culturing could offset the capital and operating costs, which makes such ideas more commercially practicable. Although the feasibility of directly using flue gas for algal cultivation was doubted by many researchers as the high CO_2 content and the presence of NO_x/SO_x might poison the culture, (Negoro et al., 1991; Negoro et al., 1992; Yoshihara et al., 1996) a contemporary study on CO_2 fixation by directly blowing flue gas from a power plant into a small algal raceway pond has proved that flue gas did not inhibit the algal growth. (Negoro et al., 1993; Hamasaki et al., 1994) Zimmerman *et al.* (2011b) also recently conducted a pilot scale trial using flue gas from a Tata Steel plant to culture *D. salina* in a 2200 L microbubble driven airlift bioreactor. The results indicate that despite the high concentration of CO_2 and trace impurities in the flue gas, microalgae still grew exponentially with a specific CO_2 uptake rate of 0.1 g L^{-1} h^{-1} achieved. Another research study (Yun et al., 1997) combining ammonia removal from wastewater discharged from a steel plant with CO_2

fixation from flue gas showed around 12430 kg of algal biomass could be produced per day with a CO_2 fixing rate of 23100 kg day^{-1}.

2.1.2.5 Microalgal culture for bio-fuel production

In terms of bio-oil production, many microalgal species are rich in oil content which can be easily extracted and converted into biodiesel by current technology. (Chisti, 2007; Banerjee et al., 2002) In fact, microalgae can produce up to 250 times greater amount of oil than soybean and 31 times greater than palm oil. (Hossain et al., 2008) Some believe producing biodiesel from microalgae may be the only way to completely displace current liquid transport fuels from petroleum. (Hossain et al., 2008; Chisti, 2008) The biodiesel produced from microalgae is also considered to be non-toxic and highly valuable. (Hossain et al., 2008; & Sheehan et al., 1998) Some microalgae species promise a direct extraction of free fatty acids and provide a good quality of oil with yield ranging from 16 to 24% of dry weight. (Aresta et al., 2005) The calorific value of the oil produced from a *Dunaliella* strain was found to be up to 36 kJ g^{-1}, (Minowa et al., 1995) much higher than the calorific value (18 kJ g^{-1}) of oil produced from other plants such as kudzu and comparable to fossil fuel oil (45 kJ g^{-1}). (Kumar and Pratt, 1996)

Most importantly, microalgae culture can combine biofuel production with carbon dioxide capture from flue gas, contributing to CO_2 mitigation and biodiesel production. Some microalgae species (e.g. *Dunaliella salina*) can directly use industrially processed gas containing different percentages of CO_2 as a carbon-rich source, which contributes to the CO_2 sequestration and meanwhile simplifies the CO_2 treatment system for industry. (Wang et al., 2008) Some microalgae species also indicated adequate-tolerance to moderate levels of NO_x and SO_x which can be effectively used as nutrients. (Matsumoto et al., 1997) The high rate algal pond (HRAP) with additional CO_2 supply was shown to produce more than double biomass. (Benemann, 2003) A proposed HRAP, sized to serve 25000 people, was estimated to produce about 2.7 tonnes of algal biomass per

day with additional CO_2 from flue gas scrubbing, and the authors suggest it could provide up to 1 million kWh of electricity per year plus further carbon credits by digesting of the biomass to methane. (Shilton et al., 2008) Kishimoto et al., (1994) reported that the cultivation of the microalga *Dunaliella tertiolecta* in a bioreactor with an additional CO_2 supply reached a biomass of 1.0 g L^{-1} after a week, with the biomass containing 10% glycerol and thermochemical liquefaction of the biomass produced a 36% conversion efficiency to oil. This indicates the capability of algal biofuel production by CO_2 fixation. In another study, Chisti proposed a process integrating microalgae biomass production with oil production, (Chisti, 2008) shown in Figure 2.1. In the biomass production stage, algae are cultured by using the CO_2 flue gas from power generation stage and nutrients separated from biomass recovery stage. The biomass recovered is then used for oil extraction which is further converted to biodiesel. Some of the remaining biomass can be used for producing other high value products or animal feeding. Most of the residual biomass is send to an anaerobic digester for biogas generation, with the effluent from that sold as fertilizer and irrigation water. The biogas, as the major source of energy, will serve for most of the production and processing and any excess energy can be sold to the grid. (Chisti, 2008) According to this conception, microalgae biofuel has the potential to be produced sustainably without CO_2 release. Sheehan et al. (1988) estimated the realistic replacement of transportation fuel with biodiesel could be achieved by culturing microalgae species containing an oil content of more than 50% in the high rate algal pond combined with a wastewater treatment plant.

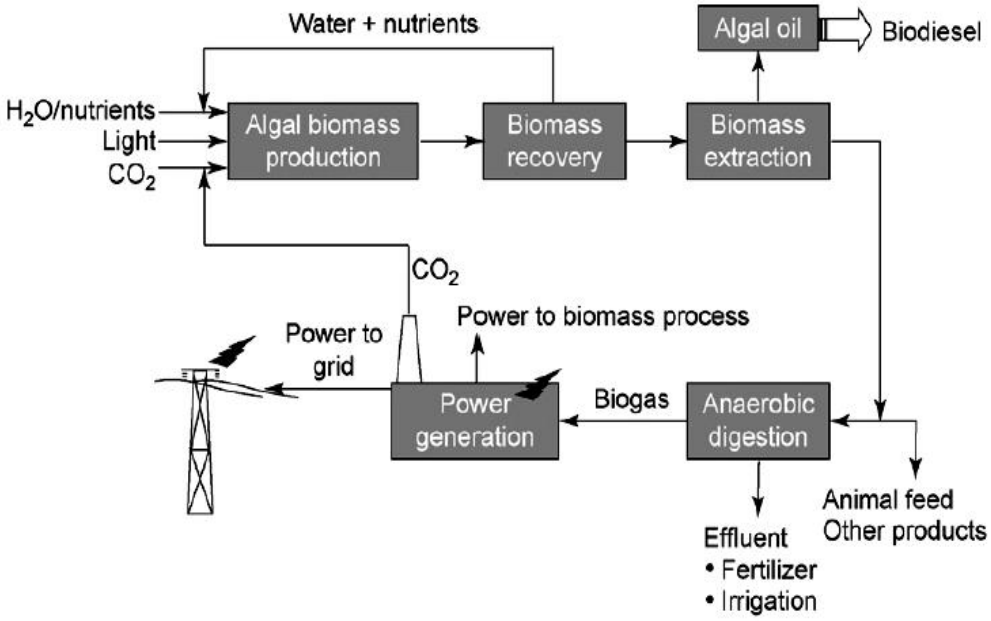

Figure 2.1: An ideal process for microalgal culture and biodiesel production. (adapted from Chisti, 2008)

2.1.3 *Dunaliella*

Dunaliella is a unicellular, biflagellate, naked, green alga. Cells of *Dunaliella*, lacking a rigid cell wall, are enclosed by a thin elastic plasma membrane covered by a mucous surface envelope. (Richmond, 2008 Ye et al., 2008;) This cellular feature allows rapid cell volume changes responding to extracellular osmotic pressure changes. *Dunaliella* species usually have a wide range of tolerance to salinity, from as low as 0.05 M to salt saturation (more than 5 M) due to their ability to synthesis and degrade intracellular glycerol. (Chen & Jiang, 2009) Besides, *Dunaliella* species have a wide tolerance to pH, ranging form pH=1 (*D. acidophila*) to pH=11 (*D. salina*). (Visviki & Santikul, 2000; Borowitzka & Borowitzka, 1988) Some *Dunaliella* species have also shown the tolerance to temperature. For instance, the halophile *D. salina* was reported to grow at temperatures up to about 40 ℃. (Wegmann, Ben-Amotz & Avron, 1980) *Dunaliella* species also have an exceptional tolerance to heavy metals (e.g.

copper and lead) and chlorinated hydrocarbons. (Borowitzka & Borowitzka, 1988; Tsuji et al., 2002) Above all, microalgae of the genus *Dunaliella* are suitable for mass cultivation, especially using outdoor cultures, due to their remarkable ability to adapt to a variety of environmental conditions.

Among the *Dunaliella* species, *salina* is the richest source of glycerol and β-carotene, (Ben-Amotz & Avron, 1983) and it was also among the first microalgae to be used commercially to produce fine chemicals. *Dunaliella salina* tolerates a wide pH range between 5.5 and 10.0. pH of 9 was found to be optimal for β-carotene production, however, the optimal pH for photosynthesis is generally lower than 9. (Borowitzka & Borowitzka, 1988) Interest in producing β-carotene from *Dunaliella* has continued to the present, with the latest research focusing on the effects of light quality onβ-carotene production (Fu et al., 2013). In terms of the tolerance to temperature, photosynthetical activity was found at temperature down to -8 ℃. (Siegel et al., 1984) This unique environmental adaptation allows successful intensive outdoor cultures in cold seasons and cold areas. The optimum temperature for *Dunaliella salina* has been reported to be around 25 ℃. (Garc á-Gonz ález et al., 2005)

In this thesis, *Dunaliella salina* was chosen for most of the studies, because its extreme salinity tolerance simplifies maintenance of a uni-algal culture. And it is also considered to be suitable for scale-up cultures (e.g. industrial scale cultures), because they grow in highly selective environments and thus can remain relatively free of contamination by other algae and protozoa even when exposed to the open air environment.

2.2 Photosynthesis

Photosynthesis represents a unique process of solar energy conversion, by which photoautotrophs convert the solar energy and inorganic compounds (CO_2 and H_2O) into chemical energy to drive metabolic functions and organic matter

(sugars), and meanwhile release O_2. (Blankenship, 2008) Although photosythsis can happen in different ways in plants, algae and cyanobacteria, the overall photosynthetic process is always similar in these organisms (see Figure 2.2), which can be summarized by the general photosynthetic equation: 6 CO_2 (aq) + 12 H_2O (liq) + photons → $C_6H_{12}O_6$ (aq) + 6 O_2 (g) + 6 H_2O (liq). (Raven, 2003) However, the photosynthesis process described by this simple equation actually involves an extremely complex series of reactions, which can be divided into two stages, the light dependent reactions and light independent reactions (dark reactions). The light reactions occur in the thylakoid membrane of the chloroplast, involving light absorption and electron transport which results in the production of biochemical reductant NADPH, high energy compound ATP and oxygen. The dark reactions, taking place in the stroma, represent the reduction of CO_2 and the synthesis of carbohydrates driven by the NADPH and ATP provided from the light reactions. **(**Richmond, 2008**)**

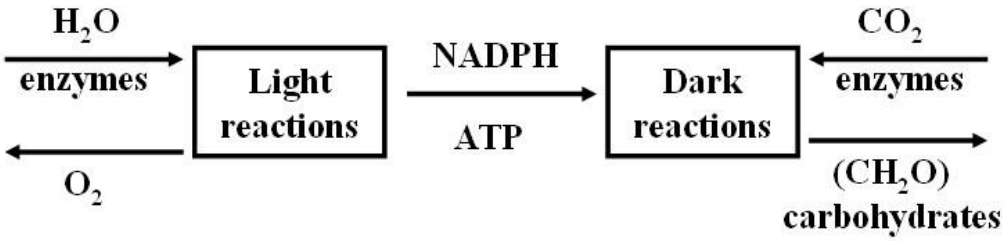

Figure 2.2: The overall process of photosynthesis **(**adapted from Richmond, 2008**)**

2.2.1 Light dependent reactions

The main role of the light reactions is to provide NADPH (biochemical reductant) and ATP (chemical energy) for the dark reactions.

The photosynthetic light reactions are located in the thylakoid membranes. In

most algae strains, the thylakoids are grouped in pairs or stacks of three. (Raven, 2003) In the thylakoid membrane, there are five major complexes that maintain photosynthetic electron transport and photophosphorylation, and they are light-harvesting antennae, photosystem I and photosystem II, cytochrome b_6/f and ATP synthase enzyme. (Lawlor, 1987) In green algae, various types of pigments can absorb the light energy, but only some special forms of *chlorophyll a* (Chl a) are able to convert the solar energy into chemical energy, forming reaction centres. All other pigments are therefore accessory pigments (forming light-harvesting antennae system) which capture photons and transfer energy to the photosynthetic reaction centres (See Figure 2.3). Since accessory pigments absorb in different parts of the spectrum, algae are able to absorb light of wide range of wavelengths. (Lawlor, 1987) Photosystem I (PS I) is composed of its reaction centre and the inner light-harvesting antenna pigments, which is maximally excited by the light of wavelength 700 nm. (Richmond, 1986) Photosystem II (PS II), located in the thylakoid membrane, is the set of its associated reaction centre (absorbs light at 680 nm), the inner antenna pigments and the oxygen-evolving complex. Electron transport between PS II and PS I is linked via the cytochrome b_6/f complex. ATP synthase is a membrane-bound enzyme which catalyzes the synthesis of ATP from ADP and P_i. (Richmond, 2008)

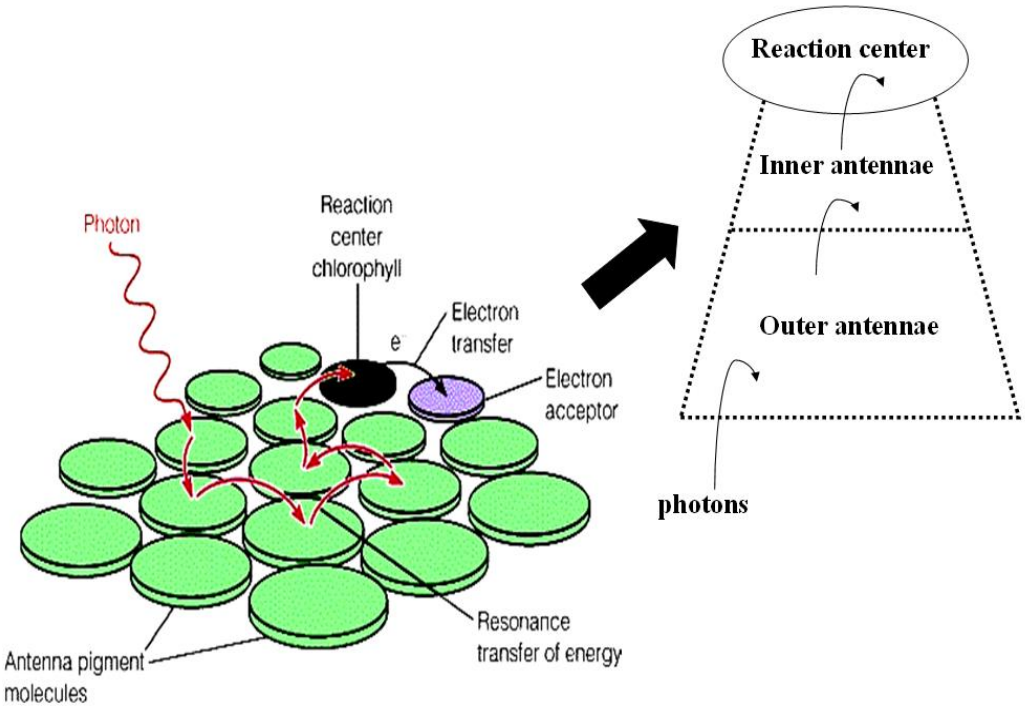

Figure 2.3: The schematic diagram showing the energy transfer from accessory pigments to reaction centre. (adapted from Richmond, 2008)

The overall processes for the light reactions are usually visualized in a 'Z-scheme', shown in Figure 2.4. (Hill & Bendall, 1960) Light energy is captured by chlorophyll and other accessory pigments and transferred to PS II reaction centres. When the chlorophyll molecules at the PS II obtain sufficient excitation energy from the adjacent antennae system, the electrons are excited and transferred to the first electron-acceptor, pheophytin. These electrons are then passed through the electron transport reactions proceeding energetically downhill (so-called electron transport chain). Meanwhile, protons are transferred from stroma into thylakoid lumen creating a pH gradient and charge difference (chemiosmotic potential), the energy of which drives ATP synthesis via the ATP synthase enzyme. (Lawlor, 1987) Usually, about four protons are required for the

synthesis of one ATP molecule. (Kramer et al., 1999) The electron then reaches the p700 reaction centre in PS I, however, its energy or reduction potential is no longer sufficient for further transport. Due to light absorption in PS I, another electron is expelled and accepted by a secondary electron-acceptor, and again passed down lowering energies of electron carriers. The energy created here is also used to move hydrogen ions across the thylakoid membrane into the lumen, which contributes to create the chemiosmotic potential for ATP synthesis, while the electron is used to reduce $NADP^+$ into NADPH. (Lawlor, 1987) The ATP and NADPH are utilized in dark reactions.

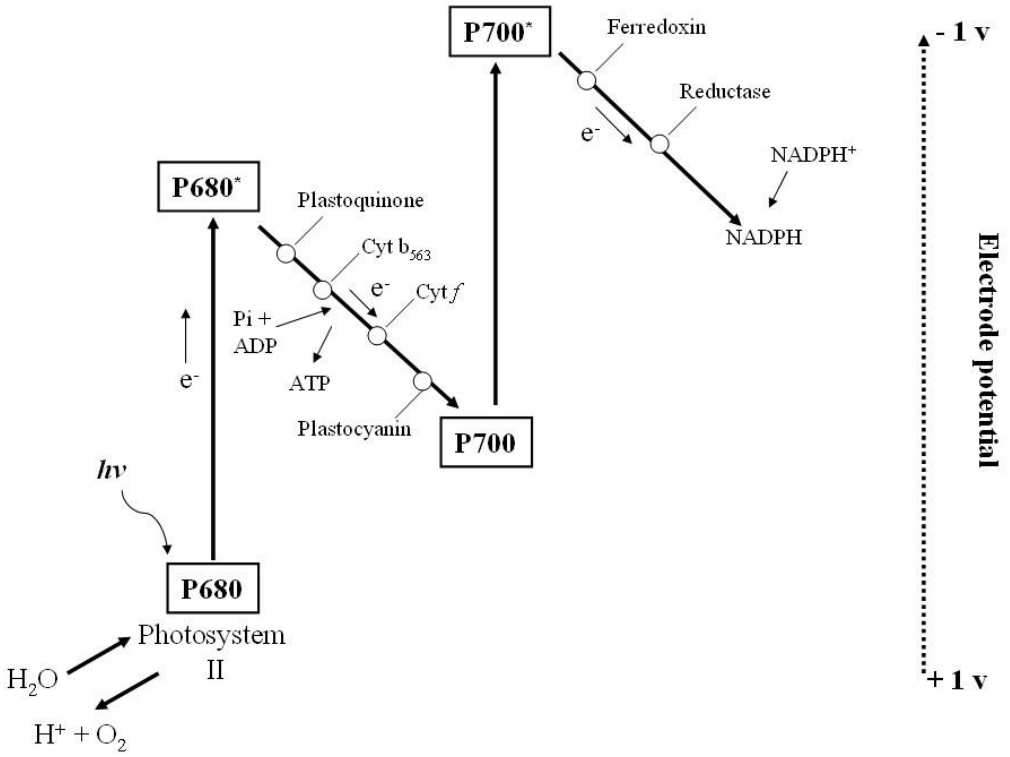

Figure 2.4: The Z scheme of photosystems and electron transport in photosynthesis (adapted from Richmond, 1986)

When the electron is expelled from PS I reaction center due to the light absorption, it leaves an empty electron 'hole' which is in turn filled by the electron expelled by illumination of PS II and arriving through the electron transport chain. This, however, leaves an electron hole in PS II. This hole is in turn filled by electrons from water through a process called water photolysis. The H^+ ions are released to the thylakoid lumen which also contributes to the build up of chemiosmotic potential that leads to ATP synthesis. Oxygen molecules generated, a 'waste' product in light reactions, are released to medium or atmosphere. (Richmond, 1986)

2.2.2 Light independent reactions (dark reactions)

In dark reactions, carbon dioxide is fixed using the NADPH and ATP provided from the light reactions. The photosynthetic carbon fixation pathways seems to be essentially the same in all photosynthetic organisms, which is called the Calvin-Benson cycle, taking place in the stroma of chloroplasts. (Berg et al., 2002) As shown in Figure 2.5, Calvin cycle comprises three stages. For stage one (carboxylation phase), in the presence of the enzyme ribulose bisphosphate oxygenase (Rubisco, located on the stromal surface of the thylakoid membranes of chloroplasts), CO_2 combines with a five-carbon sugar, ribulose 1,5-bisphosphate (RuBP), to form two molecules of phosphoglycerate (also known as PGA). In stage two (reduction phase), at the expense of NADPH and ATP, PGA is reduced to phosphoglyceraldehyde (G3P). Most of the G3P produced is used in stage three (regeneration phase) to regenerate RuBP so that the Calvin cycle can continue and more CO_2 can be fixed. Those G3P not been used for RuBP regeneration are converted to hexose phosphates, which finally yield sucrose, glucose and cellulose. (Berg et al., 2002)

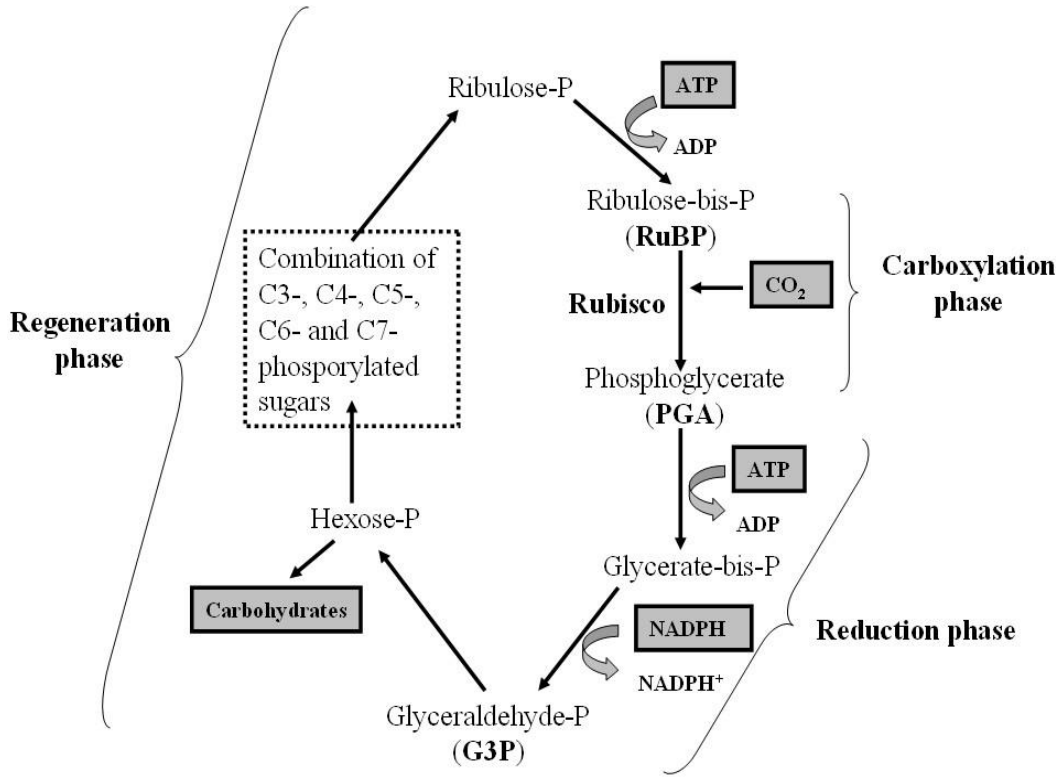

Figure 2.5: The dark reactions - Calvin-Benson cycle (adapted from Richmond, 2008)

In general, based on the basic processes of the light reactions and the dark reactions, illumination and carbon dioxide turn out to be two of the major limiting factors for photosynthesis. For light, it has the direct impact on electron transport and the generation of ATP and NADPH in light reactions, which in turn affects the amount of G3P being reduced and glucose produced. As regards to carbon dioxide, it is directly involved in the carboxylation dark reactions, determining the amount of PGA yield before PGA is reduced to form G3P at the expense of ATP and NADPH. In other words, carbon dioxide also affects the final yields of glucose formed from G3P. Besides, the enzyme that captures carbon dioxide, Rubisco, actually has a binding affinity for both carbon dioxide (carboxylation) and oxygen (oxygenation). (Richmond, 1986) When the O_2/CO_2

ratio is high (e.g. high concentration of O_2 but low concentration of CO_2), Rubisco will catalyze the reaction of O_2 with RuBP to form phosphoglycolate which after dephosphorylation, is converted to ammonia, serine and carbon dioxide. (Berg et al., 2002) This process is called photorespiration, and can often be a faster process than 'dark respiration' (Richmond, 1986). Photorespiration is not desirable because it inhibits the CO_2 fixation. (Lorimer, 1981)

2.3 Limiting factors for microalgal growth

According to the basic principles of photosynthesis, the photosynthetic activity of microalgae, in the short term (from seconds to hours), is controlled by the supply of light, CO_2, the amount of enzyme and reaction kinetics, etc. In the long term, light absorption, electron transport and enzymatic reactions of the Calvin cycle are subject to complex controls, both feedback and feedforward. The product of a reaction (e.g. RuBP), therefore, could modify the process, either stimulating or inhibiting the later ones. Complex metabolic systems adjust to conditions until the whole system returns to equilibrium, with the overall photosynthetic rate controlled by somewhat different factors. In other words, the overall rate for the long term is governed by the amount of components of the complex system which are determined by the conditions during the growth of microalgae. (Lawlor, 1987) Thereby, culture conditions, such as illumination, temperature, pH, nutrients, salinity and CO_2/O_2 ratio etc., turn out to be governing parameters for microalgal growth.

2.3.1 Light

The intensity of light is usually considered as one of the major limiting factors for algal growth, as it is directly related to the solar energy being absorbed by photosystems I and II in light reactions, affecting the amount of electron transport and the ATP/NADPH yield (assuming other components in the complex photosynthetic system are sufficient, e.g pigments in reaction centres, pigments

in antennae system, catalytic enzymes for ATP synthesis etc.) which subsequently influence the dark reactions for CO_2 fixation and glucose production.

Light energy received by microalgae is a function of the photon flux density per culture surface. In microalgae mass culture, only a small fraction of photons reaching culture surface may be reflected, while the other photons are either absorbed by the photosynthetic reaction centers or converted into heat. (Richmond, 2008) According to Iehana (1987), the light (400-670 nm) reflectance of a *Spirulina* cell was less than 2%. Goldman (1980) concluded the kinetic response of algal growth to the light intensity (illustrated in Figiure 2.6), assuming the light source is strictly the sole limiting factor for growth. As can be seen from Figure 2.6, at very low light intensities ($\approx I_c$), the algae growth rate is relatively low which is balanced by cell death rate, therefore a net growth rate of zero can be observed at compensation point. (Lee, 1986) As the light intensities increase, the photosynthetic rate shows a sharp increase until the maximal growth efficiency is achieved. A further increase in light intensities does not increase the photosynthetic activities after the light saturation (I_s) level is achieved, and the maximal growth rate is attained in the range of light saturation points. (Goldman, 1979; Lee, 1999; Richmond, 2000) Beyond these points, photoinhibition happens and any increase in light intensity will lead to a decrease in photosynthetic productivity caused by photo-oxidation which may damage the light receptors in algal cells. (Goldman, 1980)

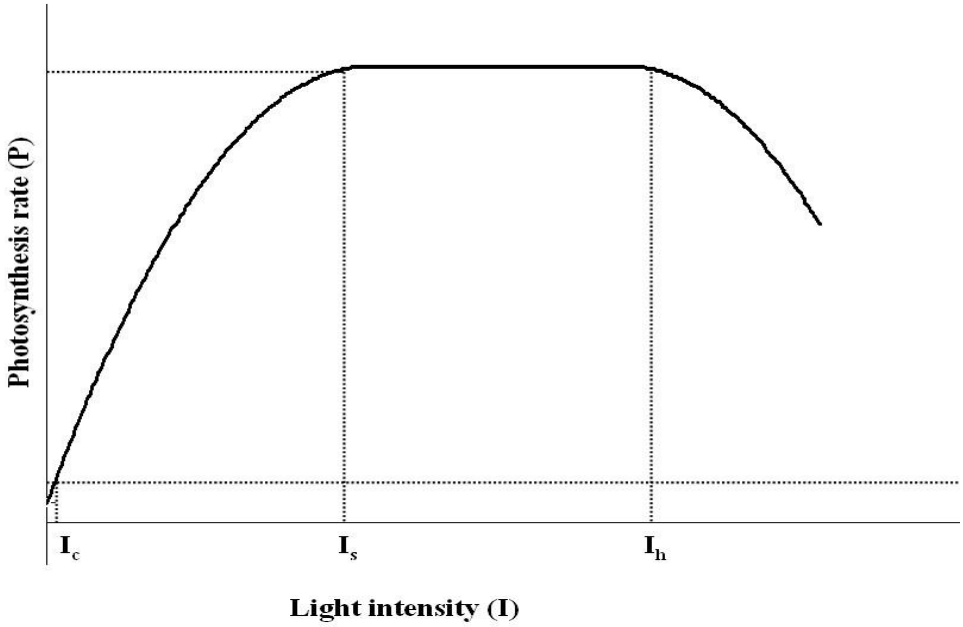

Figure 2.6: Light response curve of photosynthesis. I_c is the light compensation point, I_s means the light saturation intensity and I_h represents the light intensity value at which photoinhibitation happens. (adapted from Richmond, 2008)

For a certain high light intensity (e.g. I_s), assuming all the photons of a flux density can be captured by the algal mass culture, cell density will keep increasing exponentially until all photosynthetic available photons are absorbed. Then, cell density will increase linearly until light per cell becomes limiting which leads to a growth inhibition. (Richmond, 2008) Based on data from the light-limited chemostat continuous cultures (for *Chlorella*) conducted by Pirt et al. (1980), the relationship between biomass output rate and culture light absorption can be expressed as follows (Richmond, 2008):

$$IAY = \mu XV \quad \text{Eq. 2.1}$$

where A = irradiated culture area, I = photon flux density, μ = specific growth rate, V = culture volume, X = biomass and Y = bioenergetic growth yield. This

equation, however, assumes nutrients and CO_2 are not limited, and also the value of Y for certain algal species is a constant, implying the biomass output (μX) can be affected by the culture surface/volume ratio (A/V). Therefore, with regard to bioreactor design for algal biomass culture, high A/V ratio is usually applied to obtain high cell densities. (Chisti, 1989)

Eq. 2.1 also indicates that for a given photon flux density, A/V ratio and bioenergetic growth yield, specific growth rate decreases when culture density increases in a light limited culture. This general relationship was also reported by Richmond (2008) for a *Spirulina platensis* culture. This phenomenon can be understood by the concept 'mutual shading' (Tamiya, 1957) – when the culture becomes denser, the depth light penetrates into the culture becomes shorter which results in cells (even well suspended) receiving light intermittently. Or the available light energy per cell reduces when the population density increases. When mutual shading prevails, which is inevitable especially for batch photobioreactor cultures, two light zones are established in the culture: the light region (cells receiving sufficient light for photosynthesis) and the dark region (light intensity is below the compensation point). In microalgal culture, higher L/D ratio is usually employed for most photobioreactor designs to maximize the cell exposure time to light, so that more efficient light energy may be used for photosynthesis. (Richmond, 2008)

In conclusion, in a certain range (between I_c and I_h), increasing the light intensity leads to an increase in the photosynthetic rate. When the light intensity exceeds I_h, photoinhibition may occur. For a certain light intensity (e.g. I_s), higher cell density could result in a lower specific growth rate, although a constant output rate may be maintained. The results from the culture of the cyanobacterium Spirulina platensis demonstrated by Qiang et al. (1998) also strongly supports such a relationship between light intensity, output rate and cell density, as plotted in Figure 2.7.

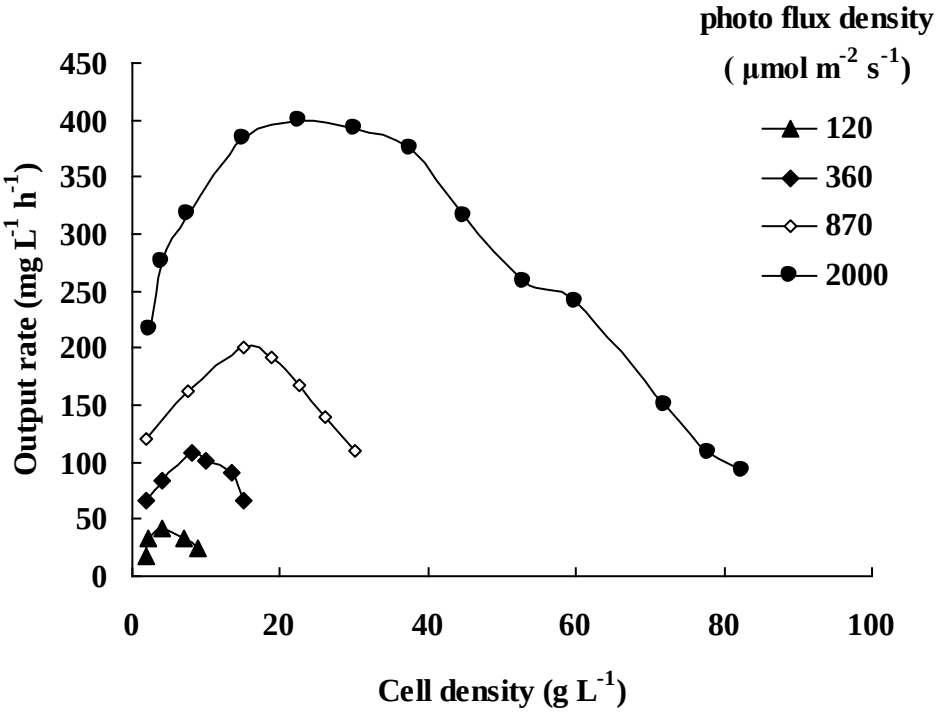

Figure 2.7: The plot of light intensity and cell density interaction on the culture productivity. (adapted from Richmond, 2008)

There are also many empirical equations, analogous to the Monod model, that have been suggested to describe the relationship between light intensity and algal growth, some examples are shown in Table 2.1. Eq. 2.2 was reported in Bannister (1979), based on each cell perceiving the illumination and that photoinhibition is absent. Eq. 2.3 takes the inhibitory effects of excessive light into consideration. (Aiba, 1982) Eq. 2.5 was developed from Eq. 2.4, accounting for photoinhibition at high irradiance and the fact that the dependence of specific growth rate on the average irradiance varies with the incident irradiance. (Molina et al., 1999) Carbon limitation was not considered in any of these examples.

Table 2.1: Models for light-denpendent specific growth rate`

Equation		Reference
$\mu = \frac{\mu_{\max} I}{(K_i^{\,m} + I^{\,m})^{\frac{1}{m}}}$	Eq. 2.2	Bannister (1979)
$\mu = \frac{\mu_{\max} I}{K_s + I + \frac{I^2}{K_i}}$	Eq. 2.3	Aiba (1982)
$\mu = \frac{\mu_{\max} I^n}{I_k^{\,n} + I^n}$	Eq. 2.4	Grima et al. (1994)
$\mu = \frac{\mu_{\max} I_{av}^{\,(b+\frac{c}{I_0})}}{[I_k(1+(\frac{I_0}{K_i})^a)]^{(b+\frac{c}{I_0})} + I_{av}^{\,(b+\frac{c}{I_0})}}$	Eq. 2.5	Grima et al. (1999)

Note:

a, b, c, m, n: parameters

I: incident photosynthetic radiation (μE m^{-2} s^{-1})

I_{av}: photosynthetically active hourly average irradiance inside culture (μE m^{-2} s^{-1})

I_k: microalgal affinity for light (μE m^{-2} s^{-1})

I_o: photosynthetically active irradiance impinging on the reactor's surface (μE m^{-2} s^{-1})

K_i: photoinhibition constant

K_s: saturation constant

μ: specific growth rate (s^{-1})

μ_{max}: maximum specific growth rate (s^{-1})

Apart from the impacts on algal growth, the light intensity also affects the algal cell composition. For example, with regard to heating value of biomass, enhancing light intensity increases the concentration of triacylglycerol in algae, however, it also results in 50-80% waste of incident light and the decrease in algal growth rate due to photoinhibition. (Benemann, 1997; Ogbonna and Tanaka, 1997) At lower light intensity, about 20-24% of visible light energy can be converted into algal biomass with a higher calorific value. (Benemann, 1997) For lipid conversion, it is reported that algae achieve higher lipid content but lower biomass concentration when algal cells are exposed to low light intensity, and inversely, higher biomass concentration but lower lipid conversion efficiency are achieved in a high light intensity culture. (Chisti, 2007)

2.3.2 Temperature

Temperature is another important parameter in algal culture, affecting biomass growth, the nature of metabolism, the nutritional requirements and cell components. (Richmond, 1986) The optimal temperature for most commonly cultured algal species ranges from 20-30℃. (Chisti, 2007) In the case of constant light intensity and no nutritional limitations, the maximum growth rate solely as a function of temperature can be described by Arrhcnius equation, (Goldman and Carpenter, 1974)

$$K = Ae^{-E/RT} \quad \text{Eq. 2.6}$$

in which K = specific growth rate, day^{-1}; A = constant, day^{-1}; E = activation energy, J mol^{-1}; R = gas constant, J K^{-1} mol^{-1}; and T = temperature, K.

The logarithmic version of Eq. 2.2 is shown as follows,

$$\log K = \log A - \frac{E}{2.30RT} \quad \text{Eq. 2.7}$$

Hence a plot of log K versus 1/T should be a straight line, with the slope of -E/(2.30R) and the intercept of log A.

The response of *Microcystis incerta* growth to variations in temperature was studied by Kruger and Eloff (1978). Figure 2.8 is the Arrhenius plot, showing the algal specific growth rate as solely a function of temperature. (Kruger & Eloff 1978) It demonstrates that for different temperature ranges the Arrhenius relations between algal growth and temperature vary. Although temperature requirements of algae vary over a wide range, in general, the algal growth will be enhanced when temperature increases until the optimum temperature is reached. However, when the upper temperature limit is exceeded, a sudden decrease in algal growth occurs. (Richmond, 1986)

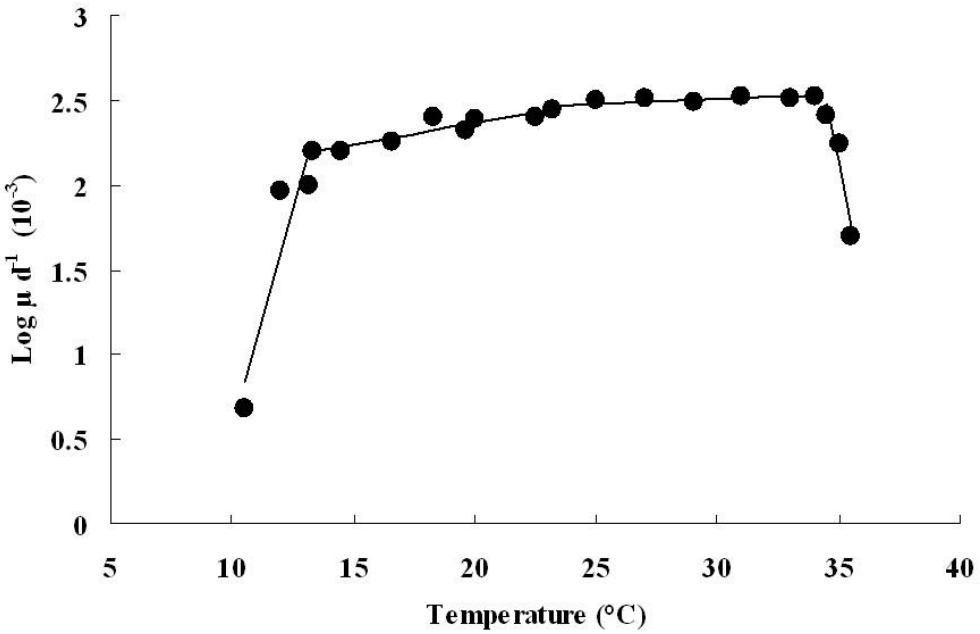

Figure 2.8: The relationship between growth rate and temperature (adapted from Richmond, 1986)

When light intensity is not held constant, the maximum specific growth rate can not be described as a function of only temperature. The effects of light and temperature on algal growth rates are interrelated. The amplitude of temperature dependence increases strongly with increasing the light intensity of the culture suspension, assuming the light intensity has not achieved the saturation point. This was demonstrated by Sorokin (1960) using a culture of *Chlorella*: under higher light intensity (1600 foot candles) the doubling times per day, compared with under lower light intensity (400 foot candles), increases much faster along with the temperature before it reaches the optimal value, while the doubling times also decrease more strongly when keeping increasing the temperature beyond the optimal level. The phenomenon indicates the higher amplitude of temperature dependence of *Chlorella* under higher light density. Besides, for both low- and high-temperature strains of *Chlorella*, it was found that the starting points of temperature for growth are higher at greater light intensities. (Sorokin 1960)

Finally, the interactions between light intensity and temperature on algal growth are well illustrated by Figure 2.9, re-plotted with comprehensive data points from Sorokin & Krauss (1962)

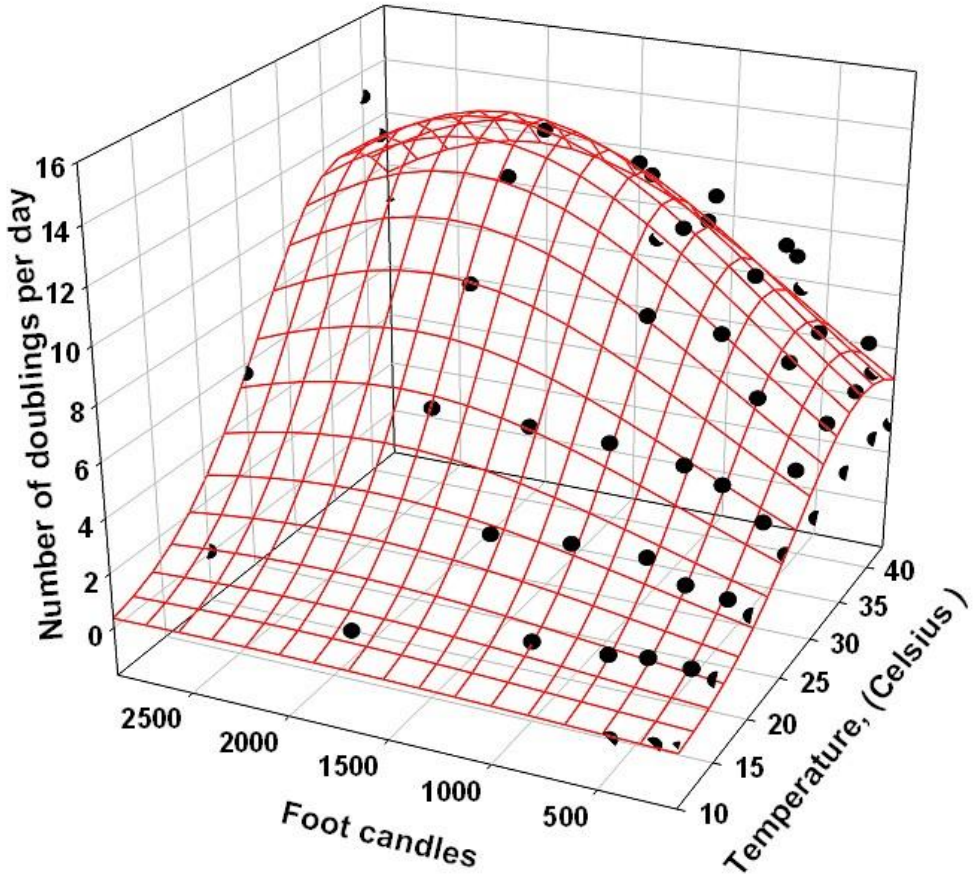

Figure 2.9: Specific growth rates for the synchronized cultures of *Chlorella pyrenoidosa*, measured at various light intensities and temperatures. (adapted from Sorokin & Krauss 1962)

For the algal culture system, particularly without temperature control (such as open culture system), temperature will be a major issue. Due to the low heat transfer efficiency from air to liquid, the algae culture temperature may be 10-15℃ lower than ambient temperatures. (Richmond, 2008) Besides, the light intensity increases fast in the morning and probably achieves an optimum level far before midday while the optimal temperature may not be achieved before midday. (Kajan et al., 1994; Singh et al., 2000; Vonshak et al., 2001) Therefore certain means such as adding a temperature controller are recommended to

increase the productivities of algae.

2.3.3 Nutrients

Nutrients required for cultures generally include macronutrients and micronutrients. Macronutrients are necessary elements that constitute the cell structure and usually required in large amounts, including nitrogen, phosphorus, carbon, calcium, magnesium, sulphur, etc. Micronutrients such as trace elements are required in relatively low concentrations (e.g. mg L^{-1}), usually involved as components of essential molecules (e.g. enzymes). The major considerations in nutrient recipe for microalgae culture are N, P and C.

Nitrogen is a quantitatively important element which contributes to the functional and structural proteins of algal cells. Under nitrogen sufficient conditions, microalgae usually have higher biomass productivities. In contrast, under nitrogen limiting conditions, lipid content in algal cells was observed to increase in many cases. (Reitan et al., 1994; Tornabene et al.,1983; Yamaberi et al., 1998) In practice, from the energetic point of view, lipids in algal cells are the most desirable components for biofuel production as the algal cells with higher lipid content and lower carbohydrates/proteins have a high calorific value and are capable of producing large quantities of oil via biomass conversion process. (Illman et al., 2000; Ginzburg, 1993; Scragg et al., 2002) However, there is a dilemma that high lipid contents usually are achieved by nitrogen limitation, while under this condition biomass productivities decrease. (Li et al., 2008a) Therefore, it is important to optimize the nitrogen concentration in culture medium to balance the production of high lipid cells with high biomass productivity, so that overall oil productivity can be increased. In cultures, the nitrogen source is commonly supplied in the form of nitrate (NO_3^-) or ammonia (NH_4^+) rather than directly by nitrogen gas. (Richmond, 1986) The effects of NO_3^- and NH_4^+ on algal cell growth and lipid accumulation vary for different algal species. For instance, in the study of *Neochloris oleoabundans*, sodium

nitrate is the better nitrogen source when compared with ammonium bicarbonate. (Li et al., 2008a) Lipid content of 38% was obtained from the culture with sodium nitrate as nitrogen source, higher than 19% obtained from the culture with ammonium bicarbonate, and the biomass productivity obtained with nitrate was more than double that obtained with ammonium bicarbonate. In another study (Giordano, 2001), the effects of NO_3^- and NH_4^+ on *Dunaliella salina* cells showed a different scenario. Specific growth rate was 50% higher with NH_4^+ than in NO_3^- medium. Besides, the cell size, protein content and carbon fixation of *D. salina* were enhanced by growth in the presence of NH_4^+.

Phosphorus is required for algal metabolism, and it is an essential element participating in the synthesis of DNA, RNA, ATP, cell membranes, etc. (Wang et al., 2008) In photosynthetic activities, large amounts of proteins which are synthesized by P-rich ribosomes are required. (Agren, 2004) Thereby, under phosphorous-limitation conditions, algal growth may be inhibited. In algal culture, phosphorus is mainly assimilated by algae in the form of $H_2PO_4^-$ and HPO_4^{2-}, (Martinez et al., 1999) however, these inorganic phosphates may react with some metal ions, forming precipitations which are not available for algae to uptake. (Yun et al., 1997) Therefore, in microalgae culture media, phosphorus elements are usually added in excess, such excess phosphorus (excepting the amount that precipitates) can be stored in algal polyphosphate bodies via ‘luxury uptake’ and used when external supply becomes insufficient, however, the amount of extra P should be very carefully controlled because most algae have low tolerance to excess phosphorus. (Richmond, 1986)

Carbon source is another macronutrient for microalgae growth. It is also one of the governing parameters for the activity of the Calvin cycle in photosynthesis. The effect of CO_2 on photosynthesis is very important, and this is discussed individually in Section 2.3.4.

2.3.4 Carbon dioxide

According to the basic fundamentals of photosynthesis outlined in section 2.2, the photosynthesis rate mainly depends on a) rates of NADPH and ATP synthesis, b) rate of RuBP synthesis, c) rate of carboxylation of RuBP (a function of e.g. carboxylation/photorespiration), and d) rate of CO_2 supply to the enzyme active sites. (Lawlor, 1987) These factors (especially NADPH/ATP synthesis) are either directly or indirectly regulated by light. At saturating light intensities, the rate of photosynthesis usually depends on the rate of CO_2 fixation, (Sukenik et al., 1987) which means the rate of RuBP carboxylation and CO_2 supply thereby become crucial for algal photosynthesis.

The enzyme Rubisco is bifunctional catalyzing the reaction of an oxygen molecule with RuBP at the same catalytic site as the carboxylation (reaction of CO_2 with RuBP). (Ghoshal & Goyal, 2001) The rate of carboxylation of RuBP in the presence of competitive inhibition by oxygenation (assuming a saturated amount of RuBP) can be expressed as Eq. 2.8, similar to the Monod equation, (Lawlor, 1987)

$$V_C = \frac{V_{C\max} \times P_{CO2}}{P_{CO2} + K_{CO2}(1 + P_{O2} / K_{O2})} \quad \text{Eq. 2.8}$$

where V_C is the carboxylation rate, V_{Cmax} is the maximum carboxylation rate, P_{CO2} and P_{O2} are the equilibrium partial pressures of CO_2 and O_2 in the chloroplast stroma, respectively. K_{CO2} and K_{O2} are the Michaelis constants (the substrate concentrations at which the reaction rate is half of V_{max}) for CO_2 and O_2 respectively.

In contrast, the oxygenation rate with saturating RuBP is

$$V_O = \frac{V_{O\max} \times P_{O2}}{P_{O2} + K_{O2}(1 + P_{CO2} / K_{CO2})}, \quad \text{Eq. 2.9}$$

where V_O and V_{Omax} represent the oxygenation rate and maximum oxygenation

rate respectively.

The competition between RuBP oxygenation (photorespiration) and carboxylation is usually described by the ratio α (Ogren, 1984), obtained by combining Eq. 2.8 and Eq. 2.9.

$$\alpha = \frac{V_O}{V_{CO2}} = \frac{V_{O\max} K_{CO2} P_{O2}}{V_{CO2\max} K_{O2} P_{CO2}} \quad \text{Eq. 2.10}$$

It indicates that ratio of RuBP photorespiration/carboxylation increases when P_{O2}/P_{CO2} becomes higher. Therefore, at high P_{O2}/P_{CO2}, the rate of photosynthesis is affected by the rate of photorespiration (the dark respiration could be negligible compared to photorespiration with high P_{O2}/P_{CO2} ratio) which consumes part of the RuBP regenerated. (Lawlor, 1987) When P_{O2}/P_{CO2} is very small, α approaches zero which means the photorespiration is negligible. In practice, it is well established that CO_2 enrichment of C3 plants (e.g. algae) can increase the photosynthetic rate and meanwhile reduce the photorespiration in the short term. (Bowes, 1991) For optimal yields in microalgal mass culture, it is necessary to minimize the photorespiration by the means of effective O_2 stripping and CO_2 enrichment. However, some researchers believe CO_2 enrichment may affect the RuBP regeneration and push the photosynthesis towards being RuBP-limited, in the long term. (Walker et al., 1986)

2.3.5 Salinity and pH

Salinity also plays an important role in regulating algal growth rate (Karsten et al, 1991). In response to an increased saline condition, microalgae enhance the capability of uptake osmoregulatory substances to counterbalance the saline circumstance. For certain algal species, commercial operators usually increase the salinity of culture medium to induce the osmoregulation process, under which conditions specific commercial products are synthesized in microalgae

cells. (Chen & Jiang, 2009) In elevated salinity conditions, glycerol was found to be more than 50% of the dry weight in *Dunaliella* (Richmond, 2008; Chen & Jiang, 2009). In the opposite case, glycerol was lost from algal cells when microalgae are cultured in a decreased salinity conditions (Gilmour et al, 1984). In the culture of either *Monodus subterraneus* or *Dunaliella* spp, lipid generation was observed to a slightly increase as the salinity increased (Borowitzka & Borowitzka, 1988). In terms of photosynthesis, it was severely inhibited if there is a large decrease or increase in salinity (Gilmour et al, 1984; Liska et al., 2004; Sudhir et al., 2004).

pH also should be considered during algal culture as one of the important factors determining productivity. In general, different algal species have various ranges of tolerance to pH. For example, the pH tolerance for most cyanobacteria ranges from 7 to 10, and inhibition of growth commonly occurs at pH between 10 and 11. (Richmond, 1986) Apart from directly acidic or alkaline inhibition caused by pH, the culture productivity also depends on the distribution of the carbon species (such as CO_2, HCO_3^-, CO_3^{2-}) and available carbon source, which are indirectly affected by pH. The photosynthetic uptake of CO_2 can lead to the increase in pH, but in response to increasing pH, CO_3^{2-} increases while HCO_3^- and CO_2 decrease, which inhibits the photosynthetic reaction and increases algal respiration. Therefore, an increase in pH in an algal culture usually indicates algal growth, whereas, over-increasing the pH beyond optimum range may jeopardize the culture. Additional CO_2 is commonly added to increase the algal productivities and also to reduce the pH value to an optimum range. (Nimer et al., 1994; Moheimani & Borowitzka, 2011; Richier et al., 2011)

2.4 Microalgae mass culture techniques and challenges

Commercial cultivation of microalgae has been studied and developed for more than 60 years. (Xu et al., 2009; Gilmour & Zimmerman, 2013) Factors which need to be considered for choosing the right culture system for algal production

include the biological properties of the alga, the type of targeted product, the cost of energy, land and labour, etc. (Borowitzka, 1992) Most reactors for algal culture can be generally divided into two types: open culture system and closed bioreactor. Some open algal ponds and closed bioreactors have already achieved economic feasibility for high value products. (Schenk et al., 2008) Regardless, open or closed systems have their own advantages and disadvantages, yet, a general trend can be found that most open systems were used in the past while more closed algal bioreactors have been employed recently. (Carvalho et al., 2006; Pulz, 2001)

2.4.1 Open culture systems

The open culture systems mainly include circular ponds, raceway ponds and shallow ponds. (Xu et al., 2009) Among them, raceway ponds are a relatively economical and simple culture system commonly used in Israel, USA, China and many other countries. (Xu et al., 2009) The raceway pond consists of a closed circulating loop channel typically less than 0.3m in depth (Jimenez et al., 2003) with paddlewheels. The algal cells are supposed to be suspended and circulated throughout the raceway channels by the paddlewheels. The pond is illuminated only by sunlight. A specially designed CO_2 sparging system has been reported recently that can be used in raceway ponds to further enhance the CO_2 absorption by algae. (Su et al., 2008) Usually, it takes 6-8 weeks for the culture to achieve maturity, and the productivity is typically about 25 g m^{-2} d^{-1}. (Chaumont, 1993 & Richmond et al., 1990)

Open ponds are usually used for large-scale economical production. They directly utilize the natural light without any artificial lighting and have a relatively lower building and operating costs compared to closed culture systems. (Borowitzka, 1999) However, open culture systems also have many disadvantages which more or less drive the development of the closed systems. First of all, because the open ponds are directly contacted to atmosphere, water in

the culture medium is significantly lost by evaporation at a rate similar to terrestrial plants, and contamination by other bacteria or unwanted species are more likely to occur than in closed systems. (Schenk et al., 2008) Additionally, only a small number of species can be successfully monocultured in open ponds by maintaining an extreme culture condition, such as high salinity (for *Dunaliella*), high alkalinity (for *Spirulina*) and high nutrition (for *Chlorella*), etc. (Lee, 1986) Second, the major CO_2 source is atmospheric which only contains 0.03-0.06% of CO_2. Such insufficient CO_2 supply may slow down the algal growth due to mass transfer limitation. (Chelf et al., 1993) Even additional CO_2 supplied from sparging systems to these large ponds can not efficiently increase algal growth and usually is uneconomical on a large scale. (Borowitzka, 1999) Thirdly, due to the open pond depth, they are always designed to be shallow to allow a good lighting distribution, a much larger land area is required compared to the same volume of closed system, (Borowitzka, 1999) which increases the capital cost and also restricts the location of the open pond, it can be only located in unproductive or waste land areas. Furthermore, it is difficult to control the culture conditions and the productivity, mainly due to weather, thus less biomass can be achieved than theoretical estimation. Compared with closed cultures, open ponds have a lower productivity. Therefore, closed culture systems have attracted more attention by many researchers rather than open ponds.

2.4.2 Closed bioreactors

Closed systems are required for future advances in microalgae culture, having a better culture condition control than open ponds so that any specific algal species of interest can be cultivated in a closed reactor (photobioreactor) with a promise of higher productivity. (Carvalho et al., 2006; Ugwu et al., 2008) There are many types of photobioreactors in use, manly including tubular reactors, flat-plate reactors, bubble column/airlift reactors etc. (Figure 2.10)

Figure 2.10: (left) the tubular bioreactor; (middle) the flat-plate bioreactors; (right) the airlift bioreactor.

The tubular photobioreactor is usually used for outdoor mass culture. (Ugwu et al., 2008; Molina et al., 2001) It consists of transparent tubes which can be arranged vertically/horizontally, coiled or looped. (Aci én Fernandez et al., 2001; Hall et al., 2003; S ánchez Miron et al., 1999) The algal medium is circulated through the tubes by a pump or airlift device to ensure even distribution of nutrients, good cell suspension, good gas exchange and equal illumination. (Xu et al., 2009; S ánchez Miron et al., 2000) The major drawback of the tubular reactor is it can not be used for quite large scale culture. Scaling up the tubular bioreactor can only be hypothetically achieved by increasing the tube diameter or length. However, the diameter of tubes is usually limited to less than 0.2 m to prevent a decrease in growth rate associated with the decrease in illumination surface/volume ratio caused by increasing tube diameter. (Jimenez et al., 2003) There are also problems with increasing the tube length. Although the photosynthesis rate could be increased due to the longer time for microalgae exposure to light and nutrients, dissolved O_2 concentration will also increase,

which may result in inhibition of photosynthesis. (Ogbonna and Tanaka, 1997)

Flat plate photobioreactors are also made of transparent material. The tilted flat plate photobioreactor is inclined at an optimal angle for maximal exposure of the culture to sunlight in order to achieve a high culture density. (Carvalho et al., 2006) However, in practice the horizontal and vertical designs are more commonly used for algal culture than inclined design because the higher capital cost of tilt configuration outweighs the gains made by the increase in productivity. (Sierra et al., 2008) Generally, these photobioreactors are suitable for either indoor or outdoor microalgal culture because they have large illumination surface area and low O_2 accumulation plus they are inexpensive and easy to build. (Xu et al., 2009) However, there are also some limitations, including some level of algal wall adhesion, inconvenience of sterilization, difficulties in culture temperature control, etc. (Pulz et al., 1995; Sierra et al., 2008; Ugwu et al., 2008)

Bubble columns and airlift bioreactors are simple, low-cost and compact culture devices, practicable for microalgae mass culture. (Sánchez Miron et al., 2000) The major feature of these bioreactors is additional CO_2, introduced in the form of bubbles generated by bubble columns and airlift device. Airlift photobioreactors are usually more favorable than bubble column reactors. In some studies, microalgae grown in airlift bioreactor showed 33-50% higher growth rates than in bubble columns, at the same aeration rate. (Merchuk et al., 1998; Xu et al., 2002) This is probably due to the airlift device, the flow pattern being more homogeneous which circularly moves algal cells from dark zone to light zone and provides a better performance on cell suspension. In the bubble column system, cell flow patterns are more random which may results in cell sedimentation and a long time residence of cells in low or high light intensities without circulation. (Xu et al., 2002; Kaewpintong et al, 2007)

Compared with open ponds, closed systems are commonly applied for

monoculture of microalgae, having several advantages such as lower contamination, higher illumination efficiency, greater biomass productivity, better temperature control etc. (Chrismadha and Borowitzka, 1994) However, some challenges still remain in closed systems, including the high energy cost associated with mixing devices, (Wijffels, 2008) algal cell adhesion to the wall, capital cost and scale up, etc.

Furthermore, there are two major operational modes for closed bioreactors, batch and continuous system. In batch culture, the algae are inoculated into the bioreactor and then go through different growth phases (lag, exponential, stationary). At the end, the products are harvested and the reactor needs to be cleaned and sterilized for another batch. In continuous culture, a culture medium is continuously fed into the reactor and meanwhile the product is drawn continuously from the reactor at the same flow rate. The advantages and disadvantages for batch and continuous culture are summarized in Table 2.2. (Doran, 1995; Williams, 2002) Compared with continuous culture, batch culture requires high labour cost for reactor filling, emptying, cleaning and sterilizing etc. but less investment cost in control and automation equipment. In contrast, continuous system reduces labour expense but increases investment cost, both due to automation. In terms of productivity, the algae in continuous culture system experience a constant and steady supply of limiting substrates/nutrients, consequently acheiveing a higher productivity than in the batch culture. Moreover, continous systems usually do not need to be shut down and cleaned as regularly as a batch reactor and therefore have a shorter ‘turn-around’ time. The major concern for industrial continuous culture system is contamination, because the promised continuous production for months may fail due to the infection, while batch culture has less risk of contamination or cell mutation due to a relatively brief growth period and less contact to the environment which may bring the infection (e.g. medium replenishment for continuous system).

Table 2.2: Comparsions between batch system and continuous system

Mode of operation	Advantages	Disadvantages
Batch	More flexible with varing product/biological system Lower investment cost Less risk of contamination or strain mutation	Much idle time (sterilization, cleaning, growth of inoculum etc.) Higher labor cost Lower productivity
Continuous	Shoter 'turn-around' time Less labor cost Higher productivity	Inflexible High costs in control and automation Risk of infection

2.4.3 Major technical concerns for microalgae culture

As mentioned previously, lack of culture control for the specific microalgae species of interest has been considered as a major unsolved problem in open culture systems, which has resulted in more focus on biomass production from closed photobioreactors. Photobioreactors usually promise higher biomass productivities, compared with open ponds. Their better control of culture conditions prevents desired algal strains from becoming contaminated and improves biofuel production, however, there also some technical concerns associated with photobioreactors, which are discussed below.

a) Illumination

The effects of illumination on microalgae growth have been aforementioned, either lower or higher light intensity can cause a reduction of algal productivities by light attenuation or light inhibition. In photobioreactors, high density of culture is easy to achieve along with the problem of algal mutual shading which reduces the available light intensity for the algal cells below the top layer of culture. Such maldistribution of light will lead to uneven algal growth and further affect the final productivity. Moreover, photoinhibiton occurs when the light flux exceeds a saturation point. To deal with these issues, increasing the surface to volume ratio of the bioreactor and reducing the light path is one way to maximize light absorbance and minimize light attenuation. (Richmond et al, 2003) An optimal light-dark cycle period can be used to maximize the photosynthetic efficiencies. (Richmond et al, 2003) For instance, in continuous light, the cells in the illuminated region are shifted to the dark area while those former ‘dark’ cells are in turn to be illuminated. This circulation pattern, so called light-dark cycle, is usually introduced by gas bubbling, and can be optimized by the proper design of the frequency of mixing (circulation time) and the geometry of photobioreactor (especially Riser/Down ratio). A comprehensive airlift bioreactor design is described in detail in Chisti (1989). In most cases, artificial light is used for either internal or external illumination. (Suh & Lee, 2003) However, introducing artificial light into bioreactor also means increasing the overall operational cost. Therefore, only relatively high productivity of desired products can offset the costs of additional lighting. In this case, combination of natural light and artificial light tends to be a more sensible choice. (Lehr & Posten, 2009)

b) Mixing

Mixing, usually combined with lighting, is necessary for good performance of a photobioreactor. Under poor mixing conditions, the distribution of radiance and

nutrients is uneven, plus algal cells settle easily and the sedimented cells are hard to resuspend again, hence the productivity of algal biomass is reduced. Increased mixing rate was demonstrated to result in a higher biomass yields, however, in a bioreactor with high mixing rates, large energy input is required, and the shear force caused by intense agitation may damage the algal cells. (Ugwu ey al., 2008) Thereby, a proper mixing partially decides the culture productivity. Usually, mixing in algal cultures is achieved by pumping, stirring and bubbling, etc. Pumping provides low mass transfer and high hydrodynamic stress, plus is always associated with high energy cost. (Jaouen et al, 1999; Carvalho et al., 2006) Stirring offers a good mixing efficiency; however, its energy cost and high hydrodynamic force also become problems. (Tredici, 2003) Compared with pumping or stirring, bubbling supplies a better gas transfer and mixing efficiency with a gentle hydrodynamic stress. (Richmond & Cheng, 2001)

c) CO_2 supply and O_2 accumulation

In practice, CO_2 is added into culture most commonly by bubbling CO_2 enriched air into porous diffusers, which promises a gas transfer efficiency of 13-20%. (Carvalho et al, 2006) Additional supply of CO_2 contributes many benefits to culture system. First of all, provision of CO_2 enhances algal metabolism, and on the other hand, it can act as a buffer solution to neutralize the increased pH caused by algal growth. Secondly, supply of CO_2 enhances the internal mixing of a bioreactor, helping to evenly distribute nutrients and the exposure time of algal cells to light. Furthermore, accumulation of O_2 in culture medium is toxic to microalgal cells and it is one of the major limiting factors for scale up of the bioreactor. (Ugwu ey al., 2008) Introducing CO_2 into culture also facilitates stripping of accumulated oxygen and hence protects algal cells from toxicity. (Pulz, 2001) However, due to low interfacial surface area between gas bubbles and culture medium, the gas-liquid mass transfer is poor, which is associated with CO_2 loss to the atmosphere. Besides, additional CO_2 supply increases the

energy costs and it does not seem to be achievable to compensate for the extra energy costs with enhanced algal yields due to the low CO_2 mass transfer.

In conclusion, technical issues associated with light have been well studied for photobioreactors, with various solutions emanating (such as using an optimal mixing rate and light/dark ratio, combining artificial light with natural light, and increasing harvest frequency etc.). Bubbling seems to hold promise for proper mixing. However, techniques to solve CO_2 supply and O_2 accumulation problems are still at the 'bottle neck' of development. Therefore, design of a bioreactor with low energy cost and particularly high gas mass transfer for both CO_2 dissolution and O_2 removal tends to be a major consideration for cost-competitive microalgae culture. The knowledge of CO_2 supply for algal biomass culture including CO_2 mass transfer principles, CO_2-pH interactions and conventional CO_2 supply problems are described in detail in Section 2.5.

2.5 CO_2 supply for microalgal culture

It is well known that CO_2 supply is essential for algal growth, and improving CO_2 mass transfer for algal culture is often considered by many bioreactor designs, however, CO_2 supply systems for algal culture are still in the early stage of development. For most lab cultures, little concern is paid on improving CO_2 supply techniques while more consideration is focused on optimizing other operational parameters such as light, nutrients and light-dark circulation etc. That is mainly because conventional CO_2 supply technologies (e.g. continuously sparging a certain percentage of CO_2 gas into the culture) are believed to be sufficient for supporting lab scale cultures, plus the problems existing in the conventional CO_2 supply may not necessarily be crucial to the good growth of lab cultures and therefore are usually neglected. However for industrial scale culture, especially with the view to using microalgal culture for CO_2 sequestration, problems with the conventional CO_2 supply techniques (Section 2.5.3) may become one of the major reasons leading to failure. To identify the

problems existing in conventional CO_2 dosing and improve the technique for industrial cultures, the knowledge behind CO_2 supply needs to be understood.

2.5.1 CO_2 gas-liquid mass transfer

The fundamental principle behind CO_2 supply is the mass transfer of CO_2 from the gas-phase into the culture medium, and subsequently to the cell-liquid interface of the suspended algae. The mass transfer of the dissolved O_2 produced by the algae is removed from liquid-phase to gas-phase via the same mass transfer process.

Two-film theory is the well known theory widely applied to explain the mass transfer process, which can be illustrated as Figure 2.11. In two-film theory (Whitman, 1962), the region between gas-phase and liquid-phase consists of a gas film, a liquid film and a gas-liquid interface. The resistance to mass transfer in each phase is assumed to lie in these two thin films, while the interface itself is assumed to offer no resistance to mass transfer. The interfacial concentrations should be determined by the equilibrium relationship according to Henry's law: at equilibrium the partial pressure of the species in the liquid phase will be proportional to the partial pressure of that species in the gas phase, $C_{Gi} = H' \times C_{Li}$ (H' is a dimensionless form of the Henry's law coefficient). (Biotol, 1992) Chisti (1989) also noted that the mass transfer through each film is assumed to be solely molecular diffusion, and that the mass flux of the diffusing species (e.g. CO_2 and O_2) is related to the concentration gradient in the films. For instance, the mass transfers of CO_2 from gas-phase to interface and from interface to liquid-phase are considered to be driven by the concentration gradients which are (C_G - C_{Gi}) and (C_{Li}-C_L), respectively. Since the gas phase diffusivities are greater than those in liquids, so that the resistances to mass transfer are usually assumed to be negligible, essentially all the resistance is localized in the liquid film. In other words, the mass transfer in liquid film dominates the overall mass transfer. The overall mass transfer rate is then given by:

$$\frac{dC_L}{dt} = K_L a(C^* - C_L) \quad \text{Eq. 2.11}$$

where dC_L/dt is the instant mass transfer rate, C* is the equilibrium concentration and K_La is the so-called volumetric or overall mass transfer coefficient.

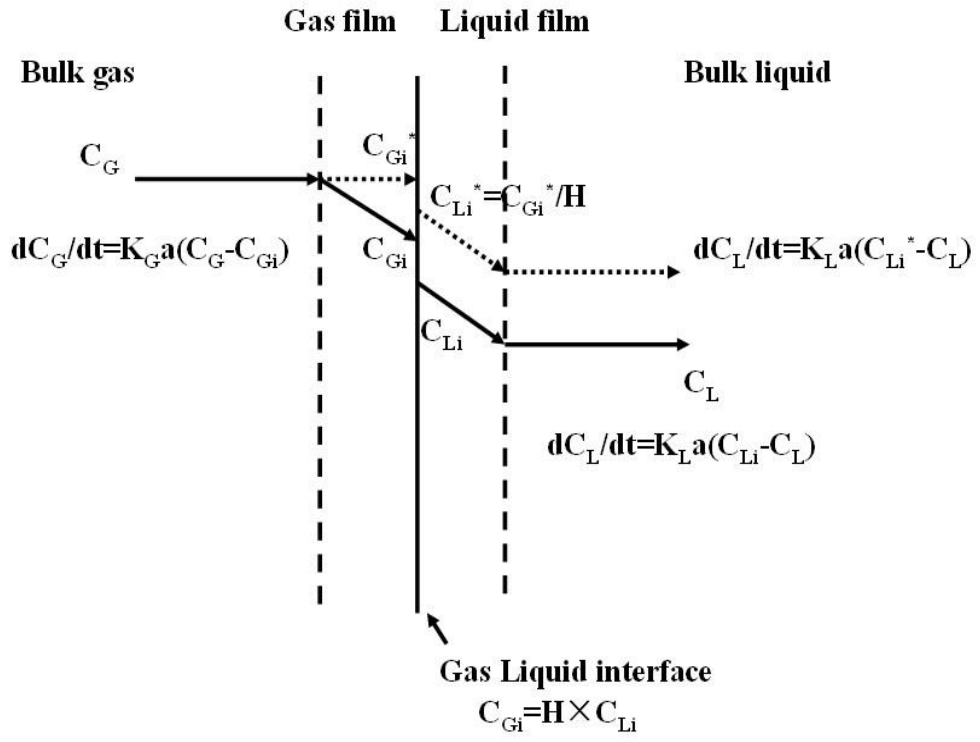

Figure 2.11: Gas-liquid mass transfer explained by two-film theory (adapted from Chisti, 1989)

Eq. 2.11 is one of the basic equations in describing mass transfer, which is widely applied in bioprocess engineering and has proven to be of great practical value. (Biotol, 1992) From the equation, the equilibrium concentration C* and mass transfer coefficient K_La are the key items governing the mass transfer rate. Take CO_2 gas-liquid mass transfer as an example, C* is proportional to the

CO_2% in the gas supply, according to Henry's law $C_{Gi} = H' \times C_{Li}$*. This explains why dosing gas of a higher CO_2% is more effective for mass transfer than e.g. CO_2 uptake from atmosphere, due to a greater driving force (C^*-C_L). For K_La, K_L mainly depends on the gas-liquid properties (e.g. density, viscosity, diffusivity and temperature etc.), and therefore is usually considered as a constant for most circumstances. The interfacial area 'a' is mainly influenced by bubble diameter (d_B) and gas hold-up (ε), which can be expressed by:

$$a = \frac{6\varepsilon}{d_B(1-\varepsilon)} \quad \text{Eq. 2.12}$$

When the ε is much less than 1, Eq. 2.8 can then be simplified into Eq. 2.9.

$$a = \frac{6\varepsilon}{d_B} \quad \text{Eq. 2.13}$$

In summary, bubble size, gas hold up and CO_2% in gas-phase turn out to be the governing parameters for mass transfer rate.

2.5.2 Relation between CO_2 dissolution and pH

When CO_2 is dissolved into water or medium, the aqueous CO_2 is in equilibrium with HCO_3^- and CO_3^-, which can be described by the following chemical reactions. (Livansky, 1990; Rubio et al., 1999)

$$H_2O \xleftrightarrow{K_w} H^+ + OH^- \quad (1)$$

$$CO_{2aq} + H_2O \xleftrightarrow{K_1} H_2CO_3 \longleftrightarrow HCO_3^- + H^+ \quad (2)$$

$$HCO_3^- \xleftrightarrow{K_2} CO_3^{2-} + H^+ \quad (3)$$

Where the relevant equilibrium constants are:

$$K_w = [OH^-][H^+] = 10^{-14}$$

$$K_1 = \frac{[HCO_3^-][H^+]}{[CO_{2aq}]} = 10^{-6.381}$$

$$K_2 = \frac{[CO_3^{2-}][H^+]}{[HCO_3^-]} = 10^{-10.377}$$

Therefore, the change in pH is highly related to the dissolving or depletion of the CO_{2aq}. Simply according to chemical reaction kinetics, when CO_2 is dissolving into the liquid, the previous equilibrium is broken and reactions (2) and (3) will move forward, producing more H^+ until achieving a new equilibrium. This explains the decrease in pH when dosing CO_2 into water. Similarly, when microalgae consume CO_2 from the medium for their growth, the depletion of CO_2 will cause the backward movement of reactions (2) and (3), which subsequently leads to a reduction of H^+ and an increase in pH. In microalgal mass culture, the rise in pH usually indicates the growth of algae and also the depletion of CO_2. The pH also affects many processes associated with algal metabolism and must be carefully controlled. (Borowitzka and Borowitzka, 1988) Measures, such as bubbling CO_2, adding $NaHCO_3$ and adding base etc., will then be taken to maintain an optimal pH range for algal growth and to prevent CO_2 limitation.

2.5.3 Conventional CO_2 supply

Conventionally, CO_2 will be dosed continuously to provide a constant supply of CO_2 and also to steadily mix the culture. However, this continuous supply of CO_2 bubbling through the culture also raises its own problems.

2.5.3.1 pH changes and the use of the buffer

The H^+ produced when CO_2 dissolves into microalgae cultures can acidify the

medium. Although Behrens (2005) notes that nitrate consumption by the algae results in an alkalisation of the medium, and so may partially counter this pH change, continued dosing of CO_2 can still produce very acidic conditions. As observed by Kong et al. (2010), continued dosing of CO_2 into the algae culture will inhibit growth and can ultimately kill the microalgae.

To control the pH of the culture, biologically benign buffers such as EPPS (4-(2-hydroxyethyl)-1-piperazinepropanesulfonic acid) may be added to the culture, although these buffers can be expensive. (Shi et al., 2009) Shi et al. (2009) note that this method of pH control has the advantage of continuously readjusting the concentration of dissolved CO_2 to a nearly constant value when it is depleted by the growing culture, but the addition of such buffers appears to affect the availability of trace metals which are required for algal growth. Scragg (1991) describes how the pH is often maintained in the desired range using controlled pulse modulated feeding of acid or base when the pH is registered to have exceeded or dropped below a set point. However, due to continually changing concentrations of inorganic carbon which are affected by the growth of the microalgae, both the pH and the partial pressure of CO_2 in a growing batch culture may be hard to control. (Shi et al, 2009) Using an automatic feedback loop to control the pH also requires energy. Therefore, pH control can be costly and hard to implement, especially for large scale industrial batch cultivation. In continuous culture system, since the concentration of algae is maintained at a steady level which means the CO_2 uptake rate is constant, pH can be maintained at a suitable level by setting the CO_2 bubbling condition to provide a CO_2 mass transfer rate equal to the CO_2 uptake rate, without applying additional buffers or pH regulator systems.

2.5.3.2 Low mass transfer and high flow rate

Another problem with CO_2 being dosed into microalgae cultures is that conventionally the bubbles used are fairly large. As Zimmerman et al. (2008)

discussed, bubbling gas through a nozzle or diffuser, can result in bubbles much larger than the aperture from where they were formed due to the buoyant force needed to detach the bubbles. They also mention the channeling effect in a nozzle bank which can occur as the gas follows the path of least resistance and so enlarge the largest bubble rather than passing through other pores and the problem of irregularly dispersed bubbles quickly coalescing after formation resulting in larger bubbles. Such bubbles will reduce the interfacial area between bubbles and the liquid in contrast with much smaller microbubbles, and will reduce the overall mass transfer for both CO_2 dissolution and O_2 stripping. Zimmerman et al. (2008)

To counteract the resulting low mass transfer, large flow rates of CO_2 enriched gas are often continuously bubbled into the cultures. While the mixing effect on the culture is beneficial for ensuring the even distribution of light and nutrients, the intense turbulence produced by large flow rate can damage the algal cells within the culture and reduce the productivity. (Molina et al., 2001) A further disadvantage of using high flow rate, especially with low mass transfer, is that most of the gas bubbled into the culture will pass through and be wasted. Carvalho and Malcata (2001) agree that when CO_2 is bubbled into algal cultures, the mass transfer is not particularly effective and considerable gas is wasted, adding to operational costs. Even with some high mass transfer dosing techniques (e.g. Dissolved Air Flotation systems), hypothetically, continuous dosing is still not a wise option, because when the concentration of dissolved CO_2 has reached an equilibrium value, the gas-liquid mass transfer process stops. Any additional input beyond this point would not increase the total amount of dissolved CO_2, but cost energy and waste CO_2.

2.5.3.3 Energy requirements and cost

Bubbling CO_2 gas continuously through microalgal cultures is both costly and energy intensive. Batan et al. (2010) considered the energy requirement of

growing *Nannochloropsis salina* in a bioreactor sparged with 2% CO_2 gas. From their study, for each kg of biomass produced, 0.46 kWh of electricity was consumed pumping and sparging the CO_2 into the culture. Along with the capital costs of building bioreactors, Zimmerman et al. (2011a) states the energy required to operate bioreactors is the biggest cost when producing microalgae at a large scale.

2.6 Microbubble dosing for microalgal culture

Since one of the major problems for conventional CO_2 supply is the relatively low mass transfer and poor mixing caused by large bubble size, various attempts, e.g. using paddle wheel, propeller and the combination of pumps and gravity flow etc., have been made to improve the mass transfer for CO_2 dissolution and mixing. (Carvalho et al., 2006; Ugwu et al., 2008) However, the adoption of additional devices for microalgal culture will mean not only increasing the operational cost (e.g. extra electricity cost) but also complicating the operational processes (e.g. the construction of additional devices and their maintenance), especially for industrial cultures. One of the straight forward ideas is to reduce the bubble size for CO_2 dosing, for instance microbubble dosing. In terms of microbubbles, there is no clear definition to give a precise range of bubble size from literature. Usually, the bubbles with a few hundered micrometers in diameter can be called as microbubbles. In this thesis, the bubbles with an average size less than 500 μm in diameter were defined as microbubbles, while the bubbles between 500 μm and 1 mm were called fine bubbles.

There are many methods for microbubble generation, their advantages and disadvantages are discussed in this subsection. An innovative microbubble generation method patented by Zimmerman et al., (2008) is emphasized and described here. General knowledge on bubble formation is also included to help in the understanding of Zimmerman's microbubble generation technology.

2.6.1 Basic principle for bubble formation

The most common way to supply gases of interest to liquid is by using bubble diffusers. The properties of bubbles generated such as bubble size, rising velocity, bubble distribution, etc directly affect the gas mass transfer rate. Understanding the bubble formation principles helps to modify or improve the bubble generation system and thereby increase the mass transfer rate.

When a bubble is formed from a single pore, it does not detach immediately but keeps growing due to the wetting force of the liquid attaching the bubble to the aperture edges which acts as an 'anchor'. (Zimmerman et al, 2008) Only when the volume of bubble increases to a certain level resulting in a sufficient buoyant force exceeding such 'anchor' restraint, will the bubble break off from the aperture. In the case of some hydrophobic material diffusers, a second anchoring force can be formed by the gas phase of the bubble, which increases the requirement for buoyant force. (Zimmerman et al, 2008) Therefore, bubble size is usually much bigger than the pore size by about an order of magnitude, even for the case of micro-porous diffuser. (Zimmerman et al, 2009)

The terminal rising velocity (assuming this can be achieved instantly) of a single bubble can be expressed by Eq. 2.16 which is obtained when the buoyancy force 'F_B' (Eq. 2.14) balancing the gravitational force and friction force 'f' (Eq. 2.15**,** Stoke's law)

$$F_B = \frac{4}{3}\pi r^3(\rho_L - \rho_G)g \quad \text{Eq. 2.14}$$

$$f = 6\pi\mu r v_r \quad \text{Eq. 2.15}$$

$$v_r = \frac{2(\rho_L - \rho_G)gr^2}{9\mu} \quad \text{Eq. 2.16}$$

where v_r is the terminal rising velocity for a single bubble with the diameter of r,

μ is the viscosity of liquid, ($\rho_L - \rho_G$) is the density difference between liquid and gas. (Chisti 1989; Zimmerman et al, 2008) From Eq. 2.16, it is clear that the rising velocity of smaller bubbles is significantly lower than for bigger bubbles, hence the residence time of the former is longer than the latter, for the same height of liquid.

2.6.2 Factors that affect bubble size

The bubble formation process depends on many parameters such as gravity, drag forces, buoyancy, and viscous forces etc. which are governed by flowrate, gas/liquid properties, orifice dimensions and material of construction. (Kulkarni & Joshi, 2005)

Liquid viscosity is a controversial parameter in the case of bubble formation. Different researchers made different observations with regard to the effects of viscosity on bubble sizes. Siemes and Kaufmann (1956) proposed an opinion on the relationship between bubble size and liquid viscosity. When liquid viscosity is low, bubble sizes are independent of liquid viscosity. Among high viscosities, higher viscosity leads to an increase in bubble size, however such observation is based on a low flowrate. (Siemes & Kaufmann, 1956) Some claims exist that the bubble size is not influenced by liquid viscosity, (Kumar & Kuloor, 1970; Benzing & Mayers, 1995) while the contradicting viewpoint that bubble size depends on liquid viscosity and increases with it have also been reported. (Khurana & Kumar, 1969; Schäfer et al., 2002; Mouza et al., 2005)

Surface tension forces acting on a bubble play an impotent role on bubble growth. During bubble nucleation process, the bubble surface close to the aperture is dragged backward by liquid and is pushed toward the aperture edges. The liquid surface tension then adheres the bubble to the orifice edge, against bubble detachment. (Zimmerman et al, 2008) Such surface tension force changes continuously along with its contact angle with the orifice and finally become

static as the contact angle reaches a constant. (Kulkarni & Joshi, 2005) During the time that the bubble is anchored by surface tension, its surface in the front portion is stretched by continuous gas supply. Eventually the volume increases to a certain level so that buoyancy can overcome the final static surface tension, and the bubble is detached from the orifice. Therefore, the delay of detaching time caused by surface tension leads to the increase in bubble size. Additionally, surface tension is also related to the diameter of aperture, it increases along with the size of aperture and consequently affects bubble size. (Gaddis & Vogelpohl, 1986; Davidson & Schüler, 1997)

Liquid and gas density also affect the bubble size to some extent. (Davidson & Schüler, 1997) For liquid density, increasing it will lead to an increase in the static head above the bubble and subsequently against the increase in bubble volume during bubble formation process. Therefore, increase in liquid density results in decrease in bubble size. Khurana & Kumar (1969) have observed the same results under the conditions of low flowrate and viscosity, however, they also observed that bubble size is independent of liquid density when the flowrate is large and the viscosity and orifice diameter are small. As regard to gas density, the increase in gas density can result in the reduction of the difference between the densities of liquid and gas phase, which subsequently leads to the decrease in surface tension and bubble size. (Kulkarni & Joshi, 2005) Some studies observed that the bubble size is smaller in the case of higher gas density because surface tension force is dominant and the detachment is delayed, however, such scenario only observed when the aperture diameter is larger; for smaller aperture, bubble size seems to be independent of gas density since the drag force becomes dominant instead of surface tension. (Idogawa et al., 1987; Wilkinson, 1991)

Orifice configuration also is involved in effecting the bubble formation size. The orifice diameter is usually made as small as possible to achieve fine bubbles. However, in practice this idea does not always work and the real bubble size

could be an order of magnitude greater than the orifice diameter, (Zimmerman et al, 2008). Some researchers reported that the effect of smaller orifice on bubble size is negligible compared to large orifice for which the bubble volume increases with the flowrate. (Tsuge & Hibino, 1983) In contrast, an opposite point was observed in the experiments on the effect of orifice diameter on bubble size in water. (Kulkarni & Joshi, 2005) For the smaller orifice, bubble size is affected significantly by flowrate and higher flowrate leads to larger bubble generation, while for larger orifice, the effect of flowrate on bubble size tends to be weaker. Apart from orifice diameter, the volume of orifice chamber also has some effect on bubble size. For a small chamber the gas flow into chamber is almost equal to the gas flow into bubble, but in terms of a large chamber, the damped pressure fluctuations inside results in an unequal flow between inlet gas volume and bubble volume. (Kulkarni & Joshi, 2005)

2.6.3 Microbubble generation

2.6.3.1 Conventional microbubble generation techniques

Typically, the best known and developed techniques for microbubble generation include electroflotation, dissolved air flotation, electrostatic spraying etc. In electroflotation method, by providing a current to the solution being treated, water molecule is split into molecular H_2 and molecular O_2 which are adsorbed by cathode and anode, separately, in the form of fine bubbles, of which the diameter is reported to achieve 22-50 μm. (Ketkar et al., 1991) Electroflotation is commonly used for the purpose of separating fine particles (such as mineral particles) from solutions and, sometimes, separating oil from oil-water emulsions. (Ahmed & Jameson, 1985; Hosny, 1992; Murugananthan et al., 2004) For dissolved air flotation (DAF) method, which is most commonly used for potable water treatment, the feed stream saturated with air under a relatively high pressure (3 – 6 atm) is released to atmospheric pressure through needle valves. (Zabel, 1985; Burns et al, 1997; Rodrigues & Rubio, 2007) Due to the sudden

reduction in pressure, the gas transfers out of liquid and forms bubbles which rise upwards to the surface of liquid. (Burns et al, 1997) The bubbles generated by this method usually range from 10 to 120 μm, with a mean size of 40 μm. (Zabel, 1985; Edzwald et al., 1992; Rodrigues & Rubio, 2007) With regard to electrostatic spraying, it is a relatively new method for microbubble generation. In this method, a high-voltage electric field is induced to the bubble generation system and the capillary is charged and acts as an electrode. Once gas flows through such a capillary, the electrical force helps to break off the bubble attached at the capillary tip and allow it to flow into the solution. (Tsouris et al., 1995) Bubbles generated in this method have an average size of 30 μm, ranging from 10 to 180 μm. (Shin et al., 1997)

Among these three methods, dissolved air flotation produced the largest mean bubble size but the narrowest distribution, while electroflotation method generated the smallest average bubble size and electrostatic spraying gives the widest bubble size distribution. (Kulkarni & Joshi, 2005) When comparing these three methods in terms of surface/power/unit time, dissolved air flotation seems to be the most efficient way to produce microbubbles. (Kulkarni & Joshi, 2005) In practice, these methods have a common disadvantage impeding their further development, which is high energy consumption. For DAF system, in order to increase the flotation efficiency by reducing bubble size, the saturating pressure should be maintained at a relatively high level, 3-6 atm. (Rijk & Blandon, 1994; Féris & Rubio, 1999; Rodrigues & Rubio, 2007) The power consumption in DAF accounts for approximately half of the total operating energy costs. (Féris & Rubio, 1999) For electroflotation and electrostatic spraying method, their dependence on high electricity energy consumption has limited their application.

2.6.3.2 Low power microfludic microbubble generation

Conventionally, a porous material diffuser with a large number of parallel micro apertures is simply introduced into an aeration system and expected to produce

simultaneously a great amount of fine bubbles. However, in real practice, instead of many desirable parallel fine bubbles, large bubbles are produced by such a porous diffuser, which is mainly because of a) the surface tension force inhibiting bubble detachment and consequently making the bubble size around an order of magnitude greater than aperture size and b) the instability of parallel percolation which can be explained by Young-Laplace law: (Zimmerman et al, 2008)

$$\Delta p = \frac{2\sigma}{r} \qquad \text{Eq. 2.17}$$

where ΔP is the pressure difference between inside and outside of a bubble, σ is surface tension and r is curvature radius of bubble. When bubble is initially formed at an orifice, its curvature radius is infinitely large but decreases as it tends to form a spherical shape. The pressure required for bubble growth therefore increases. When the bubble achieves a hemispherical shape, the situation begins to reverse. The curvature radius increases as the bubble volume increases, consequently, the pressure difference decreases, which makes the further growth easier. Air is more likely to flow into this bubble because a lower pressure difference needs to be overcome as compared with other apertures. Therefore, this particular bubble grows faster while other bubbles may cease to grow. (Zimmerman et al, 2009)

Based on the idea of breaking off the bubble when it is still a hemispherical cap, a innovative microbubble generation method has been developed by Zimmerman et al. (2008) The key idea of this method is to introduce a fluidic oscillator to a conventional porous diffuser microbubble generation system, limiting the bubble growth time by periodically switching the gas supply into apertures by oscillation. The bubble stops growing and is removed from the aperture at the end of each oscillation half-period, and the next bubble has to start anew in the next period. (Zimmerman et al, 2009) The comparison of microbubble generation by normal diffuser and by oscillator along with the same diffuser is shown in Figure 2.12.

The bubbles generated from the same diffuser under the same injection flow rate are found to be smaller and more uniformly distributed with the presence of fluidic oscillator. While bubble coalescence is taking place when produced without fluidic oscillator, which leads to bigger bubble sizes. The bubble size was measured by Brittle et al. (2014) using the high speed camera under a constant bubbling flow rate. The results showed a mean bubble diameter (d_{32}) about 388 μm for the bubbles generated from the ceramic diffuser engaged with a fluidic oscillator, and 719 μm for the bubbles directly created from the same ceramic diffuser. The bubble size distribution for each condition is shown in Appendix 1.

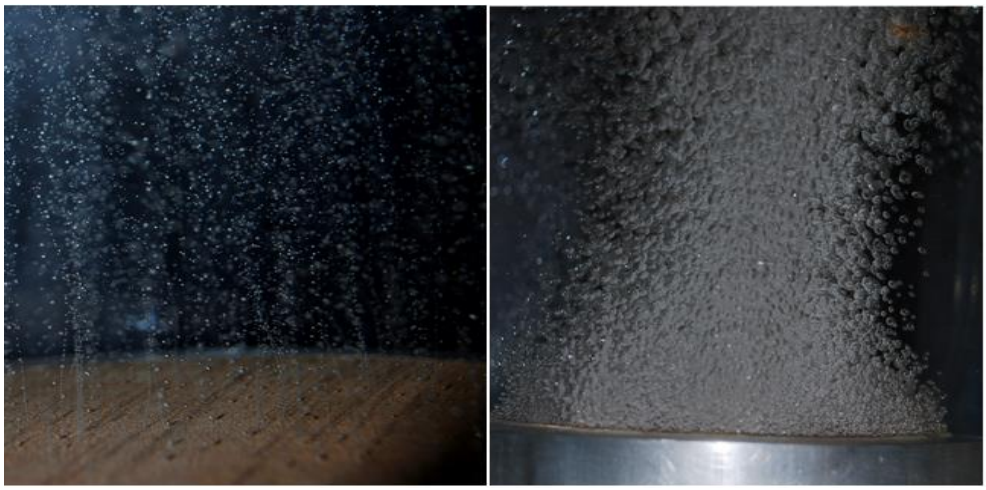

Figure 2.12 Left: with fluidic oscillator microbubble generation; Right: without fluidic oscillator bubble generation from the same ceramic diffuser

2.6.4 Benefits of microbubble dosing for algal culture by using fluidic oscillator

Additional CO_2 supply for the purpose of enhancing algal biomass productivity has been widely recognized and used in practice. However, only about 13-20% of injected CO_2 molecules are utilized by microalgae with most of them released

into atmosphere. (Carvalho et al, 2006) Such low efficiency of gas mass transfer is determined by the bubble sizes. Actually, not only mass transfer but also momentum and heat transfer are influenced by the interfacial area to volume ratio of bubbles. By using microbubbles instead of big bubbles generated from conventional aeration devices, a relatively higher surface to volume ratio can be achieved, resulting in desirable gas mass transfer, heat transfer and momentum transfer.

As expressed by Eq. 2.11 (Section 2.5.1), the overall inter-phase mass transfer flux is proportional to the interfacial area which is highly related to the bubble size (Eq. 2.13 in Section 2.5.1). Based on the same volumetric flow rate, the overall interfacial area (surface area) of small bubbles (diameter of r) is greater than the one of big bubbles (diameter of R) by the ratio of R/r. For instance, the total interfacial surface area of microbubbles with 10 μm diameter could be at least a hundred times greater than the one of normal bubbles with 1 mm diameter, under the same inlet volume. Apart from higher gas mass transfer due to the greater surface to volume ratio, microbubbles also have a longer residence time in liquid compared to normal big bubbles, which helps to further enhance the mass transfer rate. The rising velocity of microbubbles can be described by Stokes law (Eq. 2.16 in section 2.6.1). For instance, the microbubbles with 10 μm diameter are estimated to have a 10000 times longer residence time than for normal 1 mm-bubbles. In terms of momentum transfer (highly related to mixing efficiency), someone may argue that microbubbles have a lower momentum transfer compared to big bubbles due to their lower rising velocity which means less momentum. Actually, the momentum of gas injection is converted to the momentum of bubble rising and the momentum of liquid rising, assuming the heat loss is negligible. Therefore, for the same gas injection flowrate, the lower momentum for microbubbles rising means more momentum for liquid rising, which also means a better liquid mixing. (Zimmerman et al, 2009) Furthermore, the shear stress across the surface of rising microbubbles increases as the

surface/volume ratio increases. It means decreasing the bubble size can actually increase the flux of momentum. (Zimmerman et al, 2009) Such properties of microbubbles are well utilized when combining microbubble generation with airlift loop bioreactor for microalgae culture, because a sufficient mass transfer rate and proper mixing contribute to the enhancement of algal biomass productivity.

Microbubble generation by using fluidic oscillation also brings some unexpected additional advantages. First of all, unexpected hydraulic resistance can be decreased by using the oscillator. (Zimmerman et al, 2009) Typically, tee-splitter is widely used for a flow distribution system, and the flow pass through such a splitter meets a stagnation point at the geometric point of the split, near which an appreciable friction loss along the wall will happen. Whereas by using the oscillator instead of a tee-splitter, the same flow smoothly curves towards either of the outlet terminals, completely avoiding such unexpected friction loss. Secondly, the oscillation flow helps to reduce the skin friction by disrupting boundary layer formation. Flow in ducts tends to build up a viscous sublayer near the wall which induces appreciable dissipation loss, especially for statistically stationary turbulent flow. (Zimmerman et al, 2009) By introducing the fluidic oscillator, the flow is suddenly accelerated by the periodical momentum pulse which then suddenly disappears, and the inertia of the flow then trails off until the next momentum pulse comes. Therefore, due to such momentum gap, the viscous boundary layer fails to form so that the momentum pulses meet less resistance when flowing through the channel and the skin friction is reduced. (Zimmerman et al, 2009) According to the classical boundary layer problem studied by Rosenhead, (1963) it can be suggested that, for laminar flow, the time required to build up a boundary layer is long at high Reynolds number, therefore it is possible that the period of oscillation switches before the boundary layer is formed. Due to the reduced friction loss, it can be argued that this fluidic oscillator approach saves energetic consumption. Zimmerman et al.

(2007) carried out a pilot scale trial to study the efficiency of an aerator driven by fluidic oscillation. The power consumption of oscillatory flow was measured for different feedback loop lengths and volumetric air flow rates, and the results showed an 18% reduction (at the best aeration configuration) for oscillatory flow over steady flow. It was also found that the heat transfer for oscillating flow was greater than for steady flow. (Hewakandamby, 2009) For tubular flow, although the time needed for setting up a boundary layer is shorter, by giving a higher Reynolds number the skin friction reduction works as well. (Zimmerman et al, 2009)

In conclusion, in the application of microalgae culture, the microbubble generation mechanism by fluidic oscillation may play a crucial role in enhancing the biomass productivity. First, it contributes to a high CO_2 mass transfer rate by reducing the bubble size and by increasing the residence times. Second, when combined with an airlift loop design bioreactor, it provides a proper mixing feature for suspending microalgae cells and evenly distributing nutrients and illumination. Furthermore, this fluidic oscillator approach saves energetic consumption, compared to conventional microbubble generation approach, by avoiding the friction loss near the stagnation point and by disrupting boundary layer formation to reduce the skin friction loss.

Chapter 3: Methodology

3.1 Materials

The microbubble driven airlift loop bioreactors used in the work described in this thesis (for either mass transfer studies or microalgal cultures) consist of two essential parts, the airlift loop bioreactor and the fluidic oscillator.

3.1.1 Design of novel airlift loop bioreactor (ALB)

One of the key designs of the ALB is the airlift loop design, which consists of a standard design of internal draught tube, riser and down-comer regions, and a modified aeration system. Figure 3.1 shows the schematic diagram of the configuration of a single airlift loop design.

The traditional base is replaced with a tailored ceramic diffuser fed from the fluidic oscillator. This is the major modification on conventional ALB, which is expected to achieve nearly mono-dispersed and non-coalescent fine bubbles. The finite amount of kinetic energy available for free and forced convection flow depends on the flow injection and dragging of liquid by rising bubbles. (Zimmerman et al., 2009) In order to maximize the flow convection, oscillating flow is introduced to contribute to the minimization of the friction losses.

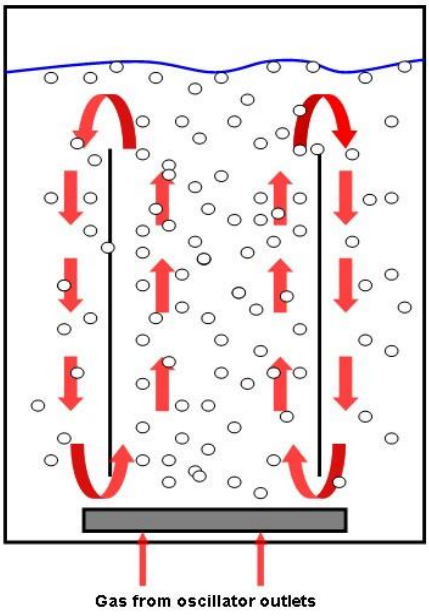

Figure 3.1: the Schematic diagram of a single airlift loop design and the flow pattern. A global stirring motion for overall mixing can be achieved by such design. Inside the draught baffle, microbubble streams rise slowly and smoothly. When the bubbles rise, they also drag liquid with them to the top of surface. Outside the draught baffle, there is a down comer region, where no aeration is provided, and the fluid will flow toward the bottom of the tank to rejoin the bubble streams due to its higher density, compared to the liquid in the riser region.

In terms of the riser region, the gas-liquid mass transfer and liquid-bioculture mass transfer are mainly happening here. Conventionally, greater bubble flux, rich in nutrients (e.g. CO_2), was generated by normal sparger, in order to achieve an intense mixing feature for increasing the mass transfer. However, such an approach requires higher gas flowrate which means more energy consumption, and the microbes can be easily killed by intense flux as the biological growth has been shown to be sensitive to flow regime. (Vial et al., 2000) Conversely, instead

of normal sparger, ceramic diffuser along with fluidic oscillator provides an energy saving approach, which uses low gas flow rate but promises the same mass transfer rate, due to the higher gas transfer efficiency achieved by microbubbles and oscillatory flow.

3.1.2 Fluidic oscillator

One of the key designs of our innovative microbubble generation system is a fluidic oscillator. It is capable of providing oscillating pluses periodically to break off the bubbles formed at diffuser orifices when they are still a hemispherical cap. The fluidic oscillator has no moving parts and only consists of a stack of laser cut Perspex plates. Its configuration and operational principle are illustrated in Figure 3.2 and Figure 3.3, respectively.

During operation, the air flow issuing from the supply terminal may equally well attach to either one of the two attachment walls, which keep the flow deflected, guide it into one of the two output terminals and maintain such stable states if no acting control signal is there. This can be explained by Coanda effect that a jet flow always tends to attach to the wall nearby. (Tesař, 2007) By connecting control terminal X_1 and X_2 with a feedback loop, the switching of flow can be achieved. Because the flow is deflected by the guidance of attachment wall, the flow trajectories inside the jet in the vicinity of control terminals are curved, and a radial pressure gradient across the jet is therefore created by such curvature. (Zimmerman et al, 2009) This result in a decrease in pressure at the nearby control terminal and thereby causes the pressure difference between two control terminals, which then draws air from the high pressure control terminals (opposite one) to the low pressure one through the feedback loop. The feedback flow gradually gains a sufficient momentum, because of the amplification effect of the valve, for switching the main jet from current output terminal to the opposite terminal. As the oscillator is symmetric, this flow switching is reproduced in the opposite way based on the same principle, thereby leading to a

periodic switching process. A delay usually happens because of the fluidic inertia which takes time for the flow in the feedback loop to stop and to begin flowing back, and the critical point for the flow switching is when the flow inside the loop channel reaches around 7% of the main supply flowrate. (Tesař et al, 2006) The frequency of generated oscillation can be simply achieved by changing the feedback loop length, which is described in detail by Tesař et al. (2006).

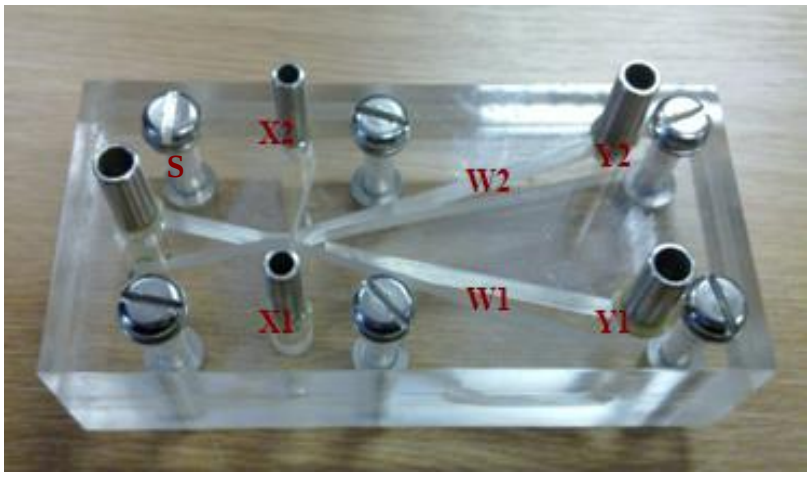

Figure 3.2: The non-moving-part fluidic oscillator. X1 and X2 are the control terminals which are connected by a feedback loop. S means supply terminal, connected to a flow inlet pipe. Y1 and Y2 are output terminals, periodically emitting output flow in sequence. W1 and W2 are two attachment walls, placed symmetrically on both sides. (adapted from Zimmerman et al, 2009)

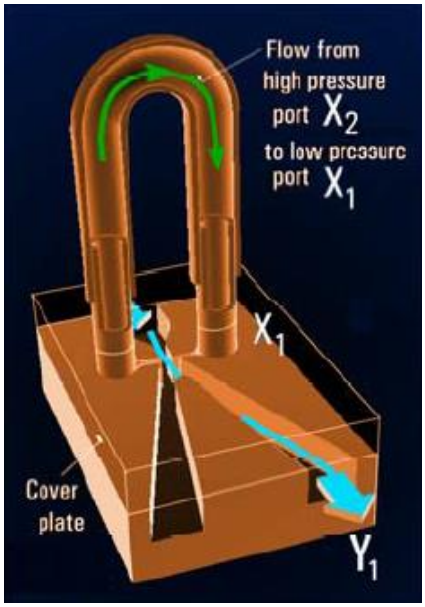

Figure 3.3: The oscillator in working mode. (adapted from Zimmerman et al. 2008)

3.2 Experimental methods

The mass transfer of both CO_2 dissolution and O_2 removal for microbubble driven airlift bioreactor (ALB with fluidic oscillator engaged) were compared with fine bubble driven airlift bioreactor (ALB with the absence of fluidic oscillator). Different bubbling flow rates, reactor volume and diffuser pore sizes were tested. The detailed experimental design is described in Chapter 4. For microalgae culture, *Dunaliella salina* was chosen as an 'indicator algae' to test the performance of microbubble driven ALB due to their features of robust, high tolerance to environmental conditions and high salinity to prevent contamination etc. Their growth in microbubble driven ALB was carefully compared with fine bubble driven ALB. The experimental designs depending on different purposes are described in detail in Chapter 5-7.

3.3 Analysis methods

3.3.1 Determination of dissolved CO_2 concentration

The dissolved CO_2 is in equilibrium with HCO_3^- and CO_3^{2-}, and can be described by the following chemical reactions. (Livansky, 1990; Camacho 1999)

$$H_2O \xleftrightarrow{K_w} H^+ + OH^-$$

$$CO_{2aq} + H_2O \xleftrightarrow{K_1} H_2CO_3 \longleftrightarrow HCO_3^- + H^+$$

$$HCO_3^- \xleftrightarrow{K_2} CO_3^{2-} + H^+$$

Where the relevant equilibrium constants are:

$$K_w = [OH^-][H^+] = 10^{-14}$$

$$K_1 = \frac{[HCO_3^-][H^+]}{[CO_{2aq}]} = 10^{-6.381}$$

$$K_2 = \frac{[CO_3^{2-}][H^+]}{[HCO_3^-]} = 10^{-10.377}$$

.

The system must satisfy the electro-neutrality constraint, therefore

$$[H^+] + [Cat^+] = [OH^-] + [HCO_3^-] + 2[CO_3^{2-}] + [An^-]$$

Assuming constant concentrations of other cations and anions, it gives

$$[H^+] = [OH^-] + [HCO_3^-] + 2[CO_3^{2-}]$$

By solving above equations, it gives

$$[CO_2] = \frac{[H^+] - \frac{K_w}{[H^+]}}{\frac{K_1}{[H^+]} + \frac{2K_1K_2}{[H^+]^2}} = \frac{(10^{-pH} - \frac{10^{-14}}{10^{-pH}})(10^{-pH})^2}{10^{-6.381}10^{-pH} + 2\times10^{(-6.381-10.377)}} \quad (mol/L)$$

Eq. 3.1

However Eq. 3.1 can only be used to calculate the concentration of CO_2 in water and when the pH is less than 7. For the $[CO_2]$ estimation in the medium containing $NaHCO_3$ modification needs to be made. The system would still need to satisfy the electro-neutrality constraint. But since $NaHCO_3$ is added into medium, other cations and anions are not equal.

$$[Cat^+] - [An^-] = \Delta[Na^+]$$

Therefore, the additional amount of Na^+ needs to be taken into consideration.

$$[H^+] + \Delta[Na^+] = [OH^-] + [HCO_3^-] + 2[CO_3^{2-}]$$

Finally, Eq. 3.1 is modified as:

$$[CO_2] = \frac{(10^{-pH} - 10^{(pH-14)} + \Delta[Na^+])10^{(-2pH)}}{10^{(-6.381-pH)} + 2\times10^{(-16.758)}} \quad (mol/L)$$

Eq. 3.2

Therefore, the dissolved CO_2 concentrations for all the experiments described in this thesis were estimated by using either Eq. 3.1 or Eq. 3.2 based on the pH which was measured by a SevenGo Duo pro (pH/DO/Ion) meter.

Eq. 3.1 and Eq. 3.2 were validated using a combination of derivations from Henry's law and the addition of experiments that would demonstrate how carbon dioxide dissolved in water. Henry's law states that the equilibrium concentration of a gas is in direct proportion to the partial pressure of that gas over the solution, (Myers, 2003) and it can be expressed as concentrations in both the gas and liquid phase (Eq. 3.3). (Lewis & Whiton, 1924)

$$C_G^* = H \times C_L^*$$ Eq. 3.3

where C_G^* and C_L^* stand for the gas concentration in the gas phase and in the liquid phase at equilibrium respectively, while H is the Henry's law coefficient.

Knowing that the solubility of CO_2 in water at 20˚C and 1 atm pressure (100% CO_2) is 0.040 mol/L (Biotol, 1992) helped to formulate an equation (Eq. 3.6) to calculate the solubility of CO_2 in water for different feed concentrations of CO_2.

$$C_{G1} = H \times C_{L1}$$ Eq. 3.4

$$C_{G2} = H \times C_{L2}$$ Eq. 3.5

$$\Rightarrow C_{L2} = \frac{C_{G2}}{C_{G1}} \times C_{L1}$$ Eq. 3.6

where C_{G1} = 100% v/v, C_{L1} = 0.040 mol/L, C_{G2} = x% v/v and C_{L2} = [CO_2 (aq)]

Eq. 3.4 represents the relationship between dissolved CO_2 in water when the gas feed is 100% CO_2. This is considered a standard as this relationship will never change and is fact. Eq. 3.5 represents the relationship between an arbitrary CO_2 feed concentration and the dissolved CO_2 that would be in the liquid at equilibrium. The Henry's constant for both scenarios are the same because the two equations represent the same species, temperature and viscosity of fluid. When Eq. 3.4 and Eq. 3.5 are combined, there is no longer a need for a Henry's constant as they cancel out and the concentration of dissolved CO_2 from a gas feed source of any CO_2% can be found. Using Eq. 3.6, the equilibrium concentration of dissolved CO_2 for each gas feed concentration is calculated. These values were compared with the equilibrium concentrations of dissolved CO_2 calculated based on pH^* by using Eq. 3.1 and Eq. 3.2, shown in Table 3.1. The pH* values were obtained from a full set of experiments, shown in Chapter 7.

From Table 3.1, it shows that the discrepancies of calculated dissolved CO_2 concentration between using Eq. 3.1/Eq. 3.2 and using Henry's law (Eq. 3.6) is no more than 6%, which indicates that the accuracy of Eq. 3.1 or Eq. 3.2 is promising. Besides, Eq. 3.6 can only be used to calculate the dissolved CO_2 concentration at equilibrium by knowing the CO_2 volume percentage in the feed gas, while Eq. 3.1/Eq. 3.2 can be used to estimate dissolved CO_2 concentration at any states (including at equilibrium) by knowing the pH.

Table 3.1: Calculated concentration of dissolved CO_2, using Henry's law, compared with results using Eq. 3.1

CO_2%	$[CO_2(aq)]$ mol/L Henry's law **(**Eq. 3.6**)**	$[CO_2(aq)]$ mol/L (Eq. 3.1 or 3.2**)**	Difference
5%	0.002	0.002	0
20%	0.008	0.008	0
40%	0.016	0.015	6%
50%	0.020	0.019	5%
75%	0.030	0.031	3%

Additionally, $[HCO_3^-]$, $[CO_3^{2-}]$ and $[C_T]$ (total carbon) can be calculated by Eq. 3.7, Eq. 3.8 and Eq. 3.9, respectively.

$$[HCO_3^-] = 10^{pH-6.381}[CO_2] \quad \text{Eq. 3.7}$$

$$[CO_3^{2-}] = 10^{2\,pH-16.758}[CO_2] \quad \text{Eq. 3.8}$$

$$[C_T] = (1+10^{\mathrm{pH}-6.381}+10^{2\,pH-16.758})[CO_2] \quad \text{Eq. 3.9}$$

The concentration of each carbon species in the water varies with pH, which can be summarized in Figure A2.1 (Appendix 2).

3.3.2 Determination of mass transfer

K_La is the essential parameter which directly reflects the effectiveness of mass transfer. The determination of overall K_La was well interpreted in Chisti (1989). The gas transfer rate is related to K_La and concentration driving force by the equation

$$\frac{dC_t}{dt} = K_L a(C^* - C_t) \qquad \text{Eq. 3.10}$$

where C_t is instantaneous concentration while C^* is equilibrium/saturation concentration. The integration form of this equation can be written as

$$\ln\frac{C^* - C_0}{C^* - C_t} = K_L a \cdot t \qquad \text{Eq. 3.11}$$

where C_0 represents the initial concentration. The usual convention is

$$E = \frac{C_t - C_0}{C^* - C_0}$$

then Eq. 3.11 can be presented as

$$\ln\frac{1}{1-E} = K_L a \cdot t \qquad \text{Eq. 3.12}$$

The K_La was calculated as the slope of a semilog plot of 1/(1-E) versus t.

For K_La estimation, the dissolved CO_2 and O_2 concentrations were measured by pH and DO probe, respectively. In terms of the pH and DO measurement, the response time for each probe needs to be considered in order to have a relatively accurate measurement. The response times for pH and DO probes used in this thesis are reported to be about 20 s and 30 s, respectively. However, the response

time on the certificate is given for stable conditions, as usually the lab use pH/DO probes are designed for single measurement. So in a stable condition, as long as the sampling time interval is longer than or equal to the response time, the reading could be as accurate as described in the instruction manual. However, for continuous use, the value displayed might not correspond to the real pH of the sample at a certain time point. In Chapter 4, pH and DO were continuously measured (every 30 s) in a liquid with the dissolved gas concentration keeping changing until reaching saturation. Therefore, take pH measurement as an example, although the time interval of sampling (30 s) was selected to be longer than the probe response time (20 s), it can still be argued that the reading displayed every 30 s might not be the real pH at that time point. However, if the sampling time interval is set to be constant, the trend of the changes in pH can still be reliable. Since the purpose of the pH measurements in Chapter 4 was to estimate the K_La for each dosing condition rather than to find out the pH value at a specific time point, the results of K_La were considered to be valid. Alternatively, certain process equipment (usually industry use) for monitoring the pH/DO over long periods of time are recommended.

3.3.3 Determination of microalgal biomass

The most convenient way to quantify the microalgal biomass is measuring their optical density (OD) by using spectrophotometer at a certain wavelength (595 nm was applied for all the OD measurements described in this thesis). Apart from OD, chlorophyll content measurement is also widely applied to quantify the microalgal biomass. (Mackinney, 1941)

1) 5 ml of microalgae sample was aseptically transferred into a 15 ml Falcon tube, which was then centrifuged at full speed (3000 g) for 10 minutes. 2) The supernatant was poured off immediately, followed by re-suspending each pellet in 1 ml of distilled water. 4 ml of acetone was then added to each tube and whirlmixed properly. 3) The tube was then centrifuged again at full speed for 5

minutes, and the pellet was checked to ensure it was completely white. 4) Finally, the optical density of the supernatant was measured at 645 nm and 663 nm separately after zeroing the spectrophotometer using 80% acetone. The chlorophyll content was then calculated according to the equation:

$$Chlorophyll\ (\mu g / ml) = \frac{OD_{645} \times 202 + OD_{663} \times 80.5}{2 \times 5} \quad \text{Eq. 3.13}$$

3.3.4 Determination of microalgal growth

Microalgal growth is usually measured as specific growth rate. The way to determine the overall specific growth rate for an algal culture is described by Scragg (1991). Algal growth rate dC_t/d_t is related to μ and concentration at time t, based on the equation

$$\frac{dC_t}{dt} = \mu C_t \quad \text{Eq. 3.14}$$

where C_t is instantaneous concentration and μ is the overall specific growth rate. The integrated form of this equation can be written as

$$\ln\left(\frac{C_t}{C_0}\right) = \mu t \quad \text{Eq. 3.15}$$

where C_0 is the initial concentration. The overall specific growth rate was then estimated from the slope of a semilog plot of $\ln(C_t/C_0)$ versus t.

3.3.5 Determination of photosynthetic O_2 generation rate

The photosynthetic O_2 generation rate was determined by measuring the changes in dissolved O_2 concentration during algal photosynthesis. The oxygen electrode was used to measure the concentration of O_2 in an algal cell suspension contained in the temperature controlled chamber of the apparatus. A teflon membrane permeable to oxygen forms the base of the chamber. Underneath this

membrane is a shallow compartment containing a 2.3 M KCl solution and two electrodes, a platinum cathode and a silver anode. A fixed polarizing voltage is applied between the electrodes and the resulting tiny current (approx. 1 microamp) is proportional to oxygen concentration. The current is determined using a chart recorder. The method is essentially polarographic, oxygen being reduced at the platinum cathode can be described as:

$$O_2 + 2\ e^- + 2\ H_2O \rightarrow H_2O_2 + 2\ OH^-$$

The current is proportional to the dissolved oxygen concentration. To ensure that the oxygen concentration in the electrode compartment follows that in the main chamber, it is essential to stir the contents of the main chamber continuously. This is achieved by mounting the whole apparatus on a magnetic stirrer, and putting a tiny magnetic stirring 'flea' in the chamber. A closely fitting stopper is used to exclude atmospheric oxygen from the system. Its position must be carefully adjusted so that the liquid exactly fills the space under it.

The oxygen electrode needs to be calibrated before measuring the algal samples. 2 ml of distilled water was added to the oxygen chamber, whilst both the chart recorder and measurement box were switched on and left for 30 min. Then box and the chart recorder were then adjusted to 950 and approximately 95, respectively. A small amount of dithionite ($Na_2S_2O_4$) was added to the oxygen chamber to flush out the oxygen (in order to calibrate the electrical zero with the oxygen zero). The liquid was removed by a Pasteur pipette as soon as the zero was established. The chamber was washed by 5 times with distilled water. After that, 2 ml of algal sample was added into the chamber and left for few minutes. The light source was then switched on to drive photosynthesis. Several minutes later the light was turned off to detect the algal respiration. The precise time for the photosynthesis (light on) and respiration (light off) was recoded by the chart recorder. The net photosynthetic oxygen generation rate was then calculated.

The calibration provided a 100% oxygen saturation point (before addition of dithionite) and a 0% oxygen point (after dithionite addition). The number of chart recorder units between 0 and 100% is known as the ‘range’. Therefore, the oxygen concentration per unit can be calculated as 100 % oxygen saturation × DW volume (2 ml) / range. The rate of oxygen change for either photosynthesis or respiration can be calculated as oxygen concentration per unit × Number of units (Y-axis) / time (X-axis) / algal cell or biomass concentration. Finally, the total photosynthetic oxygen generation rate was calculated by combining the net photosynthetic oxygen generation rate with oxygen consuming rate caused by respiration, assuming that dark respiration rate equals the respiration rate in the light.

Chapter 4: Mass transfer in the microbubble driven airlift bioreactor

It is well know that CO_2 supply is essential for algal growth, and improving CO_2 mass transfer for algal culture is often considered in many bioreactor designs, however, CO_2 supply systems for algal culture are still in the early stage of development. For most of lab cultures, little concern is paid to improving CO_2 supply techniques while more consideration is focused on optimizing other operational parameters such as light, nutrients and light-dark circulations etc. That is mainly because conventional CO_2 supply technologies (e.g. continuously sparging a certain percentage of CO_2 gas into culture) are believed to be sufficient for supporting lab scale cultures. However for industrial scale cultures, especially with the view to using microalgal culture for CO_2 sequestration, problems in the conventional CO_2 supply techniques (See 2.5.3) may become one of the major reasons leading to failure. Since a novel microalgal culture system-'microbubble driven airlift bioreactor' was proposed to improve the microalgal growth and CO_2 capture efficiency due to its improved mass transfer, it is helpful to have a better understanding on the mass transfer properties of the proposed system. In this chapter (see also Ying et al., 2013b), our proposed culture system was compared with a conventional culture system in terms of the mass transfer for CO_2 dissolution and O_2 removal. Apart from that, the impact of different liquid substrates (e.g. water, $NaHCO_3$ medium and algae medium) on CO_2 mass transfer properties was also tested. This fundamental study also contributed to the later engineering of operational parameters for our microalgal culture system described in Chapter 6.

4.1 Introduction

In most microalgae cultures, CO_2 is usually injected into the culture through bubbling CO_2 enriched air into porous diffusers. The benefits of additional

supply of CO_2 have been discussed in Chapter 2.

According to the relationship between partial pressure and Gibbs free energy (Eq. 4.1), it is found that the increase in the partial pressure of reactants (e.g. CO_2) or the reduction of partial pressure in the products (e.g. O_2) results in the value of Gibbs free energy becoming negative (Al-Mashhadani, 2011). Hence the reaction becomes thermodynamically favourable and moves towards the formation of more products (Gary, 2004). Such performance features are widely utilized for many bioprocesses to achieve a higher productivity (Pulz, 2001; Richmond, 2008). Therefore, increasing the concentration of dissolved CO_2 whilst reducing the accumulated O_2 level can be considered as an approach towards improving productivity.

$$aA + bB \rightarrow cC + dD$$

$$\Delta G = \Delta G^{\circ} + RT \ln \frac{[p_C]^c [p_D]^d}{[p_A]^a [p_B]^b} \quad \text{Eq. 4.1}$$

However, most existing CO_2 supply techniques are relatively inefficient. Due to low interfacial surface area between gas bubbles and culture medium, the gas-liquid mass transfer is poor, which is associated with CO_2 loss to atmosphere (Carvalho & Malcata, 2001). Besides, additional CO_2 supply increases the operational cost, which can not be balanced eventually by the enhancement of algal yields due to the low CO_2 mass transfer. Improving the CO_2 supply efficiency and consequently enhancing the algal productivity has become a major challenge over the years.

Due to the enhanced gas-liquid mass transfer efficiency and liquid circulation etc, airlift bioreactors (ALB) are increasingly employed for microalgae culture. Many investigations have been carried out on the performance of different ALBs; however, these studies were carried out all based on conventional gas supply

system. There are only a few studies on the effects of microbubbles on ALB performance, because normally the microbubble generation systems, for instance DAF, electro-flotation, electrostatic spraying, and mechanical agitation etc, were not profitable to be applied for most bio-processes due to their high energy cost (Ketkar et al., 1991; Edzwald et al., 1992; Rijk et al., 1994; Tsouris et al., 1995; Fóris & Rubio, 1999).

Recently, an innovative microbubble generation system (fluidic oscillator) with lower power consumption has been invented with the benefits of energy saving and improved efficiency (Zimmerman et al., 2009). Detailed information on fluidic oscillator operation and microbubble generation mechanism were described in previous studies. (Zimmerman et al., 2008; Zimmerman et al., 2009; Zimmerman et al., 2011)

This study aims to investigate the effect of microbubbbles (generated by fluidic oscillator) on mass transfer under different CO_2 dosing flow rates (5% CO_2 balanced with N_2). In addition, the impact of different liquid substrates (e.g. $NaHCO_3$ medium and algae medium) on CO_2 mass transfer properties is investigated.

4.2 Material and methods

4.2.1 Materials

A 7 L - airlift loop bioreactor based on classic ALB geometry designs (Chisti, 1989), as shown in Figure 4.1 (left), was used to study the mass transfer properties of microbubbles and fine-bubbles. Additionally, a smaller version (2.5 L) of ALB, based on a similar geometry design, was applied to study the impact of different liquids on mass transfer, shown in Figure 4.1 (right). It needs to be noted that the geometry of the bioreactors used in the experiments was not particularly designed, as the main purpose of this research was to investigate the

effect of microbubbles on mass transfer rather than the effect of geometry. Therefore, the reactor geometry was determined mainly based on the concentric draught-tube internal-loops bioreactor reported in Chisti (1989) (e.g the draught tube diameter / reactor diameter ≈ 0.75, the draught height / reactor height ≈ 0.55).

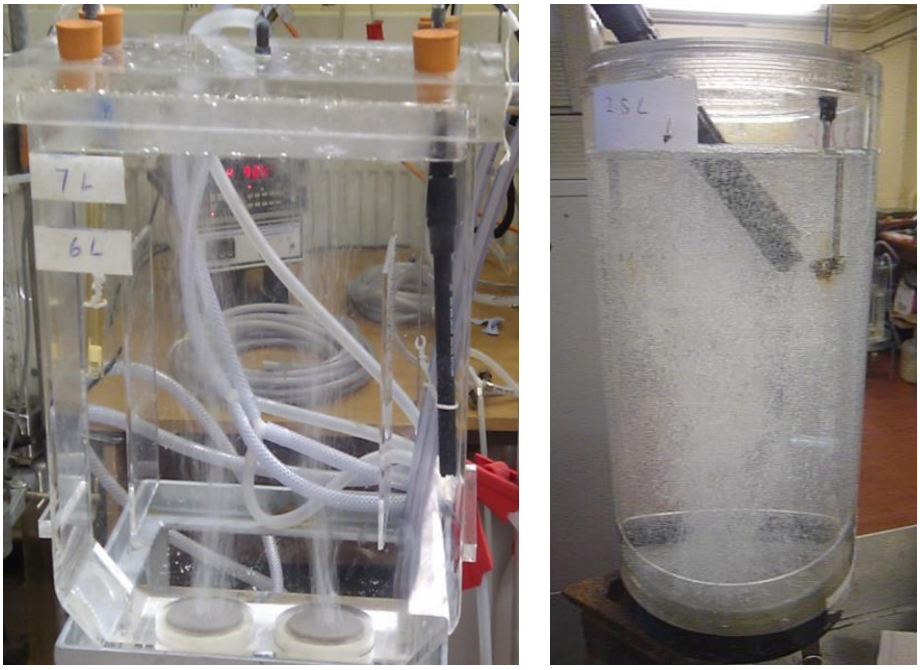

Figure 4.1: 7 L- and 2.5 L- lab scale airlift loop bioreactors. The 7L-airlift bioreactor (left) is made of transparent acrylic material with dimensions of 26 cm × 10 cm × 30 cm. Inside the bioreactor, two ceramic diffusers (d = 5 cm, h = 1 cm), with the pore size of 20 microns, are fixed at the bottom. Two draught baffles are suspended 3.5 cm above these diffusers, dividing the middle chamber into 3 regions which work as risers and downcomers. A static liquid height of 15 cm was employed to give the volume of 7 L. There are several holes drilled on the lid to allow pH and DO probes to be inserted into the reactor. The 2.5 L-airlift loop bioreactor (right) is also made of acrylic material, with the dimension of 28.5 cm in height and 12.4 cm in diameter. The air lift loop design consists of a ceramic diffuser (diameter of 7.8 cm, pore size of 20 microns) fixed at bottom and an internal draught tube (H: 17 cm, D: 9.5 cm) hanging 3 cm above the diffuser.

4.2.2 Experimental procedure

To study the mass transfer properties of microbubbles and fine-bubbles, the two inlet ports of diffusers at the bottom of 7 L bioreactor were connected to a gas cylinder by PVC tubes, through a fluidic oscillator or a Y- junction. The detailed connections for main experiments (with oscillator) and control experiments (without oscillator) are illustrated in Figure 4.2. A pH and DO probe (Mettler Toledo, UK) were inserted into the bioreactor via the holes on the lid. These holes were blocked by rubber bungs to prevent gas leakage. The outlet nozzle on the lid was connected to a flow meter to measure the outlet flowrate which is equal to the real inlet flowrate. For each set of experiment, 7L distilled water with the temperature 25±1℃ were employed. Mixture gas containing 5% CO_2 and 95% N_2 was injected into bioreactor with a selected flow rate. Five different flow rates were tested. The flow rate was measured by a flow meter which was connected to the outlet port of the bioreactor. The changes in pH and DO were monitored by pH meter and DO meter respectively. Data were recorded every 30 seconds until pH and DO were stable. For the effect of different liquids on mass transfer, the same setup as shown in Figure 4.2 was applied, except replacing the 7L-ALB with 3L-ALB. The mass transfer for CO_2 dissolution was tested in the distilled water containing certain concentration of $NaHCO_3$ and also in the real algal culture medium (containing algae). 7 different concentrations of $NaHCO_3$ were tested. The algae (*Dunaliella salina*) used in this study was 7 days old. During the test, 5% CO_2 and 95% N_2 were injected into *D. Salina* culture through microbubbles under a fixed dosing flow rate (0.7L/min), with DO and pH recorded every 30 seconds. The dissolved CO_2 concentration was calculated based on Eq. 3.1 (for water) or Eq. 3.2 (for $NaHCO_3$ medium and algal medium) (Ying et al., 2013). $[Na^+]$ in Eq. 3.2 particularly means the concentration of Na^+ obtained from $NaHCO_3$. The method of mass transfer coefficient estimation was estimated as the slope of a semilog plot of 1/(1-E) versus T, which was explained in details in Chisti. (1989)

$$[CO_2] = \frac{[H^+] - \frac{K_w}{[H^+]}}{\frac{K_1}{[H^+]} + \frac{2K_1K_2}{[H^+]^2}} = \frac{(10^{-pH} - \frac{10^{-14}}{10^{-pH}})(10^{-pH})^2}{10^{-6.381}10^{-pH} + 2\times10^{(-6.381-10.377)}} \quad (mol/L)$$

Eq. 3.1

$$[CO_2] = \frac{(10^{-pH} - 10^{(pH-14)} + \Delta[Na^+])10^{(-2pH)}}{10^{(-6.381-pH)} + 2\times10^{(-16.758)}} \quad (mol/L)$$

Eq. 3.2

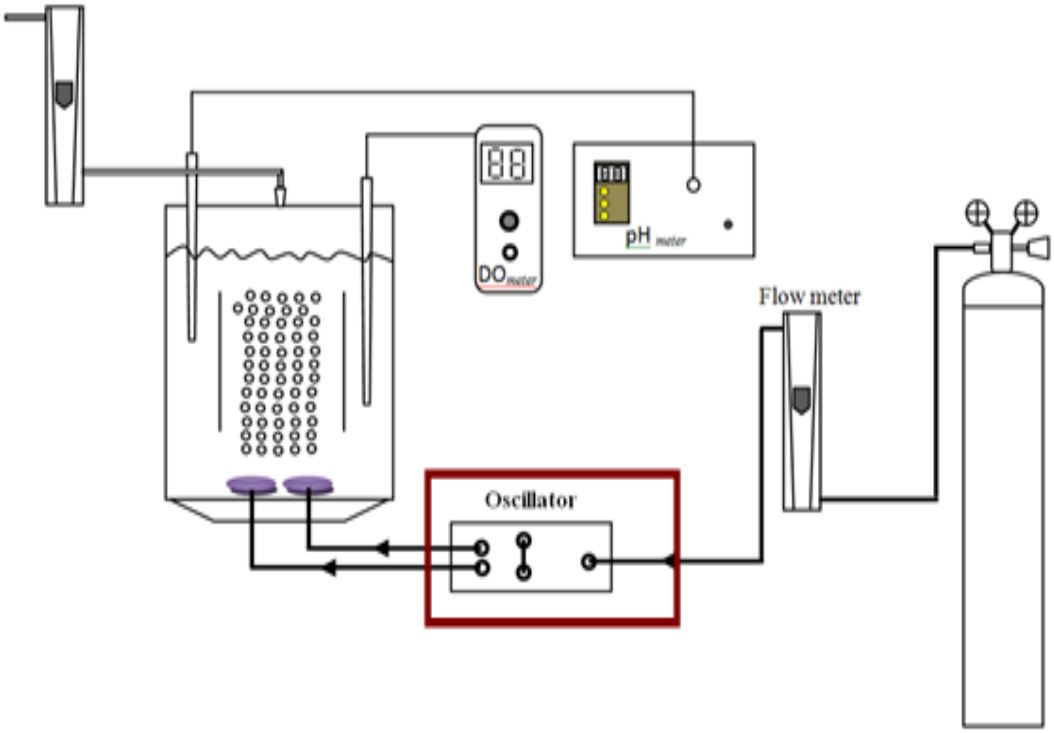

Figure 4.2: Connections for mass transfer test. For microbubble dosing, the gas ejected from cylinder flowed into a fluidic oscillator, and was shot out from the two outlet terminals on oscillator. Here a flow rate of 80 L was required to drive the oscillator. To stop this amount of gas being injected into bioreactor, most of it was bled out via bleeding pipes with less than 1% flowing into bioreactor, and the real inlet flow was measured by the flow meter at the bioreactor output. For fine-bubble dosing, the Y-junction was placed in the area marked with the red frame.

4.3 Results and discussion

4.3.1 Mass transfer for microbubble driven and fine bubble driven reactor

The effects of microbubble dosing on mass transfer for CO_2 dissolution and O_2 removal were examined by dosing 5% CO_2 mix-gas (balanced with 95% N_2) into bioreactor (containing 7 L distilled water) under 5 different bubbling flow rates, along with the control experiment (without fluidic oscillator, fine-bubbles). The K_La for CO_2 dissolution and O_2 removal under each bubbling condition were plotted in Figure 4.3. From Figure 4.3, generally K_La for either CO_2 dissolution or O_2 stripping increases along with gas dosing flow rate. For K_La, K_L mainly depends on the gas-liquid properties (e.g. density, viscosity, diffusivity and temperature etc.), and therefore is usually considered as a constant for fixed circumstances. Chisti (1989) expressed the interfacial area 'a' as a function of gas holdup (ε) and bubble diameter (d_B), shown as:

$$a = \frac{6\varepsilon}{d_B} \quad \text{Eq. 4.2}$$

For the same bubbling system (either microbubble dosing or fine bubble dosing), the bubble size can be considered as the same for different gas dosing flowrates, while the gas holdup usually increases with the bubbling flowrate, therefore, K_La was enhanced by increasing the flowrate as the total interfacial area was amplified.

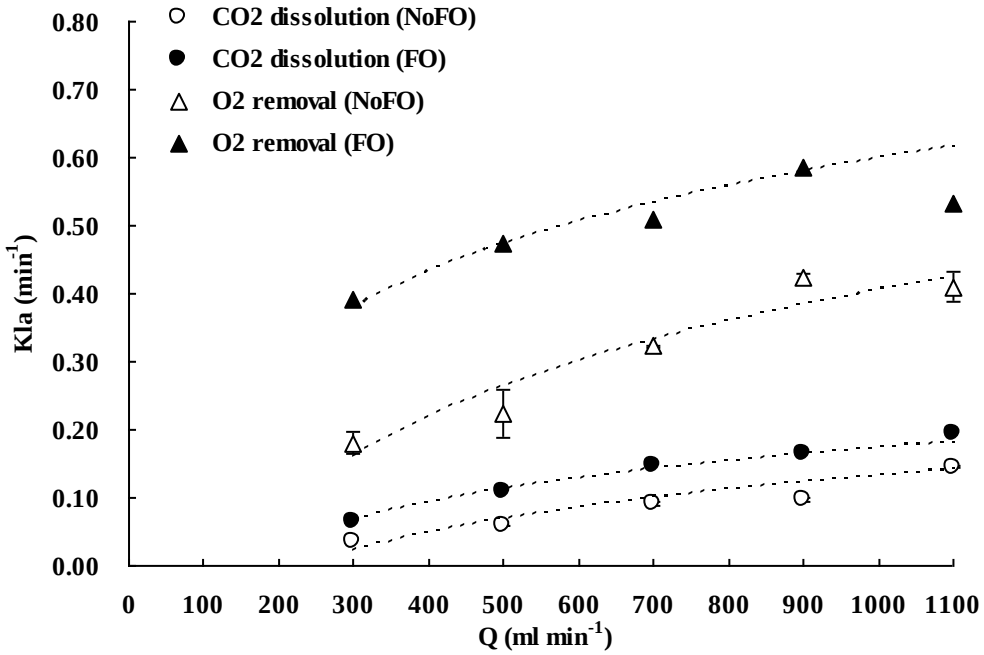

Figure 4.3: K_La under different dosing conditions. FO means 'with fluidic oscillator', representing microbubble (d_{32} = 388 μm) dosing while NoFO stands for 'without fluidic oscillator', representing fine bubble (d_{32} = 719 μm) dosing. The operational parameters (e.g. flow rate) were always slightly tuned to achieve the target level within the first 5 min during each test. The dissolved CO_2 reached saturation after 10 min of gas dosing for some bubbling conditions (e.g. under 1.1 L min^{-1} with FO). Therefore, to have a fair comparison of K_La under different bubbling conditions, the time period selected for K_La estimation was determined to be between 5 min and 10 min. The raw figures for each K_La estimation are attached in Appendix 3. Due to the lab limitations, the error bars shown in this figure was obtained from the duplication of fine bubble dosing under each flow rate (for O_2 removal, NoFO).

With regard to the comparison of K_La (either for CO_2 dissolution or O_2 removal) between microbubble dosing (FO) and fine bubble dosing (NoFO), microbubbles

had a higher K_La under each dosing flowrate. For CO_2 dissolution, the highest K_La under fine bubble dosing (0.14 min^{-1}) was achieved at dosing flow rate of 1.1 L min^{-1}, while almost the same K_La value (0.15 min^{-1}) was achieved by microbubble dosing at 0.7 L min^{-1}. Similarly, for O_2 removal the highest K_La (0.41 min^{-1}) was obtained at 1.1 L min^{-1} by fine bubble dosing, which however can be achieved at only 0.3 L min^{-1} for microbubble dosing. The potential for energy saving, especially for large scale processes, is therefore straight forward to argue. For example, in order to dissolve more CO_2 and strip off O_2 accumulated in algal bioreactor, it would typically require dosing a certain percentage of CO_2 mixture gas at a relatively high aeration rate to achieve a desired K_La. But actually, under very high flow rate, most of the gas is wasted. And an intensive agitation caused by high flow rate may damage the algal cells. However, by using the oscillator (microbubble dosing) the desired K_La can be obtained even at relatively low flow rate. It considerably saves gas usage and also the electricity cost is reduced.

In conclusion, for the same bubble generation method (the changes in bubble sizes are considered to be negligible across a wide range of dosing flow rate), increasing the gas dosing flowrate (which means enhancing the gas hold up for the same liquid volume) can increase the K_La. For the same bubbling flowrate, reducing the bubble size can lead to an improvement in K_La as well. In other words, K_La can be enhanced by either increasing the dosing flowrate (to be more accurate, flowrate/liquid volume ratio) or reducing the bubble size.

4.3.2 The improvement of Kla by using fluidic oscillator

When injecting CO_2/ N_2 mixture gas into water, CO_2 dissolution happens along with O_2 stripping. The improvements by using fluidic oscillator (microbubbles) on mass transfer for CO_2 dissolution and O_2 stripping can be simply quantified as the percentage increase in $K_{L(CO2)}a$ and $K_{L(O2)}a$, expressed in Eq. 4.3 and Eq. 4.4, respectively.

$$I_{K_{L(CO_2)}a}\% = \frac{K_{L(CO_2)}a_{FO} - K_{L(CO_2)}a_{NoFO}}{K_{L(CO_2)}a_{NoFO}} \quad \text{Eq. 4.3}$$

$$I_{K_{L(O_2)}a}\% = \frac{K_{L(O_2)}a_{FO} - K_{L(O_2)}a_{NoFO}}{K_{L(O_2)}a_{NoFO}} \quad \text{Eq. 4.4}$$

Either Eq. 4.3 or Eq. 4.4 can be turned into Eq. 4.5 which indicates the percentage increase in K_La by using microbubble dosing should be the same for either CO_2 dissolution or O_2 removal under a fixed bubbling flowrate. The percentage improvement of K_La is therefore determined by the percentage difference of the total interfacial areas for a certain dosing flow rate. Combining Eq. 4.5 and Eq. 4.2, the percentage increase in K_La is correlated to bubble diameter (d_B) and gas hold-up (ε), described by Eq. 4.6.

$$I\% = I_{K_{L(CO_2)}a}\% = I_{K_{L(O_2)}a}\% = \frac{a_{FO} - a_{NoFO}}{a_{NoFO}} \quad \text{Eq. 4.5}$$

$$I\% = \frac{\varepsilon_{FO}d_{BNoFO}}{\varepsilon_{NoFO}d_{BFO}} - 1 \quad \text{Eq. 4.6}$$

From Eq. 4.6, the efficiency of K_La improvement (I%) therefore should be the same across different flow rates, assuming 1) the gas holdups are identical between microbubble dosing and fine bubble dosing under the same flow rates, and 2) changing the flow rate dose not vary the average bubble size for either microbubbles or fine bubbles as long as 'bubble coalescence' does not happen. However, the experimental results are inconsistent with such speculation. Figure 4.4 shows the K_La percentage increase. In general, microbubble dosing enhances the K_La by 30-100% over a wide flow rate range, while the efficiency of the improvement decreases with increasing flow rate. It is speculated that the microbubble size increases with the flow rate. The fluidic oscillator provides a periodical oscillating pulse to 'shake-off' the bubbles attached to the diffuser

orifice when they are still small. But for the same surface area of diffuser, increasing the flow rate may change the oscillating properties (e.g. the attenuation of 'pulse force' due to the build up of boundary layer), and may also cause bubble coalescence, consequently weakening the efficiency of oscillator for mirobubble creation. Therefore, the microbubble size may slightly increase when the flow rate increases, resulting in a reduction of d_{BNoFO}/d_{BFO} ratio which leads to the decline of K_La improvement efficiency (I %). This phenomenon also indicates a view that using fluidic oscillator to enhance mass transfer has its limitations in terms of flow rate (or to be more accurate, flow rate over liquid volume ratio).

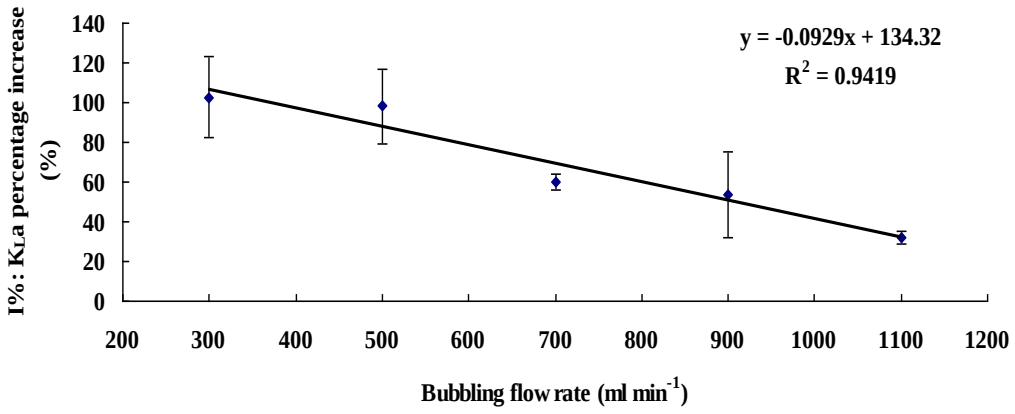

Figure 4.4: Plot of K_La percentage increase versus dosing flow rate. The value of I% under each flow rate was the average between the values calculated based on Eq. 4.3 and Eq. 4.4. The error bar represents the standard deviation between these two values.

4.3.3 The relationship between mass transfer coefficient and overall mass transfer rate

Knowing the K_La helps to indicate the capability of mass transfer, while knowing

the mass transfer rate gives a straight forward view of e.g. how fast the CO_2 is dissolving into liquid, which also helps to estimate the CO_2 capture efficiency.

The instantaneous mass transfer rate (ν_{MTR}) is interpreted as the driving force multiplied by the K_La (Chisti, 1989), shown in Eq. 4.7.

$$\nu_{MTR} = \frac{d[CO_2]}{dt} = K_L a([CO_2]^* - [CO_2]_t) \quad \text{Eq. 4.7}$$

Where K_La is the product of mass transfer coefficient K_L (m min^{-1}) and gas-liquid interfacial area a (m^{-1}), both $[CO_2]_t$ and $[CO_2]^*$ are instantaneous concentrations of CO_2 and its equilibrium concentration (mol L^{-1}), respectively. The average mass transfer rate (ν'_{MTR}) for a certain dosing time period (t_d) can be fairly represented as

$$\nu'_{MTR} = \frac{\int_0^{t_d} \nu_{MTR} dt}{t_d} = \frac{\int_0^{t_d} K_L a([CO_2]^* - [CO_2]_t) dt}{t_d} \quad \text{Eq. 4.8}$$

Assuming

$$[CO_2]_t = [CO_2]_0 + \nu'_{MTR} t \quad \text{Eq. 4.9}$$

by solving Eq. 4.8 and Eq. 4.9, it gives:

$$\begin{aligned} \nu'_{MTR} &= \frac{\int_0^{t_d} K_L a([CO_2]^* - [CO_2]_0 - \nu'_{MTR} t) dt}{t_d} \\ &= K_L a[CO_2]^* - K_L a[CO_2]_0 - K_L a \nu'_{MTR} \frac{t_d}{2} \quad \text{Eq. 4.10} \\ \Rightarrow \nu'_{MTR} &= \frac{K_L a([CO_2]^* - [CO_2]_0)}{\frac{K_L a t_d}{2} + 1} \end{aligned}$$

Where $[CO_2]_0$ represents the initial CO_2 concentration (mol L^{-1}) for a selected time period.

The accuracy of Eq. 4.10 was examined via Figure 4.5 which plots the experimental values of average mass transfer rates versus the calculated values by using Eq. 4.10. Compared with examined values, most of the data calculated by Eq. 4.10 showed less than 10% difference.

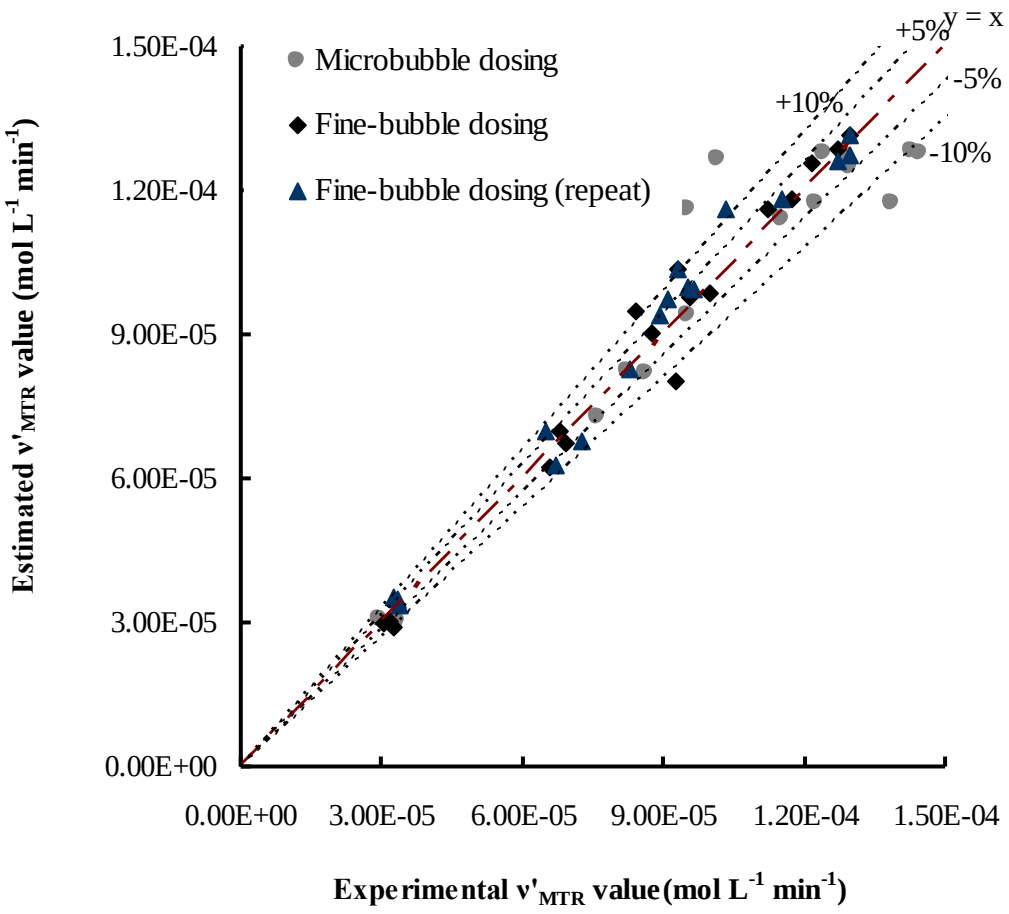

Figure 4.5: Plots of estimated average mass transfer rates versus experimental values. The K_La value for each condition was obtained based on selected time period (5 min-10 min), via the standard method described by Chisti (1989). For each dosing condition, the average mass transfer rates for selected time period (5 - 8 min, 5 – 10 min and 5 – 12 min) were estimated by Eq. 4.10 (Y-axis) and examined by $([CO_2]_t-[CO_2]_0)/t$ (X-axis).

4.3.4 CO_2 capture efficiency for microbubble dosing and fine-bubble dosing

CO_2 capture efficiency is one of the most important parameters for many bioprocesses with the purpose of CO_2 sequestration. Since the rate of CO_2 dissolving into liquid can be valuated by overall mass transfer rate using Eq. 4.10, the CO_2 capture efficiency (η) can be therefore simply described as the amount of CO_2 absorbed over the amount of CO_2 fed into the liquid (m_s/m_d) within a specific dosing time period (t_d), shown in Eq. 4.11.

$$\eta = \frac{m_s}{m_d} = \frac{V'_{MTR} \times V_L \times t_d}{CO_2\% \times Q \times P/(RT) \times t_d} \quad \text{Eq. 4.11}$$

Where CO_2% means the percentage of CO_2 in the gas supply, V_L is the volume of the liquid (m^3), Q is the gas dosing flow rate (L min^{-1}), P is standard atmosphere pressure (101.325 KPa), R is the ideal gas law constant (8.314 J K^{-1} mol^{-1}) and T is the temperature (298 K).

The CO_2 dissolving rate and the CO_2 capture efficiency under different dosing conditions were plotted in Figure 4.6 and Figure 4.7, respectively. In general, microbubble dosing by using the fluidic oscillator was found to have both higher CO_2 dissolving rate (average mass transfer rate) and CO_2 sequestration efficiency for a wide range of dosing flow rates, but the levels of improvement were attenuated as the flow rate went up (similar to the attenuation of K_La improvement, see 4.3.2). Such attenuation of improvement was caused by the increase in microbubble size due to the weakening of oscillation and bubble coalescence under higher flow rate.

Apart from reducing bubble size, increasing flow rate can also achieve a higher K_La (see 4.3.1), it is therefore not a surprise to find that the CO_2 overall mass transfer rate increases along with the flow rate (Figure 4.6). However, it is interesting that the CO_2 capture efficiency actually reduces when the flow rate

increases (Figure 4.7). Higher K_La dose mean higher CO_2 overall mass transfer rate (higher CO_2 dissolving rate), however, if the cost to achieve higher K_La is enhancing the dosing flow rate rather than reducing bubble size, then the amount of not dissolved CO_2 ('wasted CO_2') would increase, and such an increase in wasted CO_2 could not be balanced by the increase in dissolved CO_2, which ultimately lowers the CO_2 capture efficiency. Therefore, in order to achieve both higher CO_2 mass transfer rate and capture efficiency, reducing bubble size (e.g. using microbubbles) is more promising than increasing flow rate.

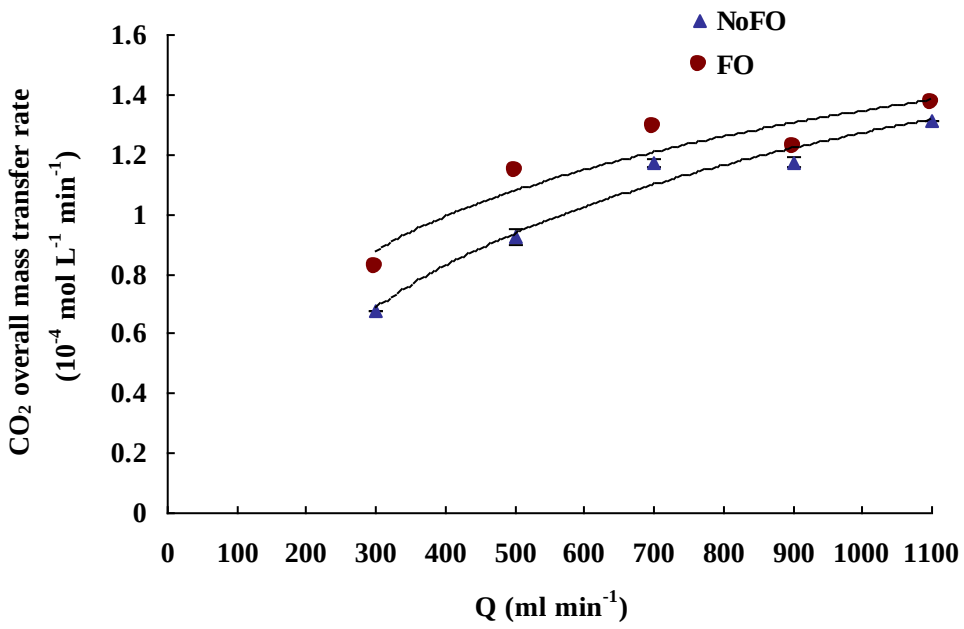

Figure 4.6: The average mass transfer rate under different dosing conditions. The average mass transfer rate was calculated based on Eq. 4.10, and the time period selected for v'_{MTR} calculation under each dosing condition was between 5 min and 10 min after starting dosing, the same time interval used for the K_La estimation.

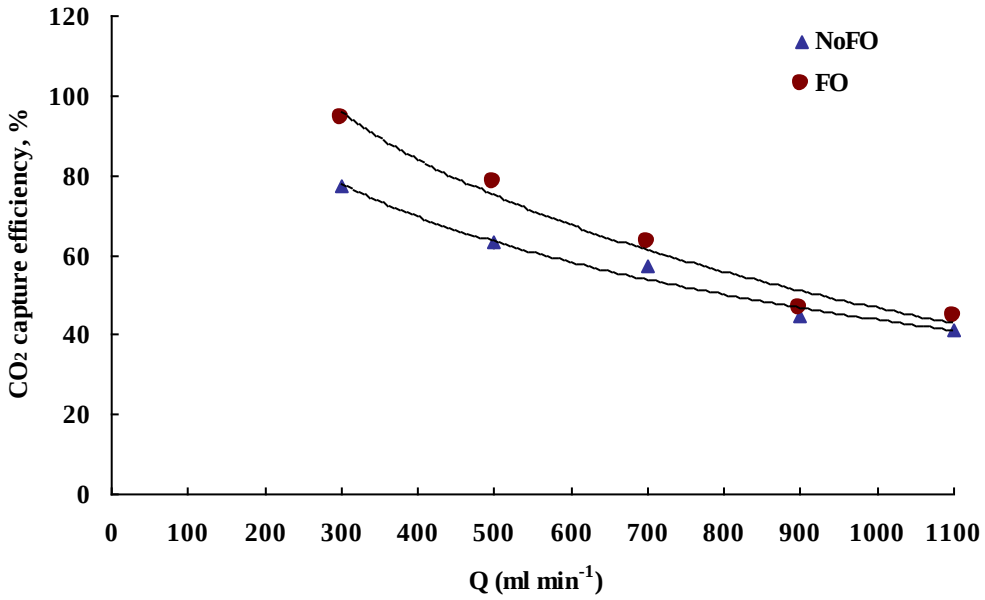

Figure 4.7: The plots of CO_2 capture efficiency versus gas dosing flowrate. The CO_2 capture efficiency for each dosing condition was calculated based on Eq. 4.11, and the time period selected for each calculation under different dosing conditions is the same as for overall mass transfer rate calculation.

4.3.5 Effect of $NaHCO_3$ on equilibrium pH and CO_2 mass transfer rate in water

In microalgae culture, CO_2 is injected into the culture medium (usually containing $NaHCO_3$) rather than pure water. When adding $NaHCO_3$ into water, $NaHCO_3$ dissociates into sodium (Na^+) and bicarbonate (HCO_3^-) ions, and these HCO_3^- ions neutralize some of the H^+ ions present in the medium to form the dissolved CO_2 and so increase the pH. So the concentration of $NaHCO_3$ clearly has an effect on pH, it is worth finding out whether the culture medium containing $NaHCO_3$ could affect the CO_2 mass transfer. Therefore, a separate experiment was carried out in a smaller version but the same design of airlift bioreactor (2.5 L).

Keeping other parameters constant (flow rate, temperature etc.), higher concentrations of $NaHCO_3$ added into distilled water should theoretically raise the minimal pH (equilibrium pH, pH^*) reached after CO_2 dosing. According to Henry's law and Two-film theory, the equilibrium concentration of dissolved CO_2 ($[CO_2]^*$) should only depend on the CO_2 partial pressure in the gas phase for fixed gas/liquid properties and temperature (assuming the changes in liquid physical properties by adding different amounts of $NaHCO_3$ to the water, e.g. viscosity, are negligible, as long as the concentration of $NaHCO_3$ is low). Therefore, different concentrations of $NaHCO_3$ in the water should not affect the $[CO_2]^*$. On the other hand, the CO_2 concentration is correlated to pH by Eq. 3.2. Since the concentration of Na^+ varies for different concentrations of $NaHCO_3$, while the $[CO_2]^*$ does not change, it is therefore reasonable to assume that pH^* changes for the water containing various $NaHCO_3$ concentrations. Indeed, this hypothesis was proved correct, in Figure 4.8, a log-linear trend was observed in the equilibrium pH values as the concentration of $NaHCO_3$ was increased. Besides, all the equilibrium concentrations of CO_2 corresponding to each equilibrium pH value under different concentrations of $NaHCO_3$ were found to be the same, which is approximately 0.0017 ± 0.0001 mol L^{-1}. In terms of mass

transfer for CO_2 dissolution, it can be seen that changing the concentration of $NaHCO_3$ does not have much of an effect on the K_La (Figure 4.9). Hence, $NaHCO_3$ could be used to control the equilibrium (minimal) pH of the medium without affecting the $[CO_2]^*$ and K_La. The pH region can also be altered depending on the particular strain of microalgae being cultured, as different algae prefer different levels of pH.

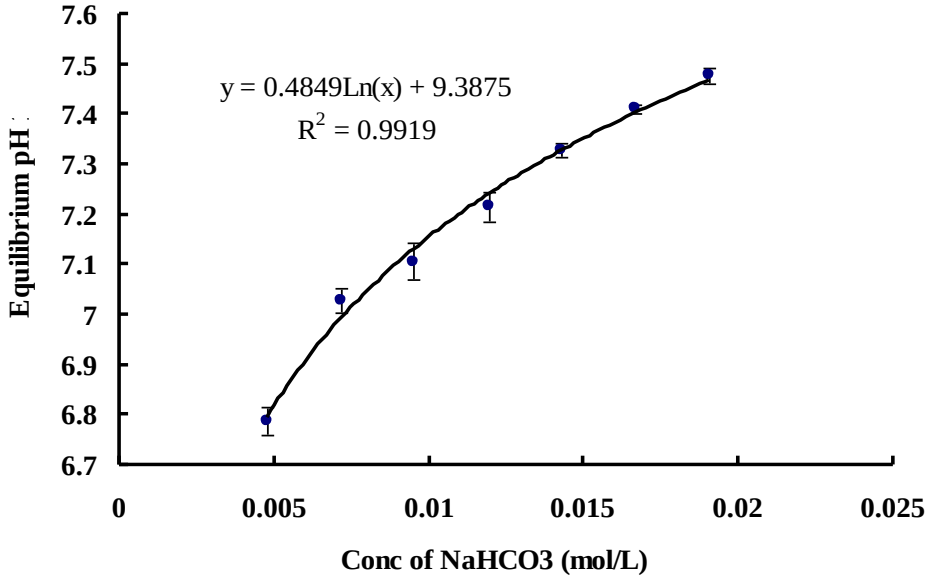

Figure 4.8: Change in equilibrium (final) pH for the liquid containing different concentrations of $NaHCO_3$.

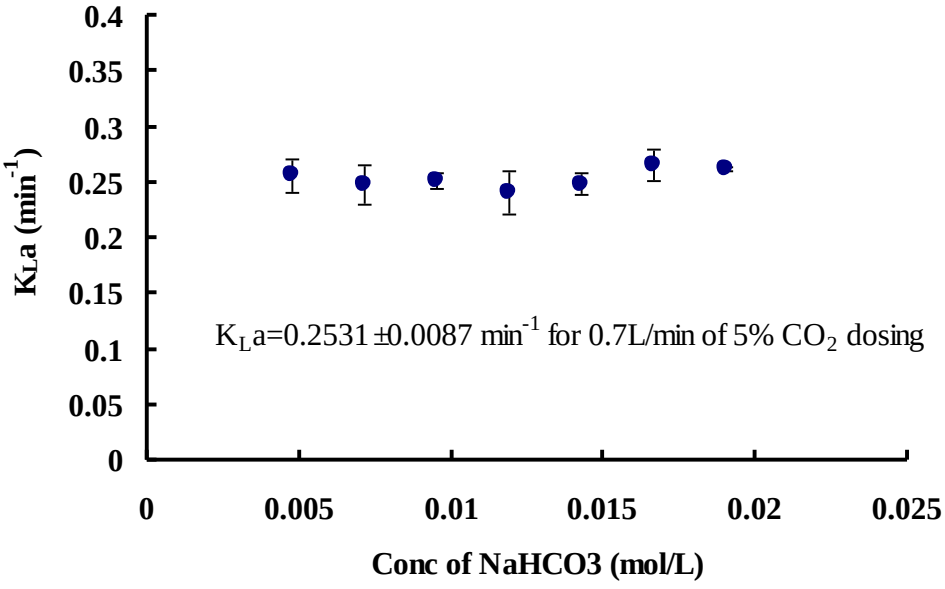

Figure 4.9: Changes in K_La (CO_2) for the liquid containing different concentrations of $NaHCO_3$.

4.3.6 CO_2 mass transfer in microalgae culture

In order to test the effect of real microalgae culture on CO_2 mass transfer, 5% CO_2 was dosed into a healthy *D. salina* culture (containing 0.012 mol/L of $NaHCO_3$) under a fixed flow rate (0.7 L/min) for 30 min, with pH recorded every 30 seconds. The results showed that there appear to be two distinct stages in terms of K_La, see Figure 4.10 for example. The calculations leading to the determination of the K_La from the slopes seen in Figure 4.10 are given in Table 4.1.

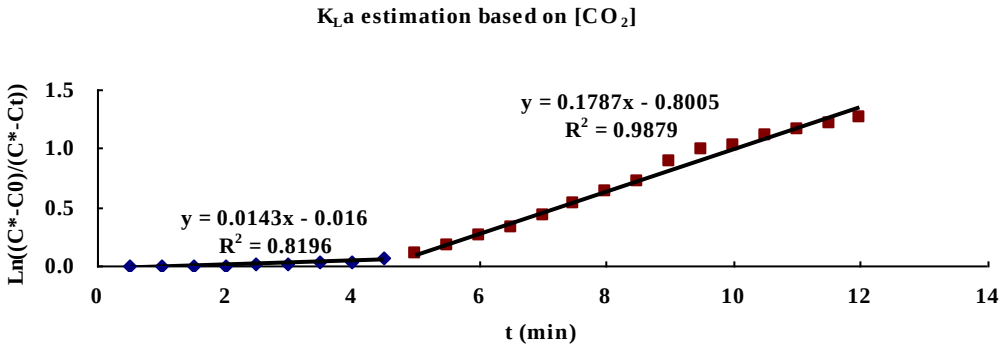

(a)

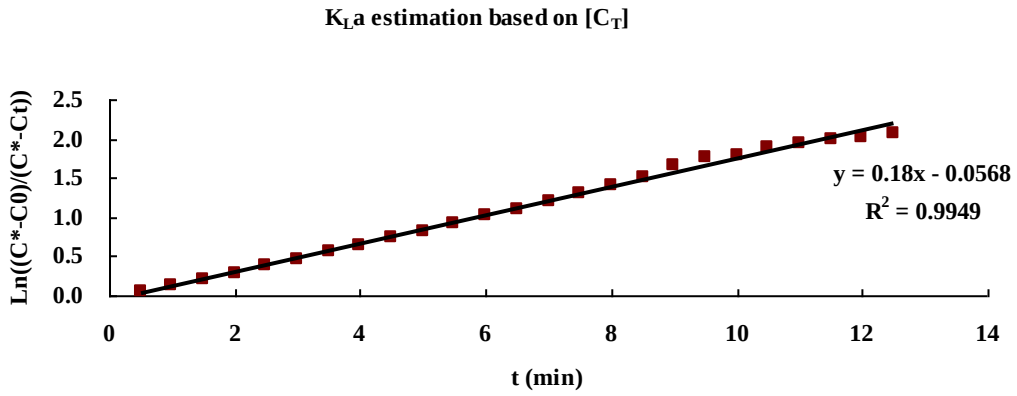

(b)

Figure 4.10: Typical plot for K_La estimation (for 0.7 L min^{-1} dosing), where the slope of straight line indicates K_La (min^{-1}). (a) The estimation of K_La based on [CO_2]; (b) The estimation of K_La based on [C_T]

Table 4.1: An example of calculations leading to the K_La for CO_2 dissolution (for 0.7 L min^{-1} dosing) The concentration of $[CO_2]$ and the total carbon $[C_T]$ was calculated by Eq. 3.2 and Eq.3.9, respectively.

Time		Estimation based on $[CO_2]$			Estimation based on $[C_T]$		
min	pH	$[CO_2]$ 10^{-6} mol L^{-1}	$\ln\frac{C^*-C_0}{C^*-C_t}$	K_La min^{-1}	$[C_T]$ 10^{-3} mol L^{-1}	$\ln\frac{C^*-C_0}{C^*-C_t}$	K_La min^{-1}
0	9.554	6.12			10.5		
0.5	9.498	7.17	0.0010		10.6	0.0556	
1	9.418	8.94	0.0026		10.8	0.1337	
1.5	9.332	11.3	0.0047		11.0	0.2144	
2	9.244	14.2	0.0074	0.0140	11.1	0.2926	0.18
2.5	9.131	19.0	0.0118		11.3	0.3854	
3	9.034	24.2	0.0167		11.4	0.4580	
3.5	8.898	33.9	0.0257		11.6	0.5488	
4	8.725	51.6	0.0424		11.7	0.6482	
4.5	8.565	75.5	0.0656		11.8	0.7289	
5	8.37	120	0.1096		11.9	0.8233	
5.5	8.208	175	0.1675		12.0	0.9100	
6	8.056	249	0.2512		12.1	1.0125	
6.5	7.969	305	0.3190		12.2	1.0880	
7	7.869	384	0.4244		12.2	1.2000	
7.5	7.801	450	0.5205	0.1790	12.3	1.2990	0.18
8	7.741	517	0.6294		12.4	1.4091	
8.5	7.699	570	0.7242		12.4	1.5041	
9	7.643	649	0.8850		12.5	1.6633	
9.5	7.616	690	0.9820		12.6	1.7587	
10	7.606	706	1.0222		12.6	1.7981	

From Table 4.1, the K_La (estimated based on $[CO_2]$) is of different magnitude comparing pH > 8.4 with pH < 8.4. This was observed from each mass transfer test in culture medium with the threshold pH value of 8.4 seen each time.

Considering the dissociation of water into hydrogen (H^+) and hydroxyl (OH^-) ions, when the pH is over 8.4, the concentration of hydroxyl ions will be much greater than that of the hydrogen ions ($[OH^-]<<[H^+]$). The $[H^+]$ produced when CO_2 dissolves will be neutralized by $[OH^-]$ present in the medium. Considering the carbonate equilibrium system (Eq. 4.12) (Corfield 2008), this will result in less dissolved CO_2 and instead, more HCO_3^-. Stemler (1980) also noted the effect of pH on the amount of dissolved CO_2 and discusses the effect of pH on the relative levels of CO_2 and HCO_3^- present within a solution. He found that in going from pH 8.0 to 7.3, the amount of HCO_3^- changed very little while the concentration of CO_2, on the other hand, increased more than 4-fold.

$$CO_{2(gas)} + H_2O \leftrightarrow H_2CO_{3(aq)} \leftrightarrow H^+_{(aq)} + HCO_3^-{}_{(aq)} \leftrightarrow 2H^+_{(aq)} + CO_3^{2-}{}_{(aq)} \quad \text{Eq. 4.12}$$

Therefore, in theory, the mass transfer rate should be greater when pH > 8.4, as the lower $[CO_2]_t$ will result in a greater driven force '$[CO_2]^*$- $[CO_2]_t$' for CO_2 mass transfer. However, according to the K_La (estimated based on the changes in dissolved CO_2 concentration), the mass transfer is lower that it should be when pH > 8.4. Hence, it can be argued that estimating the K_La based on the changes in only $[CO_2]$ is inappropriate when pH > 8.4, as most of the CO_2 transferred into the liquid exists in the forms of bicarbonate species. The total carbon ($[C_T]$), instead of $[CO_2]$, should be used for K_La estimation when pH > 8.4. As can be seen from either Figure 4.10 b or Table 4.1, the K_La estimated based on $[C_T]$ is consistent when pH > 8.4 and pH < 8.4. When pH < 8.4, the changes in the amount of total carbon are almost equal to the changes in dissolved CO_2, so it is fair to estimate the K_La based on either $[CO_2]$ or $[C_T]$. Table 4.1 also shows that

the $K_L a$ estimated based on $[CO_2]$ is almost the same as the one estimated based on $[C_T]$ when pH < 8.4. In total, from the five repetitive mass transfer tests in *D. salina* culture with 0.7 L min^{-1} of 5% CO_2 gas dosing, the $K_L a$ for CO_2 dissolution was found to be 0.174 ± 0.008 min^{-1}. The plot of each test is attached in the Appendix 4.

Comparing both CO_2 mass transfer under 0.7 L min^{-1} of dosing for water containing $NaHCO_3$ and the culture medium including microalgae (with the same concentration of $NaHCO_3$), the $K_L a$ in water (0.253 min^{-1}) was found to be greater than the one in the presence of *D. salina* (0.174 min^{-1}). That may be because the cells in the medium increased its viscosity, which could have reduced the diffusivity of CO_2 from liquid film to liquid phase. Hence the rate of CO_2 diffusion into the culture was slowed down, whilst without *D. salina* present the CO_2 could diffuse much easier through the medium. Also, because of the changes in liquid properties, the CO_2 equilibrium concentration $[CO_2]^*$ was slightly smaller in the culture (0.0011 ± 0.0001 mol L^{-1}) than that in the $NaHCO_3$ medium (0.0017 ± 0.0001 mol L^{-1}).

4.4 Conclusions

For the same bubble generation method, enhancing the gas dosing flowrate can increase the $K_L a$. For the same bubbling flowrate, reducing the bubble size can lead to an improvement in $K_L a$ as well. Compared with fine-bubble dosing, microbubbles dosing of 5% CO_2 gas by using fluidic oscillator has been proved to enhance the $K_L a$ for both CO_2 dissolution and O_2 removal by 30 – 100% across a meaningful range of flow rates. Despite that $K_L a$ can be enhanced by either increasing the dosing flowrate (to be more accurate, flowrate/liquid volume ratio) or reducing the bubble size, increasing flow rate to achieve a higher $K_L a$ would also raise the amount of CO_2 being wasted (not dissolved) which would ultimately lower the CO_2 capture efficiency. Therefore, in order to achieve both higher CO_2 mass transfer rate and capture efficiency for the

improvement of microalgal growth and CO_2 sequestration, reducing bubble size (e.g. using microbubbles) is more promising than increasing flow rate.

The K_La for CO_2 dissolution was not affected by the presence of $NaHCO_3$, and $NaHCO_3$ could be used to control the equilibrium pH of the medium without affecting the $[CO_2]^*$ and K_La. The pH region can also be altered depending on the particular strain of microalgae being cultured, as different algae prefer different pH.

In the real algal culture, due to the changes in liquid properties and carbon system equilibrium relations, the K_La as well as $[CO_2]^*$ was found slightly reduced compared to the values in water, and if the pH is more than 8.4, K_La should be estimated based on $[C_T]$ instead of $[CO_2]$.

Future work needs to be done to test the effect of different percentages of CO_2 in the gas supply on mass transfer. A mathematical model correlating mass transfer to bubble size, flow rate/liquid volume ratio and percentage of CO_2 in the gas supply etc. is expected to be established, which could facilitate the estimation of CO_2 dosing time for microalgae culture.

Chapter 5: Growth enhancement of *Dunaliella salina* by microbubble induced airlift bioreactor

Zimmerman *et al.* (2011b) have recently conducted a pilot scale trial using flue gas from a Tata Steel plant to culture *D. salina* in a 2200 L microbubble driven airlift bioreactor (see Appendix for the full text). The results indicate that despite the high concentration of CO_2 (about 23%) and trace impurities in the flue gas, microalgae still grew exponentially with a specific CO_2 uptake rate of 0.1 g L^{-1} h^{-1} achieved. The feasibility of using microbubble driven ALB for *D. salina* culture and CO2 capture was proved. However, due to limitations at the Tata Steel site, the comparison of growth between microbubble driven ALB culture and conventional ALB culture was not investigated.

In this chapter (see also Ying et al., 2013a), the efficiency of a novel microalgal culture system (an airlift loop bioreactor [ALB] engaged with a fluidic oscillator to produce microbubbles) is compared with both a conventional ALB (producing fine bubbles without the fluidic oscillator) and non-aerated flask culture. The impact of CO2 mass transfer on *salina* growth is assessed, through varying the gas (5% CO2, 95% N2) dosing flow rate. Each reactor was dosed with 5% CO_2 for 30 min every day. The results showed that approximately 6 - 8 times higher chlorophyll content was achieved in the aerated ALB cultures than in the non-aerated flasks, and there was a 20% - 40% increase in specific growth rate of *D. salina* in the novel ALB with microbubbles when compared with the conventional ALB cultures. The increase in chlorophyll content was found to be proportional to the total amount of CO2 mass transfer. For the same dosing time and flow rate, higher CO2 mass transfer rate (microbubble dosing) resulted in a greater growth rate.

5.1 Introduction

Microalgae have been considered for CO_2 capture from flue gas by many industries recently, due to their high CO_2 uptake efficiencies which are one order of magnitude (10 to 50 times) higher than those of terrestrial plants (Li, et al., 2008). Industry is one of the major CO_2 producers and fossil fuel consumers, responsible for more than 7% of total world CO_2 emissions (Sakai et al., 1995), while the flue gas produced, containing various percentages of CO_2, actually can provide a carbon-rich source for microalgae cultivation. Some microalgae species show a good tolerance to NO_x/SO_x, and can even capture them as nutrients for growth (Matsumoto et al., 1997; Nagase et al., 1998). The products from microalgae culture can be used as food, animal feed, fertilizers, valuable chemicals and as a source of biofuel production etc. (Chelf et al., 1993; Borowitzka & Borowitzka, 1988). These high value commercial products can be expected to offset the capital and operating costs.

Many studies have demonstrated the correlation between light intensity and algal productivity based on the assumption of unlimited CO_2 supply, however, in practice CO_2 mass transfer was always limited due to conventional bubble dosing (see also Chapter 2). Since an energy efficient microbubble dosing system has been developed (Zimmerman et al., 2011a) and proved to have a relatively higher K_La than normal bubble dosing (Al-Mashhadani et al., 2011; Ying et al., 2013b), the same level of dissolved CO_2 concentration can be achieved at relatively lower dosing flow rate, consequently, considerable energy saving will be made along with higher productivity. To further study the impact of microbubbles produced by fluidic oscillation, a range of ALB bench cultures of *D. salina* were set up to discover 1) the contrast between aerated ALB cultures and non-aerated flask cultures, 2) the difference between microbubble dosing and fine-bubble dosing and 3) the correlation between mass transfer and *D. salina* growth.

5.2 Materials and Methods

5.2.1 Design of Lab Scale Airlift Loop Bioreactor (ALB)

Zimmerman et al. (2009) introduced the design of the microbubble mediated ALB for a large lab scale 250 L volume. To further study the impact of using innovative ALB on microalgal cultivation, twelve 3 L-ALBs were made for screening purposes, based on a similar design. Figure 5.1 shows the configuration of a 3 L-ALB. Generally, the bioreactor is made of acrylic material, with dimensions of 285 mm in height and 124 mm in diameter. The air lift loop design consists of a ceramic diffuser (diameter of 78 mm, pore size of 20 μm) fixed at bottom and an internal draught tube (H: 170 mm, D: 95 mm) hung 30 mm above the diffuser. The flow pattern of airlift loop has been discussed in detail in previous studies (Al-Mashhadani et al., 2011; Zimmerman et al., 2009; Zimmerman et al., 2011b).

5.2.2 Experimental methods

The experimental setup for lab bench ALB cultures is shown in Figure 5.2. Generally, twelve ALBs were arranged into two rows. Each row contains a flask culture and five ALB cultures under different dosing conditions (0.3 L min^{-1}, 0.5 L min^{-1}, 0.7 L min^{-1}, 0.9 L min^{-1} and 1.1 L min^{-1}, all under 1 atm pressure). For each ALB culture flow rate was monitored through the rotameter directly connected to the output port of ALB. For the five ALBs connected to a fluidic oscillator (FO) CO_2 was dosed through microbubbles (d_{32} = 388 μm), while another five ALBs were dosed with fine-bubbles (d_{32} = 719 μm). The two flask cultures (without gas dosing) were run in parallel for error estimates. Two fluorescent lamps, one per each row, provided continuous illumination of 90 μmol m^{-2} s^{-1}. The temperature for each culture was maintained around 24 ℃, due to the empirical heat transfer from the fluorescent lamps (24 hrs illumination). The algal species for this study was *Dunaliella salina* (Zimmerman et al., 2011b),

which has a wide pH range from 6 to 9. The strain was obtained from the Culture Centre of Algae and Protozoa, SAMS, Oban, UK as CCAP 19/30. The unbuffered culture medium i.e. without 20 mM HEPES buffer, is shown in Table 5.1.

D. salina was pre-cultured (100 ml in 250 ml flasks) in a growth room (25 ± 2 ℃, light intensity 50 μmol m^{-2} s^{-1}) in a similar culture medium, but with added HEPES (20 mM) as a buffer (pH 7.5). At the beginning of the main experiments, 50 ml of pre-cultured *D. salina* was added to 2.5 L of fresh culture medium for each culture. Each ALB culture was dosed with CO_2 enriched gas (5% CO_2, 95% N_2) for 30 minutes per day. 50 ml algal samples were taken after gas dosing or mixing (for flask cultures), followed by topping up the culture with 50 ml of fresh medium. pH and DO levels in each of the bioreactors were measured daily before and after gas dosing using a SevenGo Duo Pro pH/DO meter.

The chlorophyll content of the samples of *D. salina* culture taken each day was determined by measuring the optical density at wavelengths of 645 nm and 663 nm using the method described by Zimmerman et al. (2011b) (Chapter 3). The overall specific growth rate was estimated from the slope of a semilog plot of $\ln(C_t/C_0)$ versus t (Chapter 3). The dissolved CO_2 concentration in the medium was calculated from the pH reading using Eq. 3.2, of which the detailed derivation is shown in Chapter 3. Each day, the difference between the concentration of dissolved CO_2 before and after dosing, calculated based on the pH, indicates the amount of CO_2 that has been transferred into the medium (dosed CO_2). The reading taken the following day before dosing indicates the decrease in the dissolved CO_2 and gives the amount of CO_2 uptake by *D. salina.*

$$[CO_2] = \frac{(10^{-pH} - 10^{(pH-14)} + \Delta[Na^+])10^{(-2\,pH)}}{10^{(-6.381-pH)} + 2\times 10^{(-16.758)}} \quad (mol/L) \qquad \text{Eq. 3.2}$$

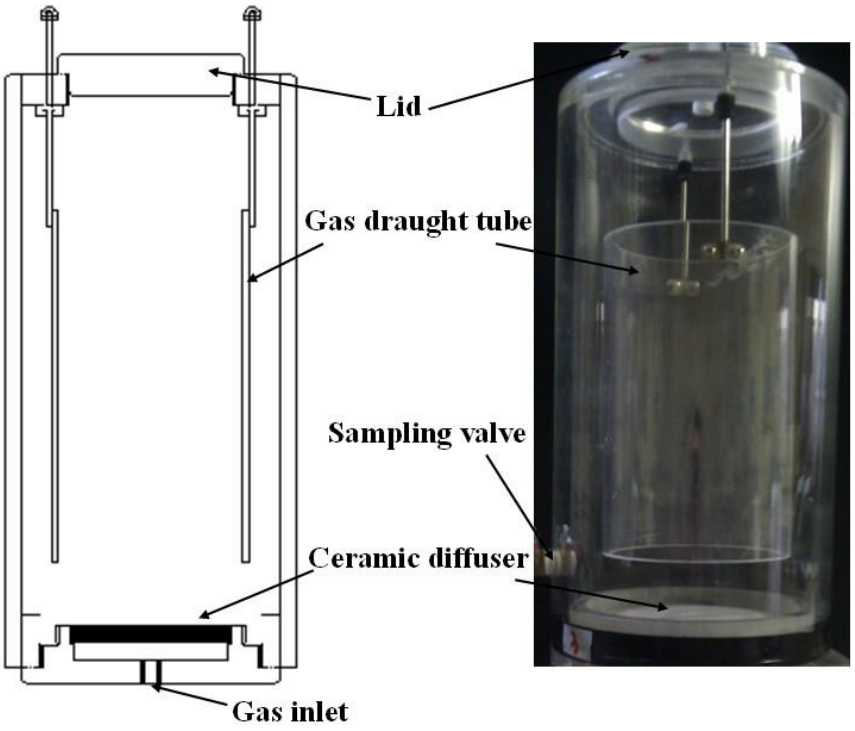

Figure 5.1: The structure of a 3 L airlift loop bioreactor

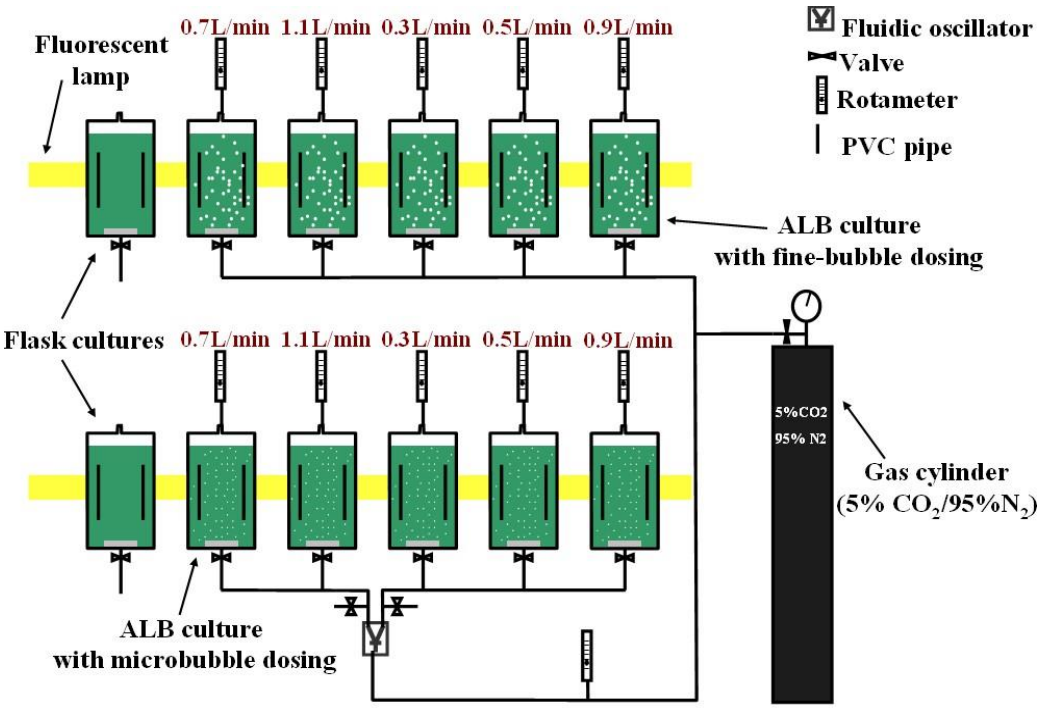

Figure 5.2: Schematic setup of ALB cultures.

Table 5.1: *D. salina* culture medium.

Composition of growth medium
1.5 M NaCl; 10 mM KCl; 20 mM $MgCl_2$; 10 mM $CaCl_2$; 24 mM $MgSO_4$; 5 mM $NaNO_3$; 0.1 mM NaH_2PO_4; 0.0015 mM FeEDTA; 2.38 mM $NaHCO_3$; 0.185 mM H_3BO_3; 0.007 mM $MnSO_4$; 0.8×10^{-3} mM $ZnCl_2$; 0.2×10^{-4} mM $CoCl_2$; 0.2×10^{-6} mM $CuCl_2$

5.3 Results and Discussion

5.3.1 Comparisons between ALB Culture and Conventional Flask Culture

5.3.1.1 Chlorophyll Content

Figure 5.3 gives the plot of chlorophyll content versus culture time for ALB cultures and flask cultures. Generally, the *D. salina* cells cultured in ALB, either with or without fluidic oscillator engaged, were growing faster compared with the flask culture. As can be seen in Figure 5.3, for the flask culture, without daily gas supply the microalgae were growing relatively slowly, with the chlorophyll content increasing from about 0.15 mg L^{-1} to eventually 4.30 mg L^{-1} through 18 days. In contrast, the algal chlorophyll content in all ALB cultures increased from the similar initial concentration to an even higher point (4.73 – 7.24 mg L^{-1}) within only 6 days. For these ALB cultures, the active growth phase started from the third day and lasted about 13 days, with the peak varying from 26.43 to 32.65 mg L^{-1} (depending on flow rate and dosing method). Entry into stationary phase was observed after about 15 days. In general, about 6 – 8 times higher chlorophyll content was achieved in ALB cultures than in the flask cultures for the same culture period. It is easily understood that the ALB engaged with micro-bubble/fine-bubble dosing enables a high mass transfer of CO_2 dissolution and O_2 removal, which makes the culture both CO_2 sufficient and O_2 stripped,

therefore, algae grew better in such 'well served' circumstances. Zimmerman et al. (Zimmerman et al., 2011b) demonstrated a pilot scale microalgal culture using a similar design of ALB as in this study, the results also showed that such ALB culture was neither CO_2 limited nor O_2 inhibited, which led to a high algal growth rate.

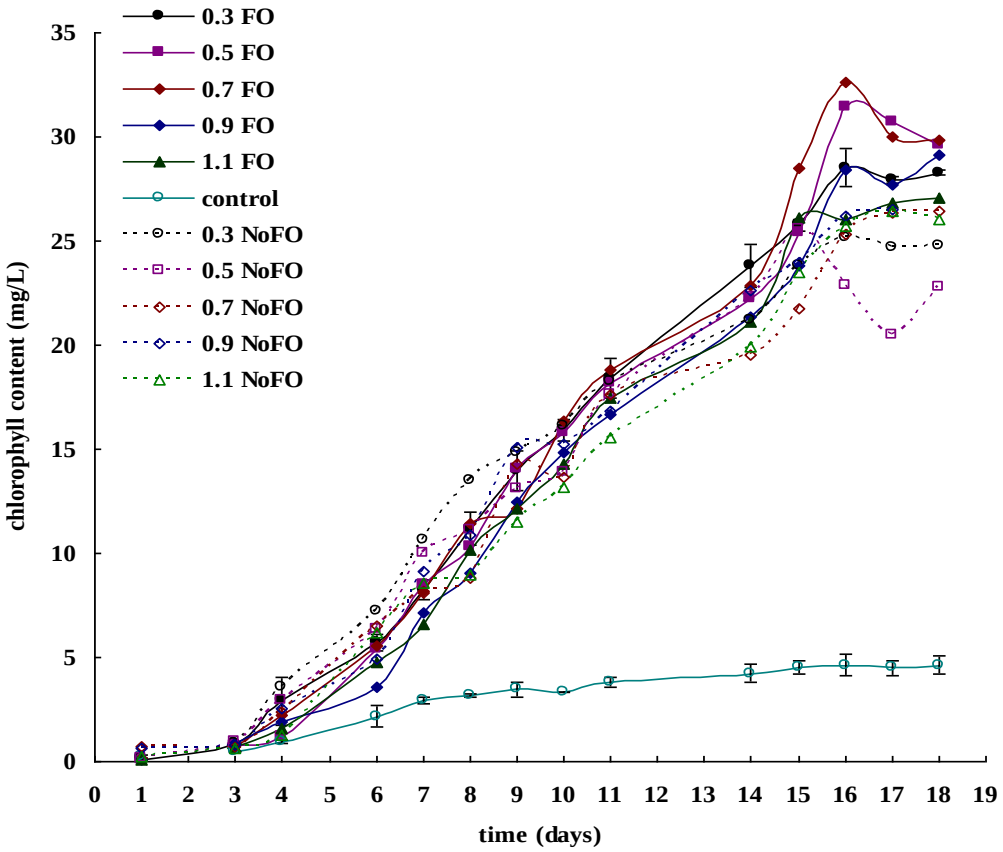

Figure 5.3: *D. salina* growth in ALBs and in flasks. FO stands for the culture with fluidic oscillator, NoFO represents the culture without oscillator, and 'control' means the control experiment (the flask cultures). The number in front of these abbreviations indicates the dosing flow rate (e.g. 0.3 stands for 0.3 L $min^{-1}$of dosing flow rate). Due to the laboratory limitations, only the control experiment and the culture dosed under 0.3 L min^{-1} using oscillator were repeated, with the error bars shown in the diagram. From day 6 to day 16, each culture was considered to be in the log growth phase, this part of the data was used to calculate the specific growth rate of each culture.

5.3.1.2 pH Changes

Apart from the relatively higher CO_2 mass transfer and an appreciable O_2 stripping by 'micro/fine-bubbling', a better pH control is also one of the reasons that explain why ALB cultures exceeded the flask cultures in productivity. Commonly, pH in the culture medium increases as the algae grows, and when the pH increases beyond the optimum range, the culture may be adversely affected. As algae grow, the photosynthetic uptake of CO_2 leads to the increase in pH, but as a consequence of increasing pH, CO_3^{2-} increases while HCO_3^- and CO_2 decrease, which inhibits the photosynthetic reaction and improves the rate of algal respiration. Therefore, for many algal cultures, either buffer solutions (e.g. HEPES) are usually included in culture medium or acid is added when pH increases over a suitable level via an auto-controlled system. However, in this study, neither buffer solution nor acid is added, because it was expected that the increasing pH could be neutralized by daily CO_2 supply via microbubble dosing technique, and indeed the results strongly supported this hypothesis.

Figure 5.4 shows the daily pH changes in ALB cultures (either with or without fluidic oscillator) and in control experiment (flask cultures). For control experiment, because of the absence of CO_2 supply and the accumulation of O_2, *D. salina* grew relatively slowly in the first 9 days, with its chlorophyll content increased from 0.15 mg L^{-1} to only 3.04 mg L^{-1} (Figure 5.3). Correspondingly, its pH also increased slowly, rising from 7.9 to 9.1 through the first 9 days (Figure 5.4). However, after 9 days the pH barely increased and was maintained at 9.1-9.5, whilst the algae almost stopped growing as well, with its chlorophyll content maintained at 3.04 - 3.33 mg L^{-1}. One of the possible reasons is that, after pH went above 9 the culture was inhibited. In terms of ALB cultures (FO engaged or not), chlorophyll increased dramatically (from around 0.05-0.15 mg L^{-1} to 26.43 – 32.65 mg L^{-1}) until the growth entered steady phase (the last 3 days) (Figure 5.8). Correspondingly, pH was expected to rise even faster than

control culture, however, due to daily micro-bubble or fine-bubble dosing, the culture pH was maintained in a suitable range of 6.5-8.5 (Figure 5.4). As can be seen, for each day, after 30 min of 5% CO_2 dosing, pH was reduced to around 7, but because of the desirable culture condition (CO_2 unlimited and O_2 free), pH increased back to about 8 to 8.5 within only one day. The next day, another 30 min of dosing dragged it back to around 6.5 to 7 again. Such a virtuous cycle kept pH within a desirable range, making the culture also not limited by pH.

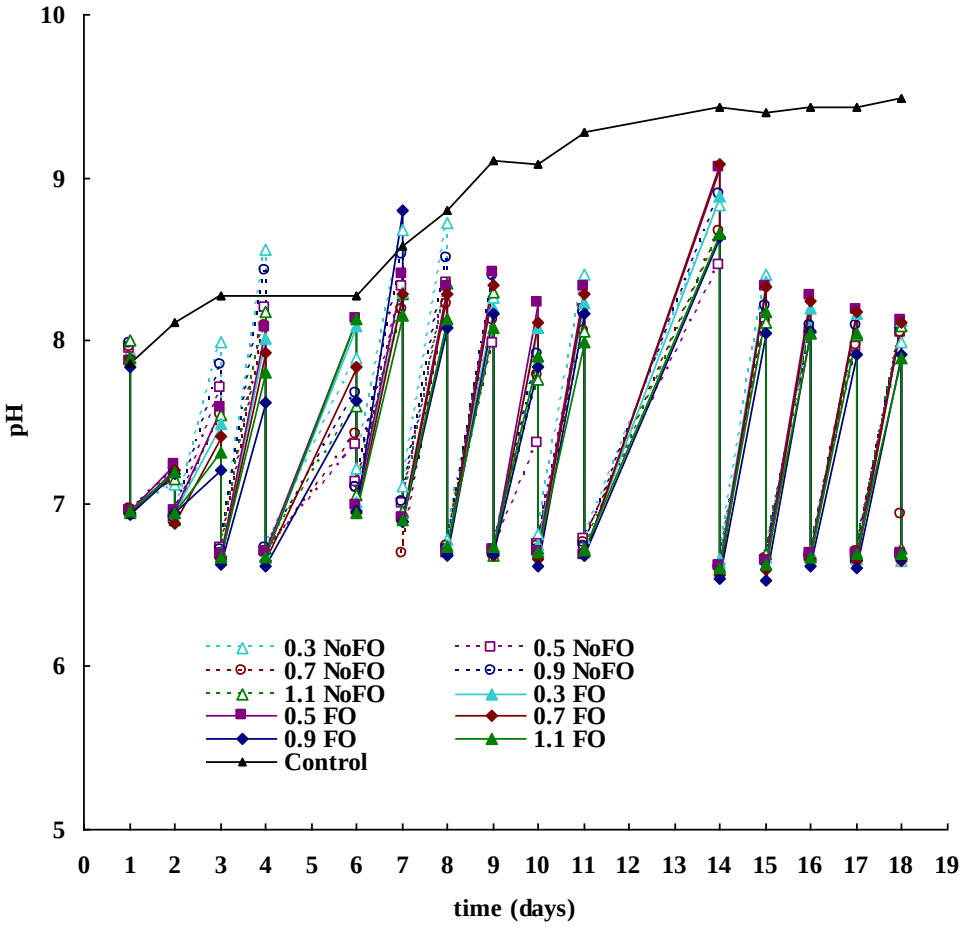

Figure 5.4: Plot of pH changes versus culture time for ALB cultures and control culture. For ALB cultures (either with or without fluidic oscillator), there are two pH values per day, a higher one and a lower one, representing the pH value before and after CO_2 dosing, respectively. Due to the lab limitations, only two pH measurements were taken per day.

One thing needs to be clarified that for all ALB cultures in this study, the pH value seems to be similar despite the different dosing flow rates or dosing methods. But theoretically, for various dosing conditions with different mass transfer capabilities, the dissolved CO_2 in the culture medium differs, correspondingly, the pH value indicating the amount of dissolved CO_2 differs as well. Such a 'contradiction' can be explained by Table 5.2. As can be seen, one magnitude of difference in the concentration (mol/L) of dissolved CO_2 only changes the pH by one unit, while the difference in the total CO_2 mass transfers (daily) for this study are in the range of 10^{-4} to10^{-3} mol/L, for different dosing conditions. Therefore, the difference in the pH value was barely affected by the different mass transfer capabilities. This also supports the hypothesis that the pH was scientifically controlled in the study, and it can be considered as a controlled parameter when comparing the impact of mass transfer on the algal growth (see 5.3.2).

Table 5.2: The corresponding dissolved CO_2 for different pH values. The amount of CO_2 was calculated based on Equation (2) and on the particulate $NaHCO_3$ concentration in medium.

pH	$NaHCO_3$ in medium, mol/L	$[CO_2]$, mol/L
6	2.38×10^{-3}	5.7×10^{-3}
7		5.7×10^{-4}
8		5.7×10^{-5}
9		5.3×10^{-6}

5.3.2 Comparisons between FO Engaged ALB Culture and Conventional ALB Culture

5.3.2.1 Effect of Fluidic Oscillator (Comparing Microbubble Dosing with Fine Bubble Dosing)

Figure 5.3 shows the comparison between the ALB cultures with fluidic oscillator engaged and normal ALB culture. Generally, for each dosing flow rate *D. salina* grew better in FO engaged ALBs (microbubble dosing) than in normal ALBs (fine-bubble dosing). The peak chlorophyll content reached 27.03 – 32.65 mg L^{-1} when FO was applied, while only 23.13 – 26.47 mg L^{-1} was achieved without FO. To quantify the comparison of *D. salina* growth under different dosing conditions, the overall specific growth rate was estimated from the slope of a semilog plot of $\ln(C_t/C_0)$ versus time, shown in Appendix 5. Hence the specific growth rate under each ALB dosing condition was obtained, which was plotted in Figure 5.5. Generally, compared with conventional ALB cultures, fluidic oscillator engaged ALB cultures presented a higher algal specific growth rate (μ), showing an approximately 20% - 40% enhancement across a wide range of flowrate. The highest specific growth rate (near 0.13 d^{-1}) for normal ALB culture was achieved at a dosing flow rate of 1.1 L min^{-1}, while the similar specific growth rate for ALB culture (with FO) was achieved at only 0.3 L min^{-1}, which shows an approximately 73% energy saving, in terms of bubbling. The detailed calculation is shown in Appendix 6.

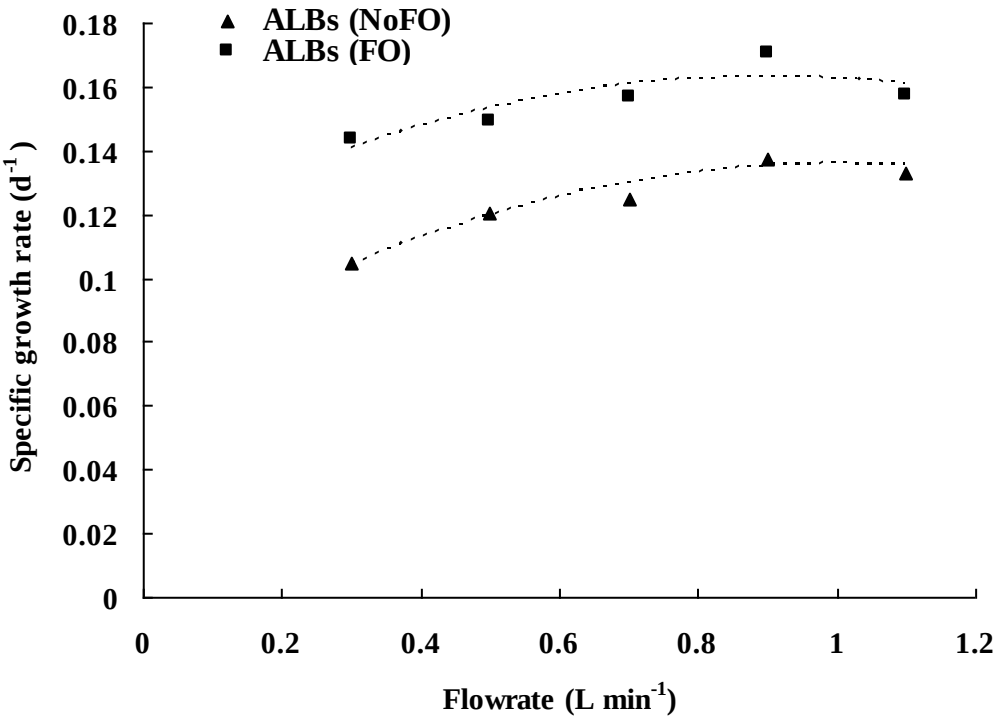

Figure 5.5: Plots correlating the overall specific growth rate with CO_2 dosing flow rate for both ALB cultures with and without fluidic oscillator. In the diagram, 'ALBs FO' represents the ALB cultures with fluidic oscillator while 'ALBs NoFO' means the ALB cultures without fluidic oscillator. Due to the lab limitations, only one culture (0.3 L min^{-1} FO) was duplicated, therefore, error bars were not obtained. Under each flowrate, the enhancement of specific growth rate, comparing 'ALBs FO' with 'ALBs NoFO', can be calculated as: $\frac{\mu(\text{FO}) - \mu(\text{NoFO})}{\mu(\text{NoFO})}$. The overall specific growth rate for each dosing condition was obtained based on the method described in 3.3.4, shown in the figures attached in Appendix 5.

5.3.2.2 Effect of Flow Rate (Comparing the Impact of Different Dosing Flow Rates on *D. salina* Growth)

Generally, the specific growth rate (μ) was found to increase along with dosing flow rate, either with or without FO engaged. The maximum μ of 0.13 d^{-1} and 0.17 d^{-1} was achieved at flow rate of 0.9 L min^{-1} for both without FO and with FO (Figure 5.5). This overall trend was found similar to gas-liquid mass transfer study (See Chapter 4). Considering both algal specific growth rate (Figure 5.5) and K_La (Figure 4.3) under different dosing flow rates, the algal growth appears to be correlated to mass transfer via following hypothesis.

For the ALB cultures with fine-bubble dosing (NoFO), within the flow rate range of 0.3-1.1 L min^{-1}, K_La (either for CO_2 dissolution or O_2 removal) increased with flow rate, and consequently CO_2 dissolution and O_2 stripping efficiency were enhanced. The culture therefore had more dissolved CO_2 available for algal uptake and less O_2 inhibition. Thus, specific growth rate increased as the flow rate went up. The same scenario was observed for the novel ALB cultures (microbubble dosing) under the flow rate of 0.3-0.7 L min^{-1}. However, the specific growth rate did not significantly increase by further increasing the flow rate when it exceeded 0.7 L min^{-1}. This can be explained by assuming that for 0.3-1.1 L min^{-1} of dosing (ALB cultures, NoFO) and 0.3-0.7 L min^{-1} of dosing (ALB cultures, FO), the daily total amount of CO_2 mass transfer (average CO_2 mass transfer rate × dosing time) did not reach or exceed the saturation concentration, therefore higher mass transfer led to a greater amount of available CO_2, which consequently resulted in a higher growth rate. For the flow rate of 0.9-1.1 L min^{-1} with microbubble dosing, the total CO_2 mass transfer is likely to be excessive (average CO_2 mass transfer rate × dosing time > CO_2 saturation). The extra CO_2 was therefore released to the atmosphere and did not contribute to the algal growth. Thus increasing the flow rate over a valid range may not effectively improve the growth. Based on the above discussion, 30 min d^{-1} of

dosing under 0.7 L min^{-1}, close enough to reach CO_2 saturation, turns out to be the optimal dosing condition for the 3 L-ALB culture (with microbubble dosing).

5.3.3 Relation Between CO_2 Mass Transfer and *D. salina* Growth

For the ALB cultures under each condition, the amount of total CO_2 uptake and the increase in the chlorophyll content were calculated for certain culture periods, which are shown in Figure 5.6a. The chlorophyll content increase shown was found commensurate with the amount of CO_2 uptake within the same culture period. It can be simply understood by the basic photosynthetic equation $6CO_2$ (aq) + $12H_2O$ (liq) + photons → $C_6H_{12}O_6$ (aq) + 6 O_2 (g) + 6 H_2O (liq), the amount of algal growth is suggested to be proportional to the CO_2 concentration. An equation describing the relation between chlorophyll increase and CO_2 consumption for the *D. salina* cultures in this study is therefore obtained via linear regression.

$$\Delta[Chl]_{(g/L)} = 2.7034_{(g/mol)} \times \Delta[CO_2]_{uptake(mol/L)} \qquad \text{Eq. 5.1}$$

Therefore, an assumption can be made that in the same time period, the CO_2 uptake rate should be proportional to the algal concentration (chlorophyll content), which is shown as follows:

$$\because \Delta[Chl] = a\Delta[CO_2]_{uptake} \Rightarrow \frac{\Delta[Chl]}{t} = a\frac{\Delta[CO_2]_{uptake}}{t} \Leftrightarrow v_{Chl} = av_{CO_{2uptake}}$$

$$v_{Chl} = \frac{d[Chl]}{dt} = \mu \times [Chl] \quad ,$$

$$\therefore \quad av_{CO_{2uptake}} = \mu \times [Chl] \Rightarrow v_{CO_{2uptake}} = \frac{\mu}{a}[Chl]$$

where μ is the overall specific growth rate (constant for a particular culture condition); v_{Chl} and $v_{CO2\ uptake}$ represent chlorophyll growth rate and CO_2 uptake rate, respectively; [Chl] and [CO_2] mean the chlorophyll content and CO_2 concentration, separately.

(a)

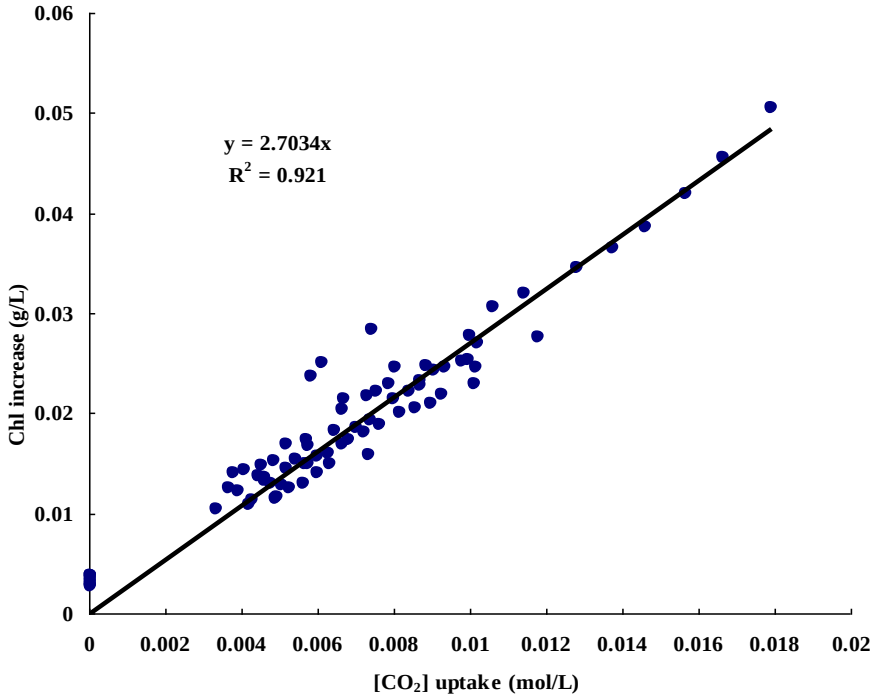
y = 2.7034x
R2 = 0.921
Chl increase (g/L)
[CO2] uptake (mol/L)
0.06
0.05
0.04
0.03
0.02
0.01
0
0
0.002
0.004
0.006
0.008
0.01
0.012
0.014
0.016
0.018
0.02

(b)

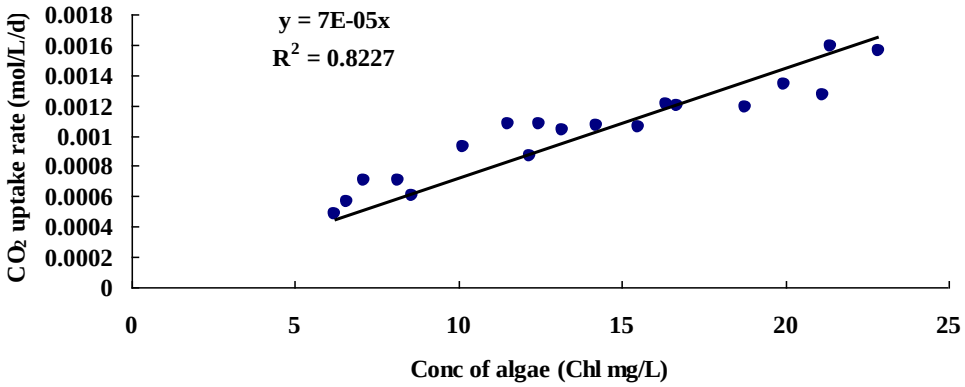
y = 7E-05x
R2 = 0.8227
CO2 uptake rate (mol/L/d)
Conc of algae (Chl mg/L)
0.0018
0.0016
0.0014
0.0012
0.001
0.0008
0.0006
0.0004
0.0002
0
0
5
10
15
20
25

(c)

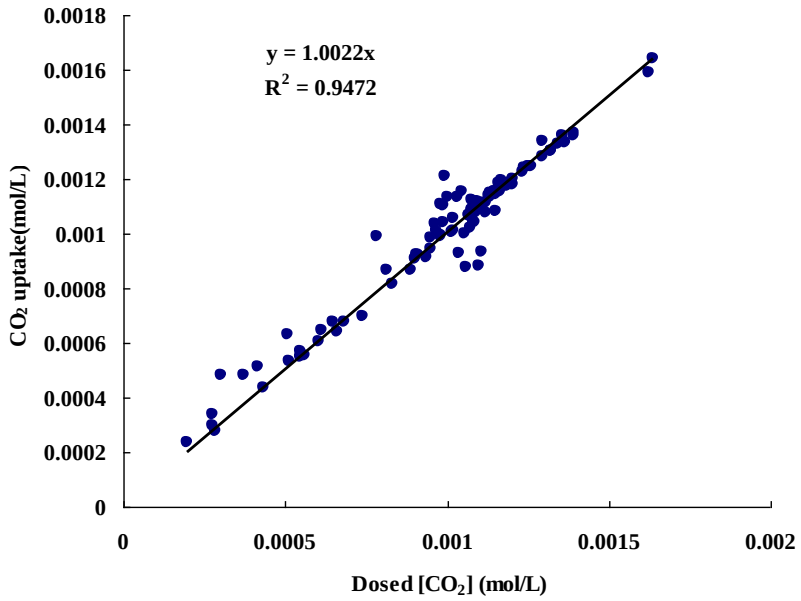

Figure 5.6: (a) The relation between CO_2 uptake and algal growth (based on chlorophyll increase); (b) Plot of CO_2 uptake versus concentration of chlorophyll content; (c) Plot of CO_2 uptake versus CO_2 input. [(a)] For each dosing condition, the total amount of chlorophyll content increase within X days (day1-dayX) was represented in Y-axis, and the total amount of CO_2 uptake within X days was represented in X-axis. X was taken as 6, 7, 8, 9 and 10. [(b)] The data come from the ALB cultures with microbubble dosing under 0.7 L min^{-1}, 0.9 L min^{-1} and 1.1 L min^{-1}, for which the daily CO_2 dosing were excessive (average CO_2 mass transfer rate × dosing time >= CO_2 saturation). [(c)] The amount of dissolved CO_2 in the medium was calculated based on pH (Eq. 3.2). For each day, the changes in the amount of dissolved CO_2 before and after dosing indicate the valid dosed [CO_2]. Till the following day before dosing, the decrease in the amount of [CO_2] gives the amount of CO_2 uptake by the algae. Data come from the ALB cultures with bubble dosing which did not exceed the valid range (average CO_2 mass transfer rate × dosing time < CO_2 saturation), including all the ALB cultures with fine bubble dosing and the ALB cultures with microbubble dosing at 0.3, 0.5, 0.7 L min^{-1}.

Indeed, the experimental data, shown in Figure 5.6b, strongly support this assumption. The daily CO_2 uptake rate is in direct proportion to the concentration of chlorophyll content, of which the equation is shown as

$$\nu_{CO_{2uptake}(mol/L/d)} = 7\times10^{-5}{}_{(mol/mg(chl)/d)} \times [Chl]_{(mg/L)}. \qquad \text{Eq. 5.2}$$

In order to correlate the algal growth to CO_2 mass transfer, the correlations between the amount of CO_2 uptake and the CO_2 transferred to the liquid still needs to be understood, which is presented in Figure 5.6c. As can be seen, the amount of daily CO_2 uptake was equal to the valid amount of CO_2 dosed, which can be described as:

$$\Delta[CO_2]_{uptake} = \Delta[CO_2]_{dosed} = \nu'_{MTR} \cdot t_{dosing}, \qquad \text{Eq. 5.3}$$

where ν'_{MTR} represents CO_2 average mass transfer rate; t_{dosing} means the dosing time.

By combining Eq. 5.1 and Eq. 5.3, it gives

$$\Delta[Chl]_{(g/L)} = 2.7034_{(g/mol)} \cdot \nu'_{MTR(mol/L/\min)} \cdot t_{dosing(\min)}. \qquad \text{Eq. 5.4}$$

From Eq. 5.4, the chlorophyll content increase has been shown to be in direct proportion to the mass transfer rate for the ALB cultures in this study, which again explains why the ALB cultures with microbubble dosing have higher growth rates than the ones with fine-bubble dosing.

5.4 Conclusions

6 to 8 fold higher chlorophyll content was found in ALB cultures, compared with the flask incubation. Instead of buffer solution (e.g. HEPES), daily 30 minutes of 5% CO_2 gas dosing maintained pH at a suitable level (6.5-8.5). Approximately 20% - 40% increase in specific growth rate was found in the FO engaged ALB cultures, over a wide range of gas dosing flow rate. Furthermore, the chlorophyll content (growth) was found to be directly proportional to the mass transfer rate for *D. salina* ALB cultures. Further modelling of these observations has been carried out (see Chapter 6).

Chapter 6: Periodical CO_2 dosing strategy for *Dunaliella salina* batch culture

From Ying et al. (2013a), the microalga (*Dunaliella salina* 19/30) thrived on only 30 min/day of gas dosing (5% CO_2/95% N_2) provided by either microbubbles or fine-bubbles. The relationship between CO_2 uptake and *D. salina* was found. In this chapter, the aspect of CO_2 dosing (involving dosing time determination, dosing interval determination and pH control etc.) was particularly studied. A periodic CO_2 dosing strategy was proposed for optimal algal (*D. salina*) biomass production and CO_2 sequestration. The model of periodic CO_2 dosing including dosing time calculation, dosing interval estimation and final biomass yield prediction was established. Experimentally, 5% CO_2/95% N_2 gas was periodically dosed into *D. salina* culture. Two different gas dosing conditions were tested. By applying the periodic dosing model, the daily pH was kept at the target range without adding expensive buffers. Notably the culture dosed periodically was seen to have the similar growth to the culture supplied constantly, but with much higher CO_2 capture efficiency (10 - 20%) compared to continuous dosing (0.25%). It shows a great potential for using periodic gas supply to reduce cost, wasted gas and energy use.

6.1 Introduction

In order to improve the algal biomass productivity and CO_2 capture efficiency, an innovative CO_2 dosing technology ('microbubbling') was studied by Ying et al. (2013 a & b). The CO_2 'microbubbling' technology was proved having a greater mass transfer and can lead to a higher microalgal growth rate. Nonetheless, the operational parameters (e.g. dosing time, dosing interval, flowrate etc.) for 'microbubbling' still need to be engineered. In this chapter, an optimal periodic CO_2 dosing strategy is proposed and a model established based on *D. salina* (19/30) cultures. The main hypothesis for this study is that by using a

microbubble driven airlift bioreactor, high mass transfer can be attained in a culture by supplying gas periodically (with little CO_2 wasted and less energy cost) and achieve similar algal growth compared to when the gas is supplied continuously.

6.2 Model of periodical CO_2 dosing

For an optimal periodical dosing strategy, three major principles need to be followed. Firstly, despite the exclusion of buffer solution and pH auto-regulating system, the pH of the culture needs to be controlled in a suitable range by periodic CO_2 dosing. Secondly, the dosing time should only be long enough for CO_2 to reach its equilibrium concentration. Meanwhile, the equilibrium pH (corresponding to CO_2 equilibrium concentration) is expected to be the lower limit of the suitable pH range for the microalgal species being utilized. Thirdly, the time period without dosing (dosing interval) should ensure that the microalgae use up the dosed CO_2, whilst ensuring that the pH increase to the upper limit is within the suitable pH range. Following these three principles, a culture with periodic dosing, compared to one with continuous dosing, should have sufficient (but not excess) CO_2 and an optimal pH range to support optimal growth (achieving similar growth as with continuous dosing), while with minimal amount of CO_2 wasted and less energy input. Based on these three principles, the dosing time, dosing interval and final algal yield can be estimated.

6.2.1 Estimation of dosing time

Assuming the suitable pH range for the culture of a particular microalga species is given between A and B, of which the corresponding concentration of $[CO_2]$ can be calculated by Eq. 3.2. To control the culture in a target pH range the amount of CO_2 needed to be transferred to the medium can simply be estimated as the difference between dissolved CO_2 level at pH=B and pH=A (assuming the CO_2 uptake rate is negligible compared with CO_2 gas-liquid mass transfer rate).

The dosing time is thereby calculated as the amount of CO_2 needed to be transferred to the medium divided by the average CO_2 mass transfer rate, shown in Eq. 6.1, where ν'_{MTR} represents CO_2 average mass transfer rate (mol L^{-1} min^{-1}) and can be calculated as Eq. 4.10. The derivation of Eq. 4.10 was explained in Chapter 4. Finally, assuming the pH before dosing was controlled at B which gives the initial dissolved CO_2 level as $[CO_2]_{pH=B}$, the optimal valid dosing time needed to drop the pH from B to A can then be estimated through Eq. 6.2, which is obtained by combining Eq. 6.1 and Eq. 4.10. As long as the suitable pH range for a particular type of algae is given and the K_La for a certain dosing condition is known, the optimal dosing time can be estimated.

$$t_d = \frac{[CO_2]_{pH=A} - [CO_2]_{pH=B}}{\nu'_{MTR}} \quad \text{Eq. 6.1}$$

$$t_d = \frac{[CO_2]_{pH=A} - [CO_2]_{pH=B}}{K_L a([CO_2]^* - [CO_2]_{pH=B}) - \frac{1}{2} K_L a([CO_2]_A - [CO_2]_{pH=B})} \quad \text{Eq. 6.2}$$

From previous study (Chapter 4), it was found that K_La estimation is more accurate based on the changes in $[C_T]$, especially when pH > 8.4. Therefore, Eq. 6.2 can also be written in terms of $[C_T]$, shown as Eq. 6.3.

$$t_d = \frac{[C_T]_{pH=A} - [C_T]_{pH=B}}{K_L a([C_T]^* - [C_T]_{pH=B}) - \frac{1}{2} K_L a([C_T]_A - [C_T]_{pH=B})} \quad \text{Eq. 6.3}$$

6.2.2 Estimation of dosing interval

The dosing interval here is defined as the time period without gas dosing. During this period, pH increases gradually because of the uptake of CO_2 by microalgae, until the pH achieves the upper limit of the suitable range, then dosing needs to

be started again. Therefore, the effective estimation of dosing interval is crucial for periodic dosing, either too long or too short could cause the pH to exceed the upper or lower limit of the suitable range and adversely affect the algal growth.

The simplest way to estimate the dosing interval is to divide the amount of CO_2 expected to be absorbed by the CO_2 uptake rate. However, the instantaneous growth rate differs with the concentration of the algae (Scragg 1991), which leads to changes in CO_2 uptake rate. Instead of instantaneous CO_2 uptake rate, the average CO_2 uptake rate for the whole active growth period is therefore used to simplify the estimation of dosing interval (Eq. 6.4).

$$t_i = \frac{[CO_2]_{pH=A} - [CO_2]_{pH=B}}{\nu'_{CO2uptake}} \qquad \text{Eq. 6.4}$$

Chapter 4 reported that when the pH was less than 8.4, the changes in the amount of total carbon almost all come from the changes in dissolved CO_2, however, when pH was more than 8.4, the changes in dissolved CO_2 can not fairly represent the CO_2 uptake by algae, as both HCO_3^- and CO_3^{2-} would generate dissolved CO_2 to compensate for the consumption of CO_2. In other words, the amount of CO_2 consumed by algae should be more than the changes in dissolved CO_2, as HCO_3^- and CO_3^{2-} would also contribute to the amount of CO_2 consumption. Therefore, the changes in total carbon [C_T] should be considered instead of the changes in [CO_2]. The [C_T] can be calculated by Eq. 3.9. Eq. 6.4 should be converted into Eq. 6.5. The dosing interval can then be estimated as long as the average CO_2 uptake rate is known.

$$t_i = \frac{\Delta[C_T]}{\nu'_{CO2uptake}} = \frac{[C_T]_{pH=A} - [C_T]_{pH=B}}{\nu'_{CO2uptake}} \qquad \text{Eq. 6.5}$$

Since the periodic dosing strategy is proposed to achieve similar algal growth as when gas is supplied continuously, the average CO_2 uptake rate is assumed to be

the same as in the culture with continuous or excessive CO_2 dosing. According to the information from previous *D. salina* cultures (Chapter 5), the correlations for CO_2 uptake rate versus algal biomass concentration (measured as chlorophyll content) was described by Eq. 5.2 (Ying et al. 2013a), and the relation between total chlorophyll content increase and total CO_2 uptake was given (based on the cultures with excessive gas dosing) as Eq. 5.1 (Ying et al. 2013a).

$$v_{CO_{2uptake}} = 7 \times 10^{-5} \times [Chl] \qquad \text{Eq. 5.2}$$

$$\Delta[Chl] = 2703.4 \times \Delta[CO_2]_{uptake} = 2703.4 \times \Delta[CO_2]_{dosed} \qquad \text{Eq.5.1}$$

For the same time period, Eq. 5.1 can be transformed into Eq. 6.6

$$v'_{Chl} = 2703.4 \times v'_{CO_{2uptake}} \qquad \text{Eq. 6.6}$$

The average CO_2 uptake rate can be fairly described as

$$v'_{CO2uptake} = \int_{t_{c1}}^{t_{c2}} \frac{v_{CO2uptake}}{t_c} dt \qquad \text{Eq. 6.7}$$

Where t_c is the selected culture time period (t_{c2}-t_{c1}), beginning from t_{c1} (the start of log growth phase) and ending by t_{c2} (the end of log growth phase).

Assuming the chlorophyll content ([Chl], mg L^{-1}) is equal to the initial concentration ($[Chl]_0$, mg L^{-1}) plus the amount of its increase ($v'_{Chl} \times t$),

$$[Chl] = [Chl]_0 + v'_{Chl} \cdot t \qquad \text{Eq. 6.8}$$

The average CO_2 uptake rate can then be obtained by solving Eq. 5.2, Eq. 6.6, Eq. 6.7 and Eq. 6.8, which gives

$$v'_{CO2uptake} = \int_{t_{c1}}^{t_{c2}} \frac{7\times10^{-5}([Chl]_0 + 2703.4\cdot v'_{CO2uptake}\cdot t)}{t_c} dt$$

$$= 7\times10^{-5}[Chl]_0 + \frac{t_c}{2}\cdot 7\times10^{-5}\cdot 2703.4\cdot v'_{CO2uptake} \qquad \text{Eq. 6.9}$$

$$\Rightarrow v'_{CO2uptake} = \frac{7\times10^{-5}\cdot[Chl]_0}{1-0.0946\cdot t_c}$$

The dosing interval is then given by

$$t_i = \frac{[C_T]_{pH=A} - [C_T]_{pH=B}}{7\times10^{-5}\cdot[Chl]_0}\cdot(1-0.0946\cdot t_c) \qquad \text{Eq. 6.10}$$

Theoretically the dosing interval is better to be shortened as the algae grows, which may in practice increase the complexity of the time control process. Using a constant dosing interval through the whole log growth period can simplify the operating process. By doing so, one of the major concerns is that the pH level may exceed the upper limit of a target range. However, one magnitude of difference in the concentration (mol L^{-1}) of dissolved CO_2 only changes the pH by one unit (Ying et al. 2013a), while the CO_2 uptake rates for *D. salina* culture are in the range of 10^{-4} to10^{-3} mol L^{-1} d^{-1}, therefore, the pH value may only increase over the upper limit of a target range by no more than 0.1 unit. Plus empirically the target pH range for algal culture can be slightly narrowed down during the dosing interval calculation in order to prevent the pH value exceeding the real upper limit. The second concern is dissolved oxygen accumulation. According to the basic photosynthetic reaction equation, the O_2 generation rate equals to CO_2 uptake rate. Therefore, 10^{-3} mol L^{-1} d^{-1} of CO_2 uptake rate could result in around 32 mg L^{-1} of daily O_2 accumulation (300% over saturation with respect to air), which will diminish the rate of photosynthesis (Richmond, 2008). Thus, the dosing interval has to be limited to no more than 1 day so that DO can be removed by CO_2 dosing in time. In terms of O_2 stripping, it takes less than 10 min to reduce the dissolved oxygen from 32 mg L^{-1} to 0.03 mg L^{-1} by microbubble (d_{32} = 388 μm) dosing of 5% CO_2/95% N_2 under 0.7 L min^{-1},

according to the previous mass transfer study (Chapter 4).

Statistically, from previous *D. salina* studies (Ying et al. 2013a), the active growth phase usually lasted for 8 days (due to the light limitation). According to the literature, *D. salina* can tolerate a pH range of 5.5 to 10 (Borowitzka and Borowitzka. 1988). A target pH range 7.5-9.5 was selected in this study. The dosing interval for *D. salina* cultures was estimated via Eq. 6.10 to give approximately 1.5 d (based on Chl_0 = 5 mg L^{-1} and t_c = 8 d). Conservatively, the dosing interval of 1d was suggested for best results in practice.

6.2.3 Prediction of final concentration of chlorophyll content

Once the dosing time t_d and dosing interval t_i are known, the total dosing time through the culture period t_c can be calculated as: $t_d \times t_c$ / (t_d + t_i). The total amount of CO_2 uptake can be predicted by Eq. 6.11

$$\Delta[CO_2]_{uptake(Total)} = \Delta[CO_2]_{transfered(Total)} = v'_{MTR} \times t_{d(Total)}$$
$$= \frac{K_L a([CO_2]^* - [CO_2]_0)}{\frac{K_L a \cdot t_d}{2} + 1} \times \frac{t_d \cdot t_c}{t_d + t_i} \qquad \text{Eq. 6.11}$$

The final chlorophyll content can be estimated by Eq. 6.12,

$$[Chl] = [Chl]_0 + \Delta[Chl] \qquad \text{Eq. 6.12}$$

By combining Eq. 6.6, Eq. 6.11 and Eq. 6.12, it gives

$$[Chl] = [Chl]_0 + \Delta[Chl] = [Chl]_0 + 2703.4 \times \Delta[CO_2]_{uptake(Total)}$$
$$= [Chl]_0 + 2703.4 \times \frac{K_L a([CO_2]^* - [CO_2]_0)}{\frac{K_L a \cdot t_d}{2} + 1} \times \frac{t_d \cdot t_c}{t_d + t_i} \qquad \text{Eq. 6.13}$$

Eq. 6.11 and Eq. 6.13 are valid only when the dosing time is in a valid range ($v'_{MTR} \times t_d \leqq [CO_2]^*$).

6.3 Methods

A set of *D. salina* batch cultures were carried out to test the hypothesis that sufficient CO_2 can be attained in a culture by 'micro-bubbling' gas periodically (with little CO_2 wasted and less energy cost) whilst similar algal growth can be achieved compared to when the gas is supplied continuously, but with higher CO_2 capture efficiency. Figure 6.1 illustrates the experimental setup.

Samples of the *D. salina* were pre-cultured in shake flask (100 ml culture in 250 ml flasks) in a 25 ± 2℃ growth room. The growth medium composition is identical to the one described in Chapter 5 (Table 5.1). For the start of the main culture, 50 ml of this *D. salina* was added to 2.5 L of fresh culture medium in ALB. The dosing time (t_d) and dosing interval (t_i) were estimated (based on Eq. 6.3 and Eq. 6.10) and applied for the cultures engaged with periodic dosing strategy (No. 2, 4 and 5). pH was measured for each culture daily (for the culture dosed periodically, pH was measured twice per day, before and after dosing). 15 ml of sample for each culture was taken after gas dosing, followed by topping up the culture with 15 ml of fresh medium (For flask cultures, a sterilized glass stick was inserted into the culture for a proper stirring. Samples were taken after that.). The chlorophyll content for each sample was determined by measuring each sample's optical density for wavelengths of 645 nm and 663 nm using the same method to that used in Zimmerman et al. (2011) and Ying et al. (2013a), previously described in Chapter 5.

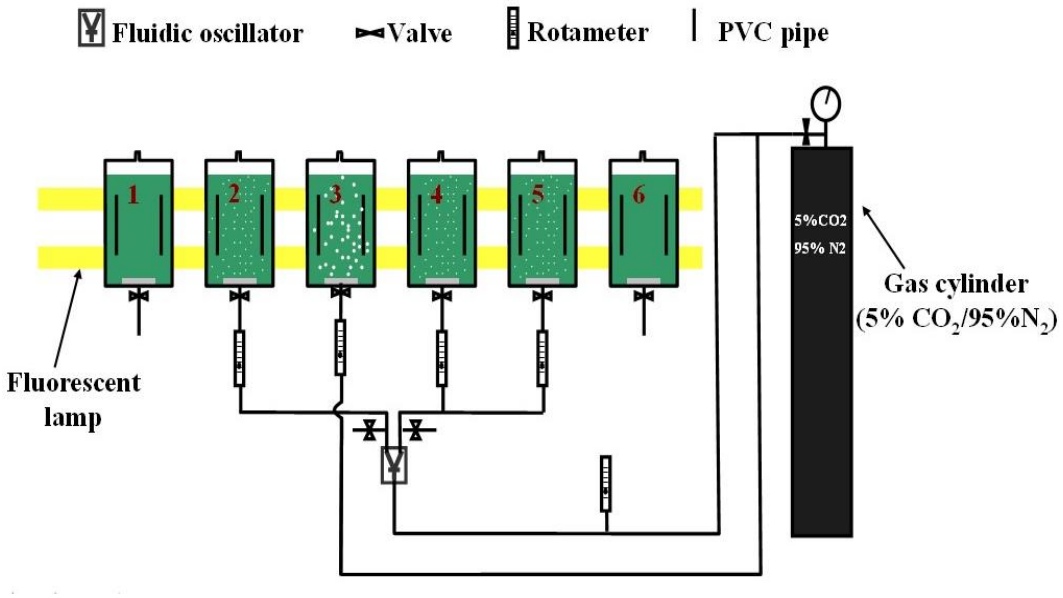

Figure. 6.1: Setup for *D. salina* cultures. Six bioreactors containing *D. salina* cultures (50 ml of inocula to 2.5 L culture medium) were used for this experiment. Two of the six (No.1 and 6) were flask cultures with no CO_2 enriched gas being bubbled through the culture. Like the other four cultures, these control cultures were kept in identical ALBs to ensure that the illumination through these cultures was the same as those being supplied with gas. The remaining four reactors were supplied with CO_2 enriched gas (5% CO_2, 95% N_2). Among them, No. 3 was dosed continuously with fine-bubbles, while No. 2, 4 and 5 were connected to a fluidic oscillator, dosed with mcirobubbles using periodic dosing strategy. No. 2 and 5 were conducted under same dosing condition for error analysis. The detailed dosing conditions for each reactor are listed in Table 6.1. The dosing time selected for each condition was estimated based on Eq. 6.3. The detailed calculation is shown in Appendix 7. The temperature for each culture was maintained at ambient temperature around 24 ℃. Two fluorescent lamps were situated behind all reactors for illumination.

Table 6.1: The dosing conditions for each culture

Reactor	**Dosing conditions**				**Represent**
	Bubbles	**Fluidic oscillator**	**Dosing flowrate**	**Dosing time** (Eq. 6.3)	
No. 1	n/a	n/a	0	0	Flask culture
No. 2	Microbubble (d_{32}: 388 μm)	Engaged	0.7 L min^{-1}	10 min d^{-1}	Periodic dosing
No. 3	Fine-bubble (d_{32}: 719 μm)	n/a	0.3 L min^{-1}	24 hr d^{-1}	Continuous dosing
No. 4	Microbubble (d_{32}: 388 μm)	Engaged	0.3 L min^{-1}	36 min d^{-1}	Periodic dosing
No. 5	Microbubble (d_{32}: 388 μm)	Engaged	0.7 L min^{-1}	10 min d^{-1}	Duplication of No. 2
No. 6	n/a	n/a	0	0	Duplication of No. 1

6.4 Results and discussion

Figure 6.2 shows the daily chlorophyll content of *D. salina* cultures supplied continuously and periodically with 5% CO_2. As can be seen, the growth of these cultures, indicated by their chlorophyll content, appears to be fairly similar. This strongly supports the idea that *D. salina* growth is proportional to the total amount of CO_2 that has been effectively transferred from gas phase into liquid phase, while extra CO_2 dosing beyond the valid range does not improve the productivity. The final chlorophyll contents for the cultures with different dosing conditions were expected to be the same, as the total amount of CO_2 mass transfer was kept identical. The contrast between the growth of the cultures fed with 5% CO_2 and the control cultures can also been seen from Figure 6.2. Unsurprisingly the chlorophyll content of the control cultures remained much lower than other cultures, and a similar phenomenon was also observed in the study of Ying et al., (2013a).

Arguably the most important finding is the comparison that can be drawn between the growth of the *D. salina* cultures supplied continuously and daily with gas. It appears that there was no significant difference between the two types of culture. The daily chlorophyll content of continuously dosed culture seemed slightly higher between day 4 and day 11, which indicates the *D. salina* grew a bit faster under continuous dosing (approximately 1 day in advance of the periodic dosed cultures). However, the cultures engaged with periodic dosing model were still competitive to the continuously dosed culture, as they achieved a similar level of final chlorophyll content although with one day of delay. Regarding the CO_2 capture efficiency, the cultures with different dosing conditions were compared (Table 6.2). As can be seen, by applying a periodic dosing strategy, CO_2 capture efficiency achieved is about 10 – 20%. It is expected that the capture efficiency could be further enhanced by improving the CO_2 mass transfer (e.g. further reduce the microbubble size). In contrast, with

continuous dosing, capture efficiency was only 0.25% of CO_2 supplied, which indicates that most of the CO_2 was wasted rather than been captured. With a view to using microalgae for CO_2 sequestration, this will mean not only wasted energy to dose CO_2, but also any CO_2 that was prevented from entering the atmosphere by fixation in the algae culture, will be greatly exceeded by the amount of CO_2 passing straight through the culture into the atmosphere. Therefore, this result shows the potential for both economic and energy savings by adopting a periodic dosing strategy, as it appears that similar algal growth to a culture supplied continuously with CO_2 can be achieved with periodic dosing, but with minimal CO_2 waste and minimal energy consumption on dosing.

Additionally, the pH control achieved using periodic dosing was also seen during these experiments (Figure 6.3). The pH in the culture supplied periodically with gas was maintained in the target region of 7.5 - 9.5 without the use of expensive buffers. This also indicates the periodic dosing model for dosing time and dosing interval estimation are accurate, so that the pH was controlled in an expected range. These results agree with the previous studies by Ying et al. (2013a) who conducted a similar experiment culturing *D. salina* in ALBs proving 30 min d^{-1} of gas (5% CO_2, 95% N_2).

Finally, the predicted final concentrations of chlorophyll content for different periodic dosing conditions (Eq. 6.13) were compared with the experimental results, shown in Table 6.3. The errors between theoretical values and experimental values were about 2 - 3 %, which indicates the accuracy of Eq. 6.13.

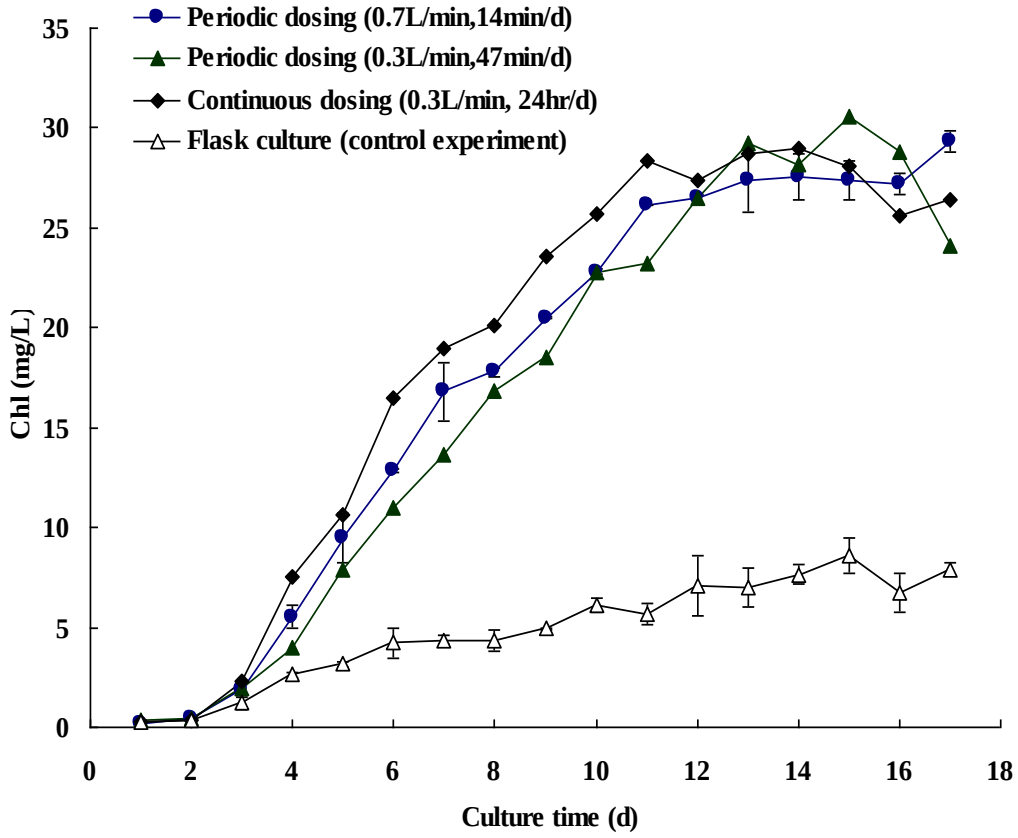

Figure 6.2: Daily chlorophyll content of the *D. salina* cultures with different dosing conditions. The cultures with 0.7 L min^{-1} of periodic dosing were conducted in parallel, as were the control cultures. Therefore, the daily chlorophyll content for these two dosing conditions shown in this graph is the average value, with the error bars given separately.

Table 6.2: Comparisons of CO_2 capture efficiency for different dosing conditions

Dosing type (5% CO_2)	**Flow rate** (1atm, 25 ℃)	**Dosing time**	**CO_2 total - absorption**	**input**	**capture efficiency**
Periodic	0.7L min^{-1}	10 min d^{-1} ×8d	0.89 g	5.03 g	18%
Periodic	0.3L min^{-1}	36 min d^{-1} ×8d	0.86 g	7.75 g	11%
Continuous	0.3L min^{-1}	24 hr d^{-1} ×8d	0.79 g	311.1 g	0.25%

Notes:

CO_2 input $_{total}$

= CO_2% × Flowrate × Dosing time × Pressure / Ideal gas constant / Kelvin temperature

CO_2 absorption = $[CO_2]_{uptake}$ (Eq. 6.11) × Culture volume

CO_2 capture efficiency= CO_2 absorption/CO_2 input

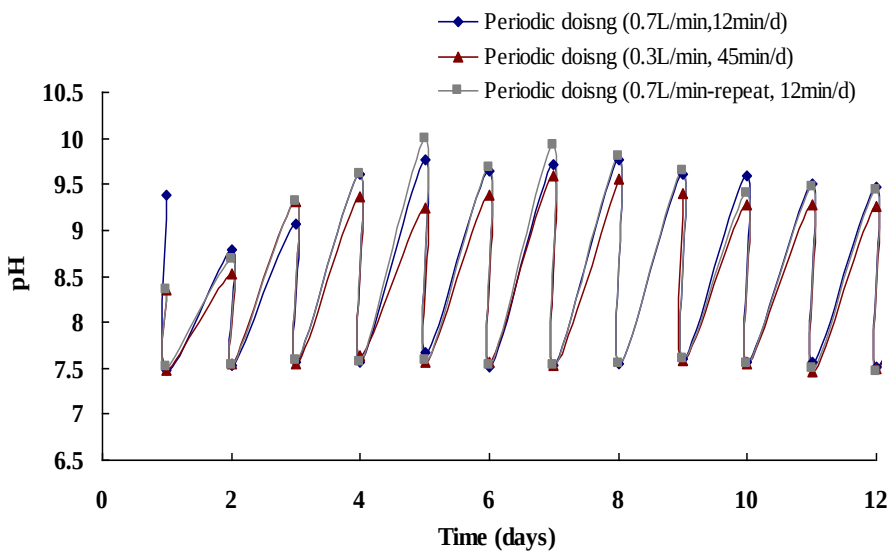

Figure 6.3: Daily pH values for *D. salina* cultures supplied periodically with 5% CO_2. There are two pH values for each day, a higher one and a lower one, representing the pH value before and after CO_2 dosing, respectively.

Table 6.3: Comparisons between estimated final concentrations of chlorophyll and real values for *D. salina* cultures with different dosing conditions

Logarithmic growth time period (d)	Dosing condition	Estimated $[Chl]_t$ (mg/L)	Real $[Chl]_t$ (mg/L)	Error
8d	0.7L min^{-1}, 10 min d^{-1}	26.90	26.09	3 %
8d	0.3L min^{-1}, 36 min d^{-1}	26.07	26.48	2 %

6.5 Conclusions

A periodic CO_2 dosing strategy for *D. salina* culture is proposed, with a model of periodic CO_2 dosing including dosing time calculation, dosing interval estimation and final chlorophyll yield prediction established. The cultures applying periodic CO_2 dosing strategy provide a similar productivity to the culture with continuous dosing, but with a greater CO_2 sequestration efficiency. The predictions of final chlorophyll yield for the cultures with different dosing conditions present an approximately less than 5% deviation to the experimental values.

Chapter 7: Effects of CO_2 and pH on growth of the microalga *Dunaliella salina*

In the previous chapter, a periodic CO_2 dosing strategy was established to enhance the CO_2 sequestration efficiency and minimize the energy cost on gas dosing. A suitable pH range rather than a specific pH value was applied in that model. It is worthwhile to find out whether the microalgae growth would be strongly affected by the pH in a suitable range. Therefore, this chapter is supplementary to the previous work. The isolated impact of either pH or CO_2 concentration on *Dunaliella salina* growth was studied. A methodology was proposed to achieve a constant pH and variable dissolved CO_2, or a constant CO_2 level and variable pH. Six different pH levels and three different dissolved CO_2 concentrations were tested.

7.1 Introduction

The cultivation of microalgae has been studied and developed for more than 60 years. (Gilmour and Zimmerman, 2012) Some parameters affecting algal growth have been well studied (e.g. light illumination) while some are still worthwhile to be studied, for instance the effects of pH and CO_2 on microalgal growth. At saturating light intensities, the rate of CO_2 supply is crucial for algal photosynthesis as CO_2 is major source for the carboxylation of RuBP. pH is also one of the important factors for algal growth as it can affect the activity of different enzymes. In general, different algal species have various ranges of tolerance to pH.

The effects of pH and CO_2 on microalgal growth have been well studied by many researchers (Hargreaves & Whitton, 1976; Moss, 1973; Azov, 1982; Gao et al., 1993; Beklioglu & Moss, 1995; Olaizola, 2003), however, neither pH nor dissolved CO_2 were solely controlled during their experiments due to the

interactions between pH and dissolved CO_2. It seems to be infeasible to keep pH constant while varying the dissolved CO_2, or vary the pH while keeping dissolved CO_2 constant. Therefore it will be interesting to find out the isolated effect of pH or CO_2 on algal growth. In this study, a method was proposed to achieve a constant pH and variable dissolved CO_2, or a constant CO_2 level and variable pH. Their effects on microalgal growth were studied based on the culture of *Dunaliella salina*. Six different pH levels and three different dissolved CO_2 concentrations were tested.

7.2 Methodology

Under a constant bubbling condition, the equilibrium concentration of dissolved CO_2 ($[CO_2]^*$), according to Henry's law and Two-film theory, should only depend on the CO_2 partial pressure in the gas phase under constant gas/liquid properties and temperature. Therefore, for a fixed CO_2 percentage in the bubbling gas, the $[CO_2]^*$ will not be altered when varying the concentrations of $NaHCO_3$ in the medium (assuming the changes in liquid physical properties by adding $NaHCO_3$ into the water are negligible, as long as the concentrations of $NaHCO_3$ are low). On the other hand, from Chapter 3, the dissolved CO_2 concentration is correlated to pH by Eq. 3.2. Since the concentration of Na^+ varies for different concentration of $NaHCO_3$, while the $[CO_2]^*$ does not change, it is therefore reasonable that the equilibrium pH (pH^*) changes for the medium with different $NaHCO_3$ concentration.

$$[CO_2] = \frac{(10^{-pH} - 10^{(pH-14)} + \Delta[Na^+])10^{(-2\,pH)}}{10^{(-6.381-pH)} + 2\times 10^{(-16.758)}} \quad (mol/L) \qquad \text{Eq. 3.2}$$

In Chapter 4, the effects of $NaHCO_3$ concentration on equilibrium concentration of dissolved CO_2 and CO_2 mass transfer rate in water were studied. The results proved the above hypothesis, indicating the feasibility of using $NaHCO_3$ to control the equilibrium pH of the medium without affecting the $[CO_2]^*$ and CO_2

mass transfer rate. However, only one concentration of CO_2 (5%) in the bubbling gas was tested, the relationship between pH^* and $NaHCO_3$ established was only suitable for 5% CO_2 dosing. Therefore, in this study, experiment a) was designed to find a comprehensive model correlating pH^*, $NaHCO_3$ and CO_2%, which would facilitate the experimental designs on b) pH impact and c) CO_2 effect on algal growth.

Experiment a): Relationship between pH^*, $NaHCO_3$ and CO_2%

To study the interaction between pH^*, $NaHCO_3$ and CO_2%, a gas mixture containing a certain percentage of CO_2 balanced with N_2 is injected to the airlift bioreactor containing 1.5 L of distilled water and a certain concentration of $NaHCO_3$. The initial temperature is adjusted to 22˚C. pH was measured by a SevenGo Duo pro (pH/DO/Ion) meter. When the pH reading stops changing for 10 minutes, this value is recorded and considered as the equilibrium pH. The experimental procedure was repeated 35 times using 7 concentrations of $NaHCO_3$ and 5 CO_2 stream concentrations tested. The equilibrium concentration of CO_2 ($[CO2]^*$) was calculated by Eq. 3.2. The experimental set up is shown in Figure 7.1.

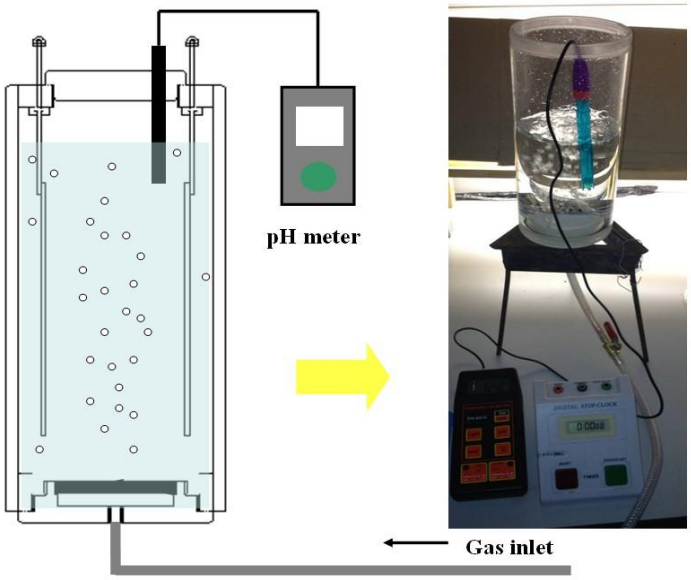

Figure 7.1: The setup for equilibrium pH measurement

Experiment b): The effect of pH on algal growth

Six 1.5 L-airlift bioreactors containing the same culture medium but with different $NaHCO_3$ concentrations were run simultaneously for *Dunaliella salina* culture. (Figure 7.2) At the beginning, 50 ml of healthy pre-cultured *D. salina* was added to 1.5 L of fresh culture medium for each culture. CO_2 gas mixture was constantly dosed into each reactor with a fixed stream concentration (5% CO_2 balanced with N_2) under 0.3 L/min. Although the algal growth may consume some dissolved CO_2, a new equilibrium would be achieved immediately after that due to the constant CO_2 dosing (CO_2 mass transfer >> CO_2 consumption, the consumed CO_2 would be balanced with the CO_2 transferred into the medium). In other words, the dissolved CO_2 is maintained constant at its equilibrium concentration. However, the equilibrium pH for each reactor differs, due to the different $NaHCO_3$ concentrations in the medium. As regard to the specific $NaHCO_3$ concentration for each culture, it was determined by the empirical model established based on the results from experiment (a). The whole set of cultures were illuminated by a fluorescent lamp providing continuous light of 90 μmol m^{-2} s^{-1}. Non-transparent baffles were placed between every two reactors to ensure even illumination for each culture. The temperature for each culture was maintained around 23℃, due to the empirical heat transfer from the fluorescent lamp. pH, OD and chlorophyll content for each culture were measured daily. The photosynthetic activity (see Chapter 3) of each culture was measured at day 5. The detailed culture condition for each reactor is listed in Table 7.1. The whole set of experiments were repeated once for error analysis.

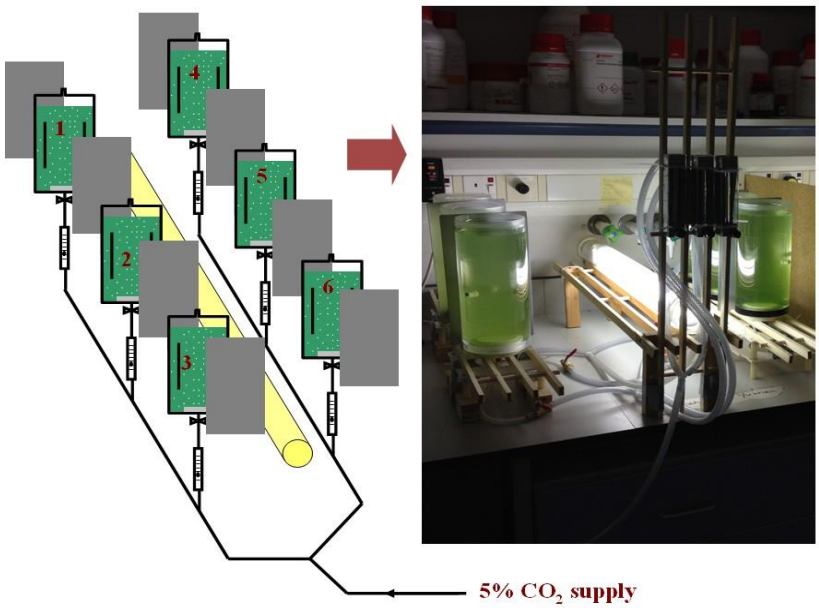

Figure 7.2: The experimental setup for studying the impact of pH on *D. salina* growth

Table 7.1: The culture condition of each reactor in the study of pH impact on *D. Salina* growth

Reactor	Culture conditions			
	Dosing condition	Concentration of $NaHCO_3$ (mol/L)	Expected pH*	Expected $[CO_2]^*$ (mol/L)
No. 1	5% CO_2 constant dosing with fine-bubbles (d_{32}: 719 μm)	5.95×10^{-4}	6	0.002
No. 2		2.03×10^{-3}	6.5	0.002
No. 3		6.97×10^{-3}	7	0.002
No. 4		8.17×10^{-2}	8	0.002
No. 5		0.280	8.5	0.002
No. 6		0.957	9	0.002

Experiment c): The effect of dissolved CO_2 on algal growth

To study the impact of dissolved CO_2 on *D. salina* growth dissolved CO_2 concentration needs to be varied while the pH for each culture should be maintained constant. To achieve this, three different CO_2 stream concentrations (5%, 20% and 50%) were applied to provide three corresponding CO_2 equilibrium concentrations. The equilibrium pH for each reactor was expected to be 7 by adding the proper amount of $NaHCO_3$. The concentration of $NaHCO_3$ required for each culture is estimated by the empirical equation found from experiment (a). The whole set of cultures was illuminated by a fluorescent lamp providing continuous light of 90 μmol m^{-2} s^{-1}. Non-transparent baffles were placed between every two reactors to ensure even illumination for each culture. The temperature for each culture was maintained around 23℃, due to the empirical heat transfer from the fluorescent lamp. pH, OD and chlorophyll content for each culture were measured daily. The photosynthetic activity of each culture was measured at day 5 and day 16. The experimental setup and culture conditions are shown in Figure 7.3 and Table 7.2, respectively.

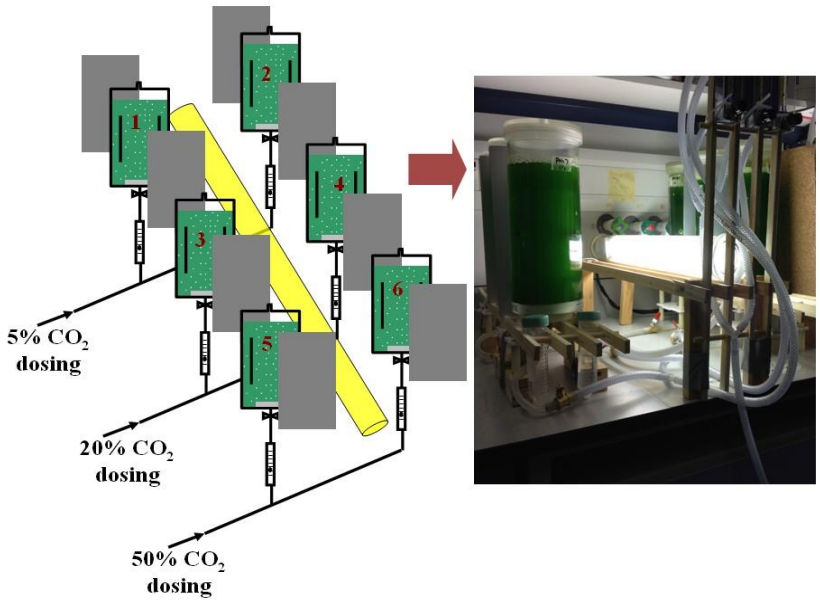

Figure 7.3: The experimental setup for studying the effect of CO_2 on *D. salina* growth

Table 7.2: The culture condition of each reactor in the study of CO_2 impact on *D. salina* growth

Reactor	Culture conditions			
	Dosing condition	Concentration of $NaHCO_3$ (mol/L)	Expected pH*	Expected $[CO_2]^*$ (mol/L)
No. 1	5% CO_2 dosing	6.97×10^{-3}	7	0.002
No. 2	5% CO_2 dosing	6.97×10^{-3}	7	0.002
No. 3	20% CO_2 dosing	3.29×10^{-2}	7	0.008
No. 4	20% CO_2 dosing	3.29×10^{-2}	7	0.008
No. 5	50% CO_2 dosing	9.19×10^{-2}	7	0.020
No. 6	50% CO_2 dosing	9.19×10^{-2}	7	0.020

7.3. Results and discussion

7.3.1 The correlations between pH^*, $NaHCO_3$ and CO_2%

Figure 7.4 summarized the relations between $[CO_2]^*$, $NaHCO_3$ and CO_2%. The results strongly support the suggestions mentioned in Section 7.2. The equilibrium concentration of dissolved CO_2 ($[CO_2]^*$) is found to be only dependent on the CO_2 stream concentration (CO_2%). $[CO_2]^*$ was enhanced with the higher CO_2% supply. The variation of $NaHCO_3$ concentration did not affect $[CO_2]^*$ when CO_2% was fixed. This phenomenon can be supported by Henry's law that the equilibrium concentration of a gas is in direct proportion to the partial pressure of that gas over the solution. In terms of equilibrium pH (pH^*), its changes along with the $NaHCO_3$ concentration and CO_2 stream concentration (CO_2%) were plotted in Figure 7.5a. As can seen, for a fixed CO_2% in the gas supply, pH^* was altered by varying the $NaHCO_3$ concentration. Higher $NaHCO_3$ concentration resulted in a higher pH^*. Such a trend is also consistent with findings from Chapter 4. An empirical equation correlating pH^* to $NaHCO_3$ and CO_2% was created in the logarithmic plot (see Figure 7.5b), shown in Eq. 7.1. The accuracy of Eq. 7.1 was examined by comparing the experimental pH^* values with the calculated values, shown in Figure 7.6. The results showed a less than 5% deviation between the real and the estimated pH^* values by using Eq. 7.1. Therefore, under a constant gas bubbling condition, pH can be controlled at a specific level for microalgae culture by choosing the right concentration of $NaHCO_3$ and CO_2% in the gas supply, without applying additional 'auto-pH regulating systems' or expensive buffers. For the gas dosing, microbubbles or fine bubbles (e.g. less than 500-600 μm in diameter) are recommended as the CO_2 mass transfer rate needs to be controlled sufficiently to balance the CO_2 consumption by algal growth. Otherwise, pH^* would not stay constant but increase.

$$pH^* = 7.6543 + 0.4063\ln(CO_2\%) - 0.4551\ln([NaHCO_3]_{mol/L})$$ Eq. 7.1

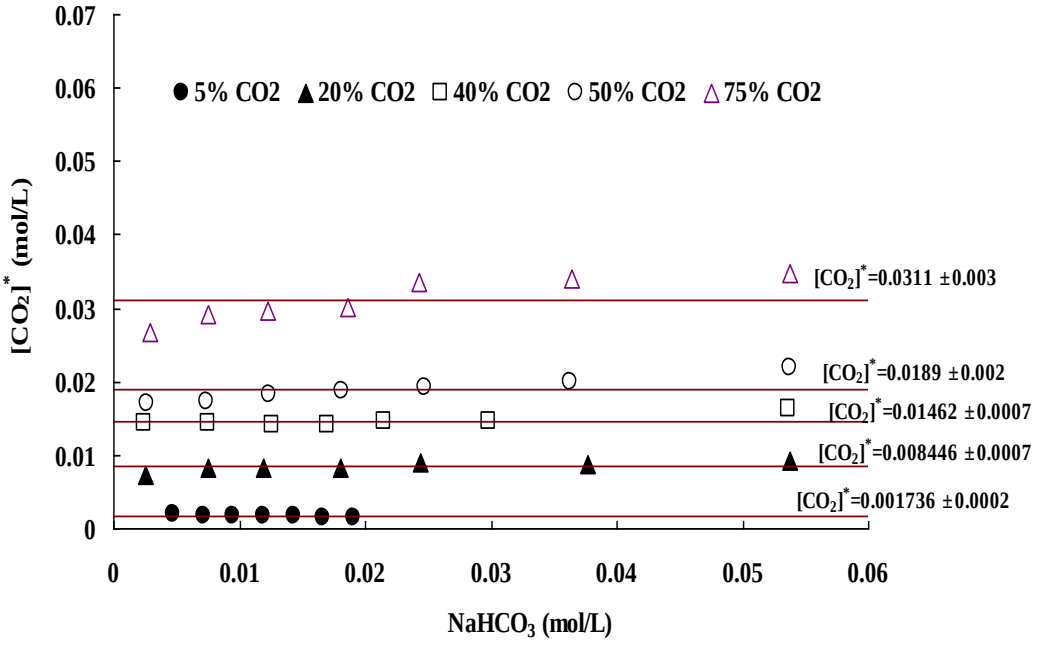

Figure 7.4: Plots of $[CO_2]^*$ versus $NaHCO_3$ concentration for different CO_2 stream concentrations

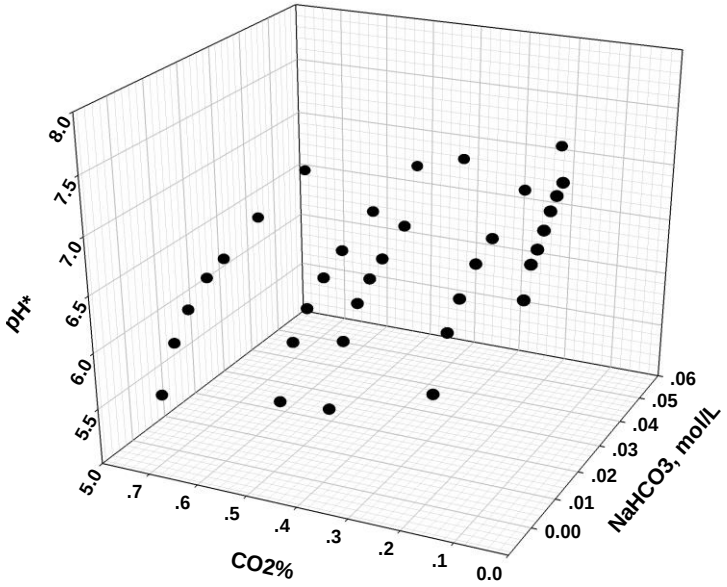

(a)

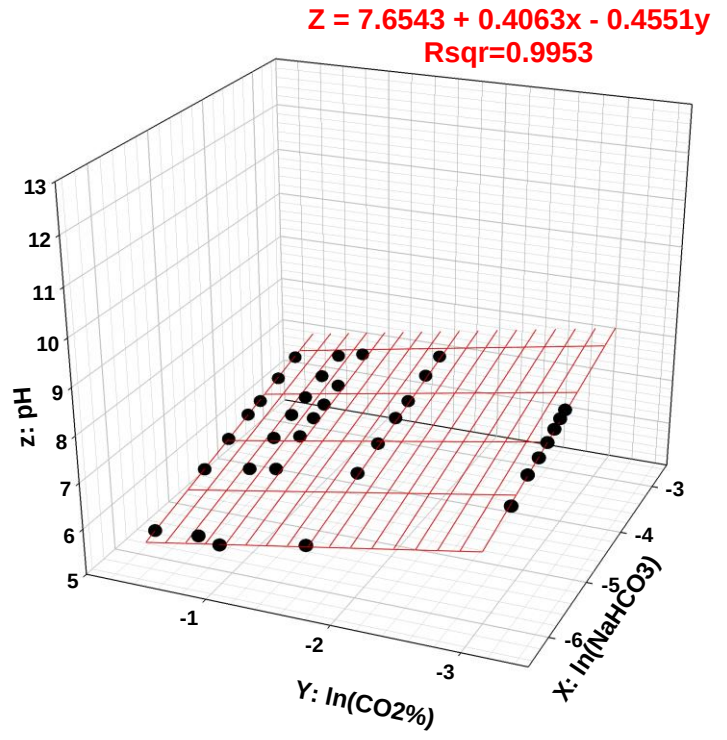

(b)

Figure 7.5: 3D-plot of the relationship between pH^*, $NaHCO_3$ and CO_2%. (a) plot of pH^* versus $NaHCO_3$ and CO_2%; (b) plot of pH^* versus $\ln(NaHCO_3)$ and $\ln(CO_2\%)$

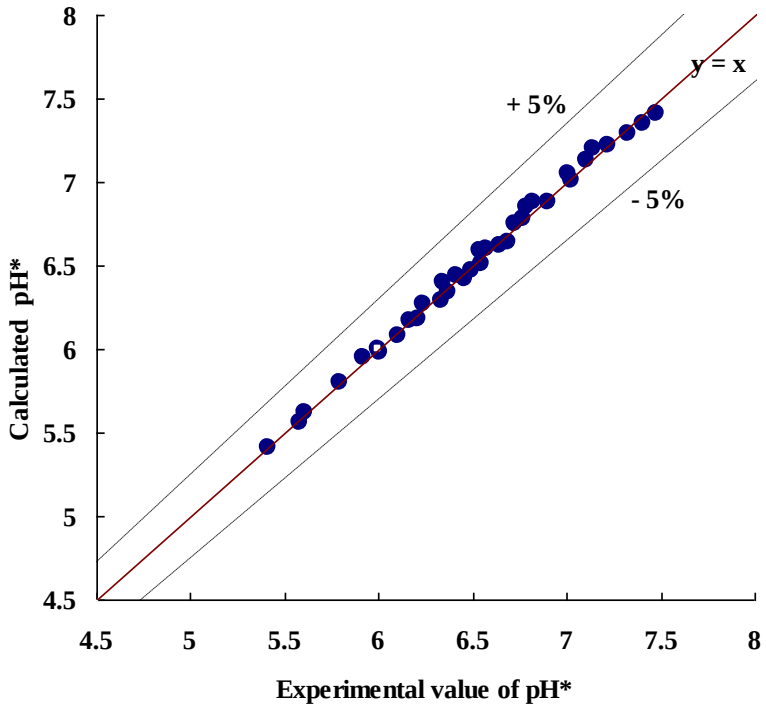

Figure 7.6: Comparison between experimental pH^* value with the one calculated based on Eq. 7.1. This figure consists of 35 points, covering the pH^* values under 7 $NaHCO_3$ and 5 CO_2 stream concentrations.

7.3.2 Effect of pH on *D. salina* growth

To study the pH effect on *D. salina* growth, six different pH levels were tested (expected pH= 6, 6.5, 7, 8, 8.5 and 9). The dissolved CO_2 concentration for each culture was maintained the same (about 0.002 mol L^{-1}) through the constant dosing of 5% CO_2. The real pH value for each culture versus the expected value was plotted in Figure 7.7. The results showed that the pH for each culture was controlled at the expected level, which again proved the feasibility of using pH^*-$NaHCO_3$-CO_2% model (Eq. 7.1) for pH control in the real algal culture. The daily algal growth under each pH level was shown in Figure 7.8. First of all, two different growth phases were observed for each culture. The growth was logarithmic in the first 5 days while 5 days after it became linear-like. The same

scenario was discussed by Richmond (2008). For a certain high light intensity, assuming all the photons of a flux density can be captured by the algal culture, cell density will keep increasing exponentially until all photosynthetically available photons are absorbed. Then, cell density increases linearly until light per cell becomes limiting which leads to growth inhibition. Therefore the cell concentration at 5^{th} day of the culture can be considered as the 'threshold' between light-unlimited growth and light-limited growth, which was about 30-40 mg/L in chlorophyll content. Secondly, no pH level between 6 and 9 was found to completely inhibit to *D. salina* growth, however, the differences in the growth for different pH conditions were also observed. The specific growth rate for each pH level was compared by plotting Figure 7.9.

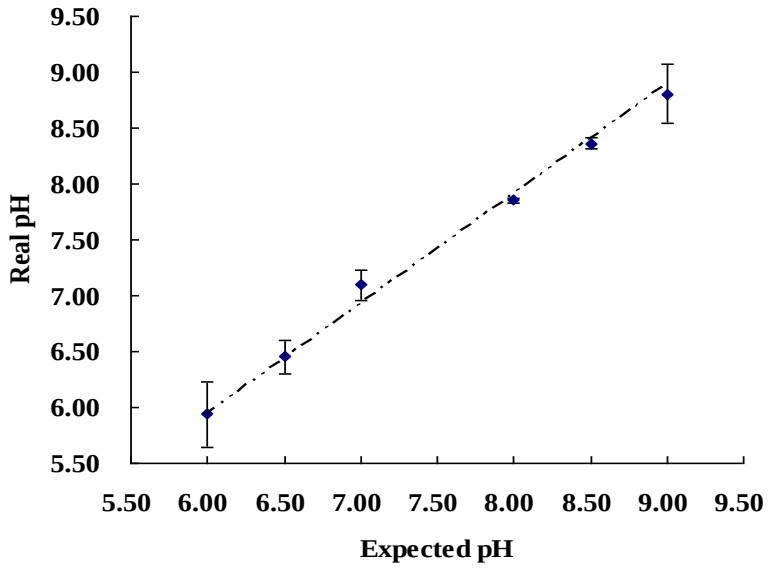

Figure 7.7: Plot of the real pH versus the expected pH for the experiment 'pH effect on *D. salina* growth'. For each culture, the real pH value presented in this figure was calculated as the average value of the daily recorded pHs of which the standard deviations are shown as error bars.

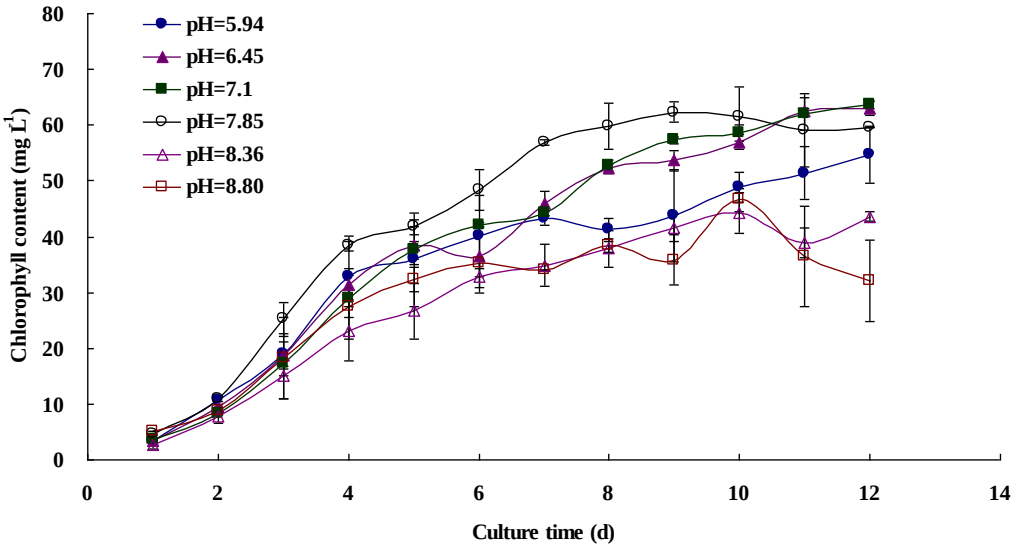

Figure 7.8: The plot of daily chlorophyll content against culture time for different pH levels. According to the diagram, from day 2 to day 5, the increase in chlorophyll was obviously quicker than the increase between day 5 and day 10. Therefore, for each culture condition, two specific growth rates were calculated on day 2 - day 5 and day 5 - day 10, separately. The method for estimating the specific growth rate was the same as the one used to obtain Figrue 5.5. The data used for each specific growth rate were plotted in the figures attached in Appendix 8.

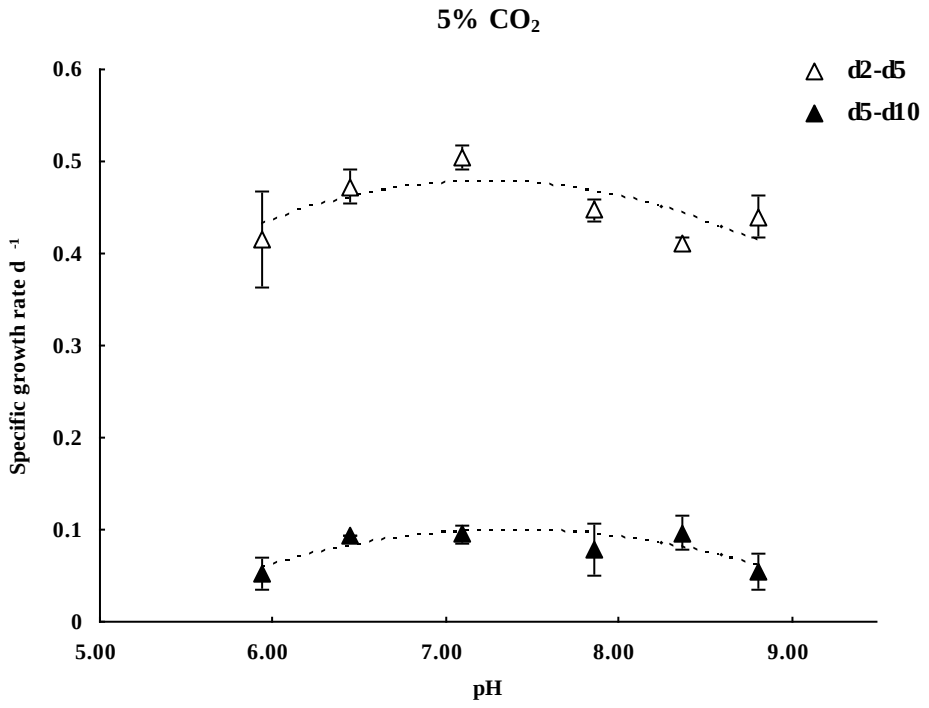

Figure 7.9: The specific growth rate of *D. salina* culture under each pH condition. The hollow triangles represent the specific growth rates of the first 5 days (light-unlimited) while the solid triangles stand for the specific growth rates between day 5 and day 12 (light-limited).

In Figure 7.9, the differences between the specific growth rates of light-unlimited growth phase and light-limited growth phase were obvious; the former were about 4 times higher than the later. Therefore, a better geometry design of ALB to extend the light-unlimited growth phase is important and should be mainly considered in future work, for example enhancing the Light/Dark ratio (Richmond, 2008). In terms of the pH effect on *D. salina* growth, the plot of specific growth rate against each pH condition presented a 'parabola trend' with an optimal value achieved at around pH 7 for either light-unlimited or light-limited growth phase. Besides, *D. salina* had a wide range of tolerance to pH, and pH between 6 and 9 was found not to completely inhibit growth. The pH

effect on growth was also studied in terms of photosynthetic O_2 yield rate. An example of the typical photosynthetic O_2 concentration versus time was plotted in Figure 7.10, from which the photosynthetic O_2 generation rate was calculated. An identical 'parabola trend' as in Figure 7.9 was obtained in Figure 7.11, again indicating the optimal pH level of around 7.

Since the concentration of dissolved CO_2 is maintained the same for each culture, the intracellular CO_2 concentration was speculated to be the same according to the two-film theory, which would suggest that the intracellular equilibrium pH for each culture is identical. In general, the results (both Figure 7.9 and Figure 7.11) indicated that even for the same intracellular pH, the changes in extracellular pH could still affect the algal growth via an as yet unknown mechanism, possibly related to the pH gradient across the cell membrane. pH around 7 was found to be the optimal pH for *D. salina* culture.

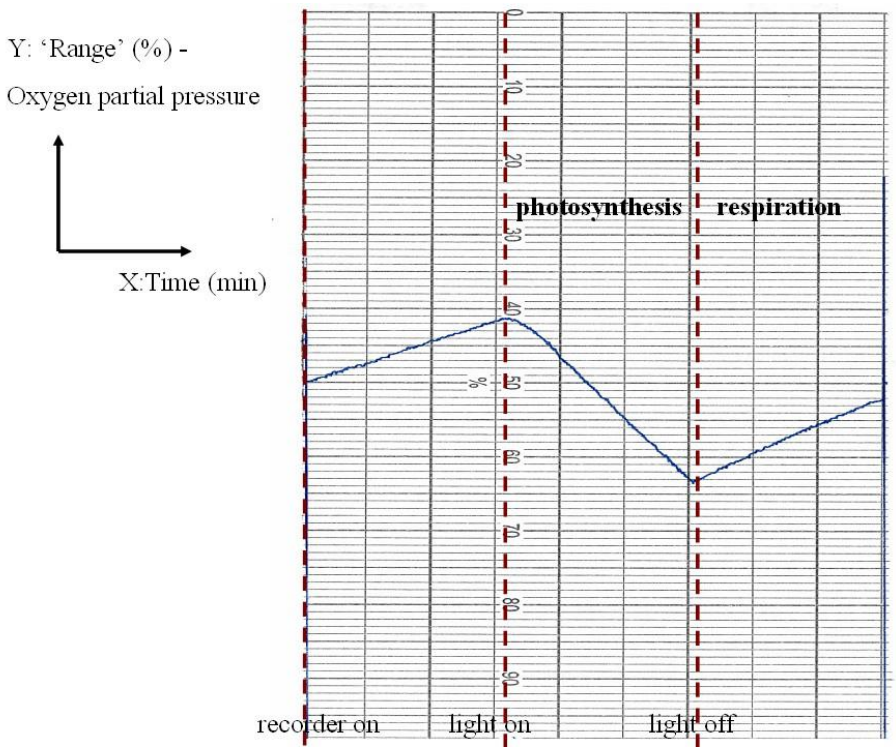

Figure 7.10: The typical graph of photosynthetic O_2 concentration (partial pressure) versus time. Each unit in X-axis was set to be 1 min. After several minutes when the recorder system was on, the light was turned on to trigger the algal photosynthetic activity, and the oxygen concentration started to increase. After several minutes, the light was turned off to observe the oxygen consumption (net respiration). The total photosynthetic oxygen generation rate was then calculated assuming that the rate of respiration in the light was the same as the respiration measured in the dark (see Chapter 3).

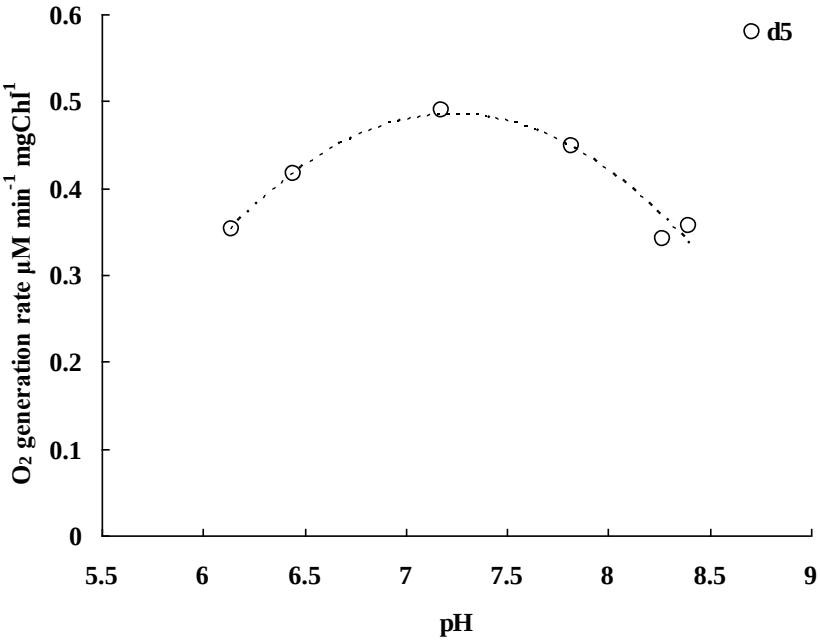

Figure 7.11: The photosynthetic O_2 yield rates under different pH conditions. The O_2 yield rates were measured on the samples taken at the 5th day of the culture (light-unlimited).

7.3.3 Effect of dissolved CO_2 concentration ($[CO_2]^*$) on *D. salina* growth

In this experiment, the pH level for each culture was designed to be 7 by using 'pH^*-$NaHCO_3$-CO_2% model' (Eq. 7.1), while the practical pH value was actually controlled at 6.88±0.08. The daily chlorophyll content change of *D. salina* under different CO_2 equilibrium concentrations was plotted in Figure 7.12. The chlorophyll content increased from 10 mg L^{-1} to 70 mg L^{-1} within 11 days under constant 5% CO_2 dosing (0.002 mol L^{-1} of $[CO_2]^*$), while a slight growth inhibition was observed when increasing the CO_2 dosing concentration up to 20% (0.008 mol L^{-1} of $[CO_2]^*$), in this case the chlorophyll content increased to less than 60 mg L^{-1} in 11 days. The 50% CO_2 dosing (0.02 mol L^{-1} of $[CO_2]^*$)

strongly inhibited the *D. salina* growth as the chlorophyll content started decreasing from day 2 onwards. Figure 7.13 and Figure 7.14 clearly show the effect of dissolved CO_2 concentration on *D. salina* growth in terms of specific growth rate and the photosynthetic O_2 generation rate, respectively. In the first 4 days, the light was still sufficient for growth due to the low concentration of algae in the culture, the specific growth rate decreased from about 0.39 d^{-1} to 0.32 d^{-1} by increasing the $[CO_2]^*$ from 0.002 mol L^{-1} to 0.008 mol L^{-1}, whilst the photosynthetic O_2 yield dropped from approximately 0.40 μmol min^{-1} mg_{Chl}^{-1} to 0.38 μmol min^{-1} mg_{Chl}^{-1}. Under 0.02 mol L^{-1} of $[CO_2]^*$, although the decrease in chlorophyll content and the negative value of specific growth rate indicated a strong inhibitation in photosynthesis, a photosynthetic activity was still detected, showing the photosynthetic O_2 rate to be 0.08 μmol min^{-1} mg_{Chl}^{-1}. Due to the significant weakening of photosynthesis at this high CO_2 concentration, the photosynthetic activity (assimilation) is highly inhibited and exceeded by the respiration activity (dissimilation), negative growth is therefore observed. When the light become limiting (d4 – d11), the effect of different dissolved CO_2 concentrations on *D. salina* growth remains the same when increasing $[CO_2]^*$ from 0.002 mol L^{-1} to 0.008 mol L^{-1}. For 0.02 mol L^{-1} of $[CO_2]^*$, neither specific growth rate nor O_2 yield showed any obvious changes, because the growth is inhibited at the beginning of the culture, which did not lead to a light-limited situation.

To sum up, under the same extracellular pH, an increase in dissolved CO_2 concentration (i.e. the CO_2% in a constant dosing condition) resulted in an inhibition of photosynthesis for *D. salina* culture at 50% of CO_2 in the dosing stream (or 0.02 mol L^{-1} of $[CO_2]^*$ in the culture), this level of CO_2 was fatal to *D. salina* growth. The possible explanation behind the situation is that despite the same extracellular pH, the intracellular pH can be affected by the extracellular CO_2 equilibrium concentration, whilst higher extracellular equilibrium CO_2 concentration leads to a lower intracellular pH which may damage or inhibit the

enzymes involved in photosynthesis.

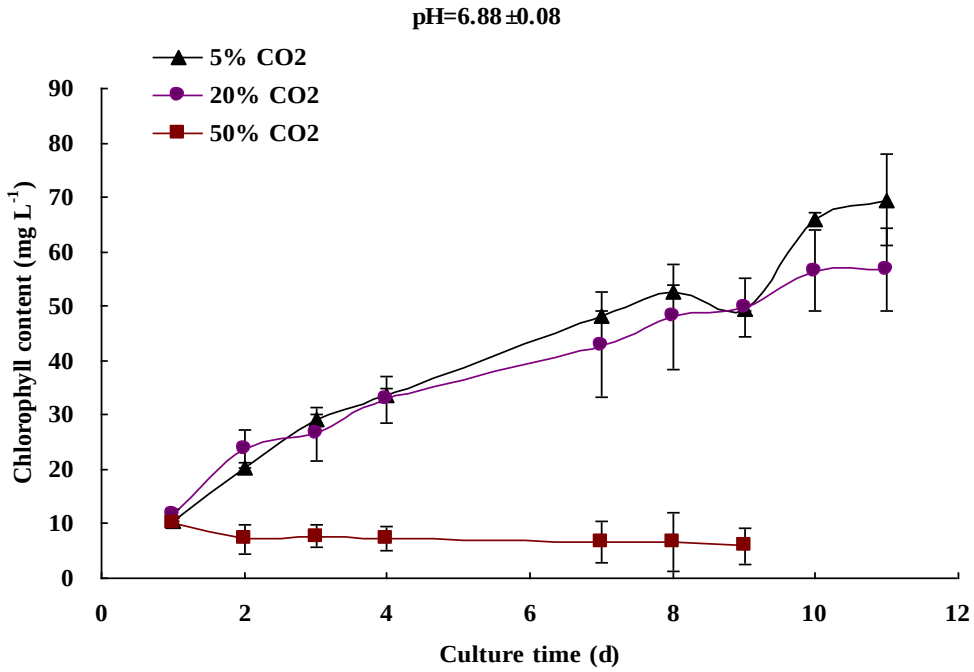

Figure 7.12: The plot of daily chlorophyll content against culture time for different CO_2 stream concentrations.

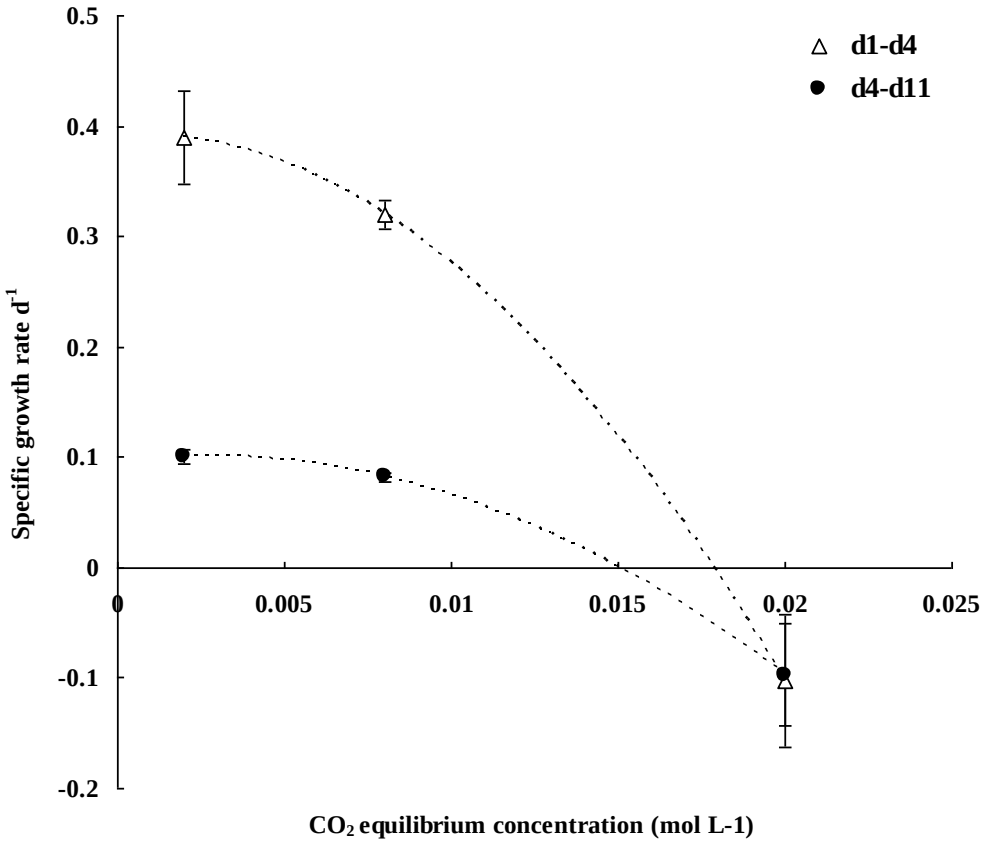

Figure 7.13: The specific growth rate of *D. salina* culture for different CO_2 stream concentrations. Under the 0.02 mol L^{-1} of dissolved CO_2 concentration, the specific growth rate was shown as negative, representing the decrease in algae concentration.

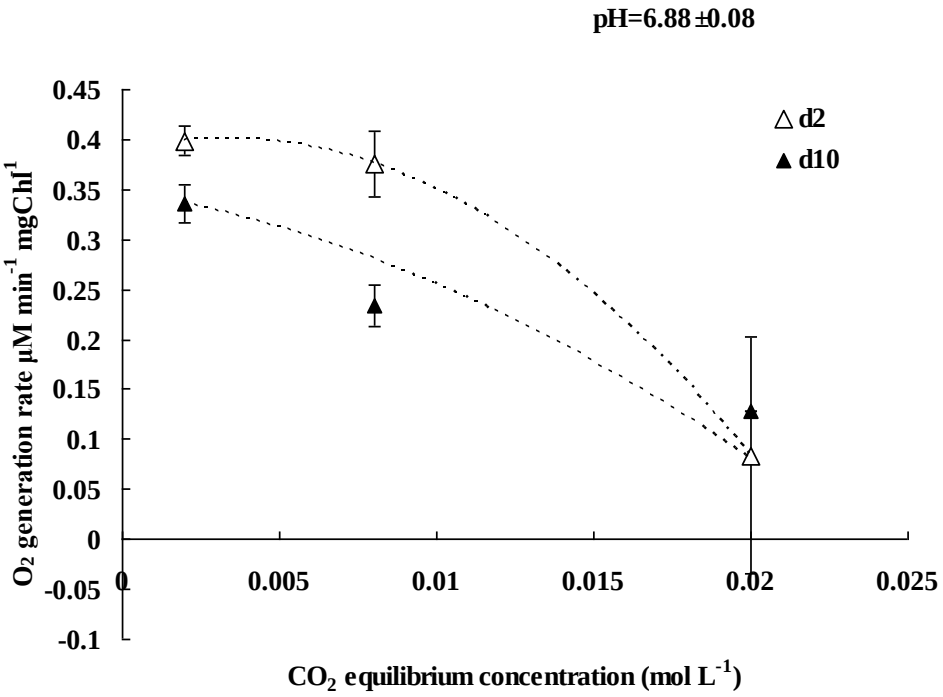

Figure 7.14: The photosynthetic O_2 yield rates under different dissolved CO_2 concentrations. The O_2 yield rates were measured on the samples taken at the 2nd day (light-unlimited) and at the 10th day (light-limited) of the culture.

7.4 Conclusions

In order to study the isolated effect of pH and CO_2 on microalgae growth, the methodology of using pH*-$NaHCO_3$-CO_2% system was introduced and tested for its performance at controlling pH constant while varying the dissolved CO_2, or varying the pH while keeping dissolved CO_2 constant. The variation of $NaHCO_3$ concentration does not change $[CO_2]^*$ when CO_2% was fixed. The pH* depended on both $NaHCO_3$ concentration and CO_2%. An empirical equation correlating pH* to $NaHCO_3$ and CO_2% is obtained. The accuracy of this empirical equation was examined by comparing the experimental pH* values with the calculated values. The results showed a less than 5% deviation between the practical and the

estimated pH^* values. Therefore, instead of applying additional 'auto-pH regulating systems' or expensive buffers, pH can be controlled at a specific level for microalgae culture by choosing the right concentration of $NaHCO_3$ and CO_2 stream concentration under a constant dosing condition.

The isolated pH effect on *D. salina* growth was studied by using 'pH^*-$NaHCO_3$-CO_2% system'. The dissolved CO_2 concentration was maintained the same for each culture, while the pH was varied. According to either specific growth rate or photosynthetic O_2 generation rate, pH around 6 - 9 was found to support growth of *D. salina* cultures. Both specific growth rate and photosynthetic O_2 generation rate versus different pH levels presented a 'parabola trend' with an optimal value achieved at around pH 7 for either light-unlimited or light-limited growth phase. The results finally indicated that even for the same intracellular pH, the changes in extracellular pH could also affect the algal growth. As regard to the isolated effect of CO_2 concentration on *D. salina* growth, the pH for each culture was controlled at 6.88 ± 0.08, while three different CO_2 concentrations (0.002 mol L^{-1}, 0.008 mol L^{-1} and 0.02 mol L^{-1}) were tested. Both specific growth rate and photosynthetic O_2 generation rate decreased when the CO_2 concentration increased. Under the 0.02 mol L^{-1} of CO_2 concentration, a strong growth inhibition was observed. More than 0.02 mol of CO_2 concentration (i.e. constant dosing of 50% CO_2) was fatal to *D. salina* growth. It was observed that increasing CO_2 stream concentration will lower the intracellular pH which may damage or inhibit the enzymes involved in photosynthesis. Therefore, in the design of an algal culture system, the CO_2 stream concentration should be carefully considered.

Due to the lab limitations, only 3 different CO_2 stream concentrations were studied, an optimal dissolved CO_2 concentration was not determined for *D. salina* culture. More CO_2 stream concentrations are expected to be tested in the future. The 'pH^*-$NaHCO_3$-CO_2% system' can also contribute to the periodic CO_2

dosing model (see Chapter 6), and should be considered in the future when developing the periodic CO_2 dosing culture system.

Chapter 8: Conclusions

The hypothesis was proved in this thesis that introducing microbubbles into an existing airlift bioreactor would improve the mass transfer for both CO_2 dissolution and O_2 stripping and consequently enhance the algal biomass productivity along with CO_2 sequestration efficiency. The mass transfer property of the proposed microbubble driven airlift bioreactor was studied acorss a wide range of flow rates. The influence of using microbubbles for microalgae (*Dunaliella salina*) culture and CO_2 sequestration was evaluated. The advantages of introducing microbubbles into an algal culture for both algal growth and CO_2 capture were confirmed. A periodic CO_2 dosing model was also established for algal batch cultures (either lab-scale or industrial-scale) to maximize the efficiency of CO_2 utilization. In this periodic dosing model, the operational parameters (dosing time, dosing interval and K_La) were also corelated to the final concentration of the microalgae. Additionally, the pure effects of both pH and CO_2 on mciroalgae growth were also studied. The detailed conclusions and major findings were sumarized as follows.

8.1 Mass transfer in the microbubble driven airlift bioreactor

The effect of microbubbbles (generated by using a fluidic oscillator: FO) on mass transfer under different gas dosing flow rates was investigated. Microbubbles (with FO) improved the K_La, average mass transfer rate and CO_2 sequestration efficiency under each dosing flow rate, compared with fine-bubbles (without FO), while the efficiency of the improvement was attenuated as the flow rate went up. Such attenuation of improvement was probably caused by the increase in microbubble size due to the weakening of oscillation and bubble coalescence under higher flow rate.

For the same bubble generation system (the changes in bubble sizes are considered to be negligible across a wide range of dosing flow rate), enhancing

the gas dosing flowrate (which means enhancing the gas hold up for the same liquid volume) can increase the mass transfer coefficient. For the same bubbling flowrate, reducing the bubble size (e.g. by using FO) can lead to an improvement on K_La as well. In other words, K_La can be enhanced by either increasing the dosing flowrate (to be more accurate, flowrate/liquid volume ratio) or reducing the bubble size. However, if the cost to achieve higher K_La is enhancing the dosing flow rate rather than reducing bubble size, then the amount of 'wasted CO_2' would increase, and such increase in wasted CO_2 could not be balanced by the increase in dissolved CO_2, which ultimately lowers the CO_2 capture efficiency. Therefore, in order to achieve both higher CO_2 mass transfer and capture efficiency, reducing bubble size (e.g. using microbubbles) is more promising than increasing flow rate. On the other hand, compared with conventional bubble dosing, a target mass transfer can be achieved under much lower gas dosing flow rate by applying microbubbles. The potential for energy saving, especially for large scale processes, is therefore straight forward to argue.

The instantaneous mass transfer rate continuously changes during the mass transfer process, as the concentration in the liquid phase keeps changing when mass transfer is taking place. Therefore, it was difficult to use a single value to represent the speed of mass transfer for a given time period. The concept of average mass transfer rate was proposed to provide an overall value which can fairly describe the mass transfer rate for a certain time period, shown as

$$v'_{MTR} = \frac{K_L a([CO_2]^* - [CO_2]_0)}{\frac{K_L a t_d}{2} + 1}.$$

The accuracy of this equation was examined via comparing the estimated values with the real values. The deviations were found to be less than 10%.

The impact of different liquid substrates (e.g. $NaHCO_3$ medium and algae medium) on CO_2 mass transfer properties was also studied. The K_La for CO_2

dissolution was not affected by the presence of $NaHCO_3$, and $NaHCO_3$ could be used to control the equilibrium pH of the medium without affecting the $[CO_2]^*$ and K_La. In the real algal culture, due to the changes in liquid properties (e.g viscocity), the K_La as well as $[CO_2]^*$ were found slightly reduced comparable to the values in water. Besides, $[CO_2]$ is no longer accurate as an indicator for K_La estimation when pH > 8.4, $[C_T]$ should be used instead. When pH < 8.4, K_La can be estimated based on either $[CO_2]$ or $[C_T]$, because the changes in $[C_T]$ are almost equal to the changes in $[CO_2]$ if pH < 8.4.

8.2 Growth enhancement of *Dunaliella salina* by microbubble induced airlift bioreactor

The perfomance of a novel microalgal culture system (an airlift loop bioreactor [ALB] engaged with a fluidic oscillator to produce microbubbles) was compared with both a conventional ALB (producing fine bubbles without the fluidic oscillator) and non-aerated flask culture. The impact of CO_2 mass transfer on *Dunaliella salina* growth was assessed, through varying the gas (5% CO_2, 95% N_2) dosing flow rate.

Approximately 6 - 8 times higher chlorophyll content was achieved in the CO_2 - aerated ALB cultures than in the non-aerated flasks. The growth of *D. salina* in these flasks was inhibited due to the lack of CO_2 supply and pH control. When compared with the conventional ALB cultures, there was a 20% - 40% increase in specific growth rate of *D. salina* in the microbubble driven ALB cultures. The highest specific growth rate (near 0.13 d^{-1}) for normal ALB culture was achieved at a dosing flow rate of 1.1 L min^{-1}, while a similar specific growth rate for ALB culture (with FO) was achieved at only 0.3 L min^{-1}, which shows an approximately 70% energy saving, in terms of bubbling. For the same type of ALB culture, the specific growth rate (μ) was found to increase along with dosing flow rate. For the same CO_2 dosing flow rate and dosing time, smaller bubbles resulted in a greater specific growth rate.

Due to 30 min/d of CO_2 periodic dosing (either microbubbles or fine-bubbles), pH was maintained in a suitable range (6.5-8.5) for *D. salina* growth.

The relation between CO_2 mass transfer and *D. salina* growth was also studied. The chlorophyll content increase was found commensurate with the amount of CO_2 uptake within the same culture period, which was described as

$$\Delta[Chl]_{(g/L)} = 2.7034_{(g/mol)} \times \Delta[CO_2]_{uptake(mol/L)}.$$

The daily CO_2 uptake rate was in direct proportion to the concentration of chlorophyll content, of which the equation is shown as

$$v_{CO_{2uptake}(mol/L/d)} = 7 \times 10^{-5}{}_{(mol/mg(chl)/d)} \times [Chl]_{(mg/L)}.$$

The amount of CO_2 uptake was equal to the amount of CO_2 dosed (assuming CO_2 is not dosed in excess), which can be described as:

$$\Delta[CO_2]_{uptake} = \Delta[CO_2]_{dosed} = v'_{MTR} \cdot t_{dosing}.$$

Finally, the chlorophyll content (growth) was found to be directly proportional to the mass transfer rate for *D. salina* ALB cultures, which also explains why the ALB cultures with microbubble dosing have higher growth rates than the ones with fine-bubble dosing.

$$\Delta[Chl]_{(g/L)} = 2.7034_{(g/mol)} \cdot v'_{MTR(mol/L/\min)} \cdot t_{dosing(\min)}$$

8.3 Periodical CO_2 dosing strategy for *Dunaliella salina* batch culture

A periodic CO_2 dosing strategy was proposed for optimal algal (*D. salina*) biomass production and CO_2 sequestration in batch cultures. The model of periodic CO_2 dosing was established, including dosing time calculation, dosing interval estimation and final biomass yield prediction, shown separately as:

$$t_d = \frac{[C_T]_{pH=A} - [C_T]_{pH=B}}{K_L a([C_T]^* - [C_T]_{pH=B}) - \frac{1}{2} K_L a([C_T]_A - [C_T]_{pH=B})}$$

$$t_i = \frac{[C_T]_{pH=A} - [C_T]_{pH=B}}{7 \times 10^{-5} \cdot [Chl]_0} \cdot (1 - 0.0946 \cdot t_c)$$

$$[Chl] = [Chl]_0 + 2703.4 \times \frac{K_L a([CO_2]^* - [CO_2]_0)}{\frac{K_L a \cdot t_d}{2} + 1} \times \frac{t_d \cdot t_c}{t_d + t_i}$$

Experimentally, 5% CO_2/95% N_2 gas was either periodically or continuously dosed into *D. salina* culture. By applying the periodic dosing model, the daily pH was kept within the target range without adding expensive buffers. Notably the culture dosed periodically was seen to have similar growth to the culture supplied constantly, but with much higher CO_2 capture efficiency (10 - 20%) compared to continuous dosing (0.25%). It shows great potential for using periodic gas supply to reduce cost, wasted gas and energy use. The predictions of final chlorophyll yield for the cultures with different dosing conditions presented an approximately 2 - 3% deviation to the experimental values.

8.4: Effects of CO_2 and pH on *Dunaliella salina* growth

The isolated impact of either pH or CO_2 concentration on *Dunaliella salina* growth was studied. An approach (pH^*-$NaHCO_3$-CO_2% control system) was proposed to achieve a constant pH and variable dissolved CO_2 concentration, or a constant CO_2 level and variable pH.

An empirical equation correlating pH^* to $NaHCO_3$ and CO_2% was obtained. The accuracy of this empirical equation was examined by comparing the experimental pH^* values with the calculated values. The results showed a less than 5% deviation between the practical and the estimated pH^* values. Therefore, instead of applying additional 'auto-pH regulating systems' or expensive buffers, pH can be controlled at a specific level for microalgae culture by choosing the

right concentration of $NaHCO_3$ and CO_2 stream concentration under a constant dosing condition.

The isolated pH effect on *D. salina* growth was studied by using 'pH^*-$NaHCO_3$-CO_2% system'. The dissolved CO_2 concentration was maintained the same for each culture, while the pH was varied. According to either specific growth rate or photosynthetic O_2 generation rate, pH around 6-9 was found to support *D. salina* culture. Both specific growth rate and photosynthetic O_2 generation rate versus different pH levels presented a 'parabola trend' with an optimal value achieved at around pH 7 for either light-unlimited or light-limited growth phase. The results also showed that even for the same intracellular pH, changes in extracellular pH could still affect the algal growth.

With regard to the sole effect of CO_2 concentration on *D. salina* growth, the pH for each culture was controlled at 6.88 ± 0.08, while three different CO_2 concentrations (0.002 mol L^{-1}, 0.008 mol L^{-1} and 0.02 mol L^{-1}) were tested. Both specific growth rate and photosynthetic O_2 generation rate decreased when the CO_2 concentration increased. Under the 0.02 mol L^{-1} of CO_2 concentration, a strong growth inhibition was observed. More than 0.02 mol L^{-1} of CO_2 concentration (i.e. constant dosing of 50% CO_2) could be fatal to *D. salina* growth. It was observed that increasing CO_2 stream concentration will lower the intracellular pH which may damage or inhibit the enzymes involved in photosynthesis. Therefore, in the design of an algal culture system, the CO_2 stream concentration and its resultant pH should be carefully considered.

8.5 Experimental challenges and future work

Due to the several challenges such as time constraints, lab limitations and general logistics, this research work was limited to the following major aspects, which should be done properly in the future.

1) In terms of the K_La for CO_2 dissolution (Chapter 4), although the effect of different bubbling flow rates on K_La were tested, only two different ranges of bubble size were compared. Futher work needs to be done to test the effect of different percentages of CO_2 in the gas supply on mass transfer. And a model ('mass transfer model') correlating K_La to bubble size, flow rate/liquid volume ratio and percentage of CO_2 in the gas supply etc. can be established, which will facilitate the estimation of CO_2 dosing time for microalgae culture. In terms of the pH/DO measurement, pH/DO probes were not particularly designed for continuous use. Alternatively, for a more accurate measurement, certain process equipment particularly designed for monitoring pH over a long time period is recommended to be used in future.

2) Only one marine species *D. salina* was used in the thesis, the major findings from Chapter 5 and Chapter 7 were valid for *D. salina*. The periodic dosing model proposed in Chapter 6 was only suitable for *D. salina* batch culture. More microalgae species should be studied following the same procedures described in Chapter 5 – 7, consequently a database (involving different algae species, operational parameters and growth properties etc.) can be established to provide a guidance facilitating industrial culture. For CO_2 periodic dosing model, it can also be further developed. For example, as the culture become denser, the dosing interval can be reduced rather than using a constant set-value. Besides, the equation for dosing time estimation can also be developed by taking 'mass transfer model' into account.

3) Batch culture system was only considered in this thesis. However, for

industrial culture, a continous culture system can promise a higher productivity. Therefore, a continuous culture system should be established in the future. The concentration of algae will be controlled at an optimal level by choosing the proper dilution rate to achieve maximal biomass productivity, whilst the 'mass transfer model' will facilitate the determination of dosing conditions (including bubble size, CO_2%, flow rate etc.) to achieve a target mass transfer rate.

4) The operational parameters studied in this thesis mainly stand for CO_2 dosing conditions, the effects of light intensity and nutrient limitations on algal growth could have been studied. Moreover, the chlorophyll content is mainly used in this thesis to indicate the biomass of the *D. salina*. Although it is a convenient measurement, it can be affected by certain culture conditions (e.g. light intensity, salt concentration and Mg^{2+} concentration etc.). Other measurements such as cell counts, dry biomass, lipid content and the residual N, P, S concentrations in the culture should have also been tested. A model to describe the algal growth (e.g the transformation of Monod equation) involving light intensity and concentration of limiting nutrients can be developed in future work.

5) The geometery of the bioreactor in this thesis was not particularly considered, the effect of different geometries (e.g down comer/riser ratio) on mixing properties and mass transfer were not investigated. Besides, the mixing effect on the algal growth was not considered in the thesis, because *D. salina* is a biflagellate alga and can well suspend in the culture even with poor mixing. However, for some algae species with no flagella, mixing could be essential for growth. Without a proper mixing, they may easily settle down to the bottom of the reactor and be inhibited due to e.g. lack of light. Therefore, the design of an airlift bioreactor geometry with an optimal mixing effect for algal growth should be considered.

References

Acién Fernández, F. G., Fernández Sevilla, J. M., Sánchez Pérez, J. A., Molina Grima, E., & Chisti, Y. (2001). Airlift-driven external-loop tubular photobioreactors for outdoor production of microalgae: assessment of design and performance. *Chemical Engineering Science*, *56*(8), 2721-2732.

Ågren, G. I. (2004). The C: N: P stoichiometry of autotrophs–theory and observations. *Ecology Letters*, *7*(3), 185-191.

Ahmed, N., & Jameson, G. J. (1985). The effect of bubble size on the rate of flotation of fine particles. *International Journal of Mineral Processing*, *14*(3), 195-215.

Aiba, S. (1982) Growth kinetics of photosynthetic microorganisms. *Advances in Biochemical Engineering*, 23, 85-156

Al-Mashhadani, M. K., Bandulasena, H. H., & Zimmerman, W. B. (2011). CO_2 mass transfer induced through an airlift loop by a microbubble cloud generated by fluidic oscillation. *Industrial & Engineering Chemistry Research*, *51*(4), 1864-1877.

Aresta, M., Dibenedetto, A., Carone, M., Colonna, T., & Fragale, C. (2005). Production of biodiesel from macroalgae by supercritical CO_2 extraction and thermochemical liquefaction. *Environmental Chemistry Letters*, *3*(3), 136-139.

Azov, Y. (1982). Effect of pH on inorganic carbon uptake in algal cultures. *Applied and Environmental Microbiology*, *43*(6), 1300-1306.

Azzi, A., & Stocker, A. (2000). Vitamin E: non-antioxidant roles. *Progress in lipid Research*, *39*(3), 231-255.

Banerjee, A., Sharma, R., Chisti, Y., & Banerjee, U. C. (2002). *Botryococcus*

braunii: a renewable source of hydrocarbons and other chemicals. *Critical Reviews in Biotechnology*, *22*(3), 245-279.

Bannister, T. T. (1979). Quantitative description of steady state, nutrient-saturated algal growth, including adaptation. *Limnol. Oceanogr*, *24*(1), 76-96.

Batan, L., Quinn, J., Willson, B., & Bradley, T. (2010). Net energy and greenhouse gas emission evaluation of biodiesel derived from microalgae. *Environmental Science & Technology*, *44*(20), 7975-7980.

Becker, E. W. (2007). Micro-algae as a source of protein. *Biotechnology Advances*, *25*(2), 207-210.

Behrens, P.W. (2005). Photobioreactors and Fermentors. In: R.A. Anderson, ed. (2005) Algal Culturing Techniques. London: Elsevier Academic Press. Ch.13.

Beklioglu, M., & Moss, B. (1995). The impact of pH on interactions among phytoplankton algae, zooplankton and perch (*Perca fluviatilis*) in a shallow, fertile lake. *Freshwater Biology*, *33*(3), 497-509.

BBC News. (2007). Q&A: EU energy plans. Available at: <URL: http://news.bbc.co.uk/1/hi/world/europe/4783996.stm>. Accessed [18/2/2013].

Ben-Amotz, A., & Avron, M. (1983). Accumulation of metabolites by halotolerant algae and its industrial potential. *Annual Reviews in Microbiology*, *37*(1), 95-119.

Benemann, J. R. (1993). Utilization of carbon dioxide from fossil fuel-burning power plants with biological systems. *Energy Conversion and Management*, *34*(9), 999-1004.

Benemann, J. R. (1997). CO_2 mitigation with microalgae systems. *Energy*

Conversion and Management, *38*, S475-S479.

Benemann, J. R. (2003). Bio-fixation of CO_2 and Greenhouse Gas Abatement with Micro-algae–Technology Roadmap. *Final report to the US Department of Energy, National Energy Technology Laboratory*, 55.

Benzing, R. J., & Myers, J. E. (1955). Low frequency bubble formation at horizontal circular orifices. *Industrial & Engineering Chemistry*, *47*(10), 2087-2090.

Berg J. M., Tymoczko J. L., Stryer L. Biochemistry. 5th edition. New York: W H Freeman; 2002. Section 20.1, The Calvin Cycle Synthesizes Hexoses from Carbon Dioxide and Water.

Available from: http://www.ncbi.nlm.nih.gov/books/NBK22344/

Biotol, Open Universiteit (Heerlen, Netherlands), Thames Polytechnic. (1992) Operational Modes of Bioreactors. *BIOTOL, Biotechnology by Open Learning Biotol Series*. Butterworth-Heinemann Limited. ISBN: 0750615087

Blankenship, R. E. (2008). *Molecular mechanisms of photosynthesis*. Wiley. ISBN: 0632043210

Borowitzka M. A. and Borowitzka L. J. (1988). Micro-algal biotechnology. Cambridge: Cambridge University Press. ISBN: 0521323495

Borowitzka, M. A. (1992). Algal biotechnology products and processes—matching science and economics. *Journal of Applied Phycology*, *4*(3), 267-279.

Borowitzka, M. A. (1999). Commercial production of microalgae: ponds, tanks, and fermenters. *Progress in Industrial Microbiology*, *35*, 313-321.

Bowes, G. (1991). Growth at elevated CO_2: photosynthetic responses mediated through Rubisco. *Plant, Cell & Environment, 14*(8), 795-806.

Brittle, S., Desai, P., Ng, W. C., Dunbar, A., Howell, R. and Zimmerman, W. B. (2014) Microbubble Size Dependence on Frequency of Oscillating Air Flow. Manuscript in preparation.

Brown, L. M. (1996). Uptake of carbon dioxide from flue gas by microalgae. *Energy Conversion and Management, 37*(6), 1363-1367.

Brown, M. R. (2002). Nutritional value and use of microalgae in aquaculture. *Avances en Nutrición Acuícola VI. Memorias del VI Simposium Internacional de Nutrición Acuícola*, *3*, 281-292.

Burns, S. E., Yiacoumi, S., & Tsouris, C. (1997). Microbubble generation for environmental and industrial separations. *Separation and Purification Technology*, *11*(3), 221-232.

Camacho, R. F. (1999). Prediction of dissolved oxygen and carbon dioxide concentration profiles in tubular photobioreactors for microalgal culture, *Biotechnology & Bioengineering*, 62 (1), 71-84.

Carvalho, A.P. and Malcata, F.X. (2001). Transfer of carbon dioxide within cultures of microalgae: Plain bubbling versus hollow-fiber modules. *Biotechnology Progress, 17*(2), 265-272.

Carvalho, A. P., Meireles, L. A., & Malcata, F. X. (2006). Microalgal reactors: a review of enclosed system designs and performances. *Biotechnology Progress*, *22*(6), 1490-1506.

Chaumont, D. (1993). Biotechnology of algal biomass production: a review of systems for outdoor mass culture. *Journal of Applied Phycology, 5*(6), 593-604.

Doran, P. M. (1995). *Bioprocess engineering principles*. Acdamic Press. ISBN: 0122208552, 277-338

Douskova, I., Doucha, J., Livansky, K., Machat, J., Novak, P., Umysova, D. & Vitova, M. (2009). Simultaneous flue gas bioremediation and reduction of microalgal biomass production costs. *Applied microbiology and biotechnology*, *82*(1), 179-185.

Chrismadha, T., & Borowitzka, M. A. (1994). Effect of cell density and irradiance on growth, proximate composition and eicosapentaenoic acid production of *Phaeodactylum tricornutum* grown in a tubular photobioreactor. *Journal of Applied Phycology*, *6*(1), 67-74.

Chelf, P., Brown, L. M., & Wyman, C. E. (1993). Aquatic biomass resources and carbon dioxide trapping. *Biomass and Bioenergy*, *4*(3), 175-183.

Chen, B. J., & Chi, C. H. (1981). Process development and evaluation for algal glycerol production. *Biotechnology and Bioengineering*, *23*(6), 1267-1287.

Chen, H., & Jiang, J. G. (2009). Osmotic responses of Dunaliella to the changes of salinity. *Journal of cellular physiology*, *219*(2), 251-258.

Cheng, L., Zhang, L., Chen, H., & Gao, C. (2006). Carbon dioxide removal from air by microalgae cultured in a membrane-photobioreactor. *Separation and purification technology*, *50*(3), 324-329.

Chengala, A. A., Hondzo, M., Troolin, D., & Lefebvre, P. A. (2010). Kinetic responses of Dunaliella in moving fluids. *Biotechnology and bioengineering*, *107*(1), 65-75.

Chisti M.Y. (1989). Airlift bioreactors, London: *Elsevier Applied Science.* ISBN: 1851663207, p119-122

Chisti, Y. (2007). Biodiesel from microalgae. *Biotechnology Advances, 25*(3), 294-306.

Chisti, Y. (2008). Biodiesel from microalgae beats bioethanol. *Trends in Biotechnology*, *26*(3), 126-131.

Corfield R (2008). The Carbon Cycle. In: Cockell C ed (2008) An Introduction to the Earth-Life System. Cambridge: Cambridge University Press. Ch.2.

Davidson, J. F., & Schüler, B. O. G. (1997). Bubble formation at an orifice in a viscous liquid. *Chemical Engineering Research and Design*, *75*, S105-S115.

Del Campo, J. A., García-González, M., & Guerrero, M. G. (2007). Outdoor cultivation of microalgae for carotenoid production: current state and perspectives. *Applied Microbiology and Biotechnology*, *74*(6), 1163-1174.

Doucha, J., Straka, F., & Lívanský, K. (2005). Utilization of flue gas for cultivation of microalgae (*Chlorella* sp.) in an outdoor open thin-layer photobioreactor. *Journal of Applied Phycology*, *17*(5), 403-412.

Croft, M. T., Lawrence, A. D., Raux-Deery, E., Warren, M. J., & Smith, A. G. (2005). Algae acquire vitamin B12 through a symbiotic relationship with bacteria. *Nature*, *438*(7064), 90-93.

Edzwald, J. K., Walsh, J. P., Kaminski, G. S., & Dunn, H. J. (1992). Flocculation and air requirements for dissolved air flotation. *Journal American Water Works Association*, 84(3), 92-100.

Emodi, A. (1978). Carotenoids--properties and applications. *Food Technology, 32(5), 38-42*.

EU Commission – Brochure (1987). The European Energy Policy. European File 2/87, January 1987. Available at: <URL: http://aei.pitt.edu/4613/>. Accessed

[28/1/2013]

Féris, L. A., & Rubio, J. (1999). Dissolved air flotation (DAF) performance at low saturation pressures. *Filtration & Separation*, *36*(9), 61-65.

Fu, W. Q., Guomundsson, O., Paglia, G., Herjolfsson, G., Andresson, O. S., Palsson, B. O., & Brynjolfsson, S. (2013). Enhancement of carotenoid biosynthesis in the green microalga Dunaliella salina with light-emitting diodes and adaptive laboratory evolution. *Applied Microbiology and Biotechnology*, *97*(6), 2395-2403.

Gaddis, E. S., & Vogelpohl, A. (1986). Bubble formation in quiescent liquids under constant flow conditions. *Chemical Engineering Science*, *41*(1), 97-105.

Gao, K., Aruga, Y., Asada, K., Ishihara, T., Akano, T., & Kiyohara, M. (1993). Calcification in the articulated coralline alga *Corallina pilulifera*, with special reference to the effect of elevated CO_2 concentration. *Marine Biology*, *117*(1), 129-132.

García-González, M., Moreno, J., Manzano, J. C., Florencio, F. J., & Guerrero, M. G. (2005). Production of *Dunaliella salina* biomass rich in 9-*cis*-β-carotene and lutein in a closed tubular photobioreactor. *Journal of Biotechnology*, *115*(1), 81-90.

Gary R. K. (2004) The concentration dependence of the ΔS term in the Gibbs free energy function: Application to reversible reactions in biochemistry, *Journal of Chemical Education*, 81(11):1599-1604.

Ghoshal, D., & Goyal, A. (2001). Carbon concentration mechanism (s) in unicellular green algae and cyanobacteria. *Journal of Plant Biochemistry and Biotechnology*, *10*(2), 83-90.

Gilmour, D. J., Hipkins, M. F., & Boney, A. D. (1984). The effect of decreasing

the external salinity on the primary processes of photosynthesis in *Dunaliella tertiolecta*. *Journal of Experimental Botany, 35*(1), 28-35.

Gilmour, D. J., & Zimmerman, W. B. (2012). Can algal biofuels play a major role in meeting future energy needs?. *Biofuels, 3*(5), 511-513.

Ginzburg, B. Z. (1993). Liquid fuel (oil) from halophilic algae: a renewable source of non-polluting energy. *Renewable Energy*, *3*(2), 249-252.

Giordano, M. (2001). Interactions between C and N metabolism in *Dunaliella salina* cells cultured at elevated CO_2 and high N concentrations. *Journal of Plant Physiology*, *158*(5), 577-581.

Goldman, J. C., & Carpenter, E. J. (1974). A kinetic approach to the effect of temperature on algal growth. *Limnology and Oceanography, 19*(5), 756-766.

Goldman, J. C., Oswald, W. J., & Jenkins, D. (1974). The kinetics of inorganic carbon limited algal growth. *Journal (Water Pollution Control Federation), 46(3)*, 554-574.

Goldman, J. C. (1979). Outdoor algal mass cultures—II. Photosynthetic yield limitations. *Water Research*, *13*(2), 119-136.

Goldman, J. C. (1980). Physiological aspects in algal mass cultures. In: *G. Shelef and C., Soeder (eds) Algae Biomass: Production and use*, p 343-360.

Grima, E. M., Camacho, F. G., Pérez, J. A., Sevilla, J. M., Fernandez, F. G., & Gomez, A. C. (1994). A mathematical model of microalgal growth in light‐limited chemostat culture. *Journal of Chemical Technology and Biotechnology*, *61*(2), 167-173.

Grima, E. M., Fernández, F. G., García Camacho, F., & Chisti, Y. (1999). Photobioreactors: light regime, mass transfer, and scaleup. *Journal of Biotechnology*, *70*(1), 231-247.

Gupta, H., & Fan, L. S. (2002). Carbonation-calcination cycle using high reactivity calcium oxide for carbon dioxide separation from flue gas. *Industrial & Engineering Chemistry Research*, *41*(16), 4035-4042.

Hall, D. O., Ación Fernández, F. G., Guerrero, E. C., Rao, K. K., & Grima, E. M. (2003). Outdoor helical tubular photobioreactors for microalgal production: Modeling of fluid- dynamics and mass transfer and assessment of biomass productivity. *Biotechnology and Bioengineering*, *82*(1), 62-73.

Hamasaki, A., Shioji, N., Ikuta, Y., Hukuda, Y., Makita, T., Hlrayama, K., Matutaki H. & Sasaki, S. (1994). Carbon dioxide fixation by microalgal photosynthesis using actual flue gas from a power plant. *Applied Biochemistry and Biotechnology*, *45*(1), 799-809.

Hargreaves, J. W., & Whitton, B. A. (1976). Effect of pH on growth of acid stream algae. *British Phycological Journal*, *11*(3), 215-223.

He, M. L., Hollwich, W., & Rambeck, W. A. (2002). Supplementation of algae to the diet of pigs: a new possibility to improve the iodine content in the meat. *Journal of animal physiology and animal nutrition*, *86*(3‐4), 97-104.

Herzog, H., Golomb, D., & Zemba, S. (1991). Feasibility, modeling and economics of sequestering power plant CO_2 emissions in the deep ocean. *Environmental Progress*, *10*(1), 64-74.

Hewakandamby, B. N. (2009). A numerical study of heat transfer performance of oscillatory impinging jets. *International Journal of Heat and Mass Transfer*, *52*(1), 396-406.

Hill, R., & Bendall, F. A. Y. (1960). Function of the two cytochrome components in chloroplasts: a working hypothesis. *Nature*, 186, 136-137.

Hosny, A. Y. (1992). Separation of oil from oil/water emulsions using an electroflotation cell with insoluble electrodes. *Filtration & Separation*, *29*(5), 419-423.

Hossain, A. B. M. S., Salleh, A., Boyce, A. N., Chowdhury, P., & Naqiuddin, M. (2008). Biodiesel fuel production from algae as renewable energy. *American Journal of Biochemistry and Biotechnology*, *4*(3), 250-254.

Iehana, M. (1987). Kinetic analysis of the growth of *Spirulina sp*. in batch culture. *Journal of Fermentation Technology*, *65*(3), 267-275.

Idogawa, K., Ikeda, K., Fukuda, T., & Morooka, S. (1987). Formation and flow of gas bubbles in a pressurized bubble column with a single orifice or nozzle gas distributor. *Chemical Engineering Communications*, *59*(1-6), 201-212.

Illman, A. M., Scragg, A. H., & Shales, S. W. (2000). Increase in *Chlorella* strains calorific values when grown in low nitrogen medium. *Enzyme and Microbial Technology*, *27*(8), 631-635.

Jaouen, P., Vandanjon, L., & Quéméneur, F. (1999). The shear stress of microalgal cell suspensions (*Tetraselmis suecica*) in tangential flow filtration systems: the role of pumps. *Bioresource Technology*, *68*(2), 149-154.

Jiménez, C., Cossío, B. R., & Niell, F. X. (2003). Relationship between physicochemical variables and productivity in open ponds for the production of *Spirulina*: a predictive model of algal yield. *Aquaculture*, *221*(1), 331-345.

Kadam, K. L. (2002). Environmental implications of power generation via coal-microalgae cofiring. *Energy*, *27*(10), 905-922.

Kaewpintong, K., Shotipruk, A., Powtongsook, S., & Pavasant, P. (2007). Photoautotrophic high-density cultivation of vegetative cells of *Haematococcus pluvialis* in airlift bioreactor. *Bioresource Technology*, *98*(2), 288-295.

Kajan, M., Tichý, V., & Simmer, J. (1994). Productivity of algae in different culture systems. *Algological Studies/Archiv für Hydrobiologie, Supplement Volumes*, *73*, 111-117.

Karsten, U., Wiencke, C., & Kirst, G. O. (1991). The effect of salinity changes upon the physiology of eulittoral green macroalgae from Antarctica and Southern Chile: II intracellular inorganic ions and organic compounds. *Journal of Experimental Botany*, *42*(12), 1533-1539.

Ketkar, D. R., Mallikarjunan, R., & Venkatachalam, S. (1991). Electroflotation of quartz fines. *International Journal of Mineral Processing*, *31*(1), 127-138.

Khurana, A. K., & Kumar, R. (1969). Studies in bubble formation—III. *Chemical Engineering Science*, *24*(11), 1711-1723.

Kishimoto, M., Okakura, T., Nagashima, H., Minowa, T., Yokoyama, S. Y., & Yamaberi, K. (1994). CO_2 fixation and oil production using micro-algae. *Journal of Fermentation and Bioengineering*, *78*(6), 479-482.

Klaui, H. (1976). Tocopherol, carotene and ascorbyl palmitate. *International Flavours and Food Additives*, *7(4)*, 165-172.

Kondili, E. M., & Kaldellis, J. K. (2007). Biofuel implementation in East Europe: Current status and future prospects. *Renewable and Sustainable Energy Reviews*, *11*(9), 2137-2151.

Kong, Q. X., Li, L., Martinez, B., Chen, P., & Ruan, R. (2010). Culture of microalgae *Chlamydomonas reinhardtii* in wastewater for biomass feedstock production. *Applied Biochemistry and Biotechnology*, *160*(1), 9-18.

Kotake-Nara, E., Kushiro, M., Zhang, H., Sugawara, T., Miyashita, K., & Nagao, A. (2001). Carotenoids affect proliferation of human prostate cancer cells. *The Journal of nutrition*, *131*(12), 3303-3306.

Kramer, D. M., Sacksteder, C. A., & Cruz, J. A. (1999). How acidic is the lumen?. *Photosynthesis Research*, *60*(2-3), 151-163.

Krüger, G. H. J., & Eloff, J. N. (1978). The effect of temperature on specific growth rate and activation energy of *Microcystis* and *Synechococcus* isolates relevant to the onset of natural blooms. *Journal of the Limnological Society of Southern Africa*, *4*(1), 9-20.

Kulkarni, A. A., & Joshi, J. B. (2005). Bubble formation and bubble rise velocity in gas-liquid systems: a review. *Industrial & Engineering Chemistry Research*, *44*(16), 5873-5931.

Kumar, R., & Kuloor, N. R. (1970). The formation of bubbles and drops. *Advances in Chemical Engineering*, *8*, 255-368.

Kumar, J. V., & Pratt, B. C. (1996). Determination of calorific values of some renewable biofuels. *Thermochimica Acta*, *279*, 111-120.

Lawlor, D. W. (1987). *Photosynthesis : metabolism, control, and physiology*. Longman Scientific & Technical; New York: Wiley, Harlow, Essex, England.

Lazo, J. P., Dinis, M. T., Holt, G. J., Faulk, C., & Arnold, C. R. (2000). Co-feeding microparticulate diets with algae: toward eliminating the need of zooplankton at first feeding in larval red drum (*Sciaenops ocellatus*). *Aquaculture*, *188*(3), 339-351.

Lee, Y. K. (1986). Enclosed bioreactors for the mass cultivation of photosynthetic microorganisms: the future trend. *Trends in Biotechnology*, *4*(7), 186-189.

Lee, Y. K. (1997). Commercial production of microalgae in the Asia-Pacific rim. *Journal of Applied Phycology*, *9*(5), 403-411.

Lee, C. G. (1999). Calculation of light penetration depth in photobioreactors. *Biotechnology and Bioprocess Engineering*, *4*(1), 78-81.

Lehr, F., & Posten, C. (2009). Closed photo-bioreactors as tools for biofuel production. *Current Opinion in Biotechnology*, *20*(3), 280-285.

Lewis, W. K., & Whitman, W. G. (1924). Principles of gas absorption. *Industrial & Engineering Chemistry*, *16*(12), 1215-1220.

Li, Y., Horsman, M., Wang, B., Wu, N., & Lan, C. Q. (2008a). Effects of nitrogen sources on cell growth and lipid accumulation of green alga *Neochloris oleoabundans*. *Applied Microbiology and Biotechnology*, *81*(4), 629-636.

Li, Y., Horsman, M., Wu, N., Lan, C. Q., & Dubois- Calero, N. (2008b). Biofuels from microalgae. *Biotechnology Progress*, *24*(4), 815-820.

Lipstein, B., & Hurwitz, S. (1980). The nutritional value of algae for poultry 1. Dried *Chlorella* in broiler diets. *British Poultry Science*, *21*(1), 9-21.

Liska, A. J., Shevchenko, A., Pick, U., & Katz, A. (2004). Enhanced photosynthesis and redox energy production contribute to salinity tolerance in Dunaliella as revealed by homology-based proteomics. *Plant Physiology*, *136*(1), 2806-2817.

Livansky K. (1990) Losses of CO_2 in outdoor mass algal cultures: Determination of the mass transfer coefficient K_L by means of measured pH course in $NaHCO_3$ solution. *Algological Studies 58*: 87-97.

Lorimer, G. H. (1981). The carboxylation and oxygenation of ribulose 1, 5-bisphosphate: the primary events in photosynthesis and photorespiration.

Annual Review of Plant Physiology, 32(1), 349-382.

Mackinney, G. (1941). Absorption of light by chlorophyll solutions. *Journal of Biological Chemistry*, *140*(2), 315-322.

Mallick, N. (2002). Biotechnological potential of immobilized algae for wastewater N, P and metal removal: a review. *Biometals*, *15*(4), 377-390.

Martinez, M. E., Jimenez, J. M., & El Yousfi, F. (1999). Influence of phosphorus concentration and temperature on growth and phosphorus uptake by the microalga *Scenedesmus obliquus*. *Bioresource Technology*, *67*(3), 233-240.

Matsumoto, H., Hamasaki, A., Sioji, N., & Ikuta, Y. (1997). Influence of CO2, SO2 and NO in flue gas on microalgae productivity. *Journal of Chemical Engineering of Japan*, *30*(4), 620-624.

Merchuk, J. C., Ronen, M., Giris, S., & Arad, S. M. (1998). Light/dark cycles in the growth of the red microalga *Porphyridium* sp. *Biotechnology and Bioengineering*, *59*(6), 705-713.

Minowa, T., Yokoyama, S. Y., Kishimoto, M., & Okakura, T. (1995). Oil production from algal cells of *Dunaliella tertiolecta* by direct thermochemical liquefaction. *Fuel*, *74*(12), 1735-1738.

Moheimani, N. R., & Borowitzka, M. A. (2011). Increased CO_2 and the effect of pH on growth and calcification of *Pleurochrysis carterae* and *Emiliania huxleyi* (Haptophyta) in semicontinuous cultures. *Applied Microbiology and Biotechnology*, 90(4), 1399-1407.

Molina, E., Fernández, J., Acién, F. G., & Chisti, Y. (2001). Tubular photobioreactor design for algal cultures. *Journal of Biotechnology*, *92*(2), 113-131.

Moss, B. (1973). The influence of environmental factors on the distribution of freshwater algae: an experimental study: II. The role of pH and the carbon dioxide-bicarbonate system. *The Journal of Ecology, 6(1)*, 157-177.

Mouza, A. A., Dalakoglou, G. K., & Paras, S. V. (2005). Effect of liquid properties on the performance of bubble column reactors with fine pore spargers. *Chemical Engineering Science*, *60*(5), 1465-1475.

Murugananthan, M., Bhaskar Raju, G., & Prabhakar, S. (2004). Separation of pollutants from tannery effluents by electro flotation. *Separation and Purification Technology*, *40*(1), 69-75.

Myers, R. (2003). *The basics of chemistry*. Greenwood Publishing Group. p.131

Nagase, H., Eguchi, K., Yoshihara, K. I., Hirata, K., & Miyamoto, K. (1998). Improvement of microalgal NOx removal in bubble column and airlift reactors. *Journal of Fermentation and Bioengineering*, *86*(4), 421-423.

Negoro, M., Shioji, N., Miyamoto, K., & Micira, Y. (1991). Growth of microalgae in high CO_2 gas and effects of SOx and NOx. *Applied Biochemistry and Biotechnology*, *28*(1), 877-886.

Negoro, M., Shioji, N., Ikuta, Y., Makita, T., & Uchiumi, M. (1992). Growth characteristics of microalgae in high-concentration CO_2 gas, effects of culture medium trace components, and impurities thereon. *Applied Biochemistry and Biotechnology*, *34*(1), 681-692.

Negoro, M., Hamasaki, A., Ikuta, Y., Makita, T., Hirayama, K., & Suzuki, S. (1993). Carbon dioxide fixation by microalgae photosynthesis using actual flue gas discharged from a boiler. *Applied Biochemistry and Biotechnology*, *39*(1), 643-653.

Nimer, N. A., Brownlee, C., & Merrett, M. J. (1994). Carbon dioxide availability,

intracellular pH and growth rate of the coccolithophore *Emiliania huxleyi*. *Marine Ecology-Progress Series*, 109, 257-257.

Ogbonna, J. C., & Tanaka, H. (1997). Industrial-size photobioreactors. *Chemtech*, *27*(7). 43-49.

Ogren, W. L. (1984). Photorespiration: pathways, regulation, and modification. *Annual Review of Plant Physiology*, *35*(1), 415-442.

Olaizola, M. (2003). Microalgal removal of CO_2 from flue gases: changes in medium pH and flue gas composition do not appear to affect the photochemical yield of microalgal cultures. *Biotechnology and Bioprocess Engineering*, *8*(6), 360-367.

Peto, R., Doll, R., Buckley, J. D., & Sporn, M. B. (1981). Can dietary beta-carotene materially reduce human cancer rates?. *Nature*, *290*, 201-208

Pirt, S. J., Lee, Y. K., Richmond, A., & Pirt, M. W. (1980). The photosynthetic efficiency of *Chlorella* biomass growth with reference to solar energy utilisation. *Journal of Chemical Technology and Biotechnology*, *30*(1), 25-34.

Pruder, G. (1983). Biological control of gas exchange in intensive aquatic production systems. *OCEANS'83, Proceedings*, 1002-1004.

Pulz, O., Gerbsch, N., & Buchholz, R. (1995). Light energy supply in plate-type and light diffusing optical fiber bioreactors. *Journal of Applied Phycology*, *7*(2), 145-149.

Pulz, O. (2001). Photobioreactors: production systems for phototrophic microorganisms. *Applied Microbiology and Biotechnology*, *57*(3), 287-293.

Qiang, H., Zarmi, Y., & Richmond, A. (1998). Combined effects of light intensity, light-path and culture density on output rate of *Spirulina platensis*

(Cyanobacteria). *European Journal of Phycology*, *33*(2), 165-171.

Raven, J. A., & Geider, R. J. (2003). Adaptation, acclimation and regulation in algal photosynthesis. In *Photosynthesis in algae* (pp. 385-412). Springer Netherlands.

Rawat, I., Ranjith Kumar, R., Mutanda, T., & Bux, F. (2011). Dual role of microalgae: phycoremediation of domestic wastewater and biomass production for sustainable biofuels production. *Applied Energy*, *88*(10), 3411-3424.

Reitan, K. I., Rainuzzo, J. R., & Olsen, Y. (1994). Effect of nutrient limitation on fatty acid and lipid content of marine microalgae. *Journal of Phycology*, *30*(6), 972-979.

Richier, S., Fiorini, S., Kerros, M. E., von Dassow, P., & Gattuso, J. P. (2011). Response of the calcifying coccolithophore *Emiliania huxleyi* to low pH/high pCO_2: From physiology to molecular level. *Marine Biology*, 158(3), 551-560.

Richmond, A. (1986). *CRC Handbook of microalgal mass culture*. CRC press. ISBN: 0849332400

Richmond, A. (2000). Microalgal biotechnology at the turn of the millennium: a personal view. *Journal of Applied Phycology*, *12*(3), 441-451.

Richmond, A., Cheng-Wu, Z., & Zarmi, Y. (2003). Efficient use of strong light for high photosynthetic productivity: interrelationships between the optical path, the optimal population density and cell-growth inhibition. *Biomolecular Engineering*, *20*(4), 229-236.

Richmond, A. (Ed.). (2008). *Handbook of microalgal culture: biotechnology and applied phycology*. Wiley-Blackwell. ISBN: 0632059532.

Richmond, A., Lichtenberg, E., Stahl, B., & Vonshak, A. (1990). Quantitative

assessment of the major limitations on productivity of Spirulina platensis in open raceways. *Journal of Applied Phycology*, *2*(3), 195-206.

Richmond, A., & Cheng-Wu, Z. (2001). Optimization of a flat plate glass reactor for mass production of *Nannochloropsis* sp. outdoors. *Journal of Biotechnology*, *85*(3), 259-269.

Richmond, A., Cheng-Wu, Z., & Zarmi, Y. (2003). Efficient use of strong light for high photosynthetic productivity: interrelationships between the optical path, the optimal population density and cell-growth inhibition. *Biomolecular Engineering*, *20*(4), 229-236.

Rijk, S. E., & Blanken, J. G. (1994). Bubble size in flotation thickening. *Water Research*, *28*(2), 465-473.

Rodrigues, R. T., & Rubio, J. (2007). DAF–dissolved air flotation: Potential applications in the mining and mineral processing industry. *International Journal of Mineral Processing*, *82*(1), 1-13.

Rosenhead, L. (1963). Laminar boundary layers: an account of the development, structure, and stability of laminar boundary layers in incompressible fluids, together with a description of the associated experimental techniques. Clarendon Press. P 629-670.

Rubio, F. C., Fernandez, F. G., Perez, J. A., Camacho, F. G., & Grima, E. M. (1999). Prediction of dissolved oxygen and carbon dioxide concentration profiles in tubular photobioreactors for microalgal culture. *Biotechnology and Bioengineering*, *62*(1), 71-86.

Sánchez Mirón, A., Contreras Gómez, A., García Camacho, F., Molina Grima, E., & Chisti, Y. (1999). Comparative evaluation of compact photobioreactors for large-scale monoculture of microalgae. *Journal of Biotechnology*, *70*(1),

249-270.

Sánchez Mirón, A., Garcia Camacho, F., Contreras Gomez, A., Grima, E. M., & Chisti, Y. (2000). Bubble - column and airlift photobioreactors for algal culture. *AIChE Journal*, *46*(9), 1872-1887.

Sakai, N., Sakamoto, Y., Kishimoto, N., Chihara, M., & Karube, I. (1995). *Chlorella* strains from hot springs tolerant to high temperature and high CO_2. *Energy Conversion and Management*, *36*(6), 693-696.

Satyanarayana, K. G., Mariano, A. B., & Vargas, J. V. C. (2011). A review on microalgae, a versatile source for sustainable energy and materials. *International Journal of Energy Research*, *35*(4), 291-311.

Schenk, P. M., Thomas-Hall, S. R., Stephens, E., Marx, U. C., Mussgnug, J. H., Posten, C., Kruse O. & Hankamer, B. (2008). Second generation biofuels: high-efficiency microalgae for biodiesel production. *Bioenergy Research*, *1*(1), 20-43.

Schäfer, R., Merten, C., & Eigenberger, G. (2002). Bubble size distributions in a bubble column reactor under industrial conditions. *Experimental Thermal and Fluid Science*, *26*(6), 595-604.

Schiedt, K., Leuenberger, F. J., Vecchi, M., & Glinz, E. (1985). Absorption, retention and metabolic transformations of carotenoids in rainbow trout, salmon and chicken. *Pure and Applied. Chemistry*, *57*(5), 685-692.

Scragg AH (1991) *Bioreactors in biotechnology: a practical approach. London: Ellis Horwood.* ISBN: 0130851434. P47-48.

Scragg, A. H., Illman, A. M., Carden, A., & Shales, S. W. (2002). Growth of microalgae with increased calorific values in a tubular bioreactor. *Biomass and Bioenergy*, *23*(1), 67-73.

Sheehan, J., Dunahay, T., Benemann, J., & Roessler, P. (1998). A look back at the US Department of Energy's Aquatic Species Program: Biodiesel from algae (Vol. 328). Golden Colorado, USA: National Renewable Energy Laboratory.

Shi, D., Xu, Y. and Morel, F.M.M. (2009). Effects of the pH/pCO_2 control method on medium chemistry and phytoplankton growth. *Biogeosciences*, *6*(7), 1199-1207.

Shi, M. & Shen, Y. M. (2003). Recent progresses on the fixation of carbon dioxide. *Current Organic Chemistry*, *7*(8), 737-745.

Shilton, A. N., Powell, N., Mara, D. D., & Craggs, R. (2008). Solar-powered aeration and disinfection, anaerobic co-digestion, biological CO_2 scrubbing and biofuel production: the energy and carbon management opportunities of waste stabilisation ponds. *Water Science and Technology*, *58*(1), 253-258.

Shin, W. T., Yiacoumi, S., & Tsouris, C. (1997). Experiments on electrostatic dispersion of air in water. *Industrial & Engineering Chemistry Research*, *36*(9), 3647-3655.

Siegel, B. Z., Siegel, S. M., Speitel, T., Waber, J., & Stoecker, R. (1984). Brine organisms and the question of habitat-specific adaptation. *Origins of Life*, *14*(1-4), 757-770.

Siemes, W., & Kauffmann, J. F. (1956). Die periodische Entstehung von Gasblasen an Dusen. *Chemical Engineering Science*, *5*(3), 127-139.

Sierra, E., Acien, F. G., Fernandez, J. M., Garcia, J. L., Gonzalez, C., & Molina, E. (2008). Characterization of a flat plate photobioreactor for the production of microalgae. *Chemical Engineering Journal*, *138*(1), 136-147.

Singh, S., Arad, S. M., & Richmond, A. (2000). Extracellular polysaccharide production in outdoor mass cultures of *Porphyridium* sp. in flat plate glass

reactors. *Journal of Applied Phycology*, *12*(3-5), 269-275.

Skjanes, K., Lindblad, P., & Muller, J. (2007). BioCO_2? A multidisciplinary, biological approach using solar energy to capture CO_2 while producing H_2 and high value products. *Biomolecular Engineering*, *24*(4), 405-413.

Sorokin, C. (1960). Kinetic studies of temperature effects on the cellular level. *Biochimica et Biophysica Acta*, *38*, 197-204.

Sorokin, C., & Krauss, R. W. (1962). Effects of temperature & illuminance on *Chlorella* growth uncoupled from cell division. *Plant Physiology, 37*(1), 37-42.

Spolaore, P., Joannis-Cassan, C., Duran, E., & Isambert, A. (2006). Commercial applications of microalgae. *Journal of bioscience and bioengineering*, *101*(2), 87-96.

Stemler A (1980). Forms of dissolved carbon dioxide required for photosystem II activity in chloroplast membranes. *Plant Physiology, 65*(6): 1160-1165

Su, Z., Kang, R., Shi, S., Cong, W., & Cai, Z. (2008). An economical device for carbon supplement in large-scale micro-algae production. *Bioprocess and Biosystems Engineering*, *31*(6), 641-645.

Sudhir, P., & Murthy, S. D. S. (2004). Effects of salt stress on basic processes of photosynthesis. *Photosynthetica*, *42*(2), 481-486.

Suh, I. S., & Lee, S. B. (2003). A light distribution model for an internally radiating photobioreactor. *Biotechnology and Bioengineering*, *82*(2), 180-189.

Sukenik, A., Bennett, J., & Falkowski, P. (1987). Light-saturated photosynthesis - limitation by electron transport or carbon fixation?. *Biochimica et Biophysica Acta (BBA)-Bioenergetics, 891*(3), 205-215.

Tamiya, H. (1957). Mass culture of algae. *Annual Review of Plant Physiology*, *8*(1), 309-334.

Tesař, V., Hung, C. H., & Zimmerman, W. B. (2006). No-moving-part hybrid-synthetic jet actuator. *Sensors and Actuators A: Physical*, *125*(2), 159-169.

Tesar, V. (2007). *Pressure-driven microfluidics*. Boston: Artech House.

Tornabene, T. G., Holzer, G., Lien, S., & Burris, N. (1983). Lipid composition of the nitrogen starved green alga *Neochloris oleoabundans*. *Enzyme and Microbial Technology*, *5*(6), 435-440.

Tredici, M. R. (2003). Closed photobioreactors: basic and applied aspects. *Proceedings of Marine Biotechnology: Basics and Applications*, 1.

Tsuge, H. & Hibino, S. I. (1983). Bubble formation from an orifice submerged in liquids. *Chemical Engineering Communications*, *22*(1-2), 63-79.

Tsuji, N., Hirayanagi, N., Okada, M., Miyasaka, H., Hirata, K., Zenk, M. H., & Miyamoto, K. (2002). Enhancement of tolerance to heavy metals and oxidative stress in *Dunaliella tertiolecta* by Zn-induced phytochelatin synthesis. *Biochemical and biophysical research communications*, *293*(1), 653-659.

Tsouris, C., DePaoli, D. W., Feng, J. Q., & Scott, T. C. (1995). Experimental investigation of electrostatic dispersion of nonconductive fluids into conductive fluids. *Industrial & Engineering Chemistry Research*, *34*(4), 1394-1403.

Ugwu, C. U., Aoyagi, H., & Uchiyama, H. (2008). Photobioreactors for mass cultivation of algae. *Bioresource Technology*, *99*(10), 4021-4028.

Van den Hoek, C. (1995). *Algae: an introduction to phycology*. Cambridge University Press. ISBN: 0521304199

Vial C., Cmarassa E., Poncin S., Wild G., Midoux N. and Bouillard J. (2000). Study of hydrodynamic behaviour in bubble columns and external loop airlift reactors through analysis of pressure fluctuations. *Chemical Engineering Science*, 55, 2957-2973.

Visviki, I., & Santikul, D. (2000). The pH tolerance of Chlamydomonas applanata (Volvocales, Chlorophyta). *Archives of environmental contamination and toxicology*, *38*(2), 147-151.

Vonshak, A., Torzillo, G., Masojidek, J., & Boussiba, S. (2001). Sub- optimal morning temperature induces photoinhibition in dense outdoor cultures of the alga *Monodus subterraneus* (Eustigmatophyta). *Plant, Cell & Environment*, *24*(10), 1113-1118.

Walker, D.A., Leegood. R.C. & Sivak, M.N. (1986) Ribulose bisphosphate carboxylase-oxygenase: its role in photosynthesis. *Philosophical Transactions of the Royal Society, London*, B 313, 305-324.

Walker, T. L., Purton, S., Becker, D. K., & Collet, C. (2005). Microalgae as bioreactors. *Plant Cell Reports*, *24*(11), 629-641.

Wang, B., Li, Y., Wu, N., & Lan, C. Q. (2008). CO_2 bio-mitigation using microalgae. *Applied Microbiology and Biotechnology*, *79*(5), 707-718.

Wegmann, K., Ben-Amotz, A., & Avron, M. (1980). Effect of temperature on glycerol retention in the halotolerant algae *Dunaliella* and *Asteromonas*. *Plant Physiology*, *66*(6), 1196-1197.

Whitman, W. G. (1962). The two film theory of gas absorption. *International Journal of Heat and Mass Transfer*, *5*(5), 429-433.

Williams, J. A. (2002). Keys to bioreactor selections. *Chemical engineering progress*, *98*(3), 34-41.

Wilkinson, P. M. (1991). Physical aspects and scale-up of high pressure bubble columns. *University of Groningen*, 1-*235*. (Dissertation)

Wijffels, R. H. (2008). Potential of sponges and microalgae for marine biotechnology. *Trends in Biotechnology*, *26*(1), 26-31.

Wijffels, R. H., Barbosa, M. J., & Eppink, M. H. (2010). Microalgae for the production of bulk chemicals and biofuels. *Biofuels, Bioproducts and Biorefining*, *4*(3), 287-295.

Xu, L., Weathers, P. J., Xiong, X. R., & Liu, C. Z. (2009). Microalgal bioreactors: challenges and opportunities. *Engineering in Life Sciences*, *9*(3), 178-189.

Xu, Z., Dapeng, L., Yiping, Z., Xiaoyan, Z., Zhaoling, C., Wei, C., & Fan, O. (2002). Comparison of photobioreactors for cultivation of *Undaria pinnatifida* gametophytes. *Biotechnology Letters*, *24*(18), 1499-1503.

Yamaberi, K., Takagi, M., & Yoshida, T. (1998). Nitrogen depletion for intracellular triglyceride accumulation to enhance liquefaction yield of marine microalgal cells into a fuel oil. *Journal of Marine Biotechnology*, *6*, 44-48.

Yap, T. N., Wu, J. F., Pond, W. G., & Krook, L. (1982). Feasibility of feeding *Spirulina maxima*, *Arthrospira platensis* or *Chlorella* sp. to pigs weaned to a dry diet at 4 to 8 days of age. *Nutrition Reports International*, *25*(3), 543-552.

Ye, Z. W., Jiang, J. G., & Wu, G. H. (2008). Biosynthesis and regulation of carotenoids in *Dunaliella*: Progresses and prospects. *Biotechnology advances*, *26*(4), 352-360.

Ying, K., Gilmour, D. J., Shi, Y., & Zimmerman, W. B. (2013a). Growth Enhancement of *Dunaliella salina* by Microbubble Induced Airlift Loop Bioreactor (ALB)—The Relation between Mass Transfer and Growth Rate. *Journal of Biomaterials and Nanobiotechnology*, *4*, 1-9.

Ying, K., Mahmood K. H. A., Hanuto J., Gilmour D. J. & Zimmerman, W. B. (2013b). Enhanced Mass Transfer in Microbubble Driven Airlift Bioreactor for Microalgal culture. *Journal of Engineering*, *5*(9), 735-743.

Yoshihara, K. I., Nagase, H., Eguchi, K., Hirata, K., & Miyamoto, K. (1996). Biological elimination of nitric oxide and carbon dioxide from flue gas by marine microalga NOA-113 cultivated in a long tubular photobioreactor. *Journal of Fermentation and Bioengineering*, *82*(4), 351-354.

Yun, Y. S., Lee, S. B., Park, J. M., Lee, C. I., & Yang, J. W. (1997). Carbon dioxide fixation by algal cultivation using wastewater nutrients. *Journal of Chemical Technology and Biotechnology*, *69*(4), 451-455.

Zabel, T. (1985). The advantages of dissolved-air flotation for water treatment. *Journal of American Water Works Association, 77*(5), 42-46.

Zaťková, I., Sergejevova, M., Urban, J., Vachta, R., Štys, D., & Masojidek, J. (2011). Carotenoid‐enriched microalgal biomass as feed supplement for freshwater ornamentals: albinic form of wels catfish (Silurus glanis). *Aquaculture Nutrition*, *17*(3), 278-286.

Zimmerman, W. B., Tesar, V., Butler, S., & Bandulasena, H. C. (2008). Microbubble generation. *Recent Patents on Engineering*, *2*(1), 1-8.

Zimmerman, W. B., Tesař, V., Bandulasena, H. H., & Omotowa, O. A. (2007) Efficiency of an aerator driven by fluidic oscillation. Part II: Pilot scale trials with flexible membrane diffusers. University Report. Available at: <URL: http://eyrie.shef.ac.uk/steelCO2/open/aerationefficiencypart2.pdf>. Accessed [18/5/2013].

Zimmerman, W. B., Hewakandamby, B. N., Tesař, V., Bandulasena, H. C., & Omotowa, O. A. (2009). On the design and simulation of an airlift loop

bioreactor with microbubble generation by fluidic oscillation. *Food and Bioproducts Processing*, *87*(3), 215-227.

Zimmerman, W. B., Tesař, V., & Bandulasena, H. C. (2011a). Towards energy efficient nanobubble generation with fluidic oscillation. *Current Opinion in Colloid & Interface Science*, *16*(4), 350-356.

Zimmerman, W. B., Zandi, M., Hemaka Bandulasena, H. C. H., Tesař, V., Gilmour, D. J. & Ying, K. (2011b). Design of an airlift loop bioreactor and pilot scales studies with fluidic oscillator induced microbubbles for growth of a microalgae *Dunaliella salina*. *Applied Energy*, *88*(10), 3357-3369.

Appendix 1: The bubble size distribution

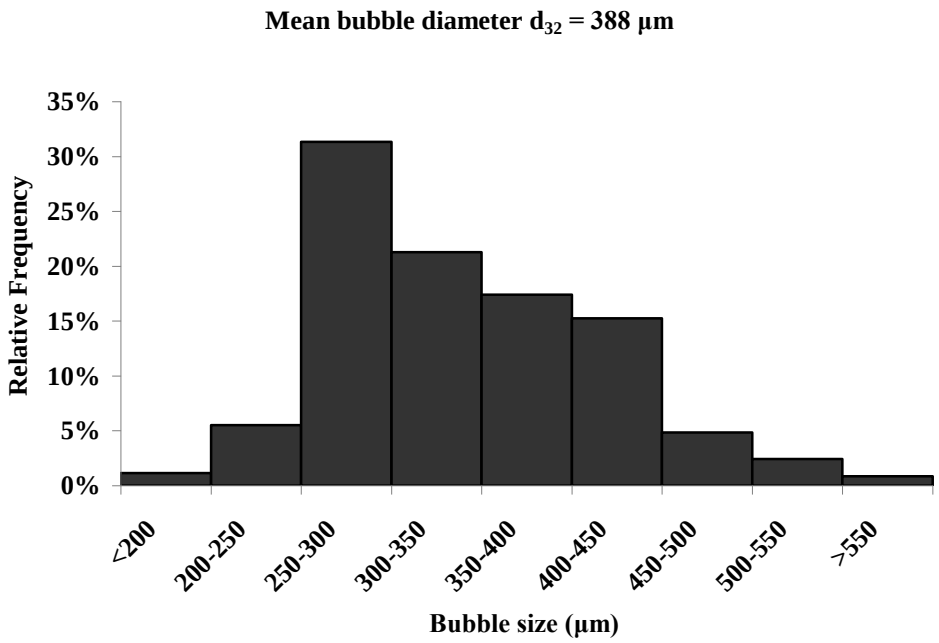

Figure A1.1: The bubble size distribution for the bubbles generated from the ceramic diffuser engaged with a fluidic oscillator. The majority of bubbles were in the size range between 250 and 450 µm. The mean Sauter bubble diameter (d_{32}) was calculated to be 388 µm.

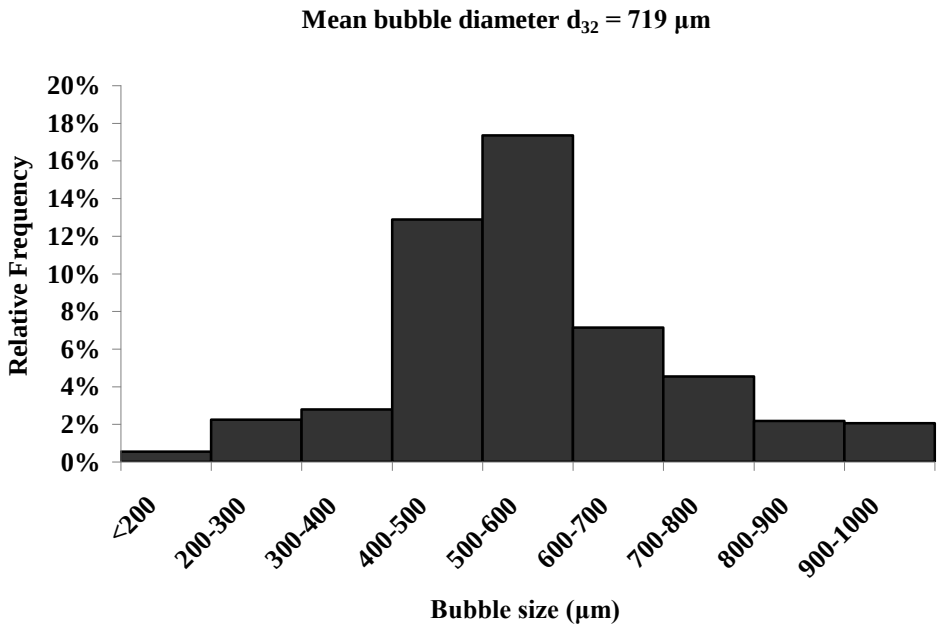

Figure A1.2: The bubble size distribution for the bubbles generated from the ceramic diffuser but without fluidic oscillator. The majority of bubbles were in the size range between 400 and 800 µm. The mean Sauter bubble diameter (d_{32}) was calculated to be 719 µm.

Appendix 2: The speciation diagram for CO_2 in water

Figure A2.1 shows the relative proportion of each carbon species (CO_2, HCO_3^- and CO_3^{2-}) in the water. Generally, the percentage distribution of each CO_2 species strongly depends on the pH level. At low pH, HCO_3^- and CO_3^{2-} will take up some of the H^+ to finally form CO_2, and therefore CO_2 has a relatively high proportion. For example, when pH is less than 5, more than 95 % of total carbon exists in the forms of CO_2. At high pH, CO_2 and HCO_3^- will tend to form CO_3^{2-}, consequently, CO_3^{2-} becomes the dominant species. For instance, more than 95 % of total carbon is CO_3^{2-} when pH > 12. At intermediate pH (e.g. 7 - 10), CO_2, HCO_3^- and CO_3^{2-} all exist, although with most of proportion taken by HCO_3^-.

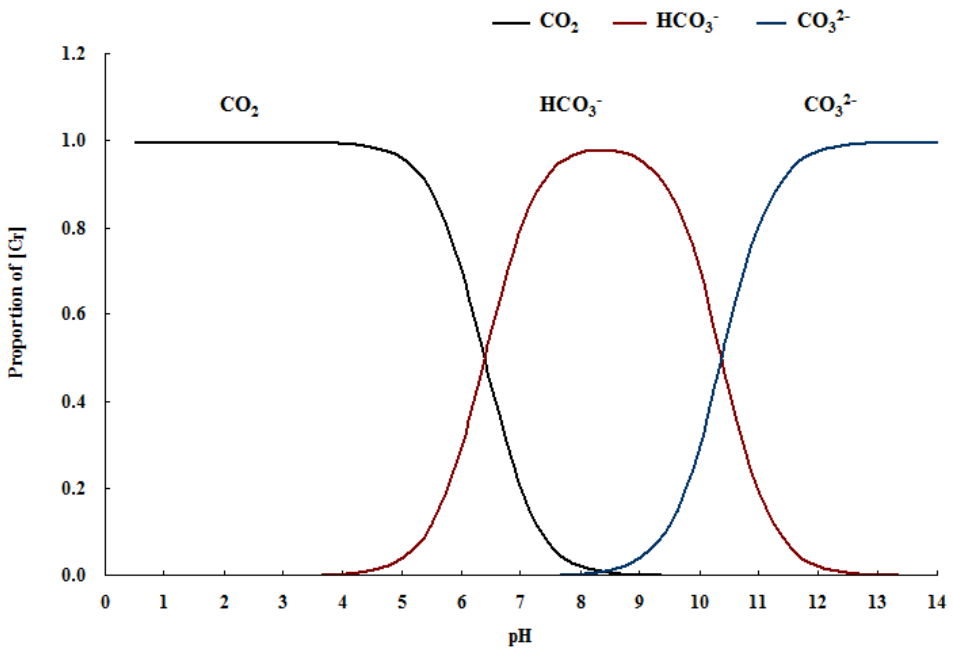

Figure A2.1: The speciation diagram for CO_2 in water showing the relative proportion of each species.

Appendix 3: K_La estimation in 7-L ALB containing DI water

The raw figures for K_La estimation are shown as follows. In each figure, the legend provides the information on the mass transfer direction (CO_2 dissolution or O_2 removal), the gas flow rate and the engagement of fluidic oscillator (FO and NoFO mean with and without fluidic oscillator respectively).

- ***K_La for CO_2 dissolution***

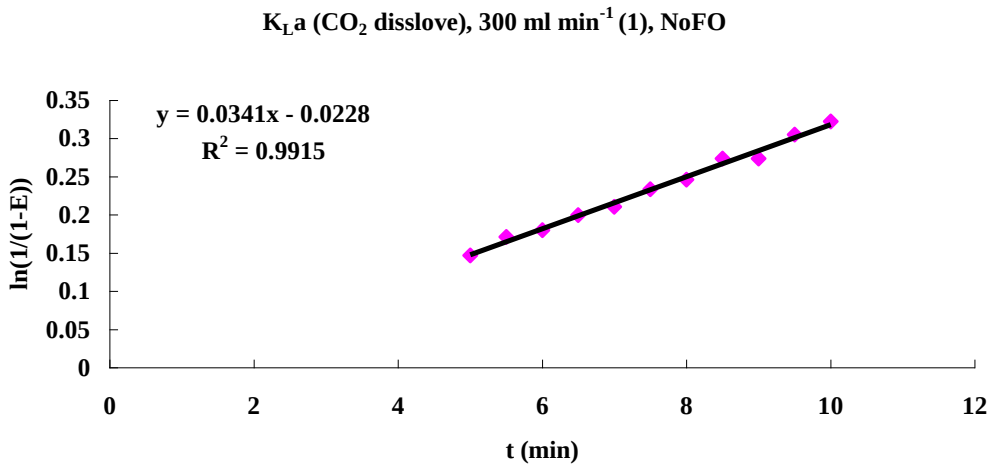

Figure A3.1: Typical plot for K_La estimation (0.3 L min^{-1}, NoFO, CO_2 dissolution) – test 1, where the slop of the linear fitting represent the value of K_La (min^{-1})

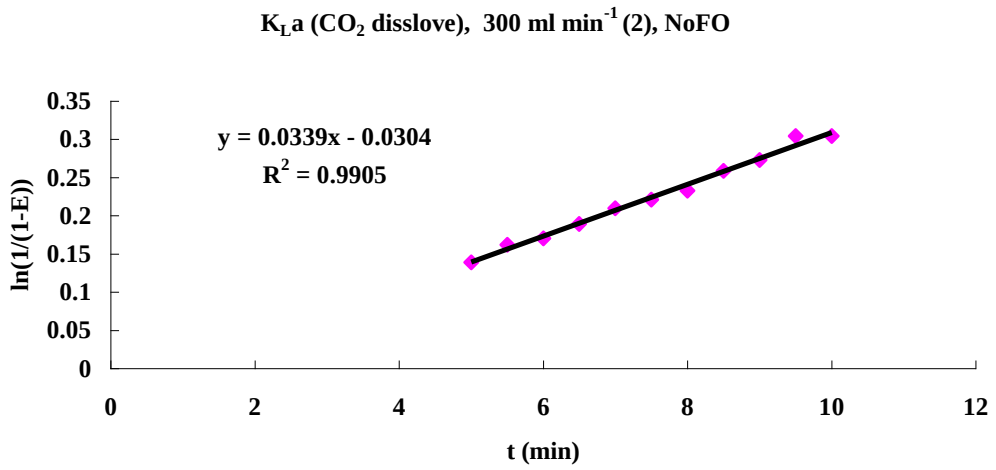

Figure A3.2 Typical plot for K_La estimation (0.3 L min^{-1}, NoFO, CO_2 dissolution) – test 2, where the slop of the linear fitting represent the value of K_La (min^{-1})

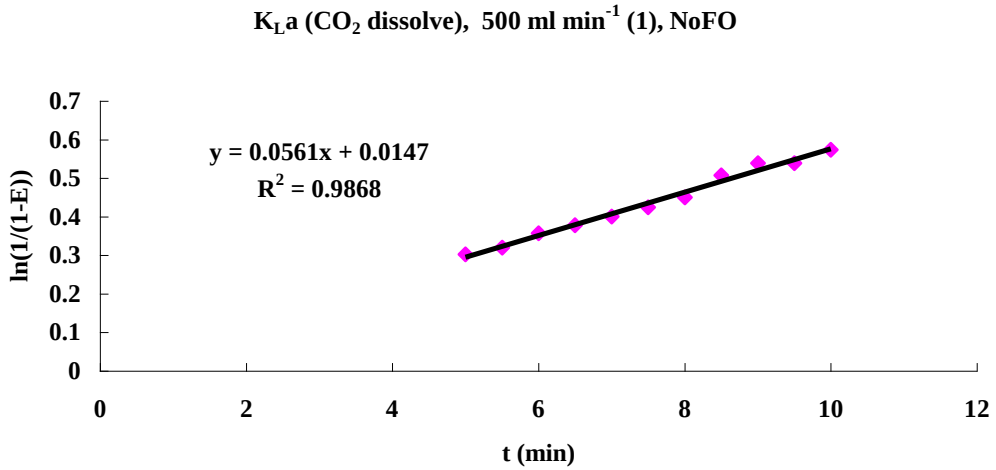

Figure A3.3: Typical plot for K_La estimation (0.5 L min^{-1}, NoFO, CO_2 dissolution) – test 1, where the slop of the linear fitting represent the value of K_La (min^{-1})

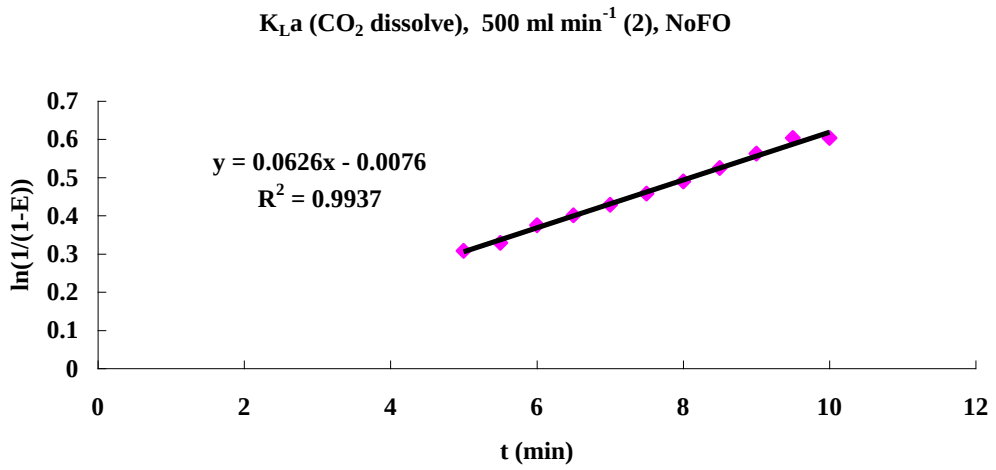

Figure A3.4: Typical plot for K_La estimation (0.5 L min^{-1}, NoFO, CO_2 dissolution) – test 2, where the slop of the linear fitting represent the value of K_La (min^{-1})

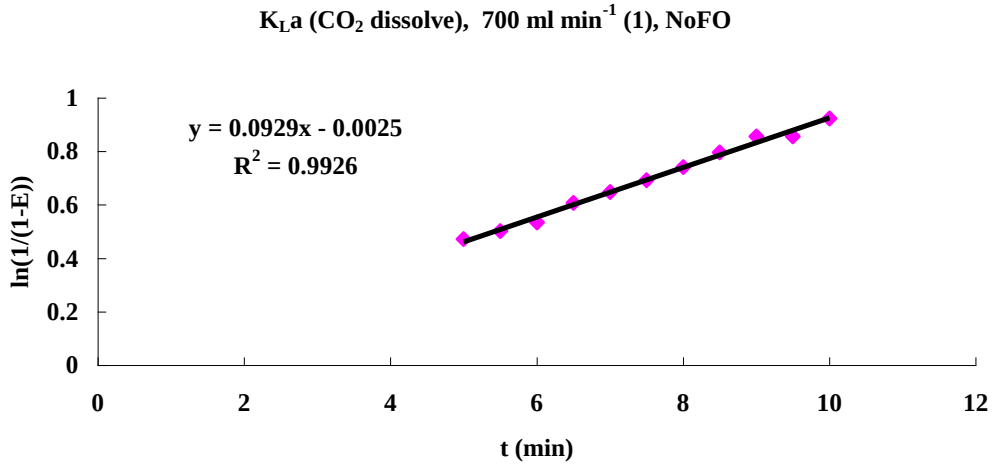

Figure A3.5: Typical plot for K_La estimation (0.7 L min^{-1}, NoFO, CO_2 dissolution) – test 1, where the slop of the linear fitting represent the value of K_La (min^{-1})

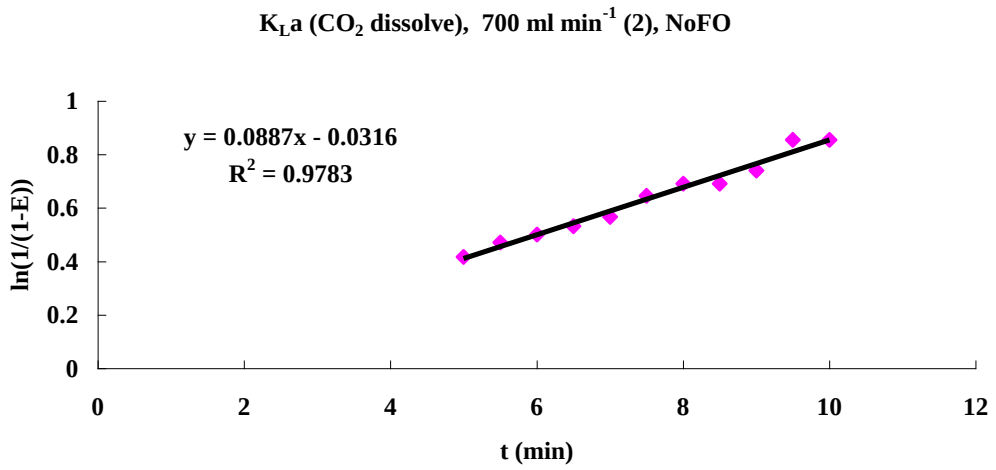

Figure A3.6: Typical plot for K_La estimation (0.7 L min^{-1}, NoFO, CO_2 dissolution) – test 2, where the slop of the linear fitting represent the value of K_La (min^{-1})

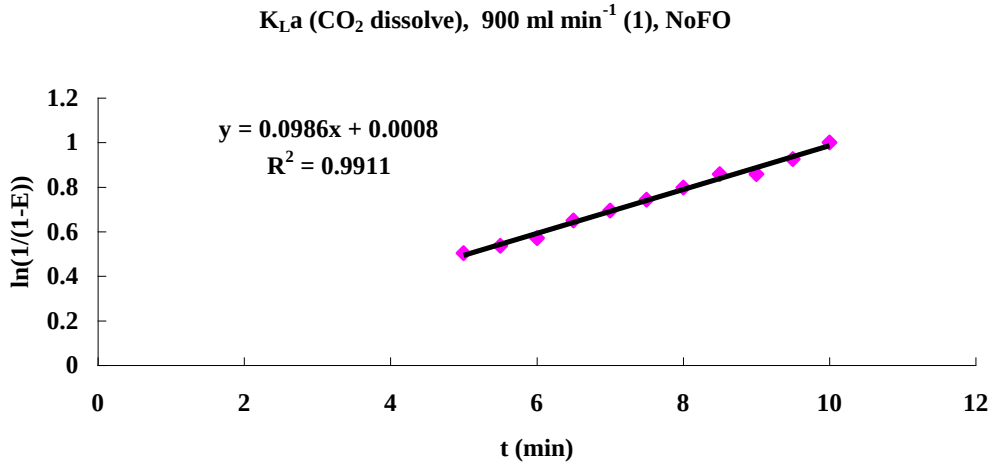

Figure A3.7: Typical plot for K_La estimation (0.9 L min^{-1}, NoFO, CO_2 dissolution) – test 1, where the slop of the linear fitting represent the value of K_La (min^{-1})

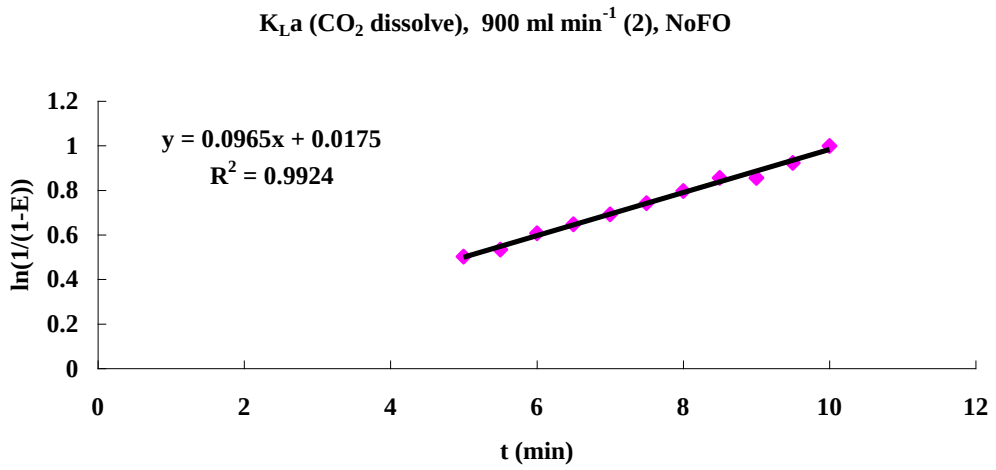

Figure A3.8: Typical plot for K_La estimation (0.9 L min^{-1}, NoFO, CO_2 dissolution) – test 2, where the slop of the linear fitting represent the value of K_La (min^{-1})

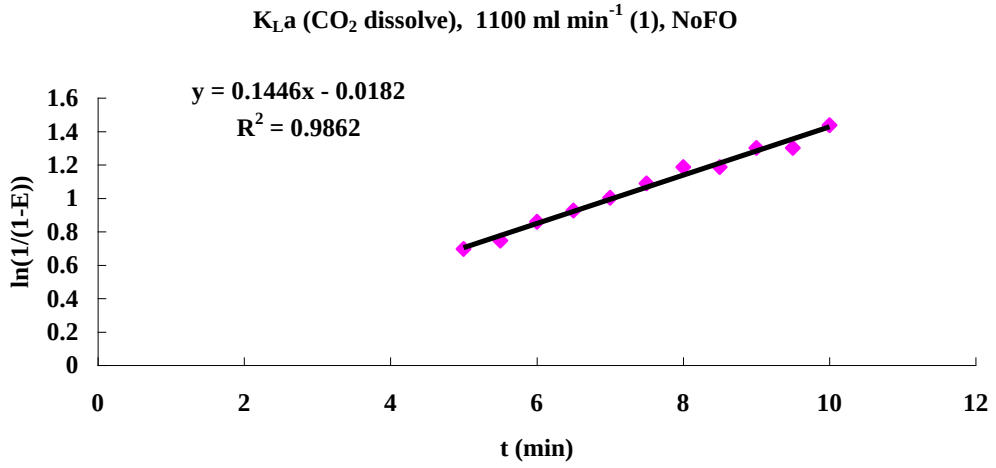

Figure A3.9: Typical plot for K_La estimation (1.1 L min^{-1}, NoFO, CO_2 dissolution) – test 1, where the slop of the linear fitting represent the value of K_La (min^{-1})

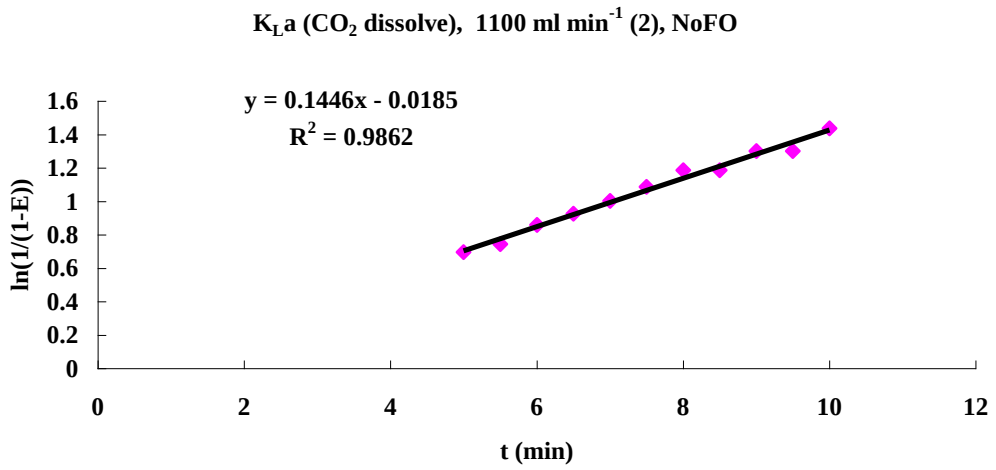

Figure A3.10: Typical plot for K_La estimation (1.1 L min^{-1}, NoFO, CO_2 dissolution) – test 2, where the slop of the linear fitting represent the value of K_La (min^{-1})

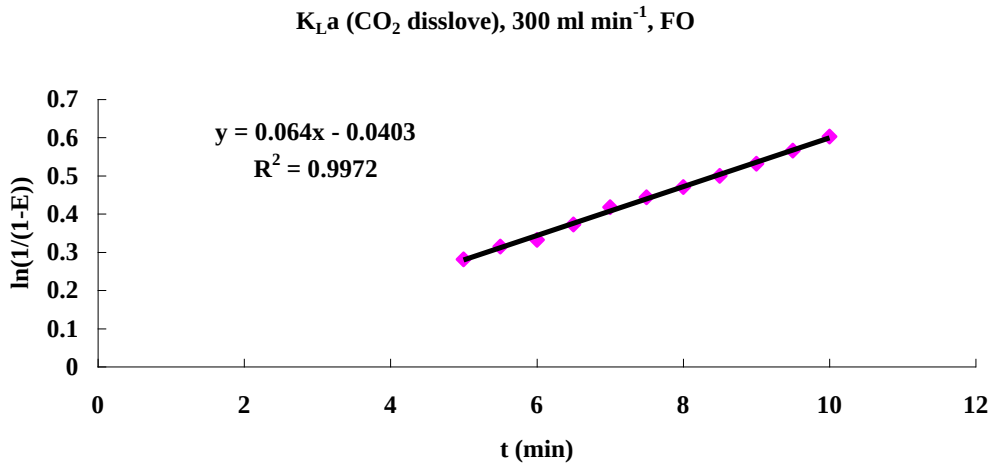

Figure A3.11: Typical plot for K_La estimation (0.3 L min^{-1}, FO, CO_2 dissolution), where the slop of the linear fitting represent the value of K_La (min^{-1})

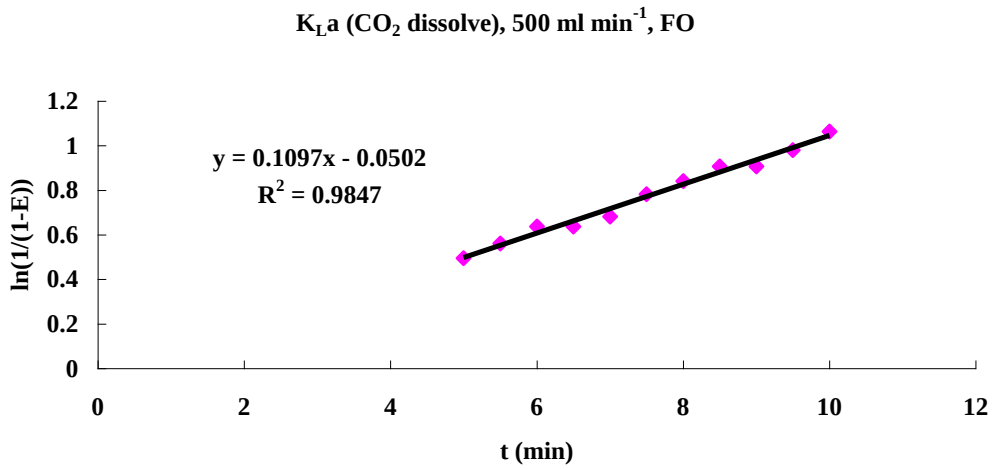

Figure A3.12: Typical plot for K_La estimation (0.5 L min^{-1}, FO, CO_2 dissolution), where the slop of the linear fitting represent the value of K_La (min^{-1})

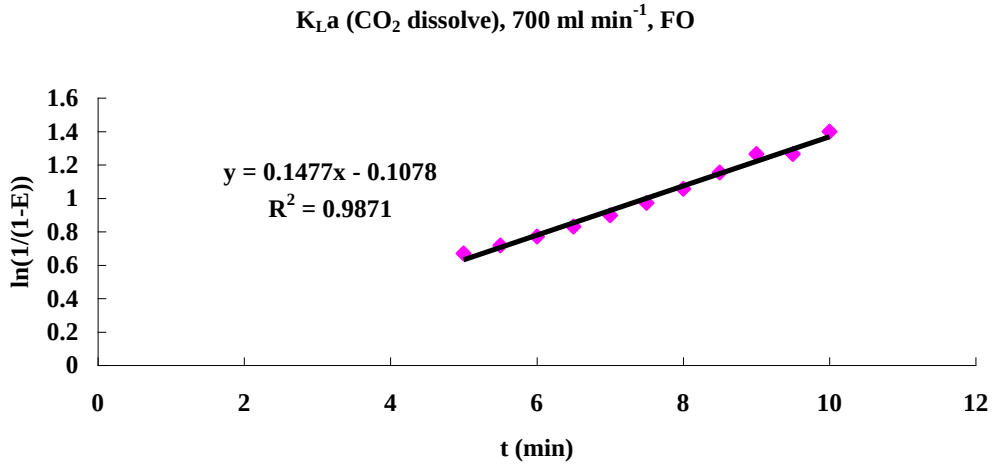

Figure A3.13: Typical plot for K_La estimation (0.7 L min^{-1}, FO, CO_2 dissolution), where the slop of the linear fitting represent the value of K_La (min^{-1})

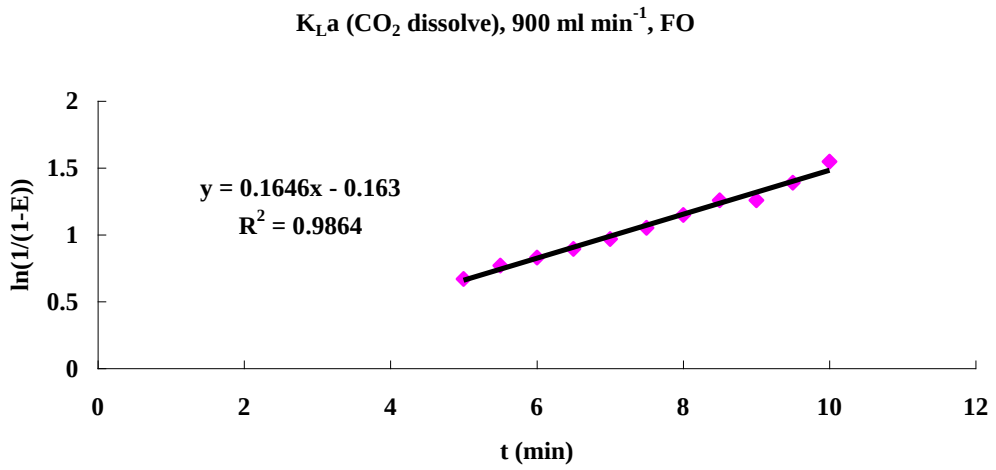

Figure A3.14: Typical plot for K_La estimation (0.9 L min^{-1}, FO, CO_2 dissolution), where the slop of the linear fitting represent the value of K_La (min^{-1})

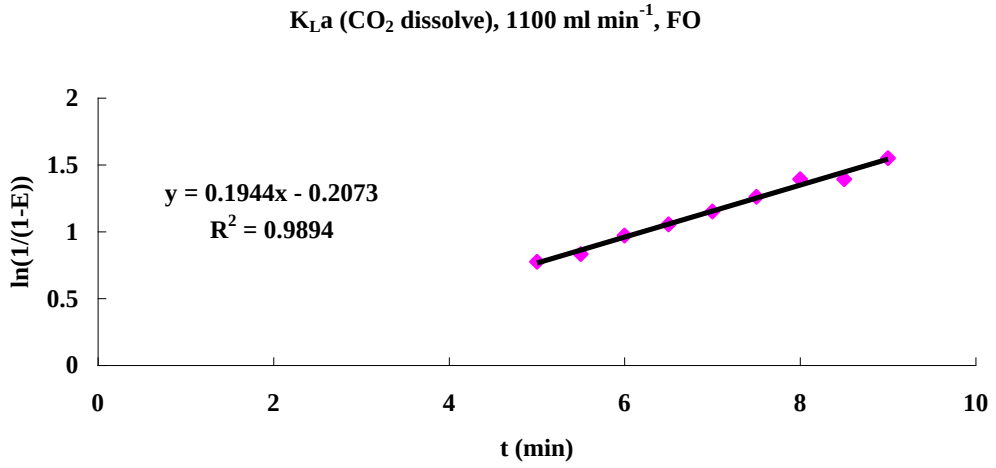

Figure A3.15: Typical plot for K_La estimation (1.1 L min^{-1}, FO, CO_2 dissolution), where the slop of the linear fitting represent the value of K_La (min^{-1})

- ***K_La for O_2 removal***

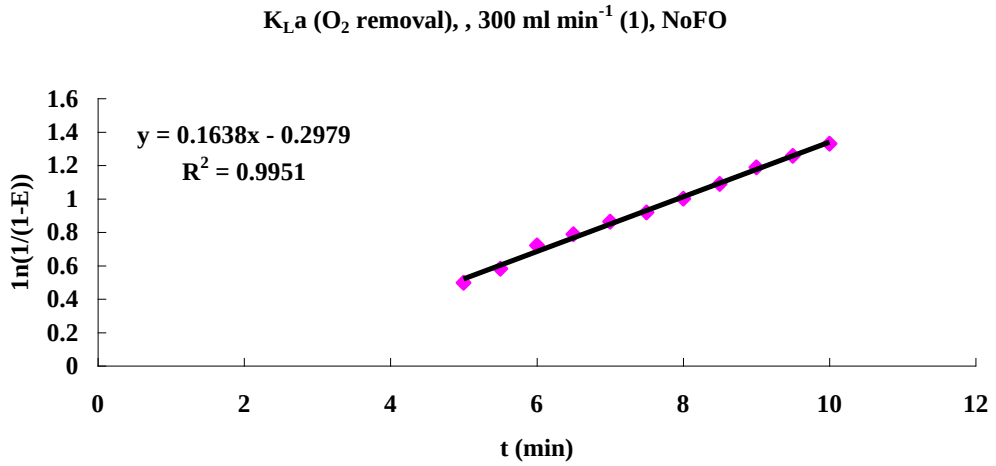

Figure A3.16: Typical plot for K_La estimation (0.3 L min^{-1}, NoFO, O_2 removal) – test 1, where the slop of the linear fitting represent the value of K_La (min^{-1})

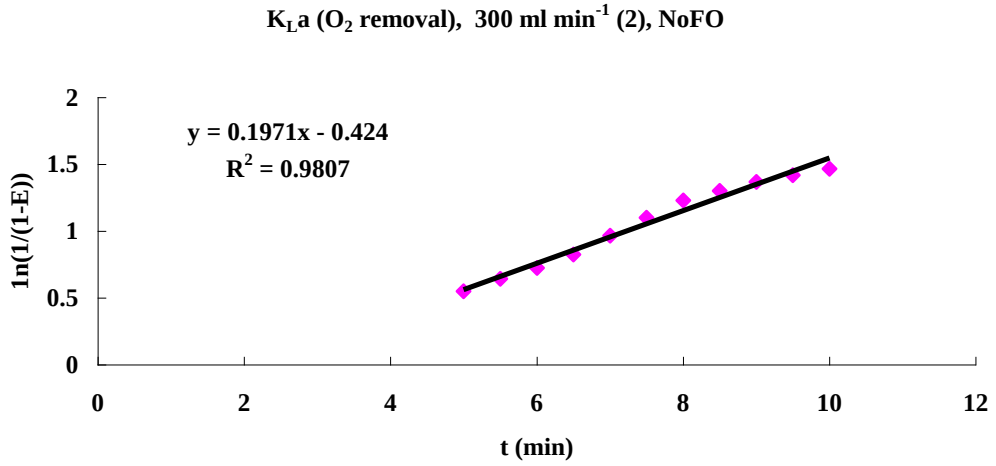

Figure A3.17: Typical plot for K_La estimation (0.3 L min^{-1}, NoFO, O_2 removal) – test 2, where the slop of the linear fitting represent the value of K_La (min^{-1})

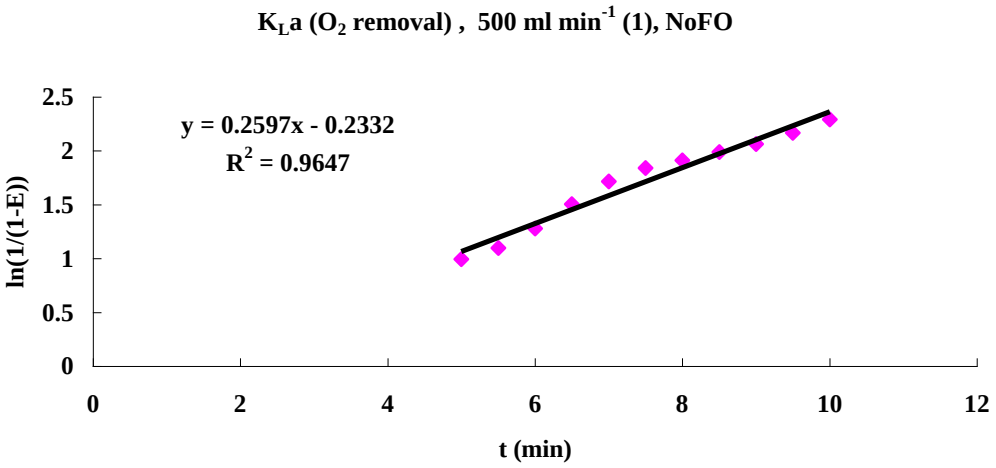

Figure A3.18: Typical plot for K_La estimation (0.5 L min^{-1}, NoFO, O_2 removal) – test 1, where the slop of the linear fitting represent the value of K_La (min^{-1})

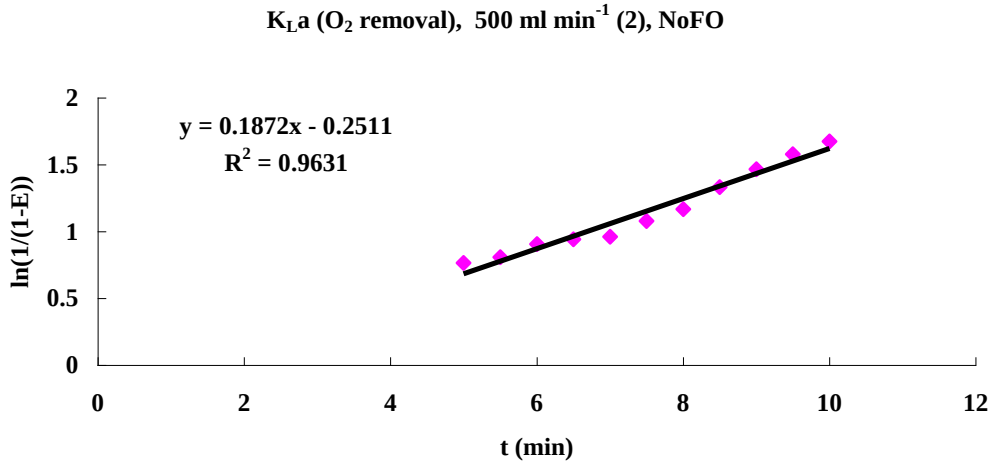

Figure A3.19: Typical plot for K_La estimation (0.5 L min^{-1}, NoFO, O_2 removal) – test 2, where the slop of the linear fitting represent the value of K_La (min^{-1})

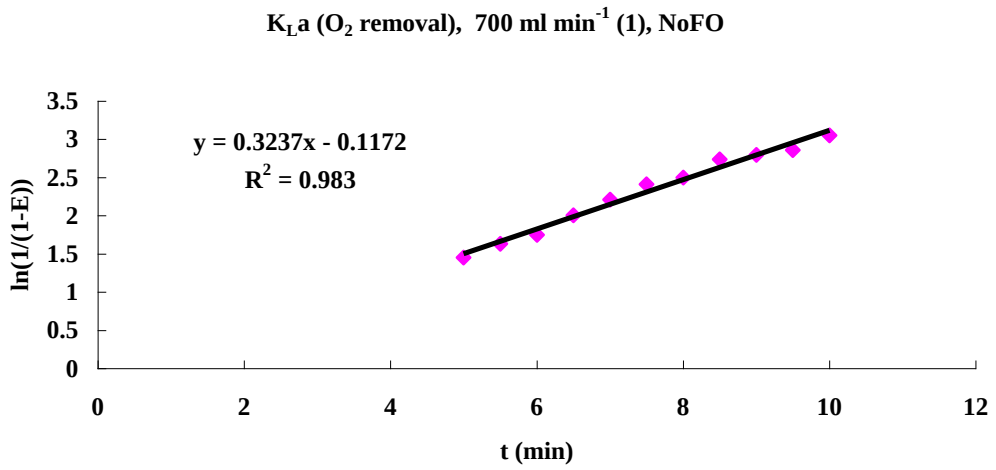

Figure A3.20: Typical plot for K_La estimation (0.7 L min^{-1}, NoFO, O_2 removal) – test 1, where the slop of the linear fitting represent the value of K_La (min^{-1})

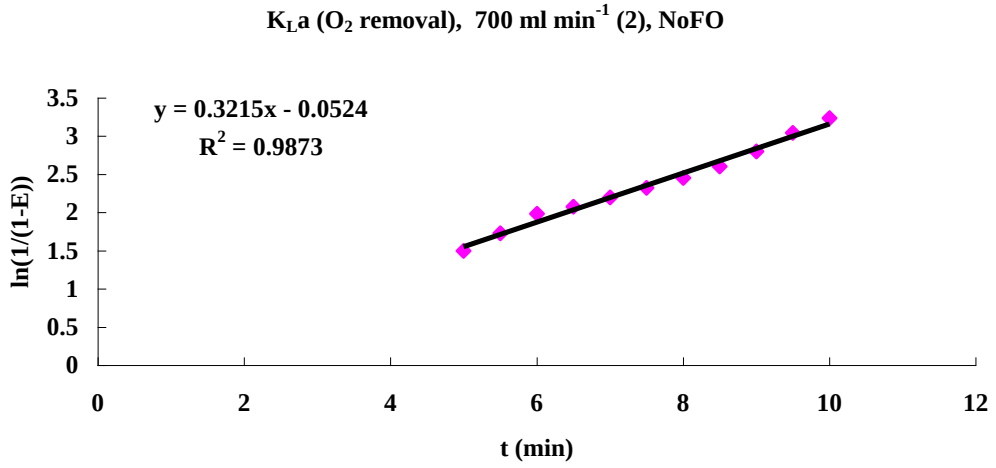

Figure A3.21: Typical plot for K_La estimation (0.7 L min^{-1}, NoFO, O_2 removal) – test 2, where the slop of the linear fitting represent the value of K_La (min^{-1})

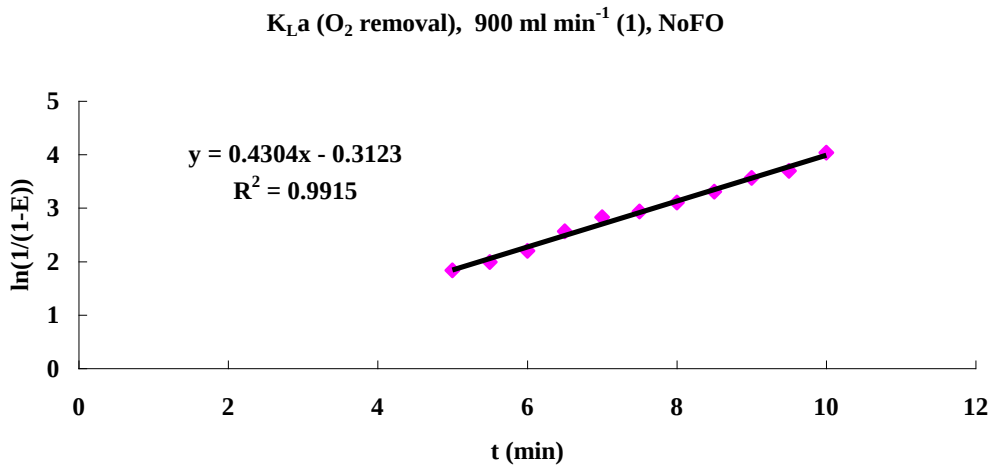

Figure A3.22: Typical plot for K_La estimation (0.9 L min^{-1}, NoFO, O_2 removal) – test 1, where the slop of the linear fitting represent the value of K_La (min^{-1})

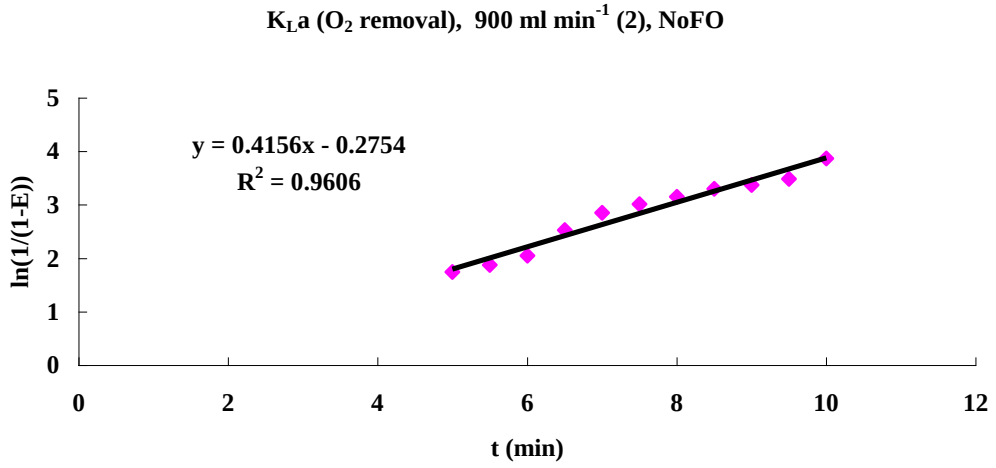

Figure A3.23: Typical plot for K_La estimation (0.9 L min^{-1}, NoFO, O_2 removal) – test 2, where the slop of the linear fitting represent the value of K_La (min^{-1})

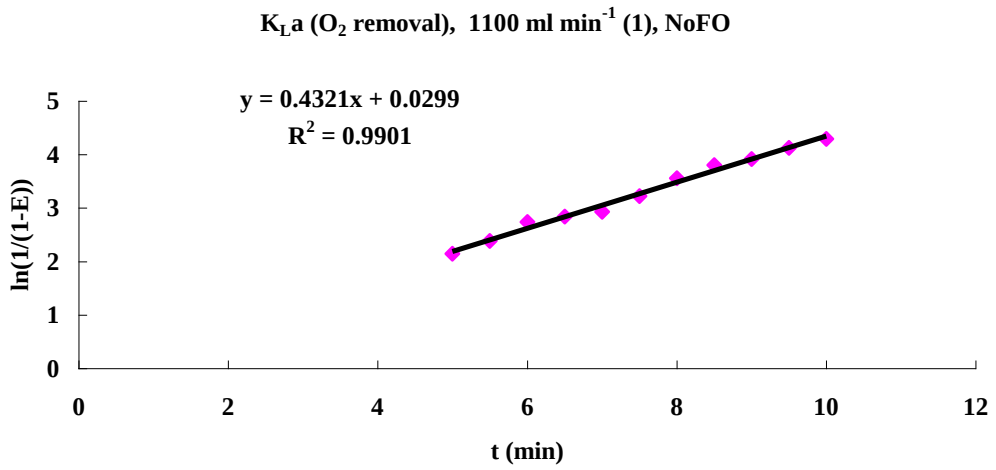

Figure A3.24: Typical plot for K_La estimation (1.1 L min^{-1}, NoFO, O_2 removal) – test 1, where the slop of the linear fitting represent the value of K_La (min^{-1})

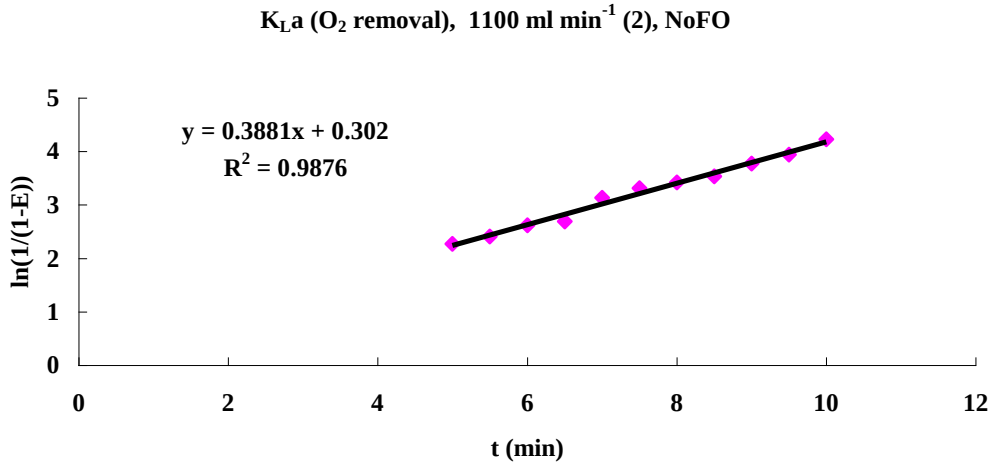

Figure A3.25: Typical plot for K_La estimation (1.1 L min^{-1}, NoFO, O_2 removal) – test 2, where the slop of the linear fitting represent the value of K_La (min^{-1})

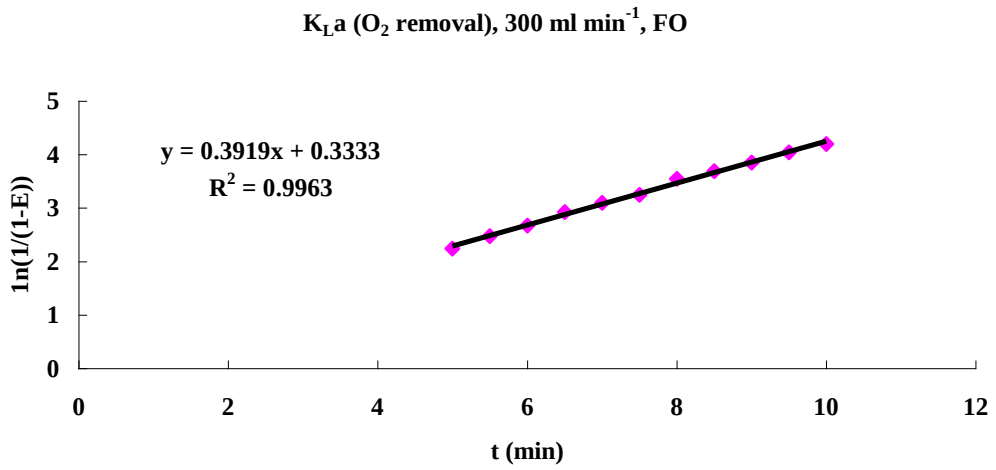

Figure A3.26: Typical plot for K_La estimation (0.3 L min^{-1}, FO, O_2 removal), where the slop of the linear fitting represent the value of K_La (min^{-1})

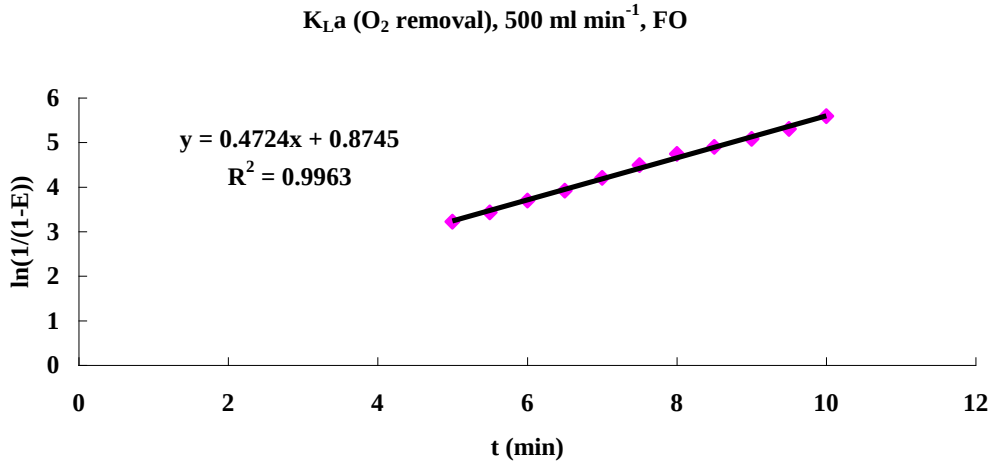

Figure A3.27: Typical plot for K_La estimation (0.5 L min^{-1}, FO, O_2 removal), where the slop of the linear fitting represent the value of K_La (min^{-1})

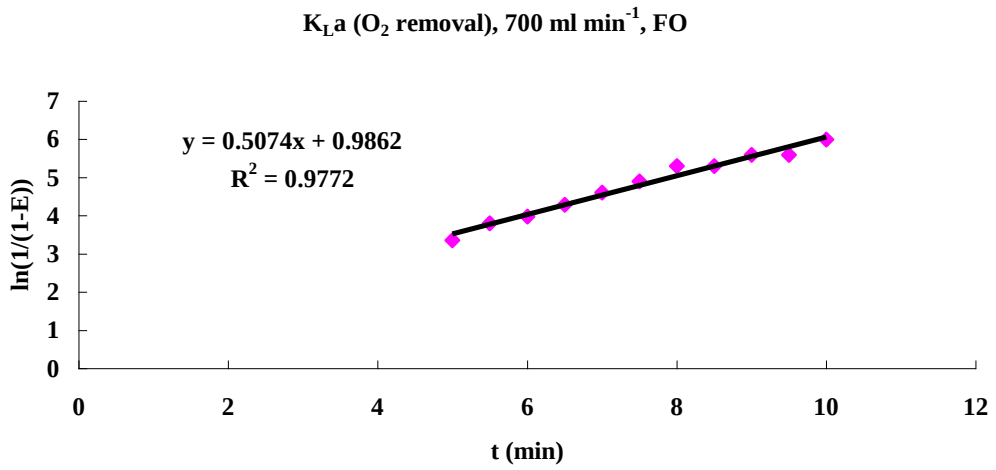

Figure A3.28: Typical plot for K_La estimation (0.7 L min^{-1}, FO, O_2 removal), where the slop of the linear fitting represent the value of K_La (min^{-1})

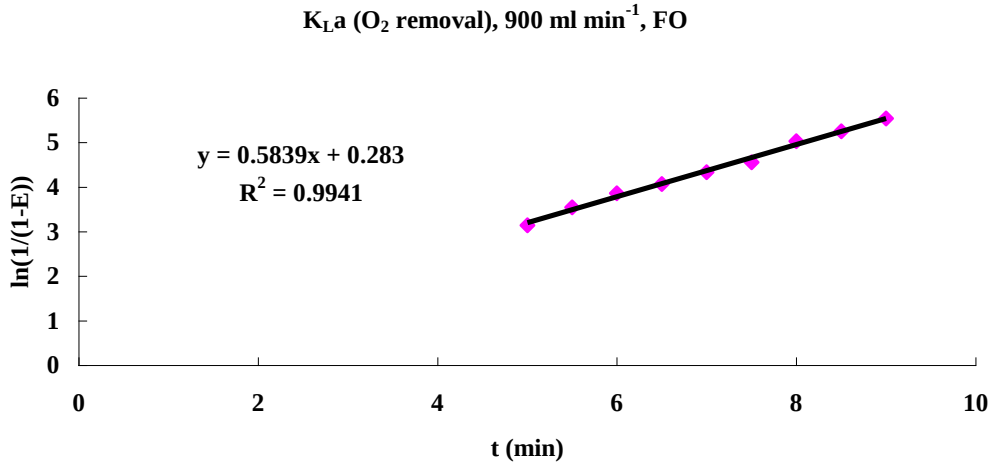

Figure A3.29: Typical plot for K_La estimation (0.9 L min^{-1}, FO, O_2 removal), where the slop of the linear fitting represent the value of K_La (min^{-1})

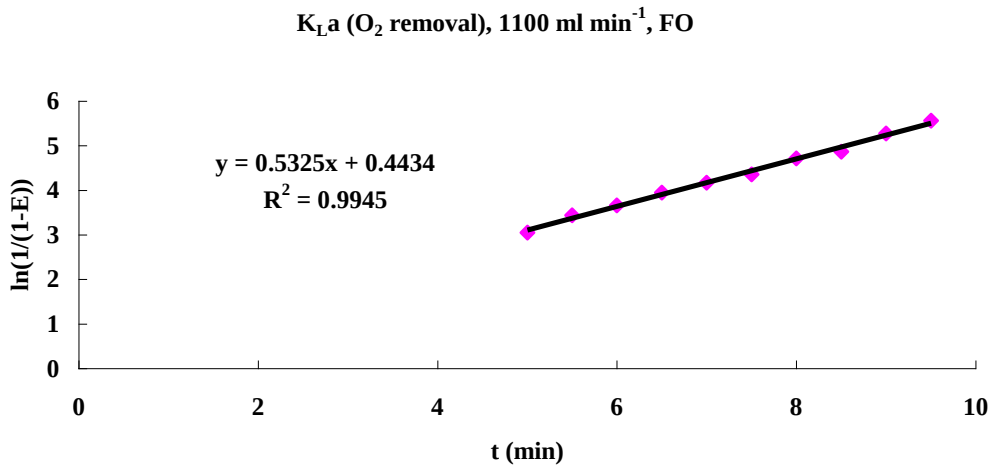

Figure A3.30: Typical plot for K_La estimation (1.1 L min^{-1}, FO, O_2 removal), where the slop of the linear fitting represent the value of K_La (min^{-1})

Appendix 4: K_La estimation in the algae culture based on $[C_T]$

The raw figures for K_La estimation (for 0.7 L min^{-1}) in the algae cultures are shown as follows.

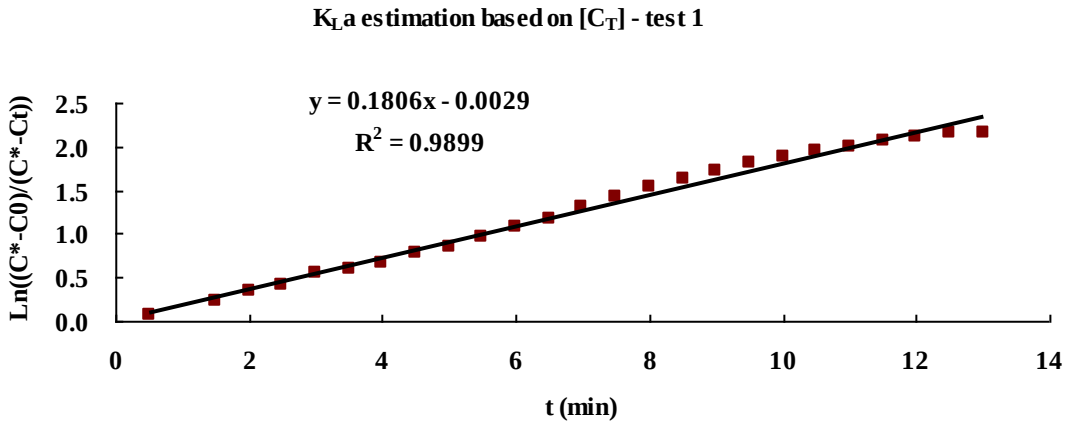

Figure A4.1: Typical plot for K_La estimation (in 3L-ALB, at 0.7 L min^{-1} dosing) – test 1, where the slop of the linear fitting represent the value of K_La (min^{-1})

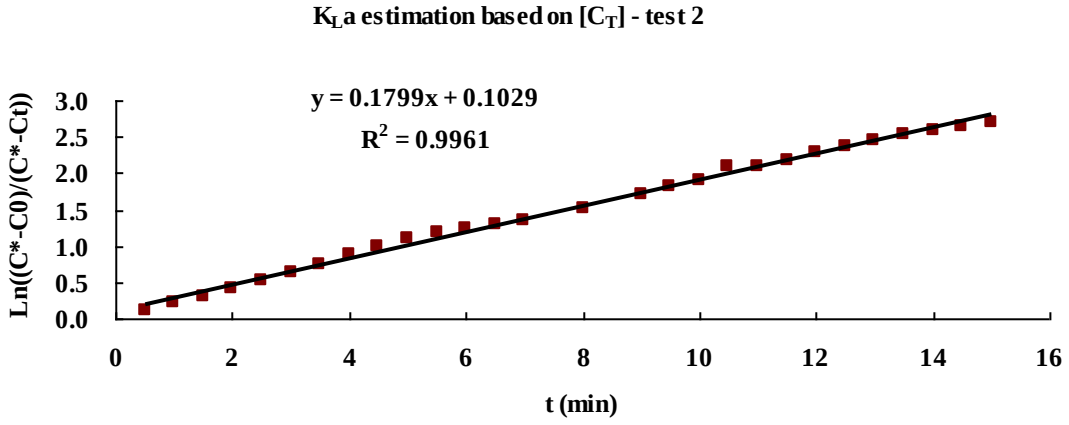

Figure A4.2: Typical plot for K_La estimation (in 3L-ALB, at 0.7 L min^{-1} dosing) – test 2, where the slop of the linear fitting represent the value of K_La (min^{-1})

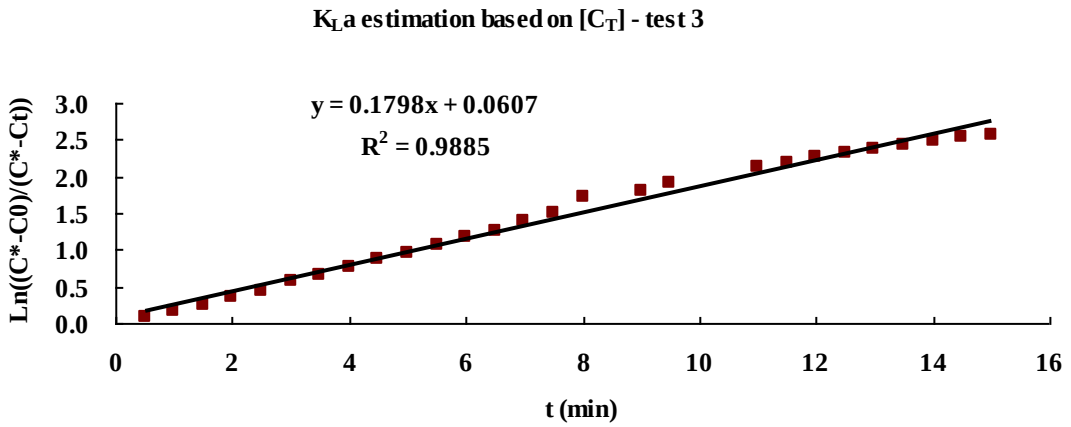

Figure A4.3: Typical plot for K_La estimation (in 3L-ALB, at 0.7 L min^{-1} dosing) – test 3, where the slop of the linear fitting represent the value of K_La (min^{-1})

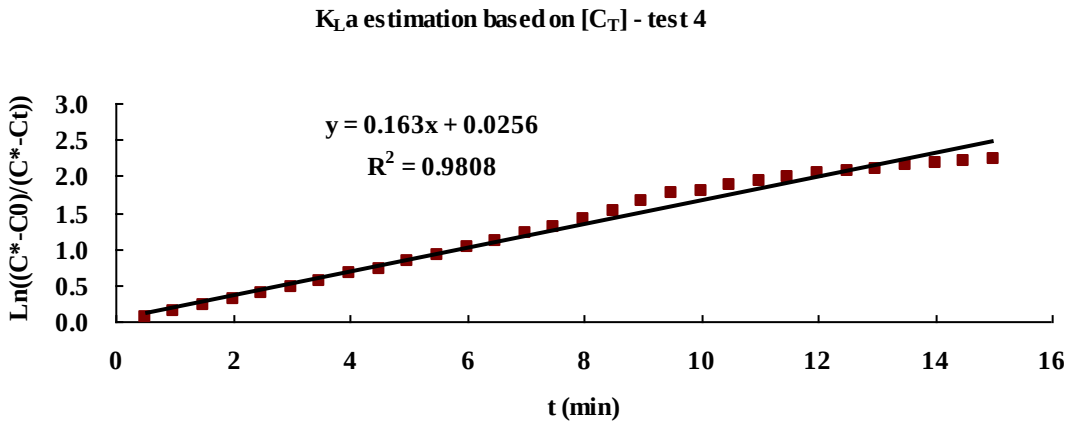

Figure A4.4: Typical plot for K_La estimation (in 3L-ALB, at 0.7 L min^{-1} dosing) – test 4, where the slop of the linear fitting represent the value of K_La (min^{-1})

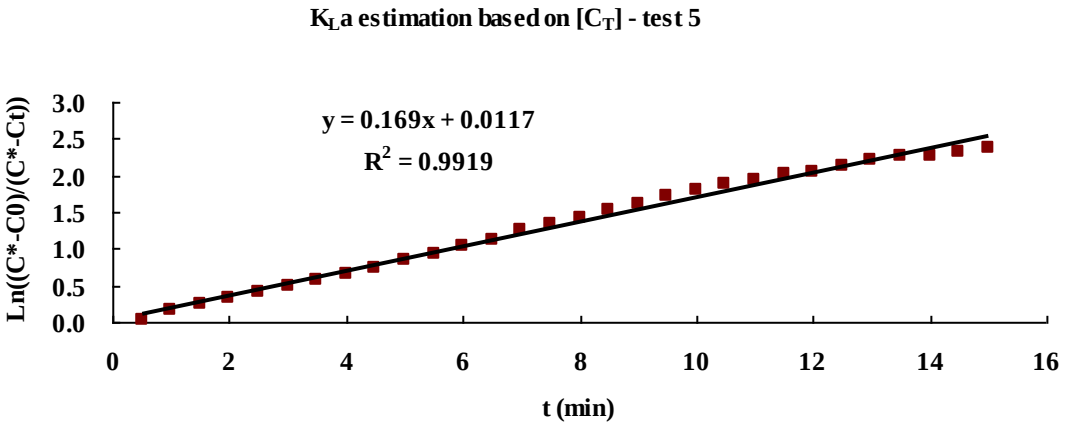

Figure A4.5: Typical plot for K_La estimation (in 3L-ALB, at 0.7 L min^{-1} dosing) – test 5, where the slop of the linear fitting represent the value of K_La (min^{-1})

Table A4.1: Summary of the K_La for each test under 0.7 L min^{-1} of 5% CO_2 dosing

Test	K_La (min^{-1})
1	0.181
2	0.180
3	0.180
4	0.163
5	0.169
Ave	**0.174**
Stdev	0.008

The raw figures for K_La estimation (for 0.3 L min^{-1}) in the algae cultures are shown as follows:

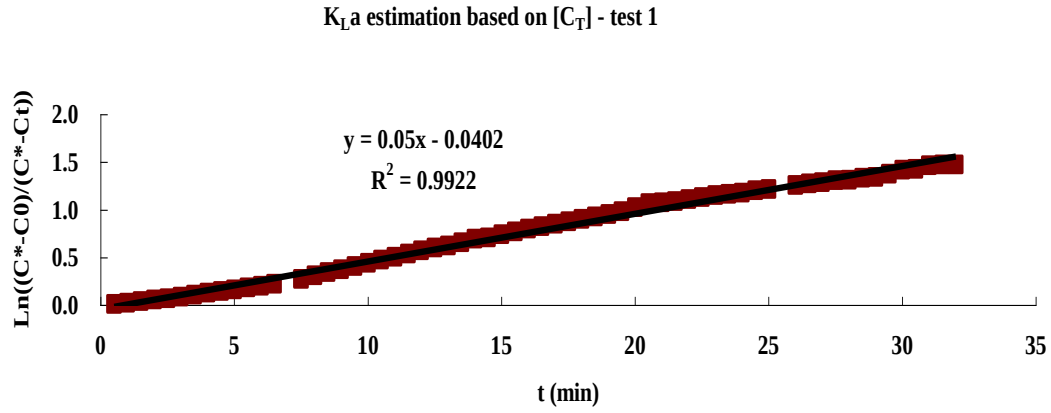

Figure A4.6: Typical plot for K_La estimation (in 3L-ALB, at 0.3 L min^{-1} dosing) – test 1, where the slop of the linear fitting represent the value of K_La (min^{-1})

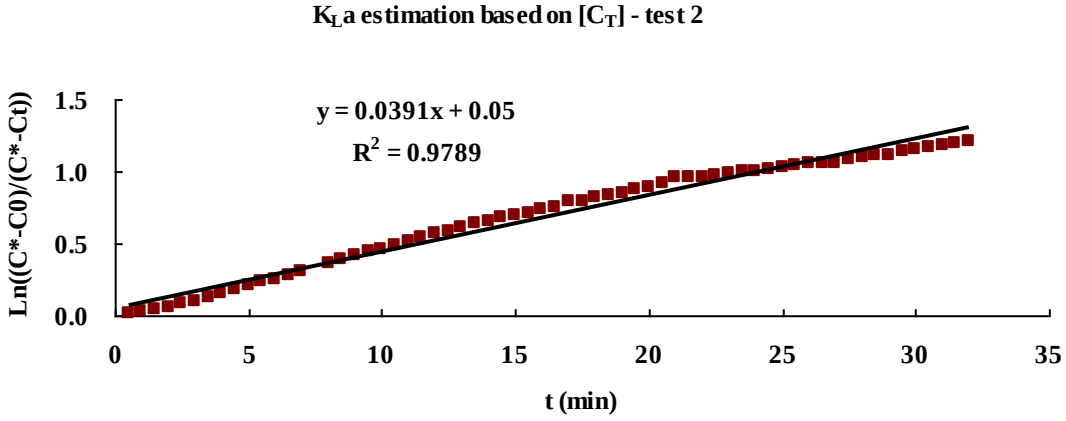

Figure A4.7: Typical plot for K_La estimation (in 3L-ALB, at 0.3 L min^{-1} dosing) – test 2, where the slop of the linear fitting represent the value of K_La (min^{-1})

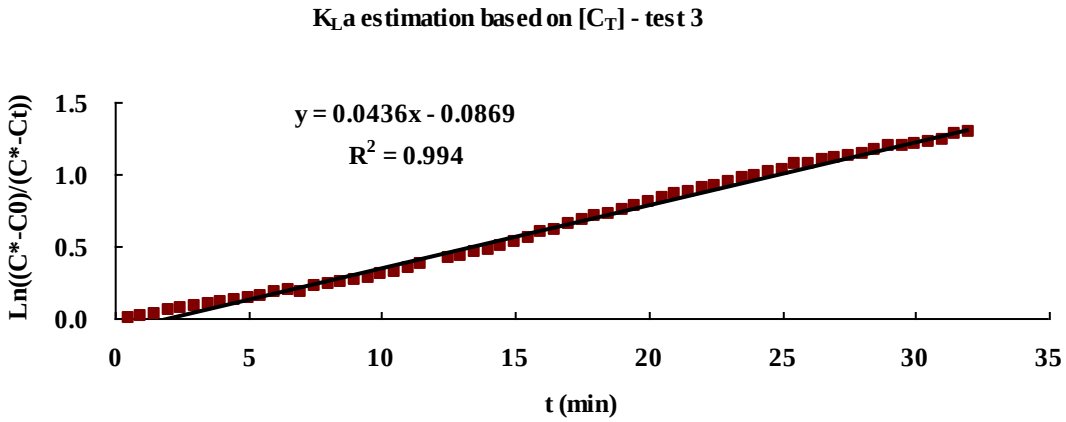

Figure A4.8: Typical plot for K_La estimation (in 3L-ALB, at 0.3 L min^{-1} dosing) – test 3, where the slop of the linear fitting represent the value of K_La (min^{-1})

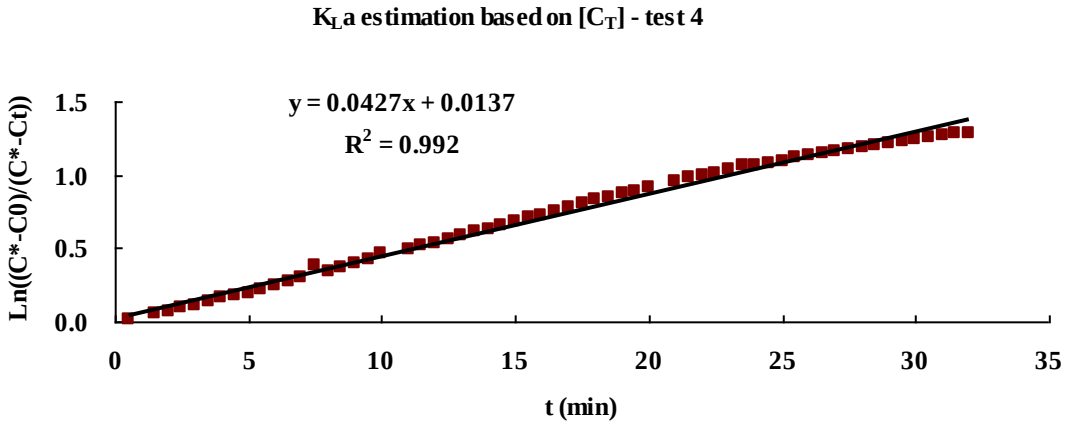

Figure A4.9: Typical plot for K_La estimation (in 3L-ALB, at 0.3 L min^{-1} dosing) – test 4, where the slop of the linear fitting represent the value of K_La (min^{-1})

Table A4.2: Summary of the K_La for each test under 0.3 L min^{-1} of 5% CO_2 dosing

Test	K_La (min^{-1})
1	0.050
2	0.039
3	0.044
4	0.043
Ave	**0.044**
Stdev	0.005

Appendix 5: The typical plots for μ estimation – the impact of FO on growth

In Figure 5.5, the specific growth rate of *D. Slina* under each dosing condition was obtained from Figure A5.1 to Figure A5.5. Each figure was plotted based on the standard method described in Section 3.3.4. The legend in each figure shows the dosing condition. For instance, '0.3 NoFO' represents 'bubbling under 0.3 L min^{-1} without fluidic oscillator', while '0.3 FO' means 'bubbling under 0.3 L min^{-1} with fluidic oscillator'. The slop of each linear fitting stands for the overall specific growth rate. Since each culture was in the log growth phase from day 6 to day 16, only this part of data was plotted to calculate the overall specific growth rate.

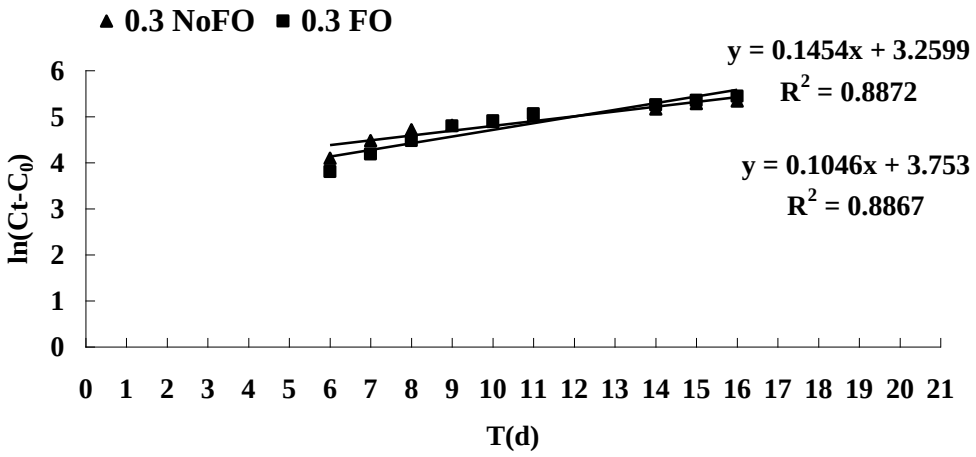

Figure A5.1: Typical plot for μ estimation (under 0.3 L min^{-1} of bubbling), where the slop of the linear fitting represent the value of μ (d^{-1})

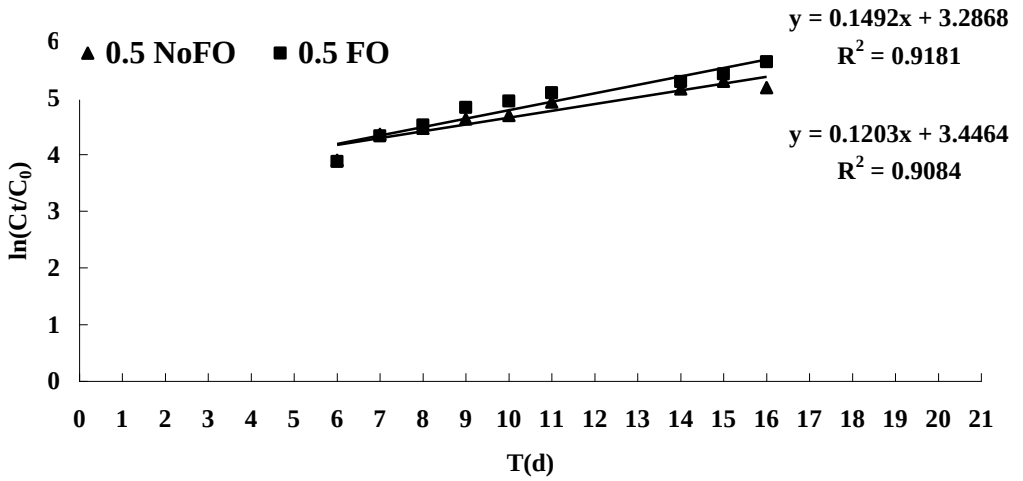

Figure A5.2: Typical plot for μ estimation (under 0.5 L min^{-1} of bubbling), where the slop of the linear fitting represent the value of μ (d^{-1})

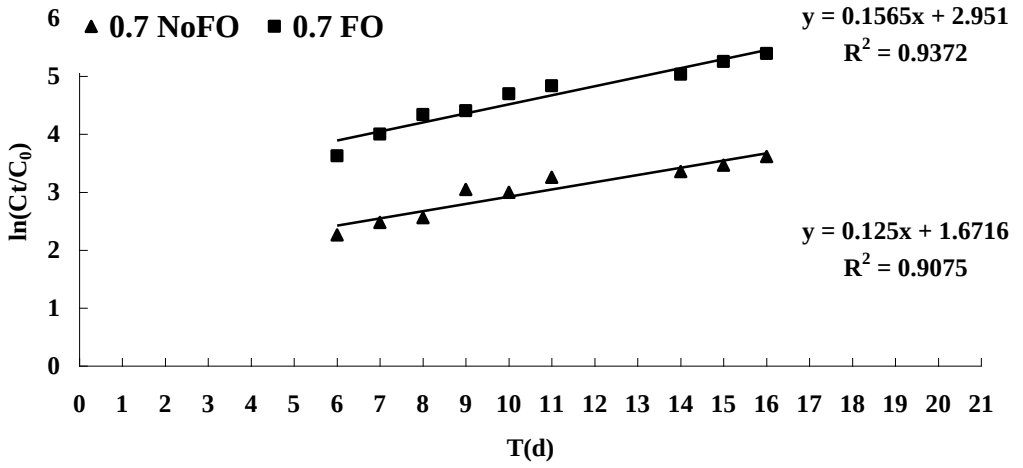

Figure A5.3: Typical plot for μ estimation (under 0.7 L min^{-1} of bubbling), where the slop of the linear fitting represent the value of μ (d^{-1})

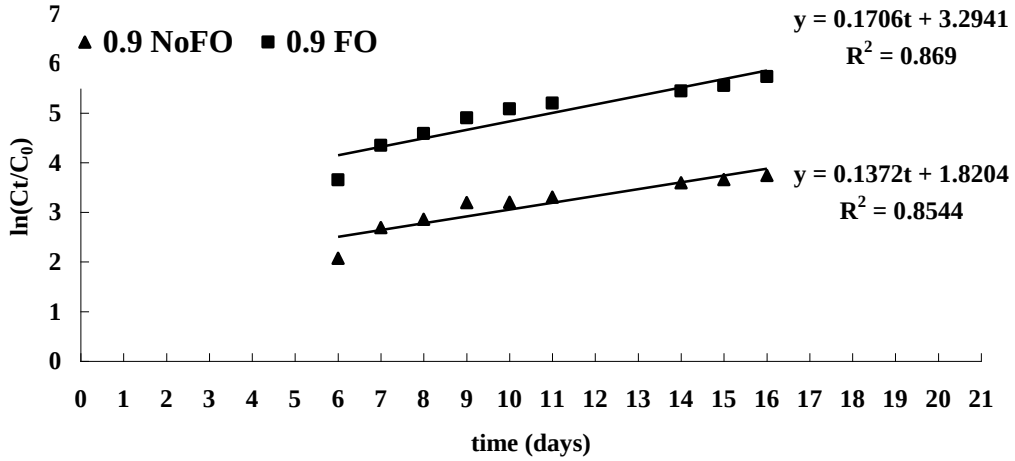

Figure A5.4: Typical plot for μ estimation (under 0.9 L min^{-1} of bubbling), where the slop of the linear fitting represent the value of μ (d^{-1})

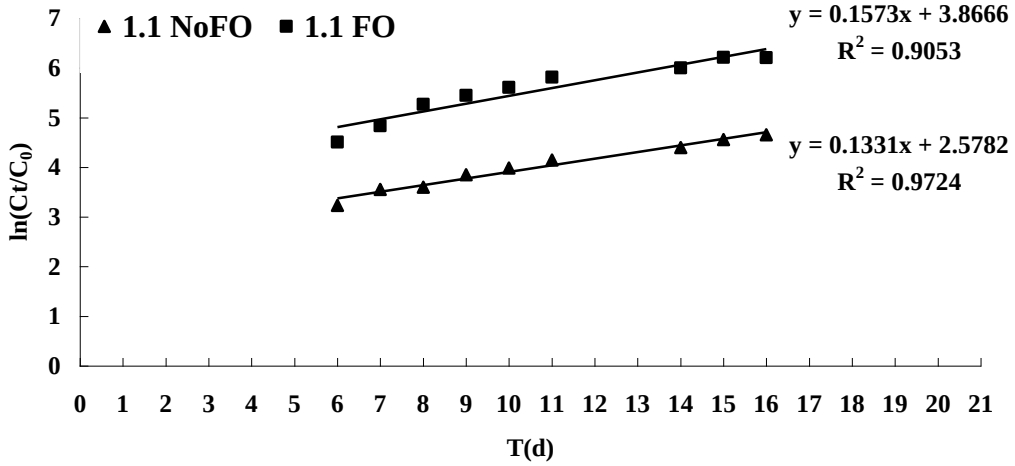

Figure A5.5: Typical plot for μ estimation (under 1.1 L min^{-1} of bubbling), where the slop of the linear fitting represent the value of μ (d^{-1})

Appendix 6: Estimation of energy consumption for bubbling

In Chapter 5, the highest specific growth rate was found to be achieved at 1.1 L min^{-1} for fine bubble dosing, however, the similar specific growth rate was achieved at only 0.3 L min^{-1} for microbubble dosing. It is interesting to find out the energy savings by using mcirobubble dosing. Therefore, the energy consumption of bubbling gas into ALB containing 2.5 L of algae was estimated for both 0.3 L min^{-1} and 1.1 L min^{-1} of dosing flow rate.

The calculations are relatively rough, based on some simplifications/assumptions, e.g. the density of algae culture medium was replaced by the water density, the energy consumption for gas passing through the diffuser chamber was assumed to be negligible compared to the total energy cost of bubbling, the friction loss in the gas pipe and diffuser chamber was assumed to be negligible, etc., shown as follows.

For 0.3 L min^{-1} of bubbling, the energy consumption for 18d of 2.5 L-culture is

$$E = F \cdot L = mg \cdot v_G t = \rho V g \cdot \frac{Q_G}{S_d} \cdot t$$

$$= 1000 \times 2.5 \times 10^{-3} \times 10 \times \frac{0.3 \times 10^{-3}}{4.8 \times 10^{-3}} \times 30 \times 18 \approx 844 J$$

where E represents the energy consumption, ρ is the water density (1000 kg m^{-3}), V stands for the liquid volume in the reactor (2.5 × 10^{-3} m^3), g is the acceleration of gravity (10 m s^{-2}), Q_G is the bubbling flow rate (0.3 × 10^{-3} m^3 min^{-1} or 1.1 × 10^{-3} m^3 min^{-1}), S_d means the diffuser area (4.8 × 10^{-3} m^2) and t is the time of dosing (30 min d^{-1} × 18 d).

Similarly, the energy consumption for 1.1 L min^{-1} can be calculated as

$$E = F \cdot L = mg \cdot v_G t = \rho V g \cdot \frac{Q_G}{S_d} \cdot t$$

$$= 1000 \times 2.5 \times 10^{-3} \times 10 \times \frac{1.1 \times 10^{-3}}{4.8 \times 10^{-3}} \times 30 \times 18 \approx 3094 J$$

The energy saving for 0.3 L min^{-1} of bubbling, compared to 1.1 L min^{-1}, is about 70%.

$$\eta = \frac{3094 - 844}{3094} \times 100\% \approx 73\%$$

Appendix 7: Dosing time and dosing interval estimation

In table 6.1, the dosing time for 0.3 L min^{-1} and 0.7 L min^{-1} were calculated based on Eq. 6.3. The detailed calculation was shown as follows.

$$t_d = \frac{[C_T]_{pH=A} - [C_T]_{pH=B}}{K_L a([C_T]^* - [C_T]_{pH=B}) - \frac{1}{2} K_L a([C_T]_A - [C_T]_{pH=B})} \quad \text{Eq. 6.3}$$

Since the selected pH range for *D. S* culture was 7.5 – 9.5, and the concentration of $NaHCO_3$ in the culture medium was 0.0119 mol L^{-1}, $[C_T]$ at pH = 7.5 and pH = 9.5 can be calculated based on Eq. 3.9, which gives:

$[C_T]_{pH=7.5}$ = 0.0128 mol L^{-1}

$[C_T]_{pH=9.5}$ = 0.0106 mol L^{-1}

The K_La for CO_2 mass transfer in the real algal culture was previously determined to be 0.044 min^{-1} for 0.3 L min^{-1} of bubbling flow rate and 0.174 min^{-1} for 0.7 L min^{-1} (Appendix 4). Finally, t_d was calculated to be about 36 min for 0.3 L min^{-1} of bubbling flow rate and 10 min for 0.7 L min^{-1}

For dosing interval estimation, it can be calculated by Eq. 6.10.

$$t_i = \frac{[C_T]_{pH=A} - [C_T]_{pH=B}}{7 \times 10^{-5} \cdot [Chl]_0} \cdot (1 - 0.0946 \cdot t_c) \quad \text{Eq. 6.10}$$

Based on the assumption that Chl_0 = 5 mg L^{-1} and t_c = 8 d, t_i is calculated to be 1.5 d. Conservatively, 1 d of dosing interval was used in the experiment so that DO can be removed by CO_2 dosing in time (see 6.2.2).

Appendix 8: The typical plots for μ estimation – the pH effects on growth

In Figure 7.9, the specific growth rate of *D. Slina* under each culture condition was obtained from Figure A8.1 to Figure A8.12. Each figure was plotted based on the standard method described in Section 3.3.4.

Since the increase in chlorophyll content was obviously different for d2 – d5 and d5 – d10. Therefore, the specific growth rate under each culture condition was estimated on d2 – d5 and d5 – d10, separately.

The legend in each figure shows the culture condition and the time period selected. For each culture condition, the experiment was duplicated, indicated as '(1)' and '(2)' and shown at left and right, respectively. The specific growth rate under each culture condition, presented in Figure 7.9, was the average value of '(1)' and '(2)'.

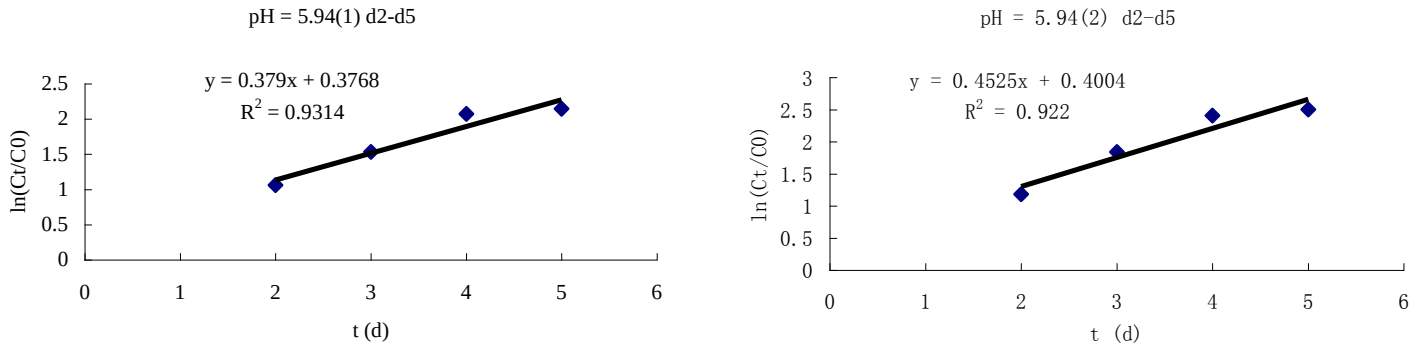

Figure A8.1: The typical plots for μ estimation (pH = 5.94, d2 – d5)

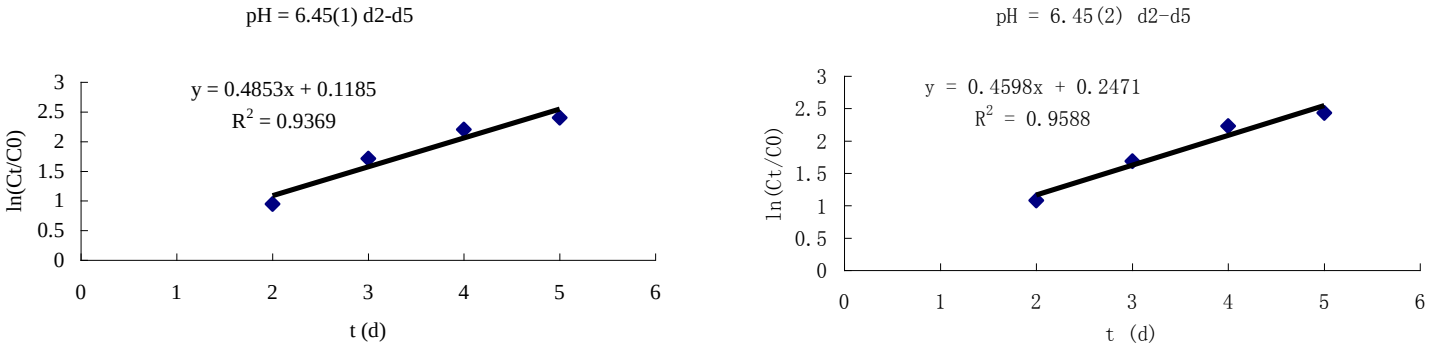

Figure A8.2: The typical plots for μ estimation (pH = 6.45, d2 – d5)

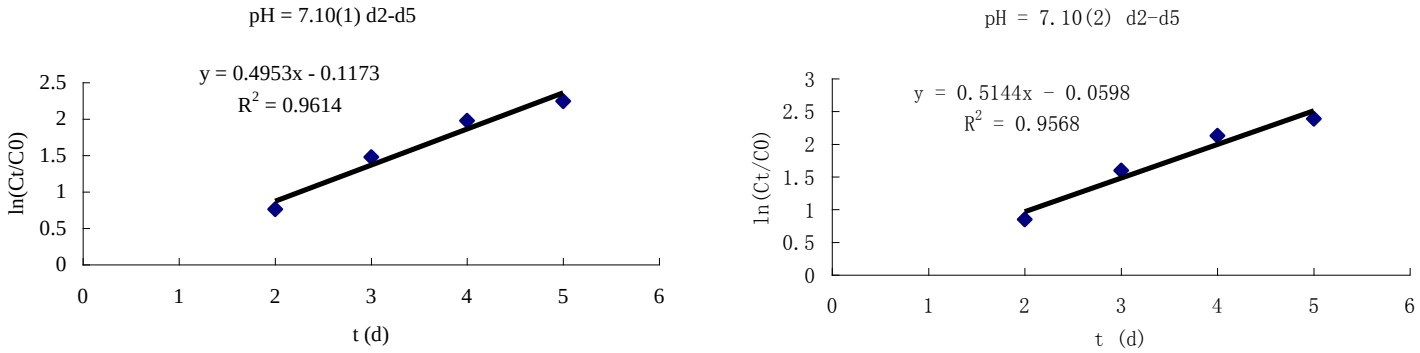

Figure A8.3: The typical plots for μ estimation (pH = 7.10, d2 – d5)

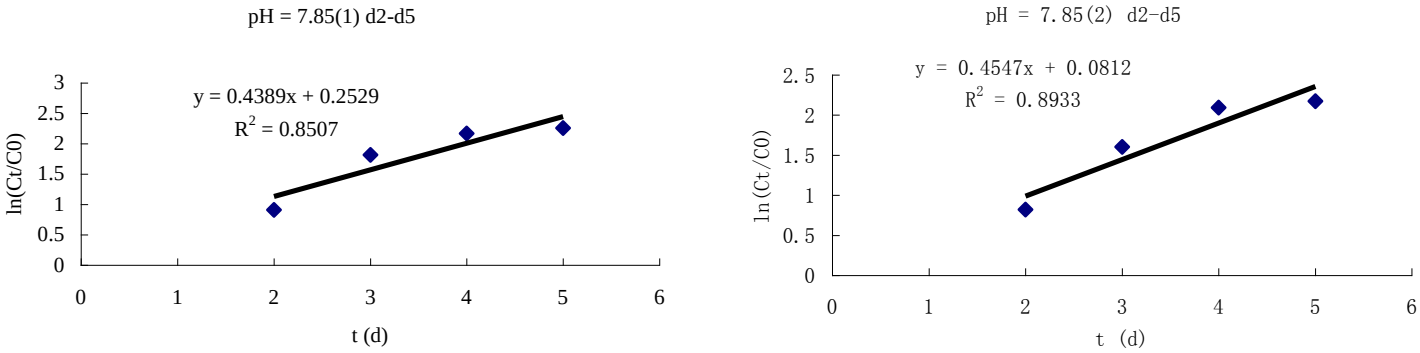

Figure A8.4: The typical plots for μ estimation (pH = 7.85, d2 – d5)

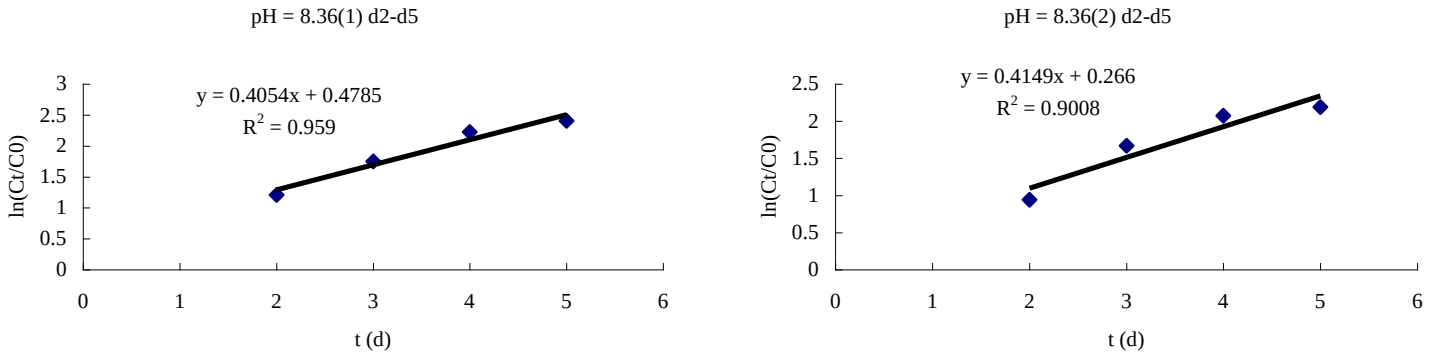

Figure A8.5: The typical plots for μ estimation (pH = 8.36, d2 – d5)

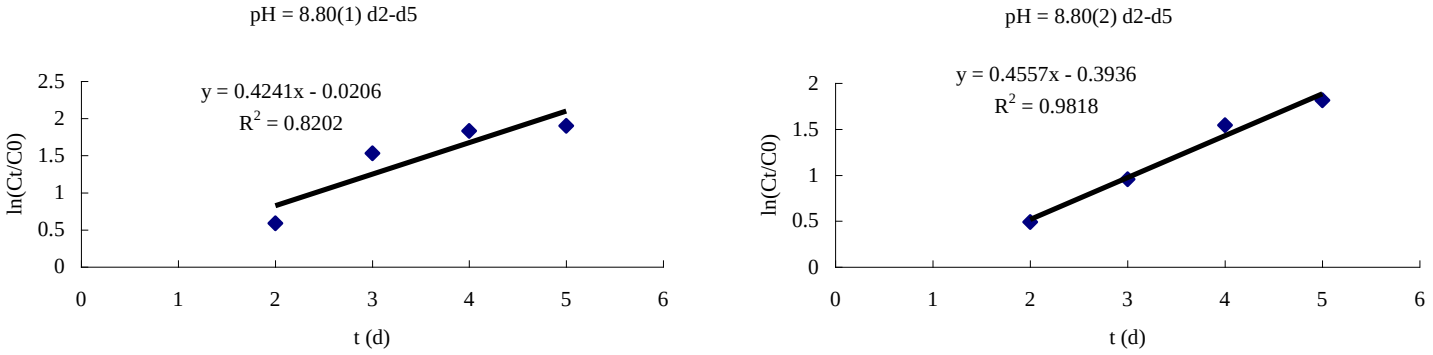

Figure A8.6: The typical plots for μ estimation (pH = 8.80, d2 – d5)

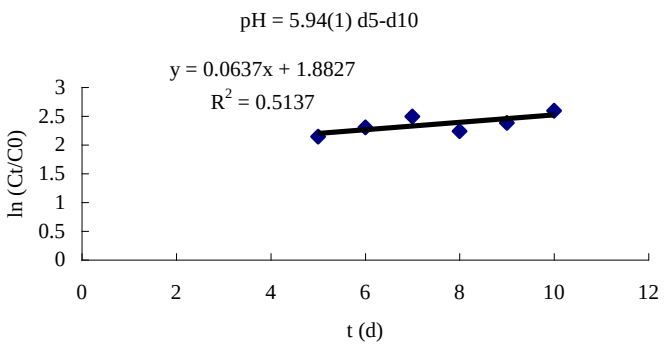

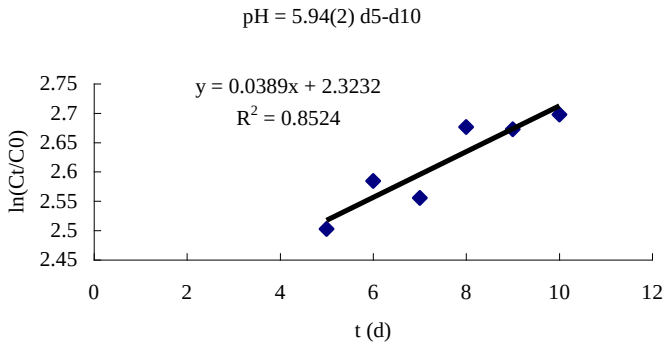

Figure A8.7: The typical plots for μ estimation (pH = 5.94, d5 – d10)

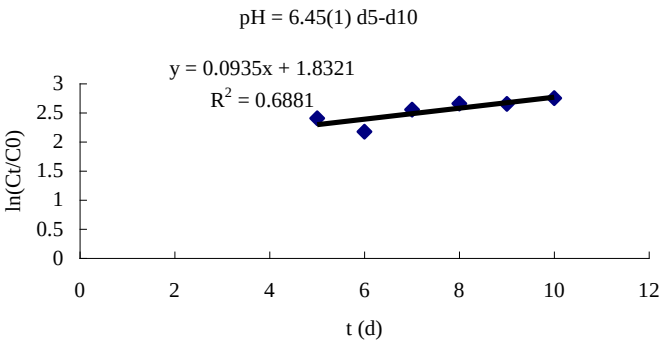

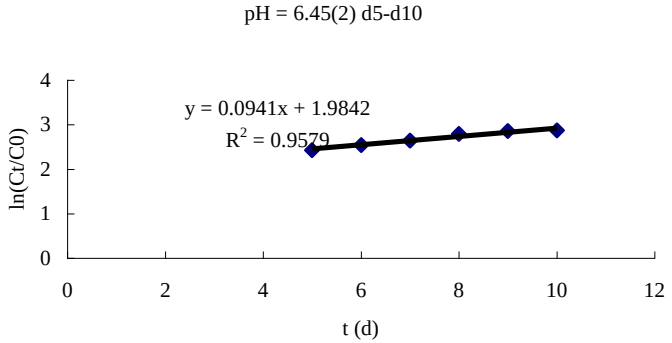

Figure A8.8: The typical plots for μ estimation (pH = 6.45, d5 – d10)

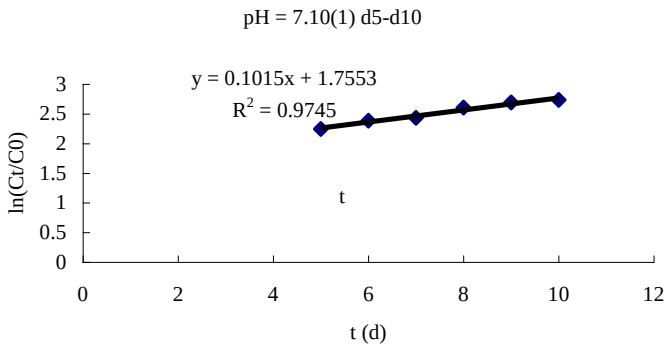

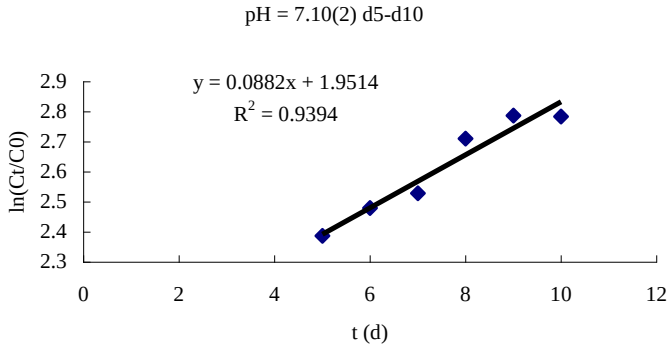

Figure A8.9: The typical plots for μ estimation (pH = 7.10, d5 – d10)

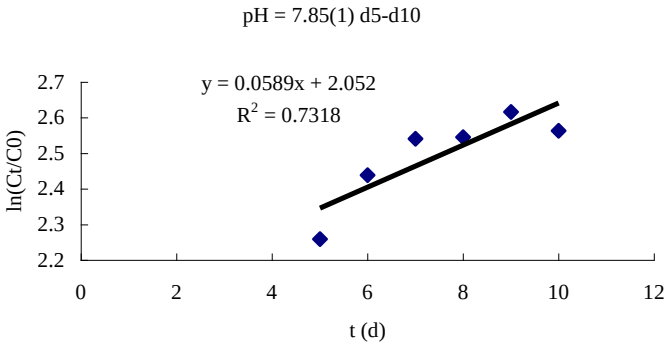

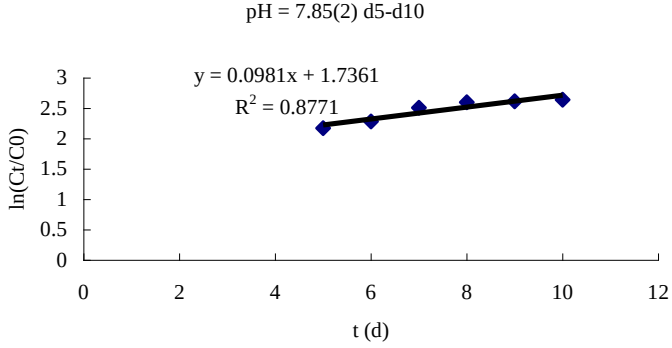

Figure A8.10: The typical plots for μ estimation (pH = 7.85, d5 – d10)

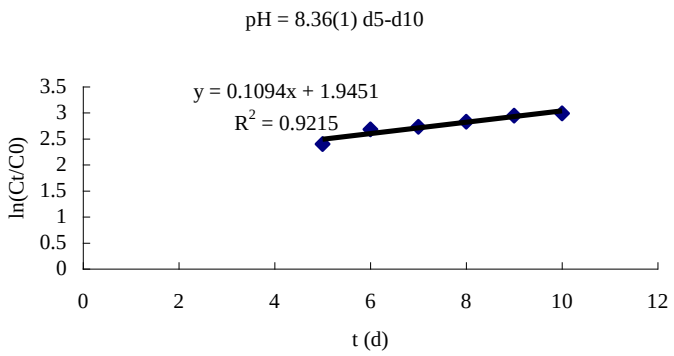

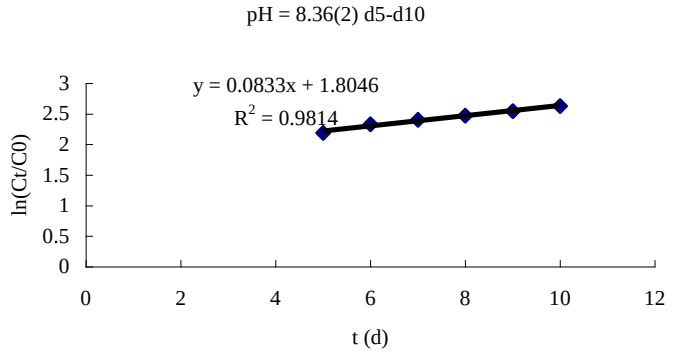

Figure A8.11: The typical plots for μ estimation (pH = 8.36, d5 – d10)

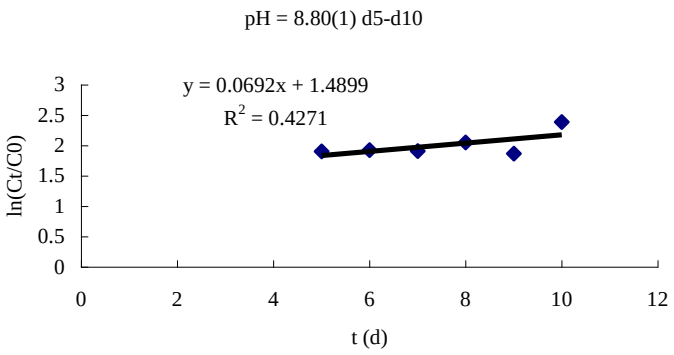

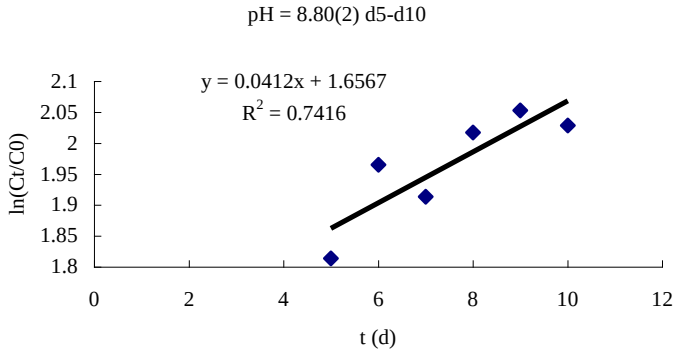

Figure A8.12: The typical plots for μ estimation (pH = 8.80, d5 – d10)

Appendix 9: List of Publications

Hanotu, J., Ying, K., Shada, O. I., Bandulasena, H., & Zimmerman, W. B. (2013). Microalgae recovery by microflotation for biofuel production using metallic coagulants. *Biofuels*, *4*(4), 363-369.

Ying, K., Gilmour, D. J., Shi, Y., & Zimmerman, W. B. (2013a). Growth Enhancement of *Dunaliella salina* by Microbubble Induced Airlift Loop Bioreactor (ALB)—The Relation between Mass Transfer and Growth Rate. *Journal of Biomaterials and Nanobiotechnology*, *4*, 1-9.

Ying, K., Mahmood K. H. A., James H., Gilmour D. J. & Zimmerman, W. B. (2013b). Enhanced Mass Transfer in Microbubble Driven Airlift Bioreactor for Microalgal culture. *Journal of Engineering*, *5*(9), 735-743.

Zimmerman, W. B., Zandi, M., Hemaka Bandulasena, H. C. H., Tesař, V., Gilmour, D. J. & Ying, K. (2011b). Design of an airlift loop bioreactor and pilot scales studies with fluidic oscillator induced microbubbles for growth of a microalgae *Dunaliella salina*. *Applied Energy*, *88*(10), 3357-3369.